HYDROCLIMATE VARIABILITY IN CENTRAL VIETNAM: PAST AND PRESENT

ANNABEL WOLF

PhD

2022

HYDROCLIMATE VARIABILITY IN CENTRAL VIETNAM: PAST AND PRESENT

ANNABEL WOLF

A thesis submitted in partial fulfilment of the requirements of the University of Northumbria at Newcastle for the degree of Doctor of Philosophy

Faculty of Engineering and Environment

May 2022

Abstract

Central Vietnam is one of only few locations within the Asian Monsoon realm, where the rainy season is associated with the Northeast Winter Monsoon. The winter monsoon in this region is characterised by strong north-easterly winds bringing moisture from the Pacific, leading to intensive rainfall during autumn and winter. This is often associated with natural hazards such as flooding and landslides, threatening the livelihood of millions in this region. Compared with the Asian Summer Monsoon, our knowledge of past and present rainfall variability related to the Northeast Winter Monsoon is more limited, which affects our ability to understand future climate scenarios in this region. This work uses stable isotopes in rainwater and the chemical composition of a stalagmite from central Vietnam to understand the climate in Southeast Asia in the present and past. Cave monitoring and climate simulations indicate that the seasonal cycle in rainwater stable isotopes from central Vietnam does not follow peak rainfall amount, but rather reflects the seasonal shift between the Indian Ocean, providing moisture during summer, and the Pacific Ocean which provides moisture during the rest of the year. This seasonal signal in rainfall oxygen isotopes is partly preserved in cave waters but low values are biased towards the season of recharge in autumn. This work presents the first high-resolution speleothem multi-proxy record from central Vietnam covering the Holocene. By using carbon isotopes and trace elements the history of the Northeast Winter Monsoon was reconstructed. In Southeast Asia, summer and winter monsoons evolved in-phase for most of the Holocene, between 8000 to 3000 years BP (before present). This in-phase relation shifts at 3000 years BP, after which the winter monsoon gets progressively wetter and the summer monsoon progressively drier. Here it is proposed that shifts in the Pacific Walker Circulation controlled the in-phase relation of the monsoons in Southeast Asia until 3000 years BP. Afterwards the summer monsoon was mainly controlled by changes in the Indian Walker Circulation and the winter monsoon by changes in Pacific sea surface temperatures. Investigating central Vietnam's climate on a seasonal scale during a cool phase between 1600 and 1300 years BP showed that the timing of the ITCZ migration is key in modulating rainfall variability. A cooling of primarily autumn/winter sea surface temperatures in the western Pacific led to a delay of the ITCZ withdrawal during this season, causing enhanced rainfall in central Vietnam. The findings of this work have far-reaching implications for future palaeoclimate studies, such as the interpretation of proxies and the understanding of the monsoonal system in Southeast Asia over

the Holocene.

Contents

List of Figures

List of Tables

List of Abbreviations

Al	Aluminium
AMOC	Atlantic Meridional Overturning Circulation
Ar	Argon
AR1	First-order autoregressive
Ba	Barium
BP	Before Present (1950CE)
Ca	Calcium
$CaCO_3$	Calcium carbonate
CE	Common Era
CO_2	Carbon dioxide
COPRA	COnstructing Proxy Records from Age models
DACP	Dark Ages Cold Period
d-excess	Deuterium excess
EASM	East Asian Summer Monsoon
EOF	Empirical orthogonal function
ENSO	El-Niño Southern Oscillation
Fe	Iron
FTIR	Fourier-transform infrared spectroscopy
GMWL	Global Meteoric Water Line
GNIP	Global Network of Isotopes in Precipitation
HCO_3	Bicarbonate
H_2CO_3	Carbonic acid
H_2O	Water
HYSPLIT	Hybrid Single-Particle Lagrangian Integrated Trajectories
Hz	Hertz
IAEA	International Atomic Energy Agency
IOD	Indian Ocean Dipole
IPCC	Intergovernmental Panel on Climate Change
IRMS	Isotope ratio mass spectrometer

ISM	Indian Summer Monsoon
ITCZ	Intertropical Convergence Zone
J	Joules
k	Number of clusters
km	Kilometre
L	Litre
LA-ICP-MS	Laser Ablation Inductively Coupled Plasma Mass Spectrometer
LIA	Little Ice Age
LMWL	Local Meteoric Water Line
m	Metre (unit)
m	Number of Principal Components
MC-PCA	Monte-Carlo Principal Component Analysis
Mg	Magnesium
mg	Milligram
min	Minutes
MJO	Madden-Julian Oscillation
mm	Millimetre
mmol	Millimole
mol	Mole
MWP	Medieval Warm Period
n	Number of time series
ng	Nanogram
NOAA	National Oceanic and Atmospheric Administration
NPSM	North Pacific Summer Monsoon
OLR	Outgoing Longwave Radiation
P	Phosphorus
Pb	Lead
PC	Principal Component
PCA	Principal Component Analysis
PCP	Prior Carbonate Precipitation

pg	Picogram
pCO_2	Partial pressure of carbon dioxide
ppm	Parts per million
PTFE	Polytetrafluoroethylene
s	Seconds
Si	Silicon
Sr	Strontium
SSTA	Sea surface temperatures anomalies
SSTs	Sea surface temperatures
Th	Thorium
Ti	Titanium
TSI	Total Solar Irridance
U	Uranium
U-Pb	Uranium-lead
U-Th	Uranium-thorium
VPDB	Vienna Pee Dee Belemnite
VSMOW	Vienna Standard Mean Ocean Water
watt	Watts
yr	Years
Y	Yttrium
Δ	Delta
δ	delta
µg	Microgram
µm	Micrometre
σ	sigma
~	Approximately
°	Degree
°C	Degree Celcius
‰	Percentage
‰	Permille

$\leqslant$	less than or equal to

Acknowledgements

I would like to express my gratitude to my supervision team for the guidance and support over the last years. Vasile Ersek - thank you for all your patience and academic guidance for and beyond this project. William Roberts - thank you for everything you taught me about ENSO, modelling and coding. Ulrich Salzmann - thank you for your help and for the fun discussions.

I am also grateful to Michael Griffiths and Kathleen Johnson for your amazing contributions to this project. Thanks to Deb Limbert for your support in Vietnam and the opportunity to follow you around in the most impressive caves! Thank you to Amanda French for your LA work and the discussions that followed. Thank you to Tobias Braun for the statistics and particularly for your endless patience in explaining maths and physics to me. I am also grateful to David McGee for the U-Th dating and inputs to this project. I am grateful to Dave and Will Thomas for the lab support, one day the IRMS will be defeated. On that note, thanks to Stefano Bernasconi, Madalina Jaggi and Sebastian Breitenbach for measuring stable isotopes when we could not. Thanks to Jack Longman for the ICP analysis and all the explanations you provided with the data! Thanks to Alison Cornforth for your support.

Many thanks to Ola and Seb for inspiring me to become an academic, but even more for making sure the fire keeps burning. Thanks to Vanessa, Tobias and Cinthya, I really enjoyed our discussions and I am grateful for your inspiring ideas over the last year.

Thank you Pip for helping me settle in when I first arrived in Newcastle and for all the fun we had learning English! Thank you to my dear friends Linh, Hannah, Johanna, Becky, Beckie, Cristina, Nick and Lucie. You made my time in Newcastle and I am grateful for all the memories! Beckie - thank you for reading every word I write.

Vielen Dank an meine Eltern, Marius, Melli und Joschka, ihr habt mich dahin gebracht, wo ich heute stehe.

Declaration

I declare that the work contained in this thesis has not been submitted for any other award and that it is all my own work. I also confirm that this work fully acknowledges opinions, ideas and contributions from the work of others.

Any ethical clearance for the research presented in this thesis has been approved. Approval has been sought and granted by the *Faculty Ethics Committee* on *11/01/2018*.

I declare that the Word Count of this thesis is 35,780 words.

Name: Annabel Wolf

Signature:

Date: 31 May 2022

Chapter 1

Introduction

1.1 Motivation

The Intergovernmental Panel on Climate Change (IPCC, 2014) identified Southeast Asia (Figure 1.1) as one of the world's most vulnerable regions to climate change. Severe flooding and droughts are threatening the livelihood and welfare of millions. Apart from the immediate catastrophic impact, changes in the hydrological cycle and the frequency of extreme rainfall events have a significant long-term impact on Southeast Asian societies. In particular, around 30% of the world's rice is grown in Southeast Asia, with rice comprising half of the daily calorie intake of an average Southeast Asian person (Yasmi, 2021). The strong dependence on rice as a major nutrient makes Southeast Asia extremely vulnerable to water supply shortages and flooding related to tropical cyclones. For example, the Lower Mekong Basin, located in southern Vietnam (Figure 1.1), has experienced increased surface temperatures; an increase in the wet to dry season rainfall ratio; and more intense floods and droughts (Hijioka et al., 2014). Anthropogenically induced changes in the local hydrology will significantly impact the food supply in Southeast Asia, a region where 9% of the population are already undernourished (Yasmi, 2021).

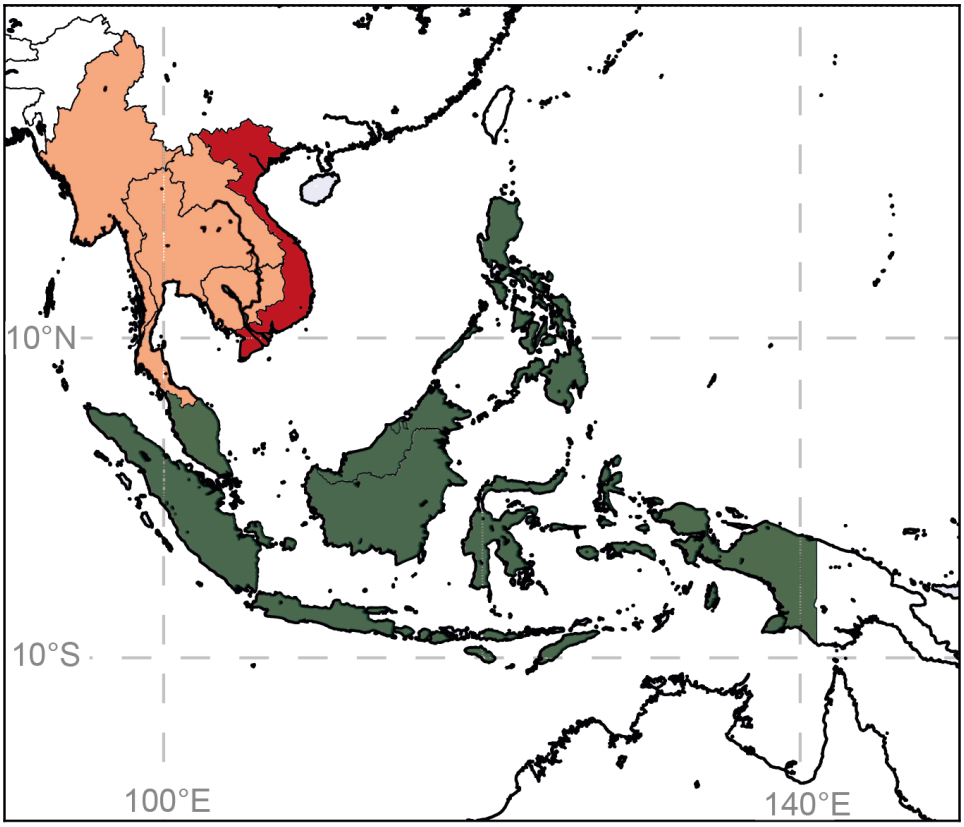

Figure 1.1: Southeast Asia (shading), with Vietnam shaded in red, mainland Southeast Asia shaded in orange, and the Maritime Continent in green.

In autumn 2020, Southeast Asia was strongly impacted by flooding related to tropical cyclones (LeComte, 2021). The region was hit repeatedly by several major typhoons in October and November, with Vietnam and the Philippines being particularly affected; around 2.4 million people were left in need of assistance and 967,000 households were destroyed or damaged (United Nations Report, 2020). 95% of all models used in the 2014 IPCC report projected an increase in heavy precipitation over East, South, and Southeast Asia for the mid- to late- 21^{st} century, a trend already observed in mainland Southeast Asia between 1955 to 2005 (Hijioka et al., 2014). Increasing heavy rainfall events and associated flooding are particularly critical in central Vietnam, where more than 75% of the annual total precipitation derives from such heavy rainfall events (Vu et al., 2015). Tropical cyclones making landfall in central Vietnam have increased in frequency since 2000, and the peak rainy season has shifted from October to November (Wang et al., 2014). Decreasing summer rainfall in combination with delayed autumn rainfall serves to prolong the dry season, applying additional stress to agriculture and water management (Phuong et al., 2018). Further complications derive from the projected sea level rise, which is predicted to lead to a loss

of 7% of Vietnam's land surface (Hijioka et al., 2014).

Despite the projected risks related to climate change in future Southeast Asia, the insufficient number of meteorological stations across the region lowers the confidence in climate model predictions (Cheong et al., 2018). Limited spatial and temporal coverage, with stations recording data for more than a decade, makes it difficult to evaluate whether the regional climate variability is captured in these simulations. This is a crucial limitation, since the effects of climate change on society in Southeast Asia have been documented over the last millennium, and are linked to the demise of advanced societies such as at Angkor Wat (Buckley et al., 2010). However, despite the growing evidence that changes in the hydrological cycle will be a critical factor for the survival of societies in Southeast Asia in the future, only limited data of past long-term climate variability is available.

This lack of long-term climate data within Asia can be resolved with palaeoclimatic reconstructions. Unfortunately, mainland Southeast Asia has received much less attention in palaeoclimate research compared to East Asia and India. A further issue arises from the diversity of rainfall patterns across Southeast Asia. Most of mainland Southeast Asia (Figure 1.1) receives peak rainfall during boreal summer, whereas the Maritime Continent (Figure 1.1) receives rainfall all year-round. Central Vietnam is an exception to this pattern, receiving the majority of rainfall from September to December unlike most northern parts of Southeast Asia. Therefore, because we can not infer how rainfall in Southeast Asia varies by extrapolating from the summer changes in the wider Asian and Indian region, the detailed behaviour of seasonal rainfalls in Southeast Asia over longer timescales and under different boundary conditions are largely unknown.

In Southeast Asia, the understanding of climate drivers and the accuracy of local climate predictions is hindered by two factors:

- The natural modern seasonal, and interannual rainfall variability is spatially heterogeneous.
- The moisture is sourced from different regions depending on the season.

These two gaps in knowledge were a direct motivation for my thesis. The work presented here focuses on modern and Holocene hydroclimate changes in central Vietnam, and addresses:

- Seasonal and interannual spatial variability of rainfall events in central Vietnam.

- Establishing a high-resolution record of hydroclimate variability in central Vietnam over the last 10,000 years.

These results have implications for resilience and flood/drought risk prevention. They might be applied not only in future climate models, but also directly for outlooks when preparing ahead for severe weather events.

1.2 Aims and thesis structure

This work aims to produce a high-resolution proxy record of winter monsoonal rainfall by using a variety of proxies, including stable isotopes and trace elements in speleothems. Central Vietnam is targeted as a study location due to its unique peak rainy season, which is dominated by the winter monsoon circulation. The aim of this work is to understand the past changes in the winter monsoon over the Holocene and use these results to understand the co-evolution of the winter and summer monsoon in Southeast Asia. To achieve this, several speleothem-based proxies are investigated to ensure a robust interpretation of the proxy data.

The following questions and problems motivate this research:

- How did the winter monsoon evolve compared to the summer monsoon over the Holocene?
- How did the monsoons in Southeast Asia evolve over the Common Era?
- What drives the long- and short-term climate of seasonal rainfall in Southeast Asia?

In order to address these questions, the following is needed:

- An overview of the theoretical background and the definitions used in this work (Chapter 1).
- A profound understanding of modern controls on climate proxies, such as δ^{18}O in meteoric water (Chapter 2).
- Processes altering the climatic signal from the surface to the climate archive (Chapter 3).
- A summary of the main methodology (Chapter 4).
- High-resolution palaeoclimate data from central Vietnam (Chapter 5).
- Comparison of the palaeoclimatic history of central Vietnam and other regions within Asia

over the Holocene (Chapter 6) and the last 2000 years (Chapter 7).

1.3 Approach

This work uses a combination of monitoring data from rain and cave waters and a suite of stable isotopes and trace elements in a stalagmite from central Vietnam to address the above listed research questions. Rain waters were collected in Tan Hoa village and Dong Hoi (GNIP dataset). Cave waters were collected from Soong Cave near Tan Hoa village. The stalagmite was collected from Thien Duong Cave (details about study site descriptions and maps can be found in Chapter 3). For this work additional published speleothem records from Laos, Thailand, Sumatra, Borneo, China, and Indonesia were used to reconstruct the summer monsoon variability in comparison to the winter monsoon variability in Southeast Asia, which was reconstructed based on the stalagmite from Thien Duong Cave.

1.4 Contributions

Contributions to this work by others are listed as follows:

Laboratory work (see Chapter 4 for details):

- Laser ablation for trace elements was conducted by Amanda French at Waikato University, New Zealand.
- U-Th dating was conducted by David McGee at MIT, USA.
- A part of the stable isotope measurements were conducted by Madalina Jaggi and Stefan Bernasconi at ETH Zürich, Switzerland.
- The collection of water samples in Phong Nha was undertaken by Deborah Limbert.

Statistical analysis (Chapter 6):

- The MC-PCA was developed and conducted by Tobias Braun at Potsdam Institute of Climate, Germany.

1.5 Climatology of Asia and the West Pacific

The following sections describe the modern climate in Asia, with a particular focus on Southeast Asia and central Vietnam. Fundamental climate forcing mechanisms for this region are defined and summarised.

1.5.1 The Intertropical Convergence Zone and Hadley Cell

The Intertropical Convergence Zone (ITCZ) is a planetary-wide band of heavy precipitation, resulting from a strong uplift where the surface northeast and southeast trade winds converge (Byrne et al., 2018). When the rising air reaches the troposphere, it diverges into a poleward motion and air descends at around 30° latitude on each Hemisphere (Robinson and Henderson-Sellers, 2014) (Figure 1.2). Equatorwards-flowing surface winds close this circulation cell, forming the Hadley Cell. The rising motion in the ITCZ is associated with the warm temperatures in the equatorial regions, and over the ocean the ITCZ tends to be collocated with the warmest SST.

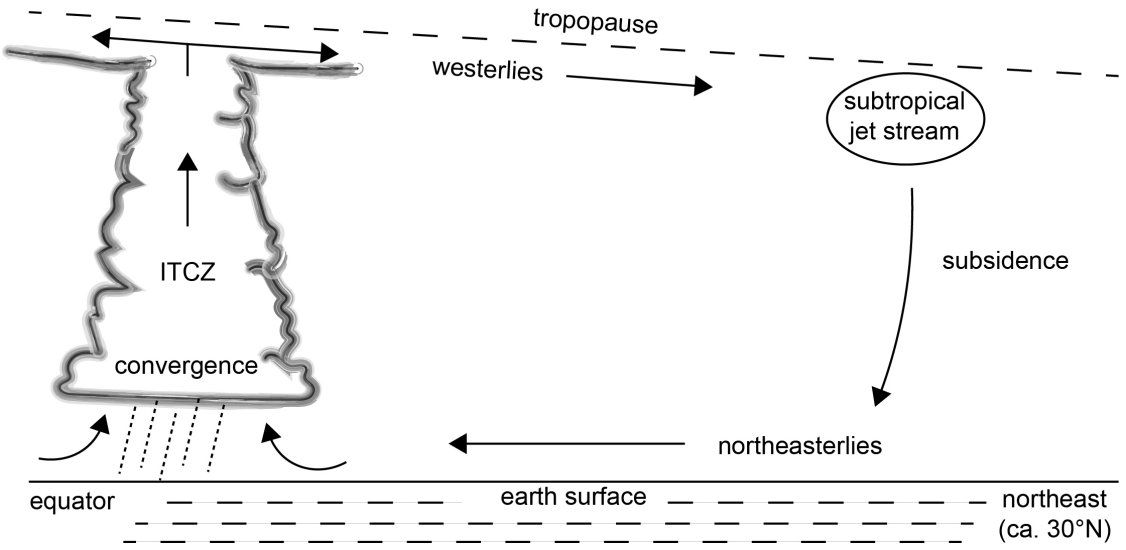

Figure 1.2: General circulation of the Hadley Cell and the associated ITCZ, modified after Robinson and Henderson-Sellers (2014).

One of the most prominent features of the ITCZ is the meridional displacement following the cycle of solar insolation. The annual mean position of the ITCZ lies about 5° north of the equator and varies from 10° degrees in Northern Hemisphere summer to 0° degrees in Northern Hemisphere winter (Byrne et al., 2018; Wodzicki and Rapp, 2016). This relatively small shift in the zonal

mean ITCZ over the course of the year hides the fact that over the ocean the ITCZ moves only a few degrees, whereas over land much larger movements are seen. For example, over the Asian continent it can extend up to 20°N during boreal summer and 8°S during winter (Schneider et al., 2014; Waliser and Gautier, 1993). This difference reflects the different dynamics driving the ITCZ over land and ocean. Over ocean, the convection in the ITCZ follows the warmest SST; over land the ITCZ is linked to the monsoon circulations. The seasonal migration drives the rainy season in Southeast Asia and peninsular India, resulting in an extended rainy season over mainland Southeast Asia between May and September (Misra and Dinapoli, 2014). By contrast, the summer monsoon season in East Asia takes place from June to August, which is controlled by the propagation of the Meiyu front (also called the Baiu front in Japan), rather than the ITCZ (Tung et al., 2020).

Observational and reanalysis studies since 1980 suggests that the ITCZ band has narrowed and precipitation has enhanced since then (Byrne et al., 2018). A narrowing of the ITCZ would leave regions at the northern or southernmost extent drier, which would reduce rainfall in the subtropics of both hemispheres (Gu et al., 2016). For Southeast Asia, this could mean a reduction of rainfalls in Thailand, Laos, and Vietnam, with severe impacts on the local agriculture.

1.5.2 The Indo-Pacific Warm Pool

The warm waters of the Indian and the Pacific Ocean meet around Southeast Asia, forming the largest warm water body in the world, the Indo-Pacific Warm Pool (Weller et al., 2016). Temperatures are around 28°C for most of the year, affecting the ITCZ position and the strength of general circulation in the region (De Deckker, 2016). The warm pool plays a significant role in the distribution of moisture and heat across Asia. Changes in the sea surface temperatures (SSTs) can impact the Asian climatic system via increased or decreased surface evaporation and associated water vapour content in the atmosphere (Yan et al., 1992). The presence of the Warm Pool is associated with the Walker Circulation, the east-west Pacific atmospheric circulation. As with the Hadley Circulation, there is ascent in the atmosphere over the warm waters of the Warm Pool and descent over the colder East Pacific cold tongue. This east to west circulation is part of the Pacific trade winds.

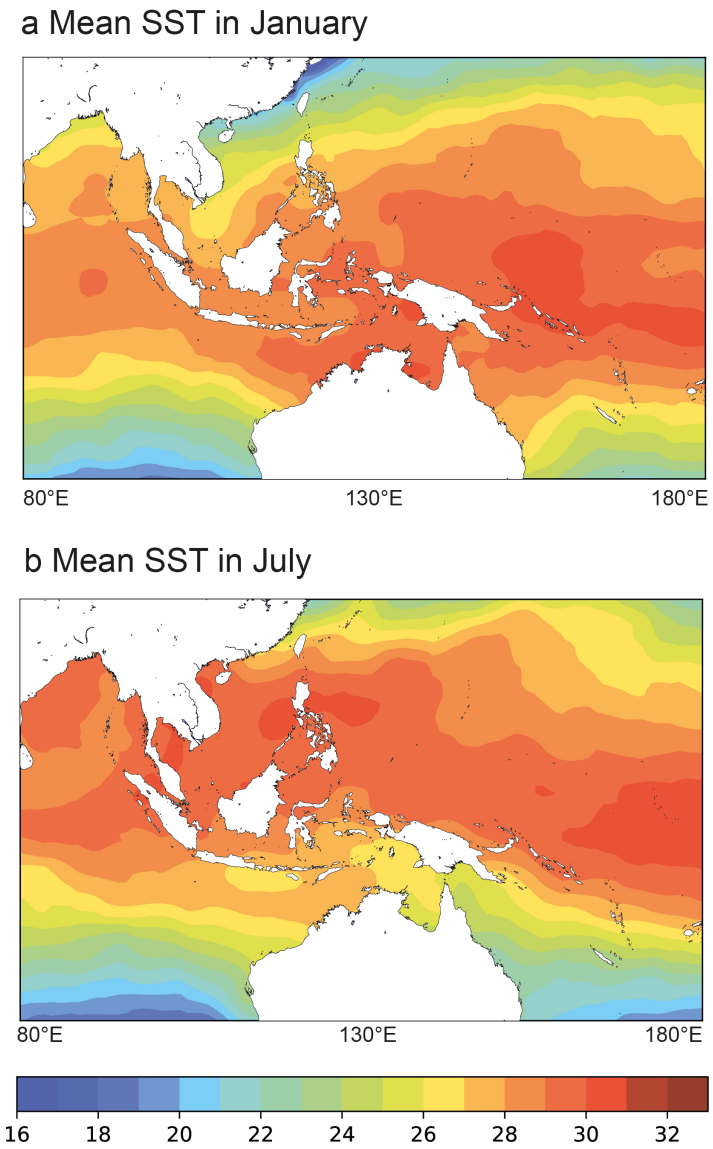

Figure 1.3: Long-term mean SSTs (1961 - 1990) in the Indo-Pacific warm pool for **a** January and **b** July. SST are the monthly means calculated from weekly values of the NOAA Optimum Interpolation (OI) SST V2 data set. Most of the region sees warm water temperatures above 28°C.

Observations since the 1950s indicate an expansion of the Indo-Pacific Warm Pool due to anthropogenic warming (Weller et al., 2016). This expansion is caused by extremely rapid warming of the Indian Ocean, which is two to three times faster than warming in the central Pacific (Williams and Funk, 2011). The unequal warming has not only extended the warm pool westwards but has also led to a westward shift of the ascending branch of the Walker Circulation, affecting rainfall patterns in Asia and Africa. Studies of past changes in the Warm Pool heat content showed that substantially higher water temperatures have feedback effects on the El-Niño Southern Oscillation, reducing event activity (Dang et al., 2020).

1.5.3 The Walker Circulation

The Walker Circulation describes the atmospheric circulation over the tropical oceans (Lau and Yang, 2015). The most prominent branch of the Walker Circulation is the Pacific Walker Circulation (Bjerknes, 1969; Julian and Chervin, 1978; Walker, 1933) (Figure 1.4). The upward branch of the Pacific Walker Circulation is centred over the Maritime Continent, causing strong convection (and rainfall) over this region (Kousky et al., 1984). The upwards motion of air over the Maritime Continent is caused by the Western Pacific Warm Pool, which creates a temperature gradient between warm waters in the Western Pacific and the cooler SST in the eastern Pacific. Surface trade winds flow towards the Maritime Continent from the eastern descending branch over the eastern Pacific and from the western descending branch over the western Indian Ocean.

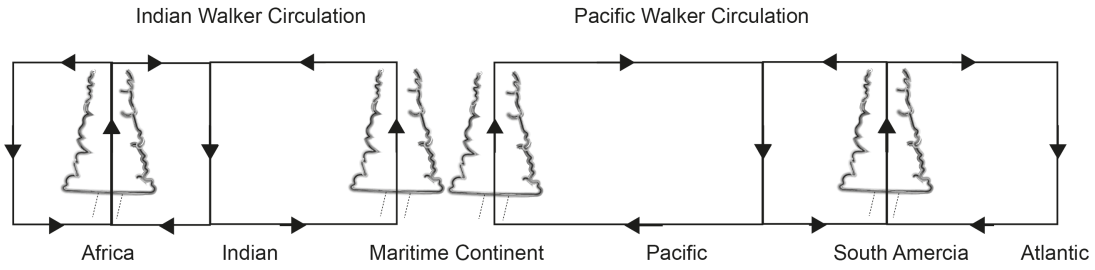

Figure 1.4: Atmospheric circulation within the Walker Circulation. Over the Pacific, the Walker Circulation has an east-west surface flow, after (Lau and Yang, 2015).

1.5.4 ENSO and the IOD

The El-Niño Southern Oscillation (ENSO) is the major source of interannual climate variability in the tropics. ENSO is a coupled ocean-atmosphere interaction in the tropical Pacific and occurs roughly every 2 to 7 years (Bjerknes, 1969). There are two extreme phases of ENSO, called El Niño and La Niña events, which are known for their strong impact on (tropical) climate world-wide (Figure 1.5). El Niño events are associated with anomalously warm SSTs in the eastern Pacific, related to decreased upwelling along the western coast of Central and South America. Low-level easterlies weaken during El Niño events or can be reversed. On the contrary, La Niña events describe cold SSTs along the east coast of South America due to enhanced upwelling in the eastern Pacific, pushing warm waters into the western Pacific. During La Niña events the easterlies are enhanced, driving a stronger Pacific Walker Circulation. The atmospheric circulation responds to ENSO events with a shift in the position and strength of the Pacific Walker Circulation. The position

of the ascending and descending branch of the Pacific Walker Circulation modulates rainfall in regions bordering the western and eastern tropical Pacific (Figure 1.5). El Niño events can lead to strongly decreased rainfall over Southeast Asia, as the Pacific Walker Circulation weakens and the ascending branch shifts away from the region. During La Niña events, surface winds over the Pacific are enhanced, shifting the ascending branch towards Southeast Asia.

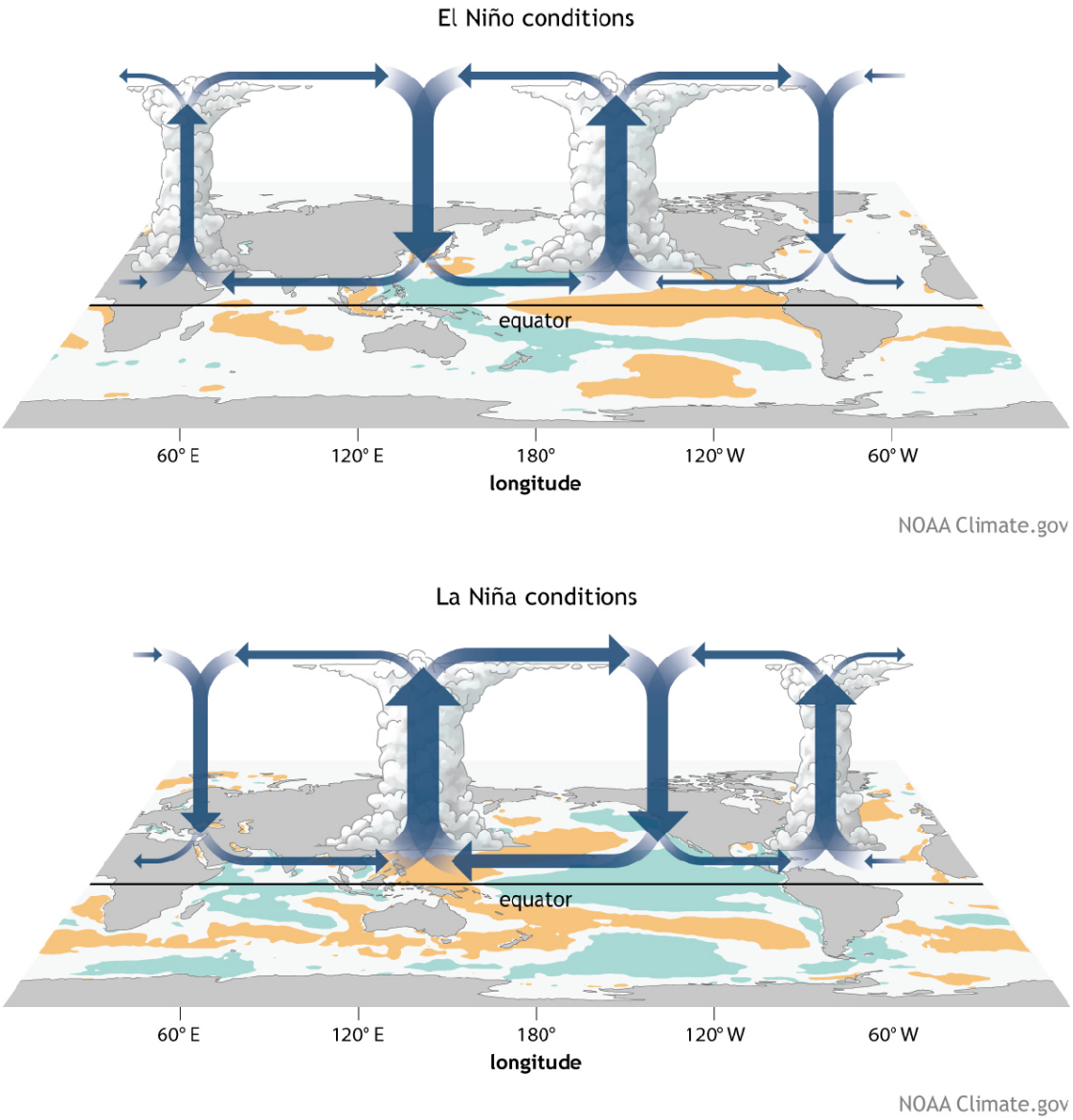

Figure 1.5: SST anomalies (shading) and the position of the Walker Circulation. Figure provided by the NOAA/OAR/ESRL PSD, Boulder, Colorado, USA,from their website https://www.esrl.noaa.gov/psd/.

A similar oscillation of SSTs is observed in the Indian Ocean and is called the Indian Ocean Dipole (IOD). Similar to ENSO, the IOD has two extreme phases, associated with anomalous SST

gradients across the Indian Ocean and shifts in the strength of the Indian Ocean Walker Circulation. A positive IOD event relates to decreased SSTs in the eastern Indian Ocean, whereas a negative IOD is associated with warmer than usual SSTs in the eastern Pacific. Due to the similar functionality and the close geographic proximity, the interaction between both oscillating systems (ENSO and the IOD) is highly important.

Warm or cold ENSO events (El Niño or La Niña) in the Pacific Ocean often co-occur with positive and negative IOD states in the Indian Ocean respectively (Izumo et al., 2010). A co-occurrence usually amplifies the effects on the ocean-atmosphere coupled climate system and can lead to an even stronger reduction or enhancement of rainfall in Southeast Asia (As-syakur et al., 2014). The opposite is true when ENSO and IOD events occur with opposing signs. The future development of ENSO and the IOD is highly uncertain, with some studies suggesting a weakening of the Walker Circulation and some a strengthening. Both oscillating systems are projected to remain the leading climate drivers in Southeast Asia (Hijioka et al., 2014), leaving future climate scenarios in this region largely unknown.

1.5.5 The Asian monsoon

The Asian monsoon is the dominant feature of seasonal climate in tropical and subtropical Asia. Therefore, past and future monsoon variability has received enormous attention in palaeoclimate and modern meteorology studies (Wang et al., 2017a). During boreal winter, cold, dry winds cross from high latitudes over vast regions of Asia. In the broadest scale, this system is reversed during summer when warm, moist air brings intense rainfall across Asia (Wang and Chang, 2012). In mainland Asia, this summer reversal of the winds and its intense rainfall is termed the Indian Summer Monsoon (also called 'South Asian Summer Monsoon') and the East Asian Summer Monsoon (Figure 1.6a). Although both regions experience strong summer rainfall, the dynamics which control them are quite separate: variability in the Indian Monsoon is not necessarily directly linked to changes in the East Asian Monsoon and vice versa. While the Indian Summer Monsoon is considered a tropical monsoon system which is strongly influenced by the ITCZ, the East Asian Summer Monsoon extends into the extratropics and precipitation derives from an east-west oriented band, known as the Meiyu or Baiu front (Geen et al., 2020; Yihui and Chan, 2005).

At the interface between these two monsoon domains lies a smaller area centred over mainland

Southeast Asia which was initially regarded as a transition or buffer zone between the two large monsoon systems (Li et al., 2014; Wang and Lin, 2002). This is likely one of the reasons why this region received substantially less attention in research, compared to either the Indian or East Asian monsoon realms. The summer monsoon in India and Southeast Asia is also named the Southwest Monsoon as winds prevail from a south-westerly direction (Sengupta and Nigam, 2019). This classification also applies to the winter monsoon in this region, which is referred to as the Northeast Monsoon.

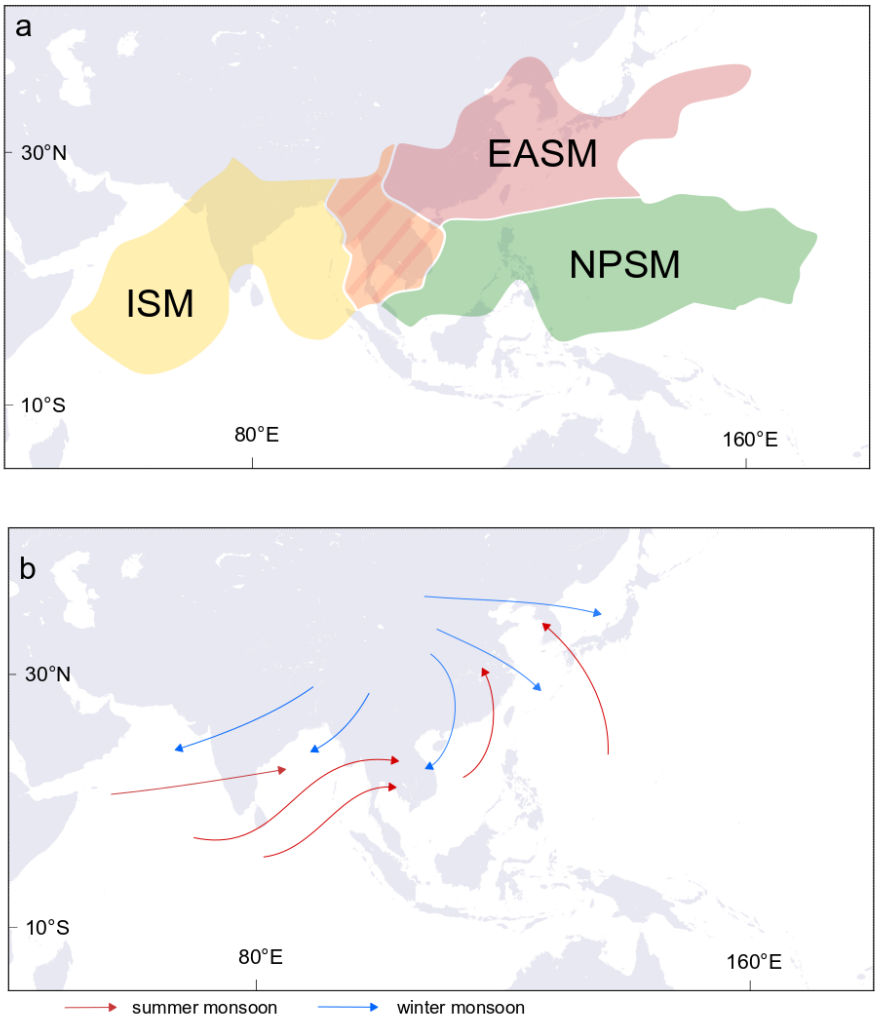

Figure 1.6: **a** Map showing the rough outline of the Asian monsoon subsystems: the Indian Summer Monsoon (ISM, yellow), the East Asian Summer Monsoon (EASM, red), the transition zone between the Indian and East Asian Monsoon (orange), and the western North Pacific Summer Monsoon (NPSM, green). Figure modified after Wang and Lin (2002). **b** Sketch of the wind directions during winter (blue) and summer (red) monsoonal circulation.

While the geographic extension of the summer monsoon is well-defined, the winter monsoon is lacking such classification. Usually, the Asian Winter Monsoon is associated with cold dry north-westerlies in East Asia and north-easterlies in Southeast Asia and India (Matsumoto, 1992; Sengupta and Nigam, 2019) (Figure 1.6b). These winds are introduced by the Siberian High, a high-pressure area over the Siberian-Mongolia region, and a low-pressure area over the Maritime Continent in winter (Chan and Li, 2004; Chang et al., 2011). For this work, the term 'East Asian Winter Monsoon' will refer to north-westerlies across East Asia. The term 'Northeast Monsoon' will refer to the winter monsoon in Southeast Asia and India, which is the winter counterpart to the Indian (or Southwest) Summer Monsoon. 'Winter Monsoon' will refer to both parts.

1.6 The climate of Southeast Asia

Southeast Asia has the longest wet season in Asia, extending from April to December (Misra and Dinapoli, 2014; Wang and Chang, 2012). The region is characterised by temporally and spatially diverse seasonal rainfall driven by complex interactions between the monsoonal circulation, the ITCZ, ENSO, the IOD, and local topography (Vu et al., 2015; Wang and Chang, 2012; Wu et al., 2018). The seasonal cycle of prevailing winds and precipitation can be described as follows: from December to April, the ITCZ lies over the Maritime Continent leading to peak rainfall over this region (Misra and Dinapoli, 2014). In mid-May, the ITCZ follows the preferential heating of the Asian landmass and moves northwards. Until August the ITCZ remains in the northern parts of mainland Southeast Asia (Zhang et al., 2004). This means a minimum of rainfall over the Maritime Continent, whereas peak rainfall occurs over northern Thailand, Myanmar, Laos, and Vietnam. Winds prevail from a south-westerly direction, while enhanced evaporation occurs over the Bay of Bengal, driving the summer monsoon in Southeast Asia from mid-May to mid-September (Lau and Yang, 1997; Zhang et al., 2004). In September, the ITCZ starts its southward migration back to the equator, reducing rainfall over northern mainland Southeast Asia. The withdrawal of the ITCZ is relatively slow, crossing mainland Southeast Asia between September to the end of November (Hu et al., 2019; Wang and Chang, 2008). During this time the Northeast Monsoon brings heavy rainfalls into central and southern parts of mainland Southeast (Sengupta and Nigam, 2019), e.g. a peak in rainfall in September to October in Bangkok, or a peak rainfall in central Vietnam from September to November and from November to December in southern Vietnam (Chapter 2). This

spatial pattern of seasonal rainfall gives the impression that several locations across mainland Southeast Asia are suitable for reconstructing rainfall related to the Northeast Monsoon. However, only central Vietnam is not receiving rainfall generated by the Southwest Monsoon, and therefore the area is suitable for a reconstruction of rainfall related to the Northeast Monsoon.

1.6.1 The climate of Vietnam

Vietnam extends as a narrow strip of land extending along the east coast of mainland Southeast Asia, located roughly between 23°N and 9°N (Figure 1.1a). The mostly mountainous country is dominated by different monsoonal regimes, mirroring the temporal variability of the monsoonal season across Southeast Asia. The north of Vietnam shows a clear summer monsoon influence with peak rainy season from June to September (Figure 1.7a), whereas southern Vietnam is influenced by a combination of boreal winter and spring/summer rainfall, showing a bi-modal distribution of rainfall from September to November and May to June (Figure 1.7c) (Chen et al., 2012a; Gobin et al., 2016; Nguyen-Thi et al., 2012; Vu et al., 2015). In general, the peak rainy months follow the seasonal movement of the ITCZ (Nguyen-Thi et al., 2012). Unique within mainland Southeast Asia is central Vietnam, which receives maximum precipitation from October to December (Figure 1.7b). At the end of boreal summer, the south-westerly monsoonal circulation declines and north-easterly winds establish over the South China Sea (Yokoi and Matsumoto, 2008). These winds carry moisture into central Vietnam pushing the moist air masses against the Truong Song mountain range and resulting in heavy orographic precipitation (Wu and Hsu, 2016; Yen et al., 2011; Yokoi and Matsumoto, 2008). Precipitation between September to November is related to SST anomalies in the South China Sea and western Pacific, which force the occurrence of tropical cyclones (Yen et al., 2011) and cold surges under the influence of the Siberian High (Chen et al., 2012a; Yen et al., 2011; Yokoi and Matsumoto, 2008) related to the Northeast Winter Monsoon. Separated from the rest of mainland Southeast Asia by a narrow mountain range, central Vietnam is sheltered from rainfalls related to the Southwest Monsoon during boreal summer. This precipitation pattern makes central Vietnam ideal for reconstructing winter rainfall related to the Northeast Monsoon.

While the rainfall pattern across Vietnam is heterogeneous, the $\delta^{18}O$ composition of rainfall shows a temporally homogeneous seasonal cycle with low values from June to September and increased values from December to April. The observed difference in isotopic composition and rainfall

amount across Vietnam is a good example for the region signal of $\delta^{18}O$ in rainfall (Figure 1.7). The discrepancy between $\delta^{18}O$ and local rainfall pattern bears potential complications for the use of $\delta^{18}O$ as a monsoonal proxy in Vietnam. Therefore, the following chapter will investigate the controlling mechanisms of $\delta^{18}O$ variability in central Vietnam rainfall.

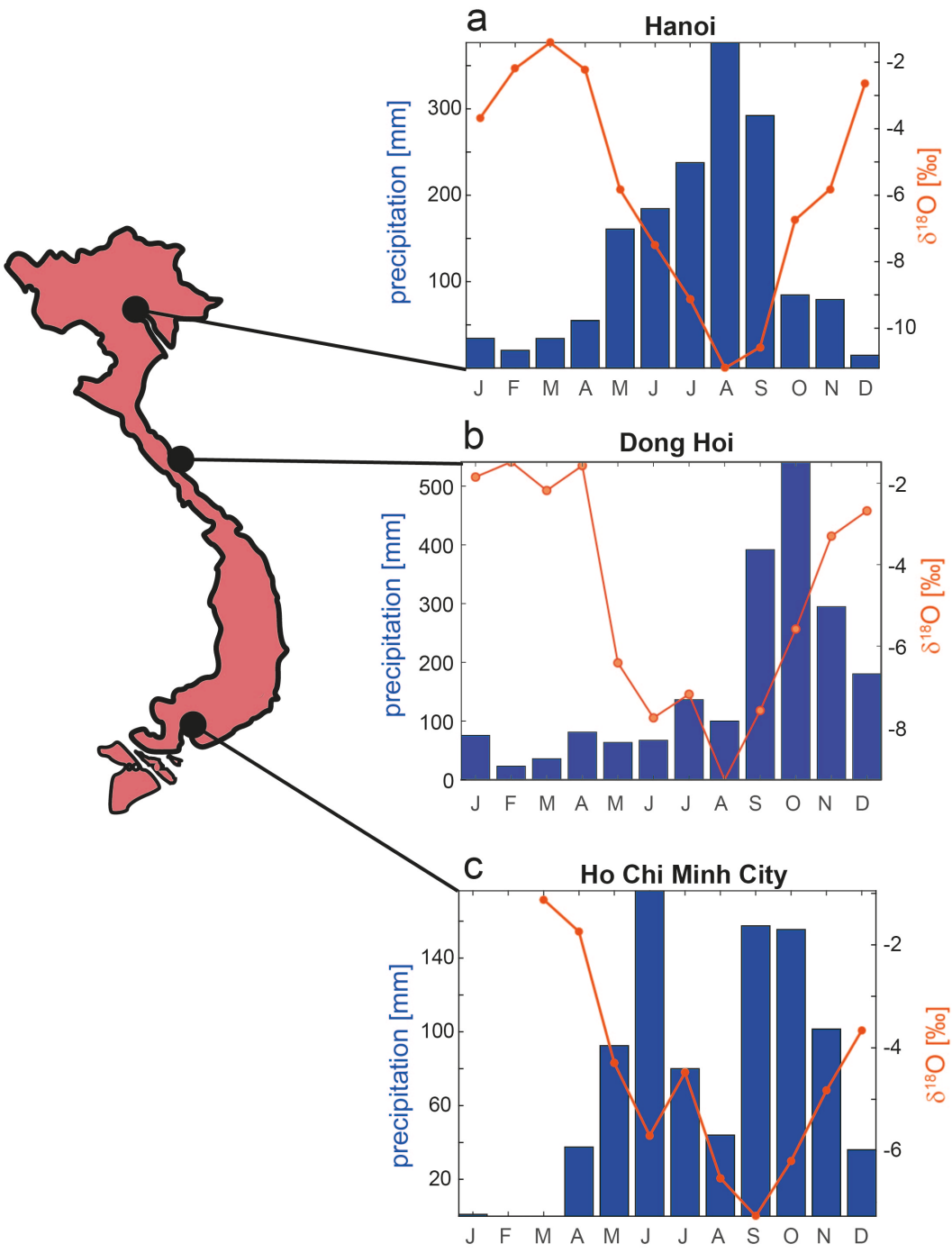

Figure 1.7: Monthly mean rainfall distribution in mm per months and monthly mean δ^{18}O in rainfall at **a** Hanoi in southern Vietnam, **b** Dong Hoi representing central Vietnam, and **c** Ho Chi Minh City, located in southern Vietnam. Data for Hanoi and Dong Hoi are provided by the GNIP database and the data for Ho Chi Minh City is from Le Duy et al. (2018) and Munksgaard et al. (2019).

1.7 Palaeoclimate archives and the climate of the past

Researching modern climatological processes has greatly advanced our understanding of climate variability and helped to simulate near-future climate change. However, the long-term processes driving climate variability can only be understood using palaeoclimate archives. Some palaeoclimate archives extend back several million years, each with certain advantages and limitations. For example, ice cores from Antarctica (Augustin et al., 2004; Petit et al., 1999) and Greenland (Johnsen et al., 2001) have a precise age control and directly record the chemical composition of surface air, but they are limited to cold regions. Other archives like marine and lake cores are distributed globally, but the age control and temporal resolution is often limited, and erosion or diagenesis can affect the proxy record. On the contrary, speleothems offer a precise age control, using uranium-thorium dating up to 640,000 years ago (Cheng et al., 2016), or uranium-lead up to hundreds of millions of years. Speleothems are calcareous cave deposits and are as such usually protected from disturbances on the surface (Fairchild et al., 2006). The advantage of using speleothems rather than ice cores is their global extent (Figure 1.8) and their potential for accurate and precise dating using U-series methods.

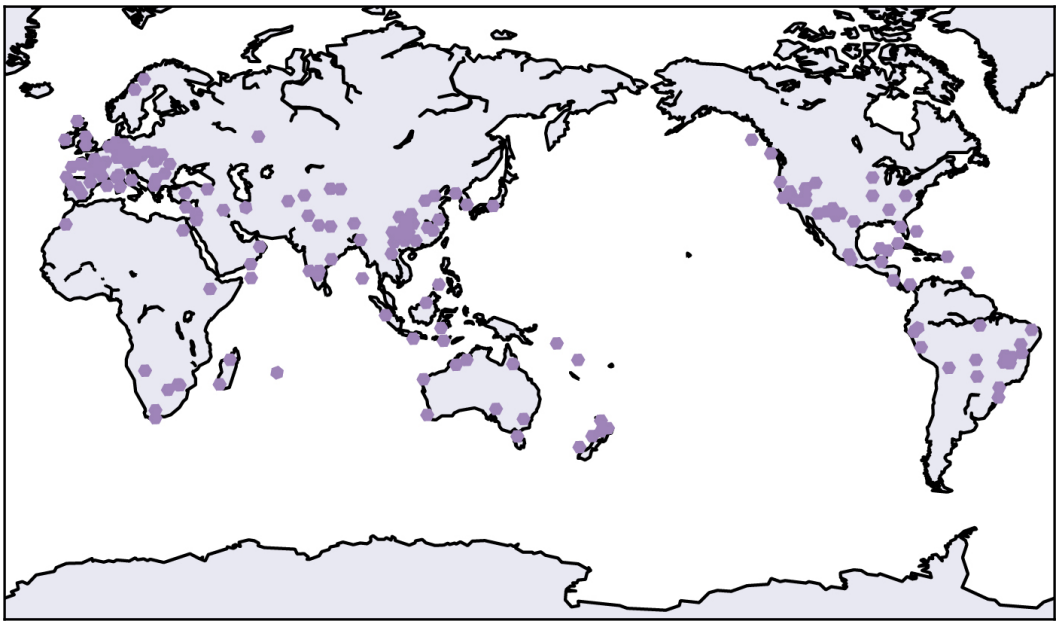

Figure 1.8: Locations yielding speleothem records (purple dots) available in SISAL_v2 database (Comas-Bru et al., 2020).

Understanding the long-term evolution of the mean climate is not the only avenue of paleoclimate

research. There is much work to understand the evolution of the shorter term, year to year, decade to decade variability. Understanding this requires climate records that can resolve at least individual years. For example, coral records have been used to understanding the evolution of interannual variability associated with ENSO in the past. The high resolution, which is usually seasonal to monthly, offers records of SST variability across the oceans going back as far as 350,000 years (Kilbourne et al., 2004) but mainly covering the last 10 000 years (Abram et al., 2007; Cobb et al., 2007, 2003, 2013; Lough, 2010). However, one of the limitations of corals is that they only provide a snapshot of SSTs usually no longer than a few hundred years. Speleothem records, on the other hand, have been shown to be able to capture ENSO variability continuously over several thousand years (Chen et al., 2016a). Air surface temperatures in high-resolution can be reconstructed from tree rings if ice cores are not available. Further tree rings can also be used for soil moisture reconstructions, not only temperature (Buckley et al., 2017). Even though the age control is extremely good with a sub-annual resolution, the extent is limited to a few hundred years. Speleothems offer a longer and continuous reconstruction instead, allowing for a more seamless understanding of climate in a specific area (Fairchild and Baker, 2012).

1.7.1 Asian climate during the Holocene

Past and future monsoon variability has received enormous attention in speleothem-based palaeoclimate studies (Cheng et al., 2012, 2016a; Chiang et al., 2015; Dykoski et al., 2005; Griffiths et al., 2020; Kutzbach et al., 2008; Liu, Song, Yuan, Sun and Yang, 2014; Maher, 2008; Pausata et al., 2011; Tierney et al., 2016; Wang, 2001; Zhang et al., 2019b). In particular, the Holocene monsoon evolution is regarded as an analogue for today's climate, because greenhouse gases were relatively stable over the last 10,000 years (10,000 Before Present (1950CE)) and ice sheet forcing was nearly absent after 8,000 BP (Törnqvist and Hijma, 2012), leaving the global sea level close to that of the present day.

Most speleothem-based monsoon reconstructions from the East Asian and Indian Summer Monsoon regions indicate enhanced summer monsoon precipitation between 11 and 8,000 BP and a declining trend towards modern times (Berkelhammer et al., 2012; Cai et al., 2012; Dykoski et al., 2005; Kathayat et al., 2016; Kaushal et al., 2018; Liu, Wen, Brady, Otto-Bliesner, Yu, Lu, Cheng, Wang, Zheng, Ding et al., 2014; Wang et al., 2005; Wang, 2001; Yang et al., 2019; Zhang et al.,

2019b). This trend follows Northern Hemisphere summer insolation, and the similarities between the speleothem $\delta^{18}O$ records hint towards insolation forcing being dominant in both monsoon realms (Zhang et al., 2019b). However, other proxy records based on pollen, lake level, and loess data suggest that Asian summer monsoon precipitation is temporally diverse, with a peak in precipitation in the early-Holocene over western China, a peak in north-central and north-eastern China during the mid-Holocene, and a late-Holocene peak in southeastern China (An et al., 2000; Herzschuh et al., 2019). The position of the westerly jet plays an important role in modulating the spatial variability of monsoon precipitation across the East Asian and the Indian Monsoon region (Chiang et al., 2015; Herzschuh et al., 2019; Wang, Liu and Herzschuh, 2010; Zhang et al., 2018). In Southeast Asia, speleothem-based palaeomonsoon reconstructions which used local proxies, such as $\delta^{13}C$ and trace elements (Chen et al., 2016a; Griffiths et al., 2009, 2020; Partin et al., 2013; Wurtzel et al., 2018), and lake records (Chawchai et al., 2015; Maxwell, 2001), also indicate more regional monsoon variability. This is influenced by the position of the ITCZ and the ascending branch of the Pacific Walker Circulation (Chawchai et al., 2015; Griffiths et al., 2020). However, the associated $\delta^{18}O$ records roughly follow insolation (Chen et al., 2016a; Griffiths et al., 2009, 2020; Partin et al., 2013; Wurtzel et al., 2018). Consequently, more local climate archives indicate a more diverse pattern of the Asian summer monsoon over the Holocene, challenging the use of speleothem $\delta^{18}O$ as a rainfall proxy of monsoon intensity (Clemens et al., 2018). Similar concerns have been raised by modern observational data, showing that the $\delta^{18}O$ signal in rainfall can be controlled by moisture source dynamics and fractionation along the transport path (Aggarwal et al., 2004; Araguás-Araguás et al., 1998; Cai and Tian, 2016; Le Duy et al., 2018; Wei et al., 2019; Yang et al., 2016). These findings limit the use of speleothem $\delta^{18}O$ as a proxy for monsoon intensity, indicating potential gaps in our understanding of the Asian monsoon.

In comparison to our understanding of the summer monsoon evolution over the Holocene, the evolution of the winter monsoon is more limited. For those records available there is no consensus among the few studies even of the same region (An et al., 2017; Hao et al., 2017; Liu et al., 2009b; Sone et al., 2013; Steinke et al., 2011; Wang, Wu, Chang, Liu, Li and Zhou, 2010; Wang et al., 2021; Wen et al., 2016; Yancheva et al., 2007; Zhao et al., 2021). Reconstructions based on marine sediment cores in the South China Sea (Huang et al., 2011; Steinke et al., 2011; Tian et al., 2010) found that the winter monsoon correlates possibly with the summer monsoon. However,

later studies from the same region found a dynamic link between cool and warm periods leading to a varying correlation of the two monsoons (Zhang et al., 2019a). Similar contrasts arise from terrestrial records in southern China, with some suggesting a positive (Wang et al., 2014) or negative (Yancheva et al., 2007) correlation of both monsoon systems over the Holocene.

Neither the millennial nor the centennial scale variability of the winter monsoon and its relation to the summer monsoon are clear in Asia. This is a critical concern for regions, such as Southeast Asia, where the winter monsoon brings extreme rainfall and flooding.

Two clear issues regarding the Asian monsoon arise from the current state of the literature:

- The use of $\delta^{18}O$ as a proxy for summer monsoon intensity might be misleading.
- Proxy data is inconclusive for the winter monsoon evolution over the Holocene.

My work addresses these issues by establishing a high-resolution palaeoclimate record based on speleothems over the Holocene.

1.8 Speleothems as climate archives

The following sections give an overview of the formation of speleothems and speleothem-based proxies, which can be used to decipher climate and environmental conditions at cave sites.

1.8.1 Speleothem formation

Speleothems are mainly secondary calcareous deposits forming in caves located in karstified host rocks. When rainwater enters the soil zone above the cave it takes up carbon dioxide (CO_2), forming a weak carbonic acid via $H_2O + CO_2 \rightarrow H_2CO_3$ (Figure 1.9). Plant and microbial activity determines the amount of CO_2 released into the soil and can thus have an influence on the water acidity (Fairchild and Baker, 2012). The water infiltrates the epikarst, the interface between the soil and the bedrock, and continues to infiltrate through the karst. The karst can be separated into the 'vadose zone', which is aerated, and the 'phreatic zone', which is saturated with water (Williams, 2008). Surface water percolates through the vadose karst and is either stored or led directly into the cave. Geological features of the karst such as bedding and fracturing determine the permeability, which in turn controls the time in which the water percolates through the karst before entering

the cave. Fracture flow (when water infiltrates along joins and bedding planes) allows for a quick flow from surface to cave, whereas intergranular flow usually extends the time for which water percolates (Baldini et al., 2006).

While percolating in the karst, the acidic water dissolves the carbonate host rock, usually limestone or dolomite, and takes up calcium (Ca^{2+}), forming aquatic bicarbonate (HCO_3) (Figure 1.9).

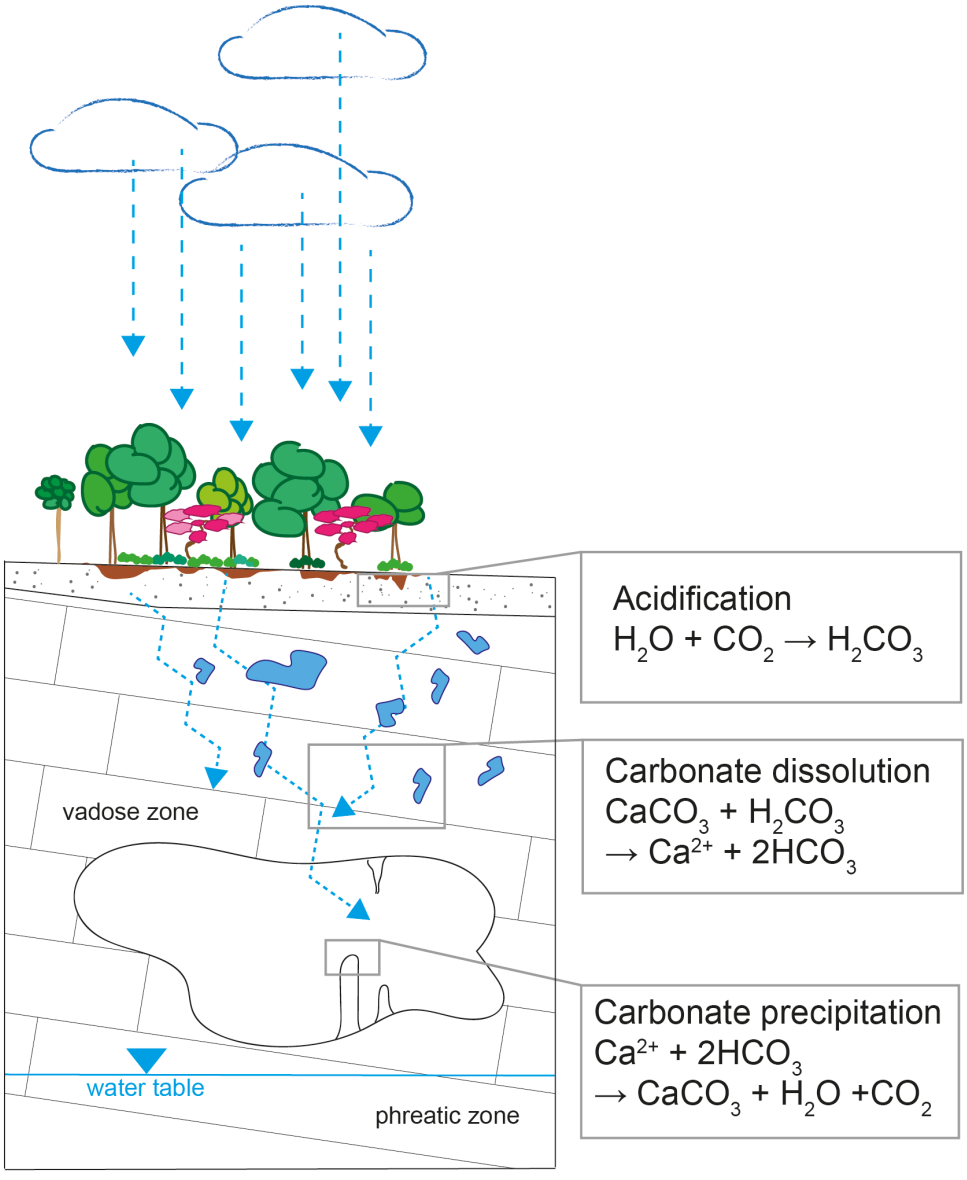

Figure 1.9: Conceptual figure showing the acidification of rain waters in the soil zone, the carbonate dissolution in the vadose zone of the bedrock, and the speleothem formation inside the cave.

The solution now enters a cave, which usually has a lower CO_2 air pressure (pCO_2), contrasting

the CO_2 concentration in the cave water. This contrast causes the degassing of CO_2 into the cave until equilibrium is reached, saturating the solution with respect to calcite or aragonite and forcing the formation of carbonate ($CaCO_3$) (Figure 1.9).

Speleothems can be formed in many shapes and locations within the cave, but the most commonly known formations are stalactites, which form at the cave ceiling, and stalagmites, which grow on the cave floor. Stalactites can be fed by water running down at the outside of the stalactite or through a central channel. Stalagmites are fed by water dripping from the cave ceiling to form layers, which are deposited in stratigraphic order (Fairchild and Baker, 2012). Stalagmites are preferred for palaeoclimate reconstructions, because age inversions are less likely due to their formation.

Most frequently, speleothems are dated using uranium-thorium (U-Th dating) which relies on the radioactive decay of ^{234}U to ^{230}Th. The timespan in which U-Th dating produces reliable results is up to 640,000 years BP (Cheng et al., 2013, 2016). For older speleothems, the longer decay chain can be applied, which describes the decay of ^{238}uranium to ^{206}lead. Uranium-lead (U-Pb) dating extends the age determination for speleothems up to 8 million years and most likely beyond that (Engel et al., 2020; Pickering et al., 2019; Woodhead et al., 2006). The use of these dating methods can be limited by low uranium concentrations or contamination with thorium during deposition. While less established as U-Th dating, radiocarbon dating can bridge the gap, allowing for age determination of 'dirty' speleothems (Hua et al., 2012; Lechleitner et al., 2016).

1.8.2 Speleothem proxies

The most commonly used proxy in speleothem-based climate reconstruction is δ^{18}O (Cheng et al., 2012; Lachniet, 2009; McDermott, 2004), but δ^{13}C has recently garnered increasing attention (Fohlmeister et al., 2020). In monsoonal regions, δ^{18}O was initially invoked as a proxy for rainfall intensity. However, this has been challenged (Chen et al., 2016a; Clemens et al., 2018; Liu et al., 2017; Zhang et al., 2019b). δ^{18}O in rainwater usually reflects the climatic conditions of an area, such as the general circulation (for more information, see Chapter 2). When formed under isotopic equilibrium, speleothems incorporate the δ^{18}O composition of cave waters, which can reflect the δ^{18}O signature of rainfall above the cave (Lachniet, 2009). The correct interpretation of δ^{18}O is complex because several processes control the δ^{18}O signature of rainfall, which is further altered

by processes which occur in the karst zone and during speleothem formation. On the other hand, $\delta^{13}C$ is characterized as a local proxy, reflecting environmental conditions above or within the cave. This proxy can also be an indicator for vegetation changes above the cave or microbial activity within the soil zone (for more information, see Chapter 5). The underlying mechanism in the use of stable isotopes, such as $\delta^{18}O$ and $\delta^{13}C$, is isotopic fractionation. This process determines the relative abundance of heavy and lighter isotopes in a certain medium. For example, during the evaporation of water, such as the ocean surface waters, the lighter water isotope (^{16}O) is preferentially evaporated, leaving the resulting water vapour with a lower $\delta^{18}O$ values compared to the remaining ocean waters. A similar mechanisms occurs during carbonate precipitation, where the lighter ^{12}C is degassed and the heavier ^{13}C incorporated into the crystal lattice. The increase in heavy isotopes is referred to as 'enrichment', while the loss of heavy isotopes is called 'depletion'.

Both proxies, $\delta^{13}C$ and $\delta^{18}O$, can have more than one controlling factor, which has led to the use of the abundance of other chemical elements in the speleothem, so-called 'trace elements' as an additional support for proxy interpretation. These other proxies have been especially helpful for deciphering whether the $\delta^{13}C$ signal is derived from processes within the karst or related to processes in the soil. Using the trace elemental concentration in speleothems as proxies for palaeoclimate variability is based on the assumption that after speleothem formation nearly no element mobility occurs (Fairchild and Treble, 2009). Therefore, changes in the trace elemental concentration in speleothems are likely to reflect changes in water chemistry at the time of crystal formation, driven by various processes. These processes include changes in rainfall amount, soil activity, water mixing processes and residence time of the water in the karst, and crystal growth (Fairchild and Baker, 2012). One exception is the conversion of aragonite to secondary calcite, where elements are reorganized in the crystal lattice leading to calcite recrystallization (Domínguez-Villar et al., 2017). These speleothems are less suitable for palaeoclimate reconstructions.

Frequently used trace elements are those which can replace calcium (Ca) in the crystal lattice via substitution, such as magnesium (Mg), strontium (Sr) and barium (Ba) (Fairchild and Treble, 2009). Other elements used are mostly products of weathering and the infiltration rate above the cave such as iron (Fe), aluminium (Al), U, phosphorous (P) and titanium (Ti) (Hartland et al., 2012). The growth rate of a stalagmite can in itself be a climate proxy. Faster growth rates are associated with

a higher water supply and lower pCO_2 in the cave, favouring carbonate precipitation. Due to the sensitivity of growth rate to the pCO_2, it can sometimes be linked to ventilation rather than water supply. Several elements can be driven by growth rate, such as strontium (Sr) and barium (Ba). An increased growth rate is usually reflected as higher Sr and Ba incorporation (Huang and Fairchild, 2001). If Sr and Ba variability is driven by growth rate, they often show a strong positive in phase correlation (Fairchild and Treble, 2009).

In addition to the abundance of certain trace elements in speleothems, their isotopes have a wide range of applications. For example, the use of $^{87}Sr/^{86}Sr$ helps to understand the amount of water-host rock interaction, thus giving an estimation of host rock weathering rates (Vaks et al., 2013; Wortham et al., 2017). This in turn can be indicative of local moisture conditions (Ward et al., 2019). Further indicators of local moisture are Ca isotopes ($\delta^{44}/^{42}Ca$). The preferential removal of light Ca during extended dry periods leads to increased $\delta^{44}/^{42}Ca$ values in the associated speleothem (Owen et al., 2016; Reynard et al., 2011). The use of uranium isotopes ($\delta^{234}U$) as an environmental indicator, such as for wet versus dry conditions at the cave side, has also increased. Similar to Ca isotopes, uranium isotopes provide insight into the local hydrology by reflecting infiltration rates (Denniston et al., 2018; Oster et al., 2012; Zhou et al., 2005). Others such as lead isotopes ($^{206}Pb/^{207}Pb$) are used to identify the sources of lead in speleothems, which can be natural or anthropogenic. Therefore, lead isotopes can help to identify past pollution events (Allan et al., 2015). Smelting, coal burning, and mining result in distinct $^{206}Pb/^{207}Pb$ ratios, which are recorded in the speleothem, allowing for an investigation of anthropogenic activity in a certain region (Allan et al., 2015).

Recent advantages of the use of water isotopes as a palaeo-temperature proxy are based on the use of clumped isotopes and fluid inclusions. Clumped isotopes (Δ_{47}) give quantitative estimates of water temperature at the time of speleothem formation (Affek et al., 2008; Gázquez et al., 2018). Fluid inclusions are microcavities that form in the speleothem matrix during precipitation. The water isotopes (oxygen and hydrogen) are trapped in the cavity without further isotopic fractionation, and thus reflect past drip water chemistry (Demény et al., 2017).

One of the easiest and most cost-effective proxies to acquire from speleothems is the grey scale profile. Changes in grey values are related to mineral density, reflecting the precipitation style which can be fast or slow. High drip rates or high super saturation levels often lead to fast and

unorganized crystallisation, leaving the crystal lattice less organized and porous (Frisia, 2014; Frisia et al., 2000). This is represented in the grey scale record with high values (Vanghi et al., 2015). Denser $CaCO_3$ mineral layers have a lower reflectance based on higher transparency, and are represented by low grey values and darker colour. This is a result of a reduced growth rate.

Due to the low organic matter content in speleothems, most studies centre around inorganic proxies. However, there are proxies available in speleothem research which allow for an investigation of plant and microbial activity above the cave, giving a more comprehensive view on past environmental conditions (Blyth et al., 2016). For example, lipid biomarkers are used to track vegetation changes, introduced either naturally or through agricultural activities. The advantage of using biomarkers is the ability to identify different biological groups (e.g. higher/lower plants, bacteria, fungi), giving a more complete picture of the local ecosystem (Blyth et al., 2006). Vegetation changes can also be reconstructed using pollen incorporated into speleothems (Matley et al., 2020; McGarry and Caseldine, 2004). However, this approach works best in well-ventilated caves (Festi et al., 2016). Another organic proxy in speleothems focuses on luminescence (Blyth et al., 2008). It can be used to determine the amount of organic matter and to some extent, differentiate between different types of organic matter (Blyth et al., 2008).

Chapter 2

Rainwater Stable Isotopes

2.1 Chapter summary

The interpretation of palaeoclimate archives based on oxygen isotopes depends critically on the detailed understanding of processes controlling the isotopic composition of precipitation. In the summer monsoonal realm, like Southeast Asia, seasonally and interannually depleted oxygen isotope ratios in precipitation have been linked to the summer monsoon strength. However, in some regions, such as central Vietnam, most of the precipitation falls outside the summer monsoon period. This chapter investigates processes controlling stable isotopes in precipitation from central Vietnam by combining moisture uptake calculations with monthly stable isotope data observed over five years. It is found that the seasonal cycle in isotopes is driven by a shift in source location from the Indian Ocean to the South China Sea. This shift is reflected in oxygen isotope ratios with low values (-8 to -10 ‰) during summer and high values during spring/winter (0 to -3 ‰), while 70% of the annual rainfall occurs during autumn. Interannual changes in precipitation isotopes in central Vietnam are governed by the timing of the seasonal onset and withdrawal of the Intertropical Convergence Zone (ITCZ), which controls the amount of vapour contributed from each source.

This chapter has been published as: Wolf, A., Roberts, W. H., Ersek, V., Johnson, K. R., & Griffiths, M. L. (2020). Rainwater isotopes in central Vietnam controlled by two oceanic moisture sources and rainout effects. *Scientific Reports*, 10(1), 1-14.

The authors contributed as follows: A. W. conducted the calculations/simulations and drafted the manuscript, E. V. and W.H.G. R. supervised the analysis and reviewed the manuscript, K.R. J. and M.L. G. reviewed the manuscript.

2.2 Introduction

Tracing the hydrological cycle with stable isotope ratios in precipitation has greatly advanced the understanding of climatic processes, due to their distinct behaviour during evaporation and condensation (Bowen, 2008; Dansgaard, 1964; Rozanski et al., 1993). Stable isotopes in precipitation are also extensively used as palaeoclimate proxies, for example when recorded in the stable isotopic composition of tree ring cellulose (Sano et al., 2012; Xu et al., 2011), leaf waxes (Yamoah et al., 2016), ice cores (Bertler et al., 2011; Jouzel et al., 2007), and speleothems (Cai et al., 2017; Dong et al., 2016; Dykoski et al., 2005; Griffiths et al., 2009; Kaushal et al., 2018; Pausata et al., 2011; Wang, 2001; Zhang et al., 2018). However, processes controlling the isotopic composition of rainfall vary strongly in space (Baker et al., 2015; Breitenbach et al., 2010; Cai et al., 2018; Konecky et al., 2019) and time (Cobb et al., 2007; Kurita et al., 2009; Moerman et al., 2013). This represents a particular challenge for palaeoclimate reconstructions. The key for interpreting the palaeoclimatic signal in water isotopes is understanding which of these processes are the most important; this can be quantified by looking at stable isotopes in modern rainfall. Traditionally, variability in the isotopic composition of tropical rainfall was explained by an inverse relationship between the local precipitation amount and the isotope ratio ($\delta^{18}O_p$), termed the 'amount effect' (Dansgaard, 1964). It was later found that this relationship is much more complex, and a variety of controlling processes explain the strong spatial and temporal variability in between sites. Seasonal changes in tropical rainwater isotopes have been attributed to changes in moisture source location and moisture history (Araguás-Araguás et al., 1998; Breitenbach et al., 2010), atmospheric processes, such as rainout along the travel path (Kurita et al., 2009; Pausata et al., 2011), and changes in convection strength (Cai et al., 2018). It has been shown that the precipitation type (e.g. convective versus stratiform (Aggarwal et al., 2016)), cloud-top height (Cai and Tian, 2016) and local microphysical processes within the cloud, such as condensation rates, re-evaporation and crystallization processes (Bony et al., 2008; Galewsky et al., 2016), can also influence the variability of the isotope ratio in tropical rainfall (Konecky et al., 2019).

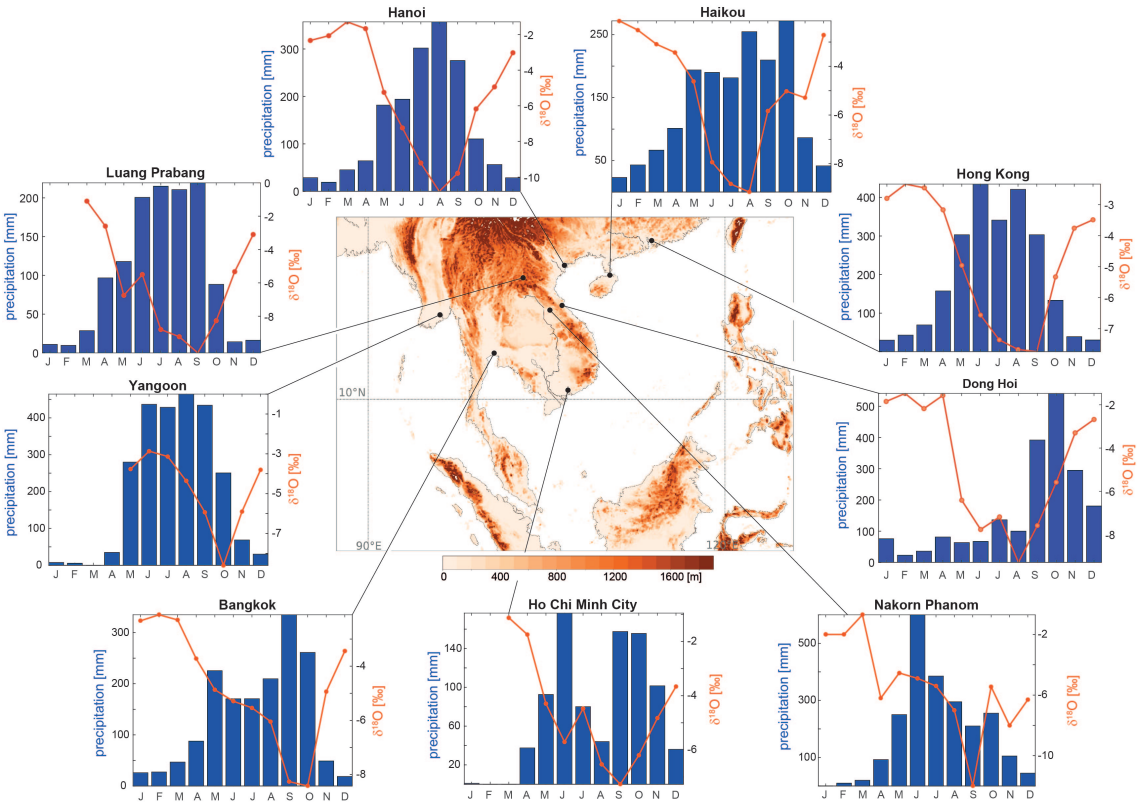

Figure 2.1: Local topography (Amante and Eakins, 2009), location and multi-annual average of precipitation and $\delta^{18}O_p$ for GNIP stations in East and Southeast Asia. Data for Ho Chi Minh City from Le Duy et al. (2018) and Munksgaard et al. (2019) and the data for Nakorn Phanom from Noipow (2015). Central Vietnams boreal autumn rainfall regime is unique in the region and is represented by the Dong Hoi station.

Understanding these processes is particularly challenging in regions with sparse and short records of rainfall monitoring, such as Southeast Asia. Thus far, seasonal variability in rainwater isotopes from Southeast Asia has been linked to source location (Aggarwal et al., 2004; Araguás-Araguás et al., 1998; Wei et al., 2018), regional and local rainfall amount (Wei et al., 2018; Yang et al., 2016), convection strength (Cai et al., 2018), and rainout along the moisture advection path (Le Duy et al., 2018; Yang et al., 2016). Research has mainly focused on the isotopic composition of the summer monsoon compared to the winter season because the shift in $\delta^{18}O_p$ between summer and winter is largest. However, it remains unclear what drives the seasonal cycle in $\delta^{18}O_p$ throughout the entire year, especially for sites with a rainy season independent of the summer monsoon. The focus on these two seasons is problematic for mainland Southeast Asia, where the timing of peak rainfall varies strongly across the peninsula and is not restricted to strong summer monsoon

rainfalls (Misra and Dinapoli, 2014) (Figure 2.1). For example, annual rainfall in central Vietnam is strongly affected by tropical cyclones that peak during autumn (September to November) and rainfall associated with north-easterly winds (Northeast Monsoon) (Chen et al., 2012a; Yokoi et al., 2007) (Figure 2.1). This makes central Vietnam ideal to investigate the impact of non-summer-monsoonal rainfall on the seasonal cycle in rainwater isotopes.

Previous modelling studies have identified the topography of mainland Southeast Asia as a crucial factor in modulating the timing of its rainfall season (Wei et al., 2019; Wu and Hsu, 2016). Autumn rainfall in central Vietnam is a direct consequence of local topography interacting with the annual migration of the Intertropical Convergence Zone (ITCZ), creating zones of intense rainfall and rain shadows depending on the season (Wu and Hsu, 2016). An inverse relationship between topography and the isotopic composition of rainfall has long been observed and is described as the 'altitude effect' (Gonfiantini et al., 2001). However, the altitude effect is less pronounced in the tropical regions (Sturm et al., 2007) and its relative importance is disputed (Jiao et al., 2020). Mainland Southeast Asia has two main mountain ranges located between Myanmar and Thailand to the west (the Tenasserim Hills), and Laos and Vietnam to the east (the Truong Son Mountains or Annamite Mountains). Therefore, central Vietnam is ideal to investigate the importance of these effects on stable isotopes in precipitation there.

In this chapter, modelling of monthly moisture uptake locations for precipitation arriving in central Vietnam is combined with monthly stable isotope ratios collected over five years. The aim is to identify controls on the seasonal cycle in precipitation isotopes from central Vietnam to understand processes at work and identify the primary controls on seasonal variability independently from the summer monsoon season. Further, the impact of rainout effects using a spatial array of precipitation isotope data from five sites in mainland Southeast Asia is investigated. Then, the investigation expands and explores interannual variability of precipitation isotopes in order to estimate the potential of stable isotopes from central Vietnam for palaeoclimate reconstructions.

2.3 Methods

2.3.1 Data collection

Meteorological and water isotopic data were obtained from the International Atomic Energy Agency (IAEA/WMO, 2020) WISER database, which gives access to data from the Global Network of Isotopes in Precipitation (GNIP). The GNIP station at Dong Hoi represents central Vietnam in this study and includes five years of data from 2014 to 2017. The year of 2015 is incomplete, with March, April, May, and August missing, and contains seven data points for stable isotopes. The deuterium excess was calculated following Craig (1961). Further, GNIP data from Yangon (Myanmar), Bangkok (Thailand), Nakorn Phanom (Thailand) and Haikou (Hainan) is used to compare observed data with the modelled spatial evolution of $\delta^{18}O_p$.

2.3.2 Modelling moisture uptake with PySplit

The Hybrid Single-Particle Lagrangian Integrated Trajectories (HYSPLIT) model (Stein et al., 2015) was developed to track air parcels moving towards or from a set location. The model incorporates meteorological data and reconstructs the movement of air masses. Backward trajectories were calculated using frequency analysis with new trajectories every 6 hours for 30 days at a height of 1500 m above mean sea level, using the NCEP Global Data Assimilation System (GDAS)(NCEP, 2020) model one-degree archive. The flow at this level is representative of the large-scale, near-surface flow in the tropics and captures the moist surface in which convergence occurs (Anders and Nesbitt, 2015; Sun et al., 2019). Moisture uptake is calculated following Sodemann et al. (2008) (Sodemann et al., 2008), using PySplit (Cross, 2015). PySplit is a Python-based application for HYSPLIT allowing for moisture flux calculation along a trajectory. Briefly, the change in humidity over 6-hour periods of a HYSPLIT trajectory is calculated. When values are positive, greater than a threshold (0.2 g/kg) and the change in humidity occurs within the planetary boundary layer, it is assumed that the moisture required is taken up from surface evaporation.

2.3.3 Modelling spatial evolution of $\delta^{18}O_p$ with simple water vapor transport model

Additionally, the Kukla et al., 2019 model is used to simulate the spatial evolution of oxygen isotopes, along a transect, affected by rainout effects and local topography (Kukla et al., 2019). The

model calculates hydroclimatic fluxes and corresponding $\delta^{18}O_p$ by combining three frameworks: an orographic rainout model (Smith, 1979), the water balance framework (Budyko et al., 1974), and a vapour transport model (Hendricks et al., 2000). This approach allows us to predict the evolution of $\delta^{18}O_p$ by incorporating orographic precipitation and the regional waterenergy budget (Kukla et al., 2019). Parameters used in this study are listed in Table 1. Initial vapour content and advective velocity are derived from the mean u and v wind fields of the ERA5 dataset (Copernicus Climate Change Service (C3S), 2020). Potential evapotranspiration from the CGIAR-CSI Global-Aridity and Global-PET Database (CGIAR-CS, 2020; Zomer et al., 2008) and dryness index was calculated using GNIP data. To understand the effects of topography on oxygen isotopes, a flat surface simulation (simulation 1) is compared with a simulation incorporating local topography (simulation 2). Two mountains are used in simulation 2, represented by simple Gaussian bell shapes with a peak elevation of 700 m and a width of 130 km for the Tenasserim Hills and peak elevation of 1500 m and a width of 160 km for the Truong Son Mountains. Both simulations use the same climatic parameters (Table 2.1), which are representing typical conditions during the period of June to August. Moisture arriving in central Vietnam only crosses landmasses during this time of the year; thus, allowing us to investigate continental rainout and altitude effects.

Table 2.1: Model input used in simulations 1 and 2 for the period of June to August. Initial vapour content and advective velocity are derived from the ERA5 dataset (Copernicus Climate Change Service (C3S), 2020). Potential evapotranspiration from the CGIAR-CSI Global-Aridity and Global-PET Database (CGIAR-CS, 2020; Zomer et al., 2008) and dryness index was calculated using GNIP data.

Nodes	500
Length of domain	3.0^6 [m]
Elevation of Truong Son and Tenasserim Hills	1500 and 700 [m]
Mean annual temperature (2 m above sea level) (IAEA/WMO, 2020)	303 [K]
Potential evapotranspiration (CGIAR-CS, 2020)	556 [mm]
Péclet number (Winnick et al., 2014)	30
Initial vapour content (Copernicus Climate Change Service (C3S), 2020)	60 [kg·m^{-2}]
Relative humidity (Held and Soden, 2006)	0.8
Advective velocity (Copernicus Climate Change Service (C3S), 2020)	3 [m·s^{-1}]
Transpired fraction of evapotranspiration (Good et al., 2015)	0.64
Starting dryness index (CGIAR-CS, 2020)	2.37
Recycling efficiency parameter (global mean) (Kukla et al., 2019)	2.6

2.4 Results and Discussion

Monthly $\delta^{18}O_p$ values from the Dong Hoi GNIP station(IAEA/WMO, 2020) show a distinct seasonal cycle, with the lowest values from May until September (-7.8 $\pm$ 1.2 ‰) and the highest $\delta^{18}O_p$ values (-1.9 $\pm$ 0.4 ‰) during December to April (Figure 2.2) over the years 2014 to 2018. This seasonal pattern is like the isotopic composition of rainfall in southern China (Hong Kong) (Cai and Tian, 2016) and Hanoi (Figure 2.1). Following removal of the seasonal cycle, no correlation ($r^2 = 0.12$, p-value $= 0.02$) between the monthly oxygen isotopes and precipitation amount in central Vietnam over the five years was found. Therefore, factors other than the amount effect must be invoked to explain the seasonal $\delta^{18}O_p$ cycle in central Vietnam. Further, there is no correlation between the monthly oxygen isotopes and the number of tropical cyclones occurring in the western North Pacific ($r^2 = 0.0002$, p-value $= 0.91$). To investigate the influence of changes in the moisture source location on rainfall in central Vietnam, the monthly moisture pathways are simulated in the following section.

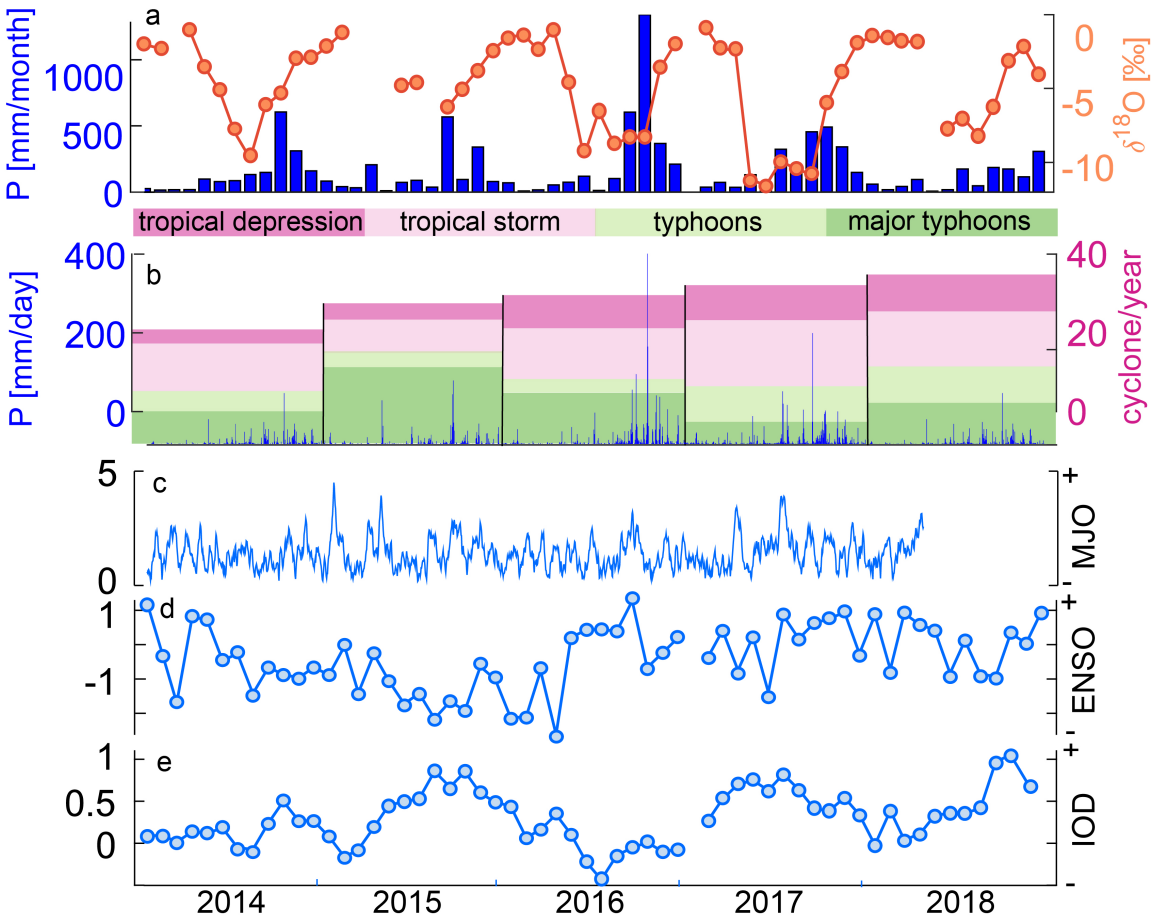

Figure 2.2: Comparison of **a** $\delta^{18}O_p$ and total monthly precipitation at Dong Hoi and **b** daily precipitation at Dong Hoi and the sum of tropical cyclones (Center, 2014-2018) in the western North Pacific, where the colours indicate the number of occurrences within each class. **c** Madden-Julian Oscillation (MJO), based on the Real-time Multivariate MJO Index (Wheeler and Hendon, 2004), **d** El Niño-Southern Oscillation (ENSO), retrieved from the Southern Oscillation Index (Ropelewski and Jones, 1987) **e** the Indian Ocean Dipole (IOD), retrieve from the Dipole Mode Index (NOAA, 2020*b*), for the years 2014 to 2018.

2.4.1 Moisture source location and large-scale circulation

There are three main air mass sources for mainland Southeast Asia: the Indian Ocean, the Pacific Ocean, and continental Asia(Aggarwal et al., 2004; Le Duy et al., 2018; Wei et al., 2018). Calculating the air mass trajectories using HYSPLIT helps to understand general air movement; however, it is of limited use for identifying the location of moisture uptake (Ruan et al., 2019). Primary evaporation can occur anywhere along the trajectory path, leaving the trajectory analysis with a given uncertainty. Therefore, the monthly moisture uptake was calculated, based on the specific humidity to estimate the uptake location for moisture arriving in central Vietnam using

PySplit (Cross, 2015).

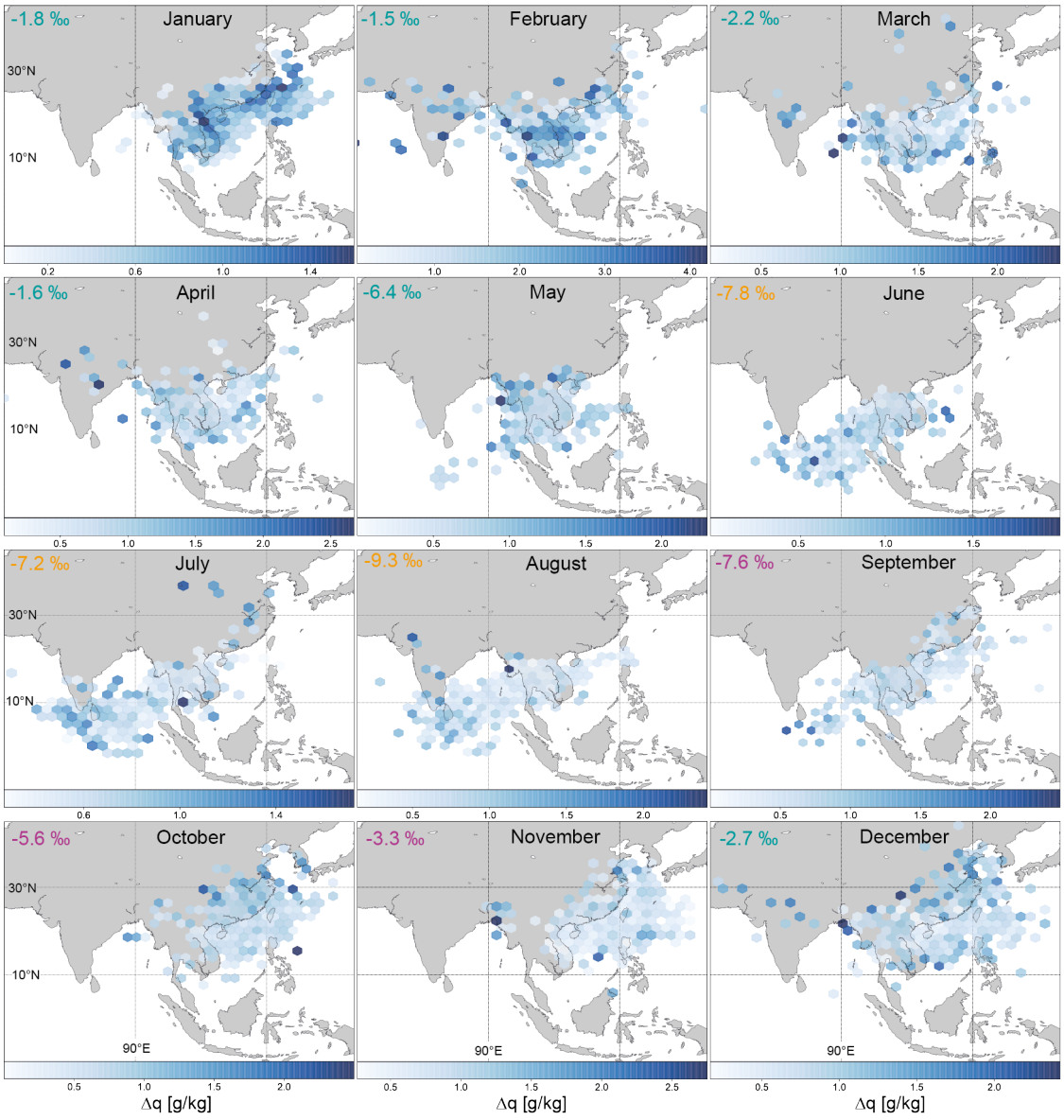

Figure 2.3: Monthly moisture uptake locations for the years 2014 to 2018 shown as hexagonal binning, with the mean value of Δq occurring in each cell. Δq describes the changes in specific humidity of an air parcel between two set time intervals. Areas with no colour show that no trajectory was projected by HYSPLIT for this point. The calculation is based on 6-hourly backward trajectories for each month. The calculation reveals a seasonal shift in moisture source location between the period of June to August and of September to May. The monthly $\delta^{18}O_p$ values are indicated in the upper left corner of each map.

The change in moisture source location is linked to the seasonal migration of the ITCZ and the associated large-scale atmospheric circulation changes. The ITCZ in the West Pacific is located around 5 °S during December to February and north of 15 °N in June to August (Lau and Yang,

1997). During April, the ITCZ begins to move northwards from near the Equator crossing southern Vietnam in early May (Wang et al., 2009). In mid-May, the ITCZ moves rapidly northwards within a few days (Wang et al., 2004), explaining the south-westerly winds, increasing the contribution of moisture to mainland Southeast Asia from the Bay of Bengal. This effect is clearly visible in central Vietnam as a shift in the moisture uptake location towards the Indian Ocean during May (Figure 2.3). The Indian Ocean remains the main moisture source location throughout summer (June to August) and mid-September (Figure 2.4). Beginning in September, the ITCZ slowly retreats southwards, resulting in northeasterlies bringing intense rainfall into central Vietnam at this time (Nguyen-Thi et al., 2012; Yokoi and Matsumoto, 2008). The moisture uptake analysis for central Vietnam shows this large-scale change in circulation pattern with a high contribution of moisture from the northern South China Sea from mid-September onwards (Figure 2.3). As the ITCZ continues to move south during October to December, easterlies weaken, and moisture is taken up more locally from mainland Southeast Asia and part of the South China Sea.

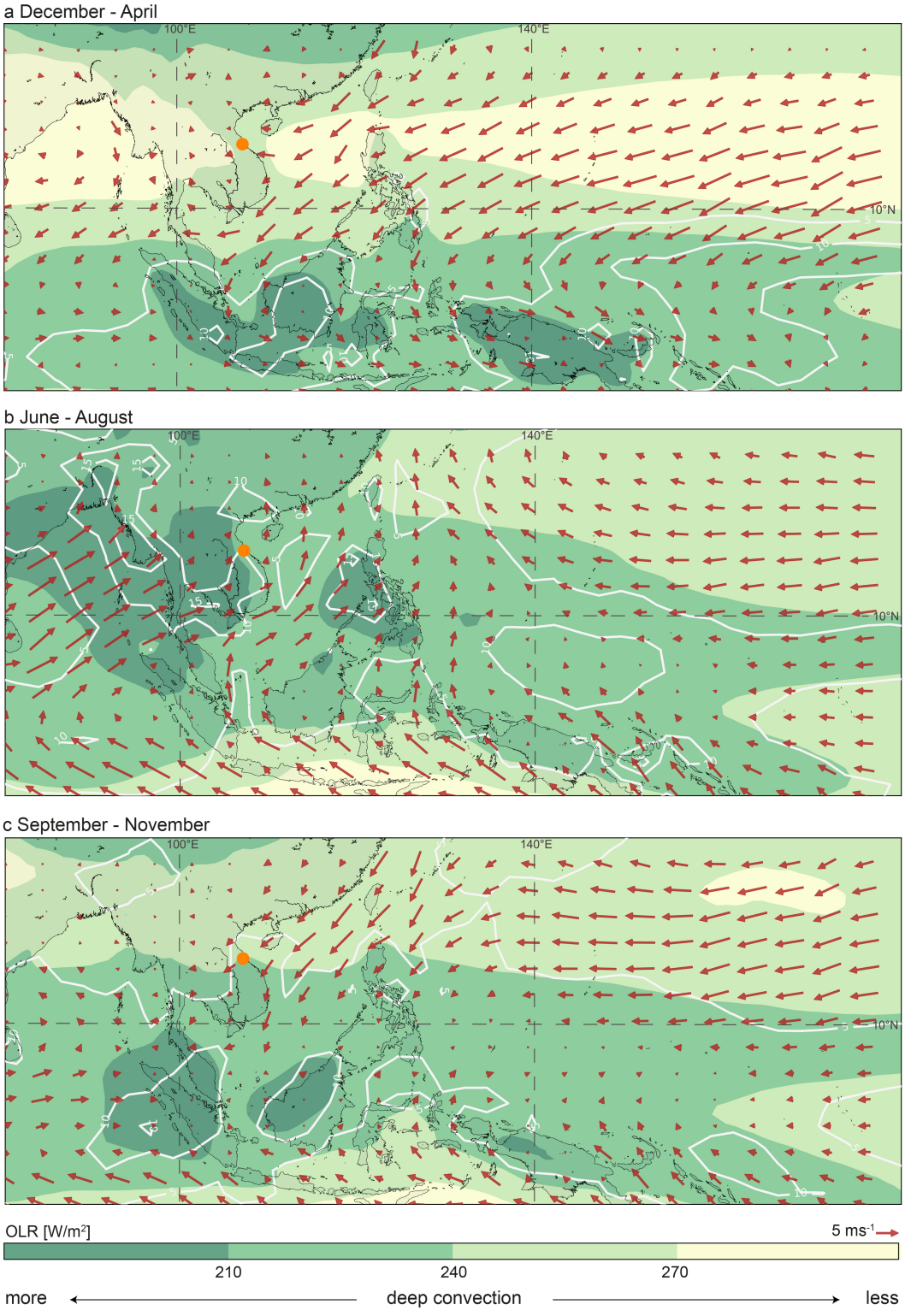

Figure 2.4: Surface wind flow pattern (monthly average of 10 m u and v component downloaded from the ERA5 dataset (Copernicus Climate Change Service (C3S), 2020)) showing the general circulation driven by the ITCZ and monthly mean Interpolated Outgoing Longwave Radiation (OLR)(NOAA, 2020*d*) data and Global Precipitation Climatology Centre (v2018)(NOAA, 2020*c*) monthly precipitation data (white contours plotted at 5, 10, 15 mm day^{-1}), reflecting zones of increased convection/precipitation during **a** December to April, **b** June to August and **c** September to November. The location of Dong Hoi is represented by the orange dot.

The findings are supported by the deuterium excess (Figure 2.5) defined as: d-excess (‰) = δ^2H - 8 $\times$ δ^{18}O (Craig, 1961). The deuterium excess is a result of the different fractionation rates of oxygen and hydrogen isotopes during kinetic fractionation (Clark and Fritz, 1997). During kinetic fractionation, hydrogen fractionation is faster than oxygen fractionation and the rate of fractionation depends on relative humidity at the evaporation site (Craig et al., 1963). Kinetic fractionation occurs mainly during evaporation, rather than condensation (Craig et al., 1963). Therefore, the deuterium excess acts as a fingerprint of climatic conditions during primary evaporation, independent of rainout processes along the travel path (Clark and Fritz, 1997). Drier source regions with low relative humidity are associated with an increased deuterium excess and vice versa (Gat and Airey, 2006). In the data, the deuterium excess in summer rainfall has lower values compared to winter and spring rainfall. Deuterium excess values of autumn rainfall clusters in between (Figure 2.5). This confirms the previous results based on moisture source location and shows that the deuterium excess reflects two oceanic sources: the Indian Ocean during summer with most of the values around 5 to 10 and Pacific Ocean during spring, autumn, and winter when most values range around 11 to 17. Further, the increased deuterium excess during winter reflects the lower relative humidity in the South China Sea during this time. The relative humidity in the Bay of Bengal is high during summer due to the strong convection related to the Indian Summer Monsoon, which is reflected by low deuterium excess values (Figure 2.5).

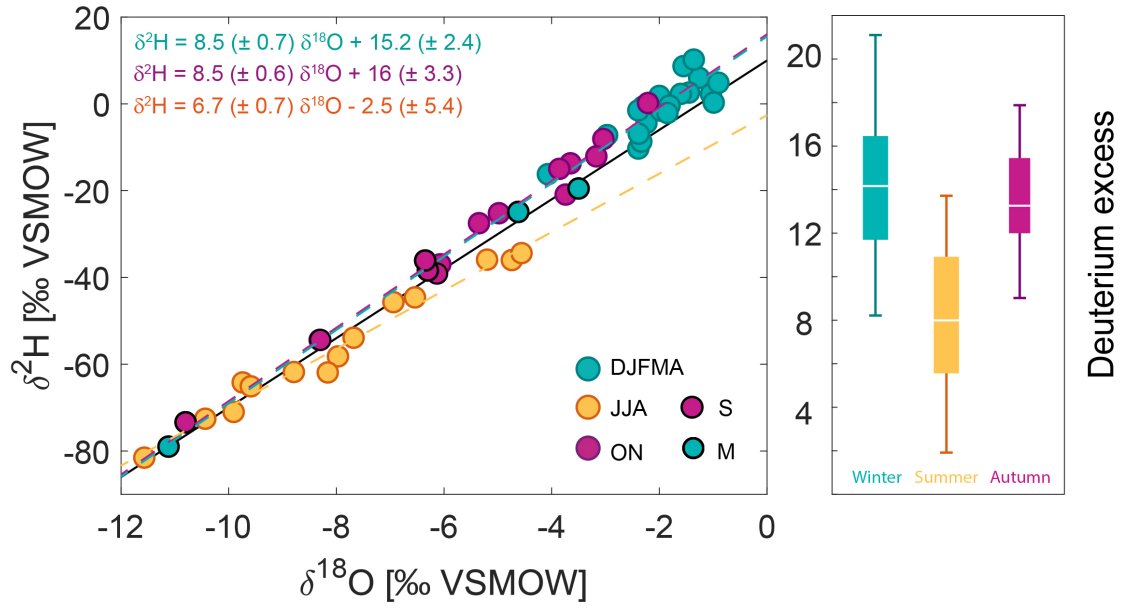

Figure 2.5: Local Meteoric Water Line (LMWL) in central Vietnam for September, October, and November (purple), December to May (turquoise) and June to August (yellow). Since September and May are the transition months where the moisture source changes, they are highlighted with a black outer circle. Monthly data points for the deuterium excess are coloured according to each season. The Global Meteoric Water Line (GMWL) is colour-coded in black and local meteoric water lines are colour-coded according to each season. Deuterium excess values are lower during summer and higher during winter/spring. This is empathized in the box-and-whisker plot on the right, showing that summer strongly deviates from the rest of the year.

The isotopic variability of rainfall during the transition periods between moisture sources in May and September (Figure 2.3), when the deuterium excess shows a large variability (Figure 2.5) is now considered in detail. The deuterium excess depends on the relative contribution from each source, which can vary from year to year. Waters from May 2017 are strongly depleted, which is caused by a generally larger range of moisture source regions, compared to 2014 (Figure 2.6 left column). Lower values in 2017 can be linked to an increased contribution of more distal moisture sources compared to 2014 and 2016. This is a first hint that interannual variability of oxygen isotopes in rainfall can be linked to the source location.

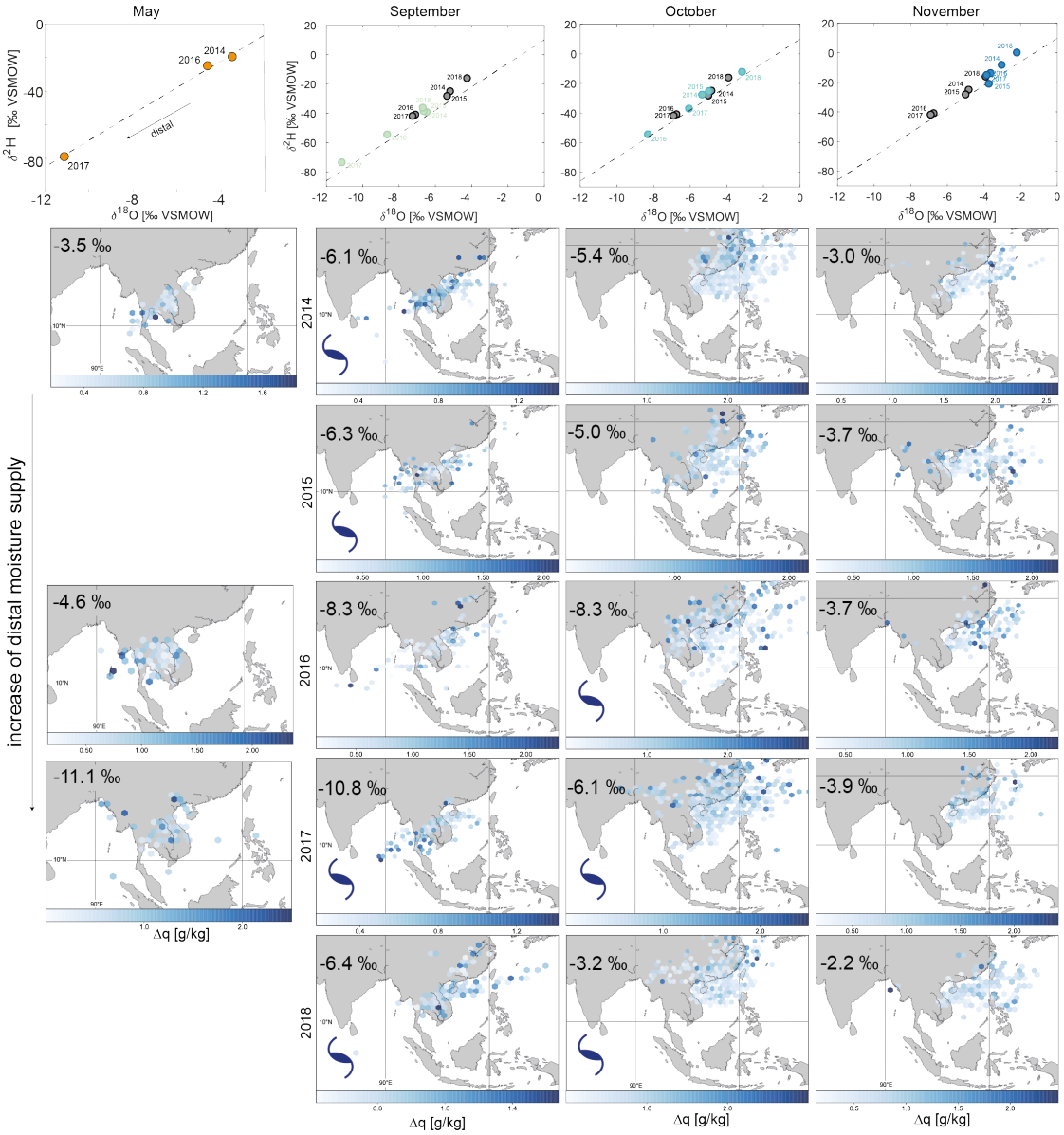

Figure 2.6: Plots of δ^2H–δ^{18}O for May (orange), September (mint), October (turquoise), and November (blue), with the annual means of September, October and November in grey. Grey dashed line shows the GMWL. The maps show hexagonal binning of moisture uptake for each month of the years 2014 to 2018. Months with tropical cyclones (Center, 2014-2018), that made landfall (NOAA, 2020*a*) in central Vietnam are highlighted with a dark blue whirl symbol.

Additionally, the link between source location and interannual variability is evident during September to November rainfall (Figure 2.6). Considering the averaged values for this time, two clear clusters for 2014/15 and 2016/17 are evident (Figure 2.6). This relation is reflected in the source location (Figure 2.6 middle columns). In 2016 and 2017, moisture arrives from a more distal location, such as near Sri Lanka and the Gulf of Thailand (Figure 2.6). This is not the case in

2014/15 and 2018, when moisture arrives from the proximal eastern Bay of Bengal and off the coast from northern and central Vietnam (Figure 2.6). This interannual variability in moisture source is related to the timing in the withdrawal of the ITCZ from Vietnam (Hu et al., 2019). An early withdrawal (2014/15) causes the formation of an anti-cyclonic circulation in the South China Sea, partly blocking the south-westerly flow from bringing moisture from the Bay of Bengal to central Vietnam. This leads to more positive deuterium excess. A late withdrawal enables more moisture contribution from the southern Bay of Bengal (south of Sri Lanka) and the Gulf of Thailand (Figure 2.6) (Tan et al., 2019; Wu and Hsu, 2016), leading to more negative deuterium excess values. Several studies highlighted that tropical cyclones affect interannual autumn rainfall variability in central Vietnam (Chen et al., 2012a; Le Duy et al., 2018; Vu et al., 2015), thus it is of importance to consider tropical cyclone activity as a potential factor in modulating δ^{18}O. Tropical cyclones can result in unusually low δ^{18}O values in related rainfall (Sánchez-Murillo et al., 2019). Using the Joined Typhoon Warning Center annual reports (Center, 2014-2018), tropical cyclones are identified, that made landfall in central Vietnam during autumn 2014 to 2018 (Figure 2.6). In general, the numbers of tropical cyclones in the western North Pacific show an increasing trend over the years from 2014 to 2018 (Figure 2.2). In the dataset, cyclones in September 2014, September 2015, October 2016, September and October 2017 and September and October 2018 (Figure 2.6) are identified.The only September during the data period without a cyclone is 2016. Rainfall in September 2017 has the lowest δ^{18}O value compared to other years, which can be explained by the strong contribution of moisture from the Bay of Bengal (Figure 2.6). A similar pattern is evident for September 2016. Therefore, low δ^{18}O is not necessarily the result of tropical cyclone activity. During October 2014 to 2018, there is no moisture source in the Bay of Bengal; rather, moisture was sourced from the South China Sea. The Octobers with lowest δ^{18}O values (October 2016 and 2017) appear to have received moisture from a more distal source, north of the Philippines. However, the difference in distal source contribution appears to be limited. In October 2016, the typhoon Aere brought strong rainfall into central Vietnam, which resulted in the highest recorded rainfall amount in the dataset (Figure 2.2). The possibility cannot be excluded, that typhoon Aere contributed to the depleted δ^{18}O in October 2016; however, this is a single event and does not allow for further conclusions. October 2018 shows that moisture is contributed mainly from a proximal source, which potentially explains the high δ^{18}O values during this year, despite the potential influence of typhoon Yutu. In the months of May and November, no tropical cyclones

made landfall in central Vietnam during the timespan of the dataset.

Several studies linked the seasonal cycle in rainwater isotopes in Asia to a shift from oceanic to continental sources including Southeast Asia (Aggarwal et al., 2004; Araguás-Araguás et al., 1998), Taiwan (Peng et al., 2010), Thailand (Wei et al., 2018) and southern China (Tang et al., 2015). The findings suggest that in central Vietnam, $\delta^{18}O_p$ is controlled by a shift between two oceanic sources, rather than a shift between a continental and oceanic source (Figure 2.3). Establishing the Local Meteoric Water Line (LMWL) is a useful tool to investigate the contribution of continental moisture or secondary evaporation along the travel path. Plant transpiration returns the water vapour with nearly no change in deuterium excess, whereas open water or soil evaporation leads to an increased deuterium excess and sub-cloud evaporation to a decreased deuterium excess (Gat et al., 1994). This means that an increased deuterium excess represents an increased continental moisture contribution, and a decreased deuterium excess indicates secondary evaporation. The LMWL for central Vietnam is: $\delta^2H = (8.6 \pm 0.3\ ‰) \times \delta^{18}O + (15 \pm 2\ ‰)$ with an r^2 of 0.98 (n = 54) calculated following Sachs (1984). The LMWL is calculated for each season and find that during autumn, spring, and winter, the LMWL slope is increased by 0.5 ‰ and the intercept by 5.6 ‰ compared to the GMWL (Figure 2.5). This deviation suggests a limited contribution of continental moisture (lake, river or soil moisture) from mainland Southeast Asia during this time of the year (Gat et al., 1994). During summer, the LMWL has a slope of 6.7, which is less than 8 of the GMWL and an intercept of -2.5 ± 5.4 ‰ (Figure 2.5). This decrease again suggests a limited influence of continental evaporation. The depletion in the deuterium excess could be a result of re-evaporation of raindrops after condensation (sub-cloud evaporation) (Clark and Fritz, 1997; Dansgaard, 1964; Gat et al., 1994).

2.4.2 Spatial variability of $\delta^{18}O_p$ across mainland Southeast Asia

Thus far, the focus was on explaining the mechanisms controlling the temporal variability of rainwater isotopes in central Vietnam. However, the spatial evolution has not been explained, nor fully considered processes occurring during condensation, rather than evaporation. Investigating how rainwater isotopes vary along the moisture travel path helps understand the importance of rainout processes. These effects are strongest when moisture travels via landmasses and for central Vietnam this is the case during summer (June to August). To explore the spatial variability of

$\delta^{18}O_p$ in mainland Southeast Asia during this time, the effects of local topography and rainout are investigated. Rayleigh fractionation due to rainout does not only occur while moisture travels landwards, but also due to orographic uplift (Gonfiantini et al., 2001). During summer, air masses reaching central Vietnam have a western source and cross two mountain ranges before reaching the study site (Wang and Chang, 2012), making this time ideal to understand these processes.

Two simulations are performed: one with mainland Southeast Asia being represented as a flat land surface and one considering local topography to understand the effects of rainout and orographic uplift, respectively. Simulation 1 (Figure 2.7) models the rainout in water isotopes from the Bay of Bengal to Hainan (Haikou) and predicts a rainout effect of -0.68 ‰ per 1000 m. Considering the GNIP $\delta^{18}O_p$ data across the transect, the rainout effect alone cannot correctly explain this spatial variability. Simulation 2 shows that the spatial development of $\delta^{18}O_p$ along the transect is better simulated when topography is included in the model (Figure 2.7). Effects of the Tenasserim Hills (700 m elevation in the simulation), positioned between Myanmar and Thailand and of the Truong Son Mountains (1500 m elevation in the simulation), located between Laos and Vietnam are simulated. The simulation predicts a negative shift in oxygen isotopes of -1.44 ‰ for the Tenasserim Hills and of -2.89 ‰ for the Truong Son Mountains, which is an isotopic lapse rate of -0.3 ‰/100 m and -0.2 ‰/100 m, respectively. These values are within typical rates for the altitude effect of -0.15 to -0.5 ‰ per 100 m (Poage and Chamberlain, 2001). This simulation is in good agreement with observed data (Figure 2.7) and shows that the altitude effect alone can explain 70% of the spatial variability in rainwater isotopes during summer. During the summer months, the vertical temperature gradient is greater compared to winter, amplifying the altitude effect during this time (Peng et al., 2010). The altitude effect has also been shown to be larger during the rainy season, related to stronger rainout (Sturm et al., 2007). While the dry season is during summer in central Vietnam, Figure 2.4 shows that this is not the case for the rest of the Peninsula, which undergoes the rainy season during summer. Sturm et al. (2007) simulated the altitude effects in tropical South America and found that during the rainy season, more than 60% of the $\delta^{18}O_p$ variance is related to altitude according to observed data, which is similar to the results presented in this chapter. The simulations suggest that the rainout and altitude effects combined can explain the spatial variability of oxygen isotopes in mainland Southeast Asia during summer. However, the relation between $\delta^{18}O_p$ and altitude in mainland Southeast Asia needs

more detailed investigation, ideally using isotope-enabled general circulation models. The results are preliminary and hint towards the importance of orography and local advection for the spatial evolution of water stable isotopes.

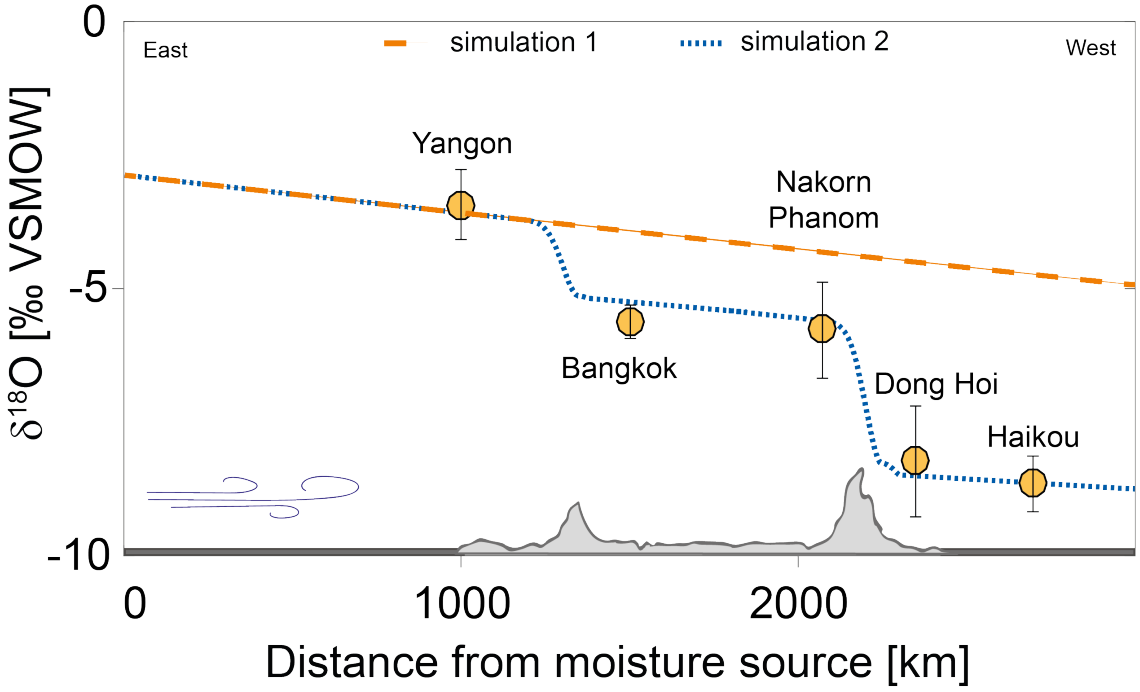

Figure 2.7: The spatial evolution of oxygen isotopes in precipitation over mainland Southeast Asia. Simulation 1 (orange line) simulates mainland Southeast Asia as a flat surface. Simulation 2 (dashed blue line) includes local topography. Observed long term means of GNIP data are shown in yellow, with error bars indicating the standard deviation in oxygen isotopes for each location.

2.4.3 Implications for palaeoclimate research

The seasonal variability of rainwater isotopes in central Vietnam is controlled by a seasonal shift between two moisture source locations: the Bay of Bengal and the South China Sea. This shift in source location is regulated by the position of the ITCZ (Figure 2.8). The timing of the seasonal migration determines the duration of each source's moisture contribution, thus, the ITCZ is controlling the year-to-year variability in average $\delta^{18}O_p$. Hence, the results show that $\delta^{18}O_p$ in central Vietnam is sensitive to small-scale variations in the position of the ITCZ. This offers the opportunity for palaeoclimate archives, such as speleothems and tree ring cellulose, to use changes in $\delta^{18}O$ as indicators of ITCZ dynamics, especially for periods where large changes have been inferred (Chawchai et al., 2013; Schneider et al., 2014; Tan et al., 2019a).

Further, variability in the ITCZ position is tightly linked to broader tropical ocean dynamics including ENSO and the IOD (Donohoe et al., 2013). This link is mainly established via variability in the local Hadley circulation, which is modulated by changing SSTs in the western Pacific and thus ENSO (Guo and Tan, 2018). An extensive body of literature based on tree ring cellulose $\delta^{18}O$ (Sano et al., 2012; Xu et al., 2019, 2018, 2015, 2011; Zhu et al., 2012) and $\delta^{18}O$ in precipitation (Wei et al., 2018; Yang et al., 2016) has confirmed the importance of SST variability in the Pacific and Indian Oceans for $\delta^{18}O_p$ in mainland Southeast Asia. Tree ring cellulose $\delta^{18}O$ from Thailand (Xu et al., 2018), Laos (Xu et al., 2011), Cambodia (Zhu et al., 2012) and Vietnam (Sano et al., 2012) shows a clear link between $\delta^{18}O$ and ENSO, with El Niño events leading to higher $\delta^{18}O$ and La Niña to lower $\delta^{18}O$ values. This relation can be enhanced or reduced by modulations of Indian Ocean SST (Xu et al., 2019; Yang et al., 2016). In addition, positive $\delta^{18}O$ anomalies during June to September in rainfall from Laos have been linked to more proximal moisture sources from the Bay of Bengal (Yang et al., 2016). This pattern is comparable to an early ITCZ withdrawal in the $\delta^{18}O$ dataset, showing more proximal sources in the Bay of Bengal as well. These similarities suggest a link between interannual variability in $\delta^{18}O_p$, and the ITCZ position and ENSO events across mainland Southeast Asia. This means that palaeoclimate records from central Vietnam based on $\delta^{18}O_p$ can potentially be used to reconstruct regional climate dynamics related to ocean SST anomalies and the evolution of ITCZ through time.

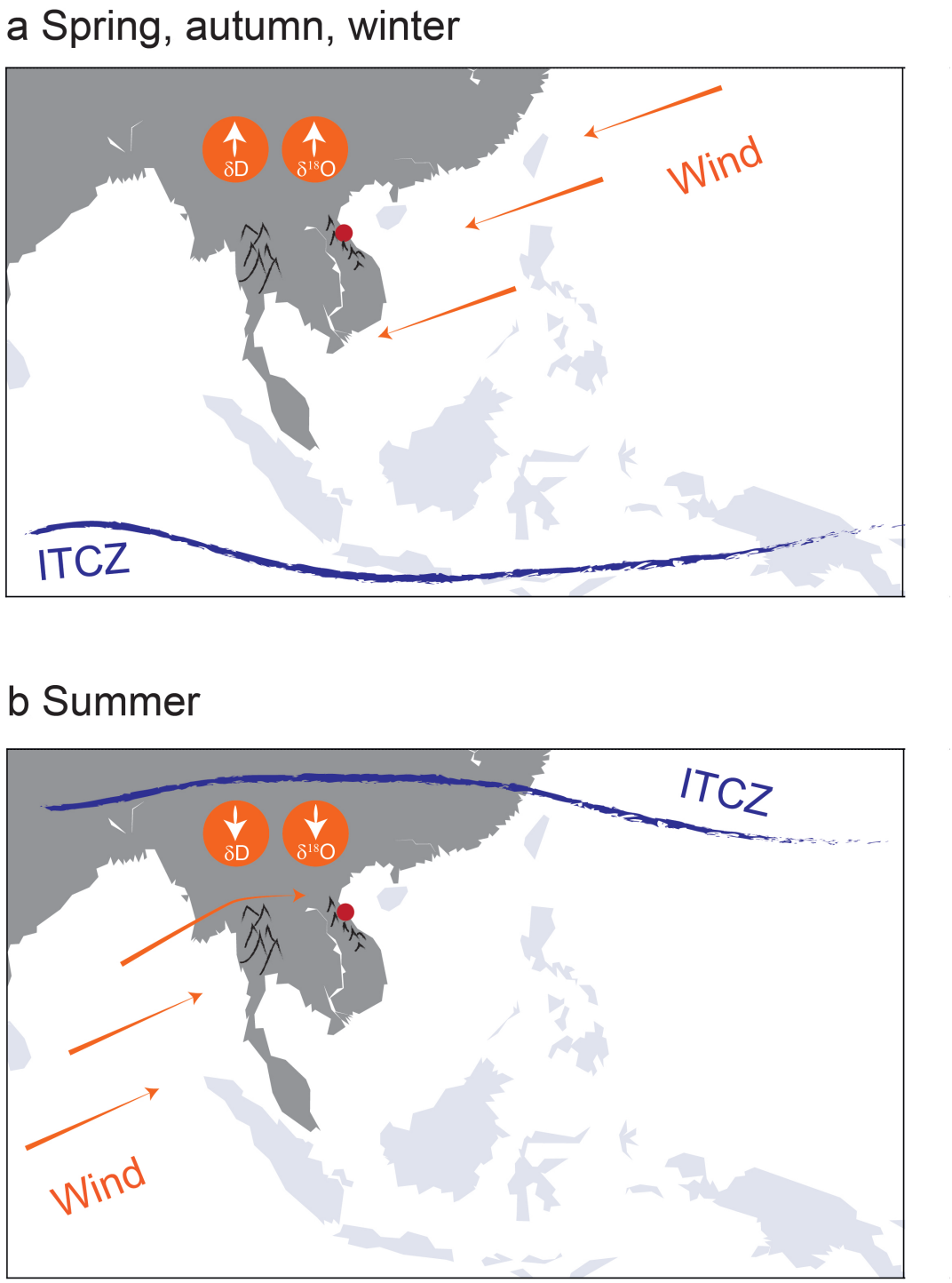

Figure 2.8: General circulation pattern (orange), oxygen isotopes (δ^{18}O) and deuterium excess (δD) in central Vietnam reacting to the ITCZ position (blue) during **a** spring autumn and winter and **b** summer.

In addition to $\delta^{18}O_p$ variability across mainland Southeast Asia, studies also investigated the effects of ENSO and the IOD on local rainfall amount. They found a strong spatial variability in

the relation of SST anomalies and rainfall anomalies across the Peninsula (Misra and Dinapoli, 2014) and throughout the seasons (Duc et al., 2018). This emphasises that rainfall amount and $\delta^{18}O_p$ do not necessarily correspond, since the impact of ENSO on $\delta^{18}O_p$ appears to be consistent across the Peninsula, whereas ENSO induced rainfall variability is spatially inhomogeneous (Ge et al., 2017a). Therefore, $\delta^{18}O_p$ from mainland Southeast Asia can potentially be used to trace large-scale circulation patterns, like shifts in the ITCZ and ENSO, while proxies for local rainfall can be used to investigate how these climate drivers control the local hydroclimate. However, the dataset is limited in time and restricts any long-term observations.

2.5 Conclusion

The timing of the rainy season in central Vietnam differs strongly from the rest of mainland Southeast Asia, with peak rainfall from September to November. Therefore, central Vietnam offers the opportunity to investigate the seasonal evolution of stable isotopes in precipitation unconfounded from the summer monsoon strength. The data show that there is a strong seasonal cycle in the isotopic composition, with low values during summer and high values during spring/winter, while the seasonal cycle in precipitation amount peaks in autumn. It was found that the seasonal isotopic variability in $\delta^{18}O$ and $\delta^{2}H$ is controlled by a shift between two oceanic moisture sources. During summer, the Bay of Bengal is the main source location and during the remaining part of the year, the South China Sea contributes most moisture. Thus, precipitating moisture arriving in central Vietnam crosses mainland Southeast Asia only during summer. By simulating the spatial variability of $\delta^{18}O$ in summer precipitation, it was found that rainwater isotopes across mainland Southeast Asia are mainly related to the altitude and rainout effect. Thus, both effects amplify the seasonal difference in the isotopic composition between summer and spring/autumn/winter rainfall even further.

By investigating the transition period from one source to the other (once in May and again in September to November), it was found that during May the relative distance of moisture uptake within the Bay of Bengal differs from year to year, and thus, drives interannual variability in the isotopic composition of precipitation. A similar process can be observed in September to December, where lower values in $\delta^{18}O$ and $\delta^{2}H$ are related to a longer travel distance of moisture within the Bay of Bengal, but also to an additional source of moisture contributed from the southern

South China Sea. During years with higher mean values for September to November, this second source within the southern South China Sea is absent and moisture from the Bay of Bengal arrives from a more proximal location, close to the coast of Myanmar and Thailand. These small changes within each moisture source are governed by the timing in ITCZ migration varying per year. This means that the relative travel distance and contribution of moisture from each source is regulated by the duration in which the ITCZ remains north of central Vietnam.

To conclude, palaeoclimate archives from central Vietnam, based on stable isotopes, have the potential to capture changes in the relative moisture contribution sourced from the Indian Ocean versus the South China Sea, and thus, track variability in the past position of the ITCZ. The findings suggest that a long-term northwards displacement of the ITCZ would result in more negative values in the isotopic composition of precipitation in central Vietnam and a southwards displacement in more positive values.

Chapter 3

Cave Monitoring

3.1 Chapter summary

Cave monitoring is fundamental for interpreting speleothem records, providing crucial insights into the processes controlling the transfer of the surface climate signal to speleothem geochemistry. Several processes, such as flow pattern and the mixing of waters in the epikarst, can alter the isotopic composition of drip waters. The following chapter describes internal processes of the Thien Duong and Soong Cave. Stalagmite TD3 was collected from Thien Duong Cave, however, due to restricted access to the cave, environmental monitoring was conducted at Soong Cave. Both caves were developed in the same geologic unit and under the same climatic regime. A strong seasonal cycle in δ^{18}O, with low values in summer and high values in winter, is observed in drip water samples from Soong Cave. A comparison of δ^{18}O in surface and drip water suggests that the seasonal cycle in surface precipitation is transmitted into the drip water, but the amplitude is reduced and the signal is smoothed. Furthermore, there is a positive correlation between δ^{18}O in rainwater normalized to the precipitation amount at Dong Hoi and δ^{18}O in the drip waters of Soong Cave. These results suggest that drip water δ^{18}O is likely biased towards the season of peak rainfall. This chapter describes internal processes in central Vietnamese caves and lastly summarises cave monitoring observations from other cave sites in Southeast Asia. Local rainfall patterns at each cave site are introduced and the potential of speleothem records from these regions is described.

Deborah Limbert and the Oxalis team regularly visited Soong Cave and collected surface and cave

water samples.

3.2 Introduction

The assumption that $\delta^{18}O$ in cave waters reflects the $\delta^{18}O$ signal of meteoric precipitation is fundamental to speleothem-based palaeoclimate studies. However, the coupling between surface precipitation $\delta^{18}O$ and drip water $\delta^{18}O$ remains poorly understood at many locations. Processes within the soil/epikarst zone and inside the cave can alter the isotopic composition of cave waters. For example, the degree of water-mixing prior to carbonate deposition controls the temporal resolution of the climate signal preserved in speleothems. The sensitivity of cave drips to rainfall and the lag response, determines the resolution at which a climate signal can be extracted from speleothems. A fast drip response makes the drip site more sensitive to individual rain events, but increases the background noise in drip rate and $\delta^{18}O$ signal (Mahmud et al., 2018). A lag of several months might allow for thorough mixing of the drip water and a reduction in the noise, but this can also lead to the loss of seasonal dynamics (Breitenbach et al., 2019).

The lag response is mainly controlled by the residence time, which describes the time that water percolates in the epikarst before entering the cave. The flow rate of waters through the cave is determined by the geology of the bedrock. The infiltrating water passes the bedrock either as matrix flow, which describes intra-granular permeability, or as fracture flow, which is water movement along bedding plane partings and joints (Baldini et al., 2006). The relative importance of each flow type determines the residence time of water in the bedrock, and controls the degree of mixing (Baldini et al., 2006; Fairchild and Baker, 2012; Nava-Fernandez et al., 2020). The lag response of a given drip to infiltration can vary from hours to years (e.g. Mawmluh Cave: <1 month (Breitenbach et al., 2015), Golgota Cave: ca. 6 months lag (Mahmud et al., 2018), Soreq Cave: 26-36 years (Kaufman et al., 2003)).

In many tropical regions, caves are characterised by intra-annual changes in water supply, which are dominated by a pronounced rainy season. The air temperature variability is limited throughout the year, but rainfall is strongly seasonal. In these regions, $\delta^{18}O$ in drip water can be biased towards the season of recharge, which is mostly during the wet season (Baker et al., 2019). Consequently, the study suggested that drip water $\delta^{18}O$ in caves, where the mean annual temperature is higher than

16°C, might reflect recharge processes in the karst rather than rainwater δ^{18}O (Baker et al., 2019). Therefore, these results challenge the use of δ^{18}O in tropical speleothems as a proxy for surface precipitation δ^{18}O. This is particularly critical for speleothem-based monsoon reconstructions because the reported proxy records would reflect recharge variability, rather than changes in the monsoon intensity inferred from δ^{18}O of precipitation.

One of the limitations of this study is the lack of any cave monitoring from mainland Southeast Asia (Baker et al., 2019). As a result, it remains unclear whether this region follows a similar pattern. This is crucial because the rainy season in mainland Southeast Asia varies temporally (Misra and Dinapoli, 2014). For example, the seasonal cycle in southern China shows maximum temperature and precipitation during summer, when δ^{18}O values are lowest (Cai and Tian, 2016). In contrast, central Vietnam has its strongest rainfall in autumn when temperatures are lower. This means that secondary evaporation will be less pronounced during the recharge season. Additionally, another cave monitoring study at several cave sites in northern Borneo showed that some tropical regions with all-season rainfall do not follow the proposed pattern, and instead reflect amount-weighted δ^{18}O of surface precipitation (Ellis et al., 2020).

3.3 Cave sites

Stalagmite TD3, which is used for palaeoclimate reconstructions in this PhD work, was sampled from Thien Duong Cave in 2015. Thien Duong Cave is located in the Phong Nha-Ke Bang National Park ca. 60 km from Dong Hoi City (Figure 3.1). For conservation reasons it is not permitted to install cave monitoring devices inside the national park and any related caves. Therefore, monitoring as part of this work was carried out in Soong Cave (Figure 3.1) which is near to the national park (ca. 50 km) and part of the same geological unit.

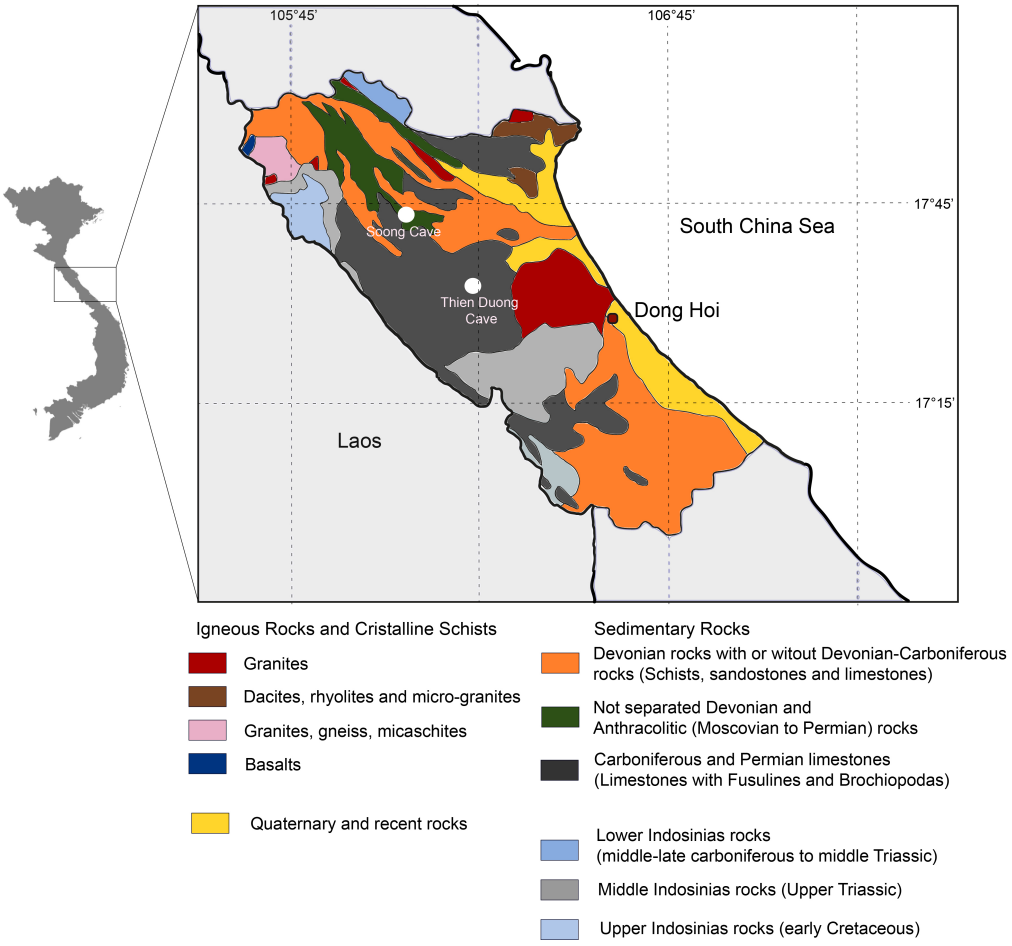

Figure 3.1: Geological map of Quang Binh Province (adapted from Fromaget et al., 1971). White stars indicate the location of Thien Duong Cave, where stalagmite TD3 was collected, and the location of Soong Cave where the cave monitoring was installed. Thien Duong Cave is part of the Phong Nha Caves and Soong Cave is hosted in the Tu Lan Karst Area (Limbert et al., 2020).

3.3.1 Thien Duong Cave

Thien Duong Cave has a length of 31 km with multiple entrances, and is covered by an overburden between 20 to 350 m in thickness (Trinh et al., 2018). Characteristic to the cave is the large volume with a ceiling height of up to 100 m and a width of up to 150 m. Thien Duong Cave lies within partly dolomitized Carboniferous-Permian Limestone (Debevec et al., 2012), and the bedrock surface is smooth but well-fractured with bedding planes visible. Even though it was not possible to install cave monitoring as part of this PhD, few data are available which have been sampled sporadically during spring and summer 2014 to 2016 (Trinh et al., 2018). Based on the GNIP data in Dong Hoi (ca. 50 km from the cave site), the surface air temperature in central Vietnam varies between 30

and 17°C, with a mean annual temperature of 25°C. Cave air temperature in Thien Duong Cave varies between 20 and 22°C. The pCO_2 concentration in the cave ranges between 470 and 1,190 ppm (Trinh et al., 2018), which is in contrast to the highly saturated waters deriving from the soil, with around 3,400 and 1,600 ppm (Trinh et al., 2018). Dripping is still active and new speleothem formation can currently be observed. Sample TD3 was found broken in one of the cave side passages but the original growth position of this sample could not be ascertained precisely.

3.3.2 Soong Cave

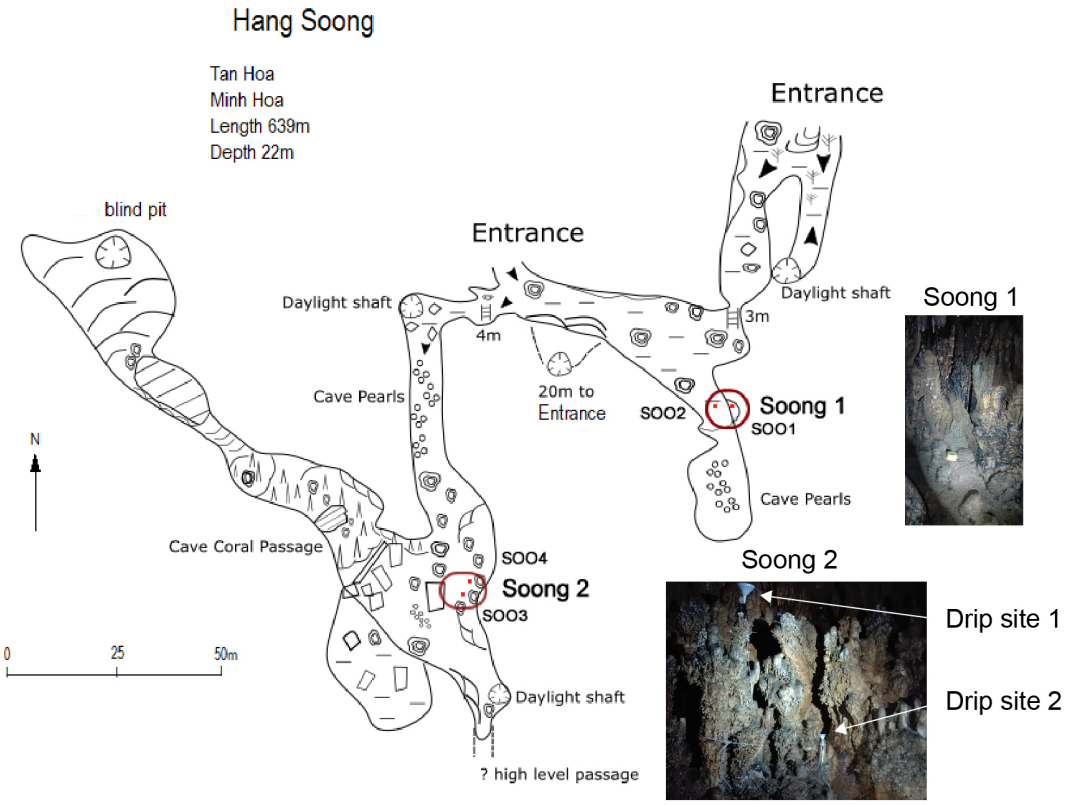

Figure 3.2: Map of Soong Cave (provided by the Oxalis Team), showing the location of monitoring devices in two locations (Soong 1 and Soong 2) marked with a red circle.

Monitoring devices were installed in two locations of Soong Cave (Figure 3.2). A TinyTag Plus 2 (TGP-4017) temperature logger was installed in location Soong 1 (Figure 3.2). Location Soong 2 was chosen for cave environment and water monitoring. One TinyTag Plus 2 (TGP-4017) was used for temperature measurements and both devices recorded data at 15 minutes intervals with a precision of ±0,6 °C. Water collecting devices for water stable isotope measurements

were installed. The devices were plastic canisters with air tight caps, to avoid evaporation during sample collection, which were connected to funnels via plastic tubes (Figure 3.2). A rain gauge (Pluvimate) was installed in Tan Hoa village ca. 2 km from Soong Cave and water was collected at monthly intervals. The cave and rainwater was collected in 4.5 mL glass vials sealed with septum caps. Additionally, the vials were sealed with parafilm and stored in fridges to minimize evaporation.

Cave air temperature in Soong Cave ranges between 23 and 17°C, with the lowest values occurring during boreal winter (December to March). Temperatures are relatively stable between April and November.

3.4 Rainwater analysis

Water samples were prepared for stable isotopes analysis by transfer into 1.5 mL glass vials sealed with PTFE septum caps. Samples containing cave material, such as clay particles, were filtered beforehand. Isotope measurements were performed on a Los Gatos Research LWIA-24EP liquid water isotope analyser (model 912-0050) coupled with a LC PAL AutoInjector. A full set of standards were run at the beginning and end of each ran, and a standard was measured after every 5^{th} sample. Each sample is injected eight times for high precision and vaporised immediately by injection from a 1.2 µL Hamilton syringe and injection port was heated to 80°C. Then, the resulting vapour was transferred into the pre-evacuated high-reflectivity mirror chamber, where laser absorption is measured. The precision is 0.2 ‰ for δ^2H, 0.03 ‰ for δ^{17}O and 0.03 ‰ for δ^{18}O. Results are reported against Vienna Standard Mean Ocean Water (VSMOW). The reference material used is listed in table 3.1.

Table 3.1: Reference material and values used for water stable isotope measurements.

Name	δ^2**H**	δ^{18}**O**	δ^{17}**O**
lgr1e	-165.7	-21.28	-11.26
lgr2e	-123.8	-16.71	-8.79
lgr3e	-79.6	-11.04	-5.83
lgr4e	-49.2	-7.81	-4.12
lgr5e	-9.9	-2.99	-1.52

In order to estimate the effect of the precipitation amount on δ^{18}O in rainfall close to the cave, the GNIP data from Dong Hoi station was used. It should be noted that the two time series, δ^{18}O from

Dong Hoi and drip water δ^{18}O from Soong Cave, were collected in different years. Therefore, δ^{18}O is normalised relative to precipitation as follows: $\delta^{18}O_{month}$ x $\frac{P_{month}}{P_{annual}}$

Where $\delta^{18}O_{month}$ and P_{month} refers to the monthly δ^{18}O values and monthly precipitation amount respectively. P_{annual} describes the annual total precipitation amount for each year. The results were averaged for the years 2014 to 2017.

3.5 Drip water stable isotopes

Rainwater isotopes in central Vietnam show a strong seasonal cycle and interannual variability, mainly related to moisture source effects and changes in the large-scale circulation (Chapter 2). However, the climate signal of rainwater δ^{18}O is not necessarily transferred directly into the speleothem carbonate (Baker et al., 2019). In order to estimate the lag time in Soong Cave, rain water and cave water stable isotopes are used for an investigation of the surface climate signal transfer (Figure 3.3). Rainwater isotopes range between -0.15 and -12 ‰ for δ^{18}O and between -90 to 10.2 ‰ for δ^{2}H, whereas the cave water isotopic composition has a reduced amplitude of -7.3 to -1.3 ‰ for δ^{18}O and -44.7 to -1.8 ‰ for δ^{2}H (Figure 3.3). The local drip water line is δ^{2}H $= (8.5 \pm 0.99$ ‰$) \times \delta^{18}$O + $(11 \pm 6.5$ ‰$)$ with an r^2 of 0.96, which is similar to the GMWL and suggests the limited influence of secondary evaporation (Dansgaard, 1964; Merlivat and Jouzel, 1979). The local drip water line closely resembles the local meteoric water line calculated in Chapter 2: $\delta^{2}H = (8.6 \pm 0.3$ ‰$) \times \delta^{18}$O + $(15 \pm 2$ ‰$)$, further suggesting that evaporation is limited in Soong Cave.

A recent study by Limbert et al. (2020) analysed groundwater samples collected in February 2016 in Phong Nha-Ke Bang and Tu Lan Karst Area, finding a range of -7.44 and -5.02 ‰ for δ^{18}O, and -43.7 and -20.5 ‰ for δ^{2}H. This contrasts with drip waters from Soong Cave collected during January and December 2019 and March 2020, with an average δ^{18}O of -3.7 ‰. Minimum drip water δ^{18}O values coincide with low amount-normalized δ^{18}O values at Dong Hoi station. A positive correlation between amount-normalized δ^{18}O and drip water δ^{18}O of r=0.78 (p-value=0.0045) further hints at a response of drip water δ^{18}O to δ^{18}O in surface precipitation, if the amount of precipitation is considered (Figure 3.3).

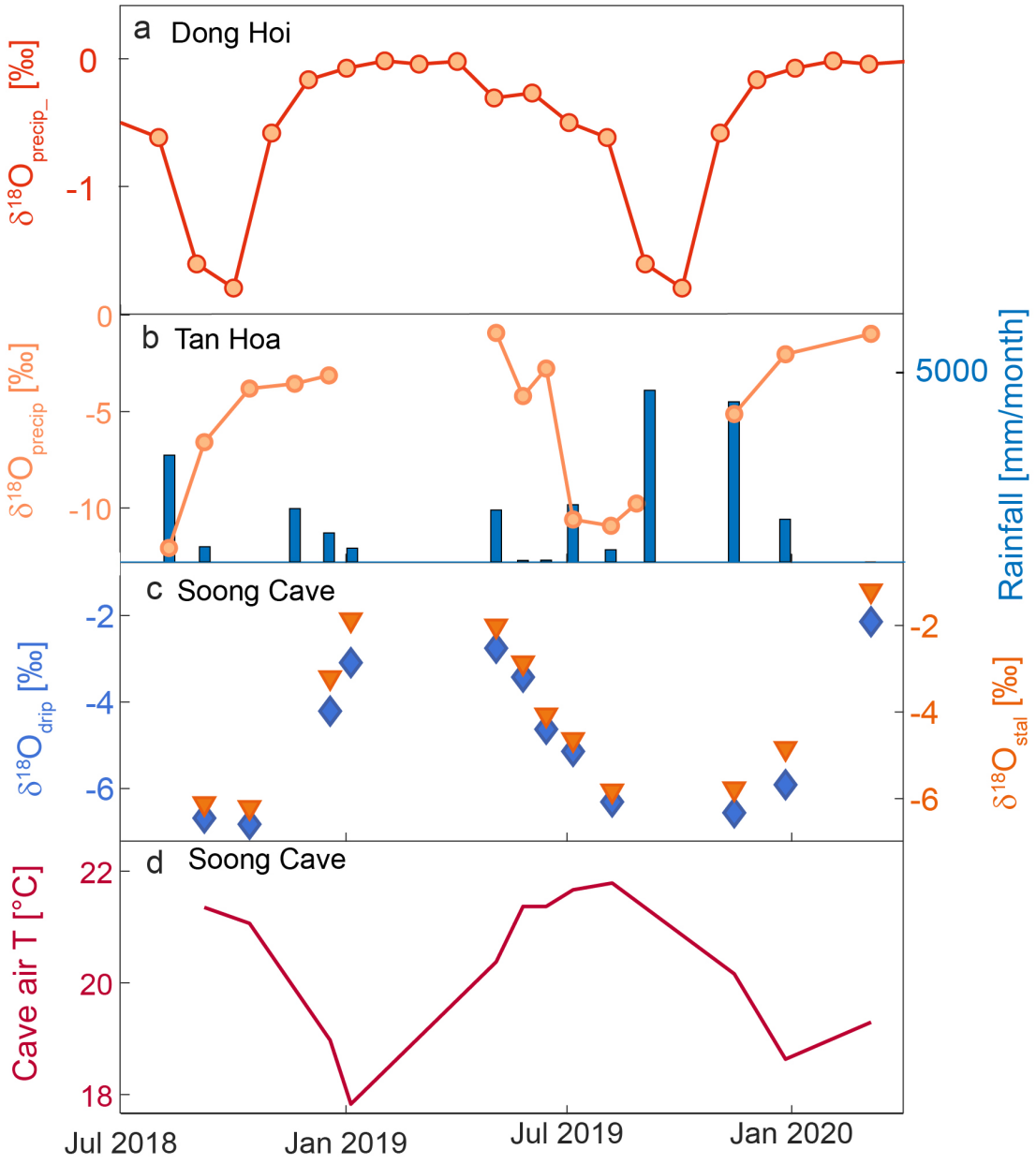

Figure 3.3: **a** Amount-normalized δ^{18}O calculated from GNIP data at Dong Hoi station. This time series shows the monthly mean for the years 2014 to 2017. **b** δ^{18}O values for surface precipitation (circles) and surface rainfall amount (bar plot), collected at Tan Hoa village, near Soong Cave. **c** drip waters (blue diamonds) and calculated δ^{18}O values estimating the δ^{18}O of associated carbonate (orange triangles). Drip water δ^{18}O is the mean of two simultaneously collected waters at drip sites 1 and 2, in location Soong 2 (Figure 3.2 bottom picture). **d** Monthly mean cave air temperature at drip site 1, used to calculate the δ^{18}O of carbonates.

The bias in low δ^{18}O values towards the season of strongest precipitation is also evident from the deuterium excess. For the surface precipitation at Dong Hoi and Tan Hoa village, the lowest values occur during the summer months, from June to August (Figure 3.4). The colour-coded δ^{2}H

vs δ^{18}O plot shows that the lowest values in drip water occur from September to November 3.5. Autumn is the time of highest rainfall in central Vietnam.

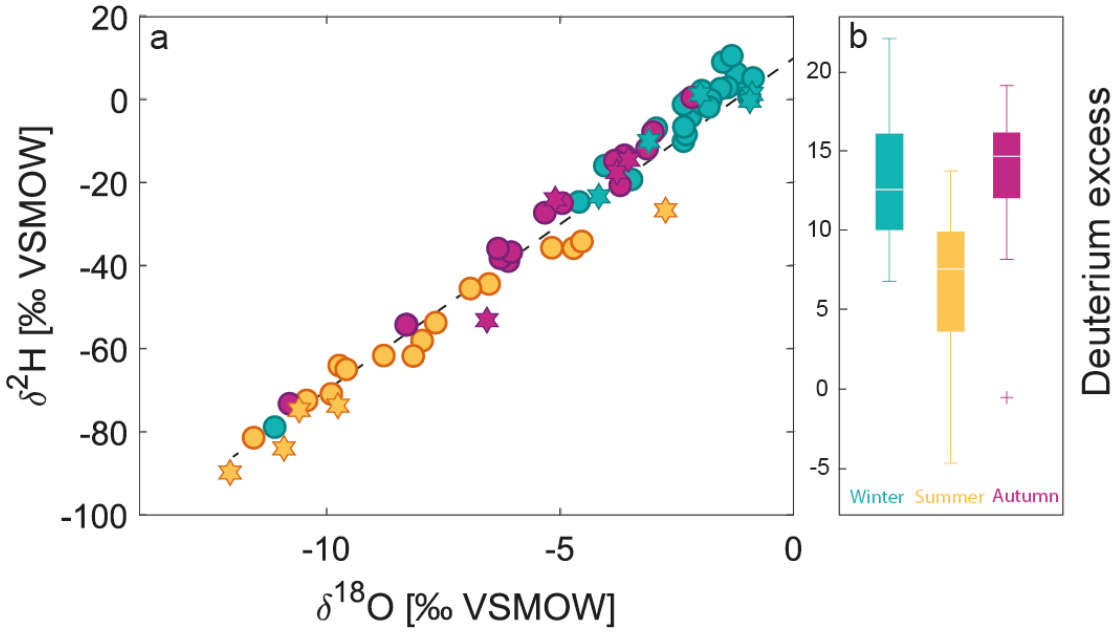

Figure 3.4: **a** δ^{2}H vs δ^{18}O plot of GNIP (large circles) and collected rainwaters (stars) in Tan Hoa village. **b** Box-and-wishers plot of the deuterium excess colour-coded according to each season. Winter is from December to May, summer from June to August, and autumn from September to November. Dashed line indicates the LMWL.

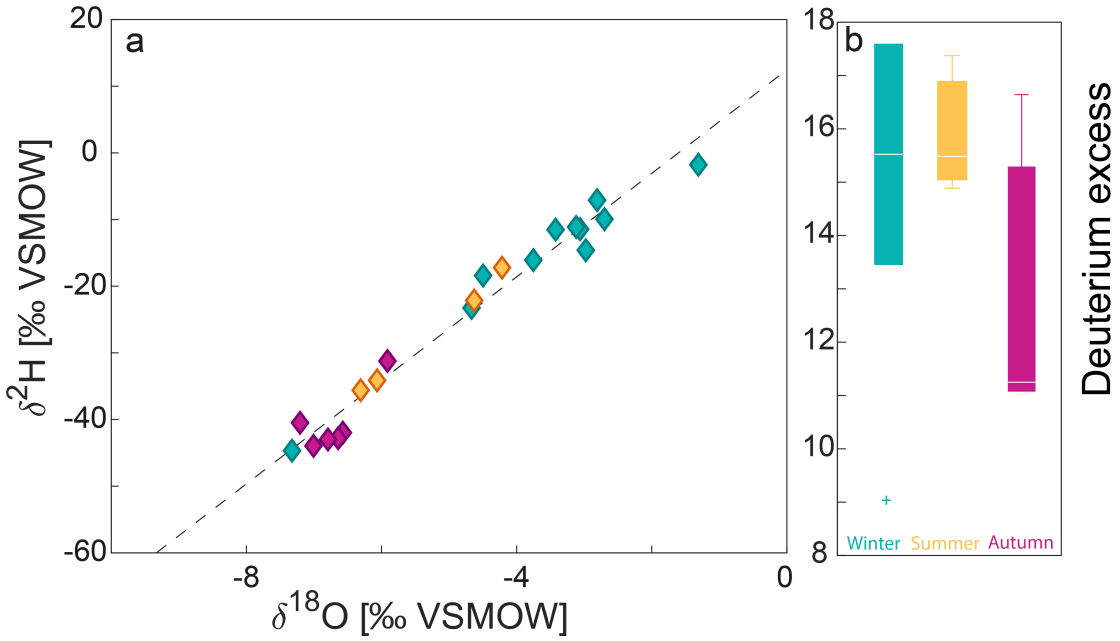

Figure 3.5: **a** δ^{2}H vs δ^{18}O plot of drip waters, colour-coded per season, as in Figure 3.4. **b** Box-and-wishers plot of the deuterium excess, colour-coded according to each season. **a** Shows values for each individual drip, where as **b** was calculated from the mean of simultaneously sampled drip waters. Dashed line indicates the local drip water line.

A fast response between rainfall and drip waters is not the only limiting processes within a cave environment. Isotopic fractionation can also occur during carbonate precipitation and alter the isotopic signal of a speleothem. The seasonal amplitude of the drip water is about -6 ‰ compared to -12 ‰ in rainwater. Oxygen isotope fractionation during carbonate formation is approximately -0.24 ‰ at 25°C (McDermott, 2004). Figure 3.3b shows the estimated offset between drip water δ^{18}O and δ^{18}O in an associated carbonate, following Tremaine et al. (2011). Isotopic fractionation is stronger (-0.981) when cave air temperature is low (18°C) and weaker (-0.242) when temperatures are higher (21°C). However, the temperature dependent fractionation is negligible compared to the seasonal cycle in δ^{18}O (Figure 3.3c). These calculations are based on the assumption that isotopic fractionation occurred under equilibrium conditions. However, there is also a potential for non-equilibrium or kinetic fractionation to occur in Soong Cave. The large seasonal differences in cave air temperature or fast carbonate precipitation rates, which might occur during the rainy season, could lead to kinetic fractionation. Further monitoring is need to determine if or to what degree kinetic fractionation controls the isotopic composition of cave water in Soong Cave.

3.6 Conclusion

δ^{18}O in rainfall from central Vietnam shows a pronounced seasonal cycle and interannual variability (Chapter 2), and this chapter investigates the transfer mechanisms of rainwater into Soong Cave drip waters. It is found that the seasonal cycle in rainwater isotopes is transferred into the drip water, but the δ^{18}O signal is likely biased towards the rainy season. The reduced amplitude in drip water isotopes suggests that some mixing of existing and newly arriving rainwaters occurs in the karst system. The temperature-controlled isotopic fractionation occurring during speleothem deposition has a limited effect on the resulting speleothems δ^{18}O, and the amplitude of the seasonal signal is much larger than the temperature-dependent fractionation. Therefore, δ^{18}O proxy records based on stalagmites from Soong Cave and other caves in the region can be used for palaeoclimate reconstructions with an annual and lower resolution. However, δ^{18}O in the stalagmite likely reflects δ^{18}O of precipitation with a bias towards the rainy season. Consequently, carbonate δ^{18}O can be a proxy for both, the local hydrology and the δ^{18}O signal in rainfall.

3.7 Caves in Southeast Asia

In the following section, local climate and cave internal processes are outlined for cave sites within Southeast Asia which have speleothems records covering the Holocene. The climate in Southeast Asia is characterised by temporally and spatially diverse seasonal rainfalls driven by complex interactions between the monsoonal circulation, movements of the ITCZ, ENSO, the IOD, and local topography (Misra and Dinapoli, 2014; Wu and Hsu, 2016). For mainland Southeast Asia, these interacting processes create the longest wet season within Asia and the strongest interannual variability in the length of the rainy season (Misra and Dinapoli, 2014). Due to the spatial variability of the on and offset of the rainy season, it is important to understand the local climate at each cave site. In particular, the source region for rainfall needs to be identified because the timing of seasonal rainfalls in this region does not reflect the association with a monsoon system. For example, the October rainfalls in central Vietnam are related to the Northeast (Winter) Monsoon, but October rainfalls in Sumatra are related to the Southwest (Summer) Monsoon. Thus far, there are six speleothem records covering the Holocene available from Southeast Asia (Figure 3.6).

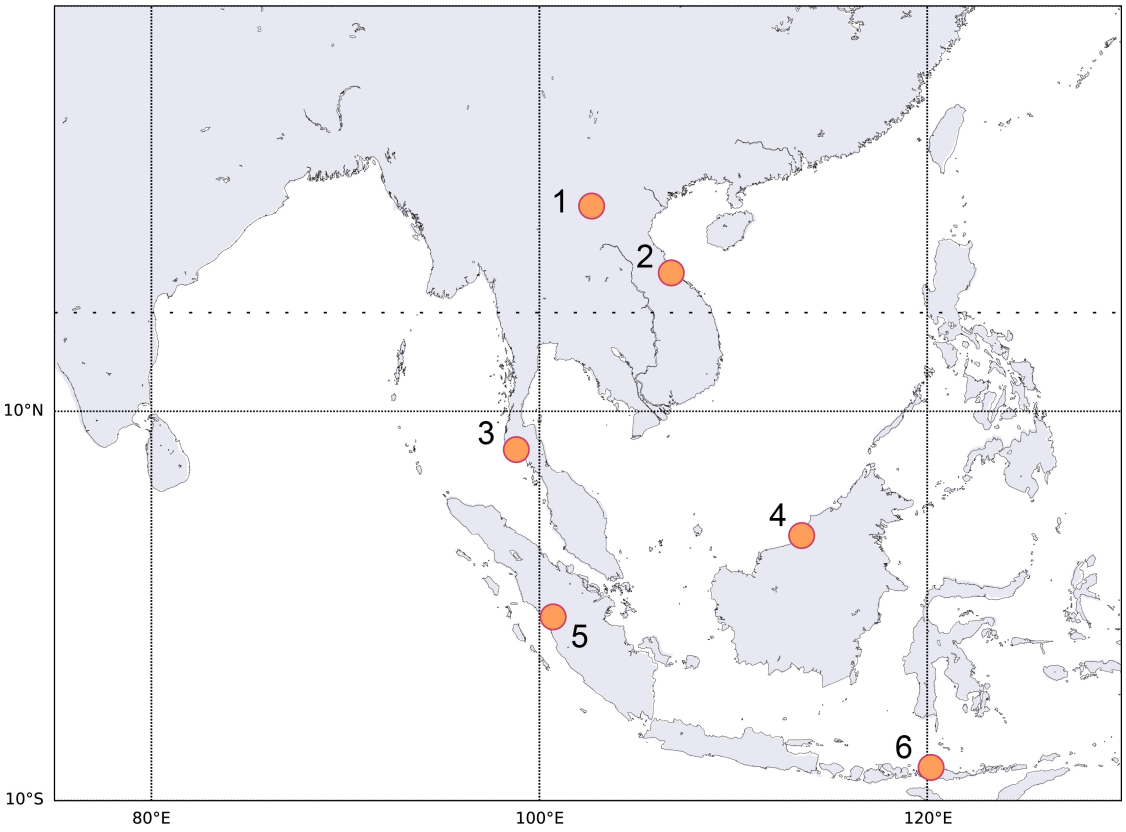

Figure 3.6: Map showing cave site with available speleothem records in Southeast Asia, covering the Holocene. **1** Tham Mai Cave in Laos, **2** Thien Duong Cave in Vietnam, **3** Klang Cave in Thailand, **4** Bukit Assam Cave in Borneo, Tangga Cave in Sumatra and **5** Liang Luar Cave in Flores, Indonesia.

3.7.1 Tham Mai Cave

Tham Mai Cave (20.75°N, 102.65°E) is located in northern Laos and receives most rainfall (67%) during the summer monsoon season (Figure 3.7a). This rainfall is sourced from the western Indian Ocean and related to the strength of the Southwest Monsoon (Wang et al., 2019). δ^{18}O in rainfall at Tham Mai Cave mirrors upstream rainout over the Indian Ocean and Indo-Pacific Warm Pool, and meteorological conditions in the equatorial Indian Ocean (Yang et al., 2016). Therefore, δ^{18}O in northern Laos can reflect increased moisture pathways (distal versus proximal) in the Indian Ocean, and increased rainout due to the Indian Summer Monsoon. ENSO is a controlling mechanism of interannual variability in δ^{18}O via moisture source variability, and leads to increased δ^{18}O values during El Niño, the opposite occurs during La Niña. This effect appears to be amplified by the IOD (Yang et al., 2016).

3.7.2 Thien Duong Cave

Thien Duong Cave receives most rainfall during autumn (Figure 3.7b). This rainfall is mainly sourced from the South China Sea and western Pacific, related to the Northeast Monsoon circulation. Local rainfall is modulated by the seasonal migration of the ITCZ, and interannual variability of rainfall amount is associated with ENSO (Chen et al., 2012a; Vu et al., 2015). As shown in Chapter 2, δ^{18}O in rainfall of central Vietnam is controlled by the relative contribution of moisture from the Indian versus Pacific Ocean (Wolf et al., 2020). The timing of ITCZ withdrawal and ENSO influence the interannual variability of δ^{18}O via moisture source dynamics. However, based on the observation of drip waters in a cave nearby it is likely that δ^{18}O in TD3 reflects local hydrological processes as well as the δ^{18}O signal of rainfall.

3.7.3 Klang Cave

Klang Cave (8.20°N, 98.44°E) is located in southern Thailand and most rainfall falls from May to October (Figure 3.7c). This rainfall is linked to the Southwest Monsoon, and 75% of the annual rainfall is sourced from the Indian Ocean (Tan et al., 2019a). The Northeast Monsoon delivers moisture from the South China Sea and western Pacific during the remaining time (November to April). While ENSO and the IOD were found to have limited effects on summer monsoonal rainfall in southern Thailand, the effects of ENSO and the IOD on rainfall amount from December to February are significant (Bridhikitti, 2012). Tan et al. (2019a) argues that δ^{18}O in rainfall in southern Thailand reflects the amount effect in the northern central Indo-Pacific, based on observations from the Bangkok GNIP station.

3.7.4 Bukit Assam Cave

Bukit Assam Cave is located in the Gunung Buda National Park in Malaysia, Borneo (4°N, 114°E), which lies within the core region of the ITCZ (Cobb et al., 2007). Rainfall falls year-round with limited seasonality (Figure 3.7d), although a minor increase in rainfall is observed between September and December and in late spring, from April to May (Cobb et al., 2007). The general circulation over Borneo shows strong seasonality with southwesterly monsoonal winds during summer, and northeasterly monsoonal winds during autumn/winter (Cobb et al., 2007; Moerman et al., 2013). Generally, 67% of the moisture arrives from the western Pacific and Sulu Sea, and

31% are sourced west of Borneo in the Karimata Strait and Java Sea (Wurtzel et al., 2017). The interannual variability of rainfall in northern Borneo is strongly controlled by ENSO, leading to increased rainfall during La Niña and decreased rainfall during El Niño events. Rainfall amount is affected throughout all seasons, but with the strongest effects on autumn and winter precipitation (Cobb et al., 2007). Monitoring studies found that rainfall δ^{18}O in northern Borneo is representative of regional convective activity, with ENSO events explaining about 40% of the variance in δ^{18}O (Moerman et al., 2013).

3.7.5 Tangga Cave

Tangga Cave (0.36°S, 100.76°E) is located in central West Sumatra, Indonesia, bordering the western edge of the Indo-Pacific Warm Pool (Wurtzel et al., 2018). Local rainfall falls year-round, with a minimum during boreal summer (Figure 3.7e) when the ITCZ lies at its northernmost location. Around 70% of the annual rainfall is sourced from the equatorial Indian Ocean, and 30% of rainfall are related to the Indo-Austral and Asian summer monsoon. Due to the proximity to the Indian Ocean, the IOD is one of the main drivers of interannual variability (Wurtzel et al., 2017), with a positive IOD reducing rainfall by 33%. ENSO plays only a minor role and no significant influence on rainfall variability was found at Tangga Cave (Wurtzel et al., 2018). δ^{18}O in rainfall has been explained by the relative contribution from the Indian Ocean versus the South China Sea, and an extended moisture transport from more distal locations within the Indian Ocean (Wurtzel et al., 2017).

3.7.6 Liang Luar Cave

Liang Luar Cave (8.32°S, 120.26°E), located on Flores Island, Indonesia, lies at the southerly limit of the ITCZ during boreal winter, and 70% of the annual rainfall occurs during the Indo-Australian summer monsoon (Griffiths et al., 2009) (Figure 3.7f). This rainfall is mainly sourced from the southern South China Sea, where the remaining portion of annual rainfall is sourced by easterly trade winds north of Australia and from the southern Indian Ocean (Griffiths et al., 2009; Wurtzel et al., 2017). δ^{18}O reflects the relative contribution of moisture from each source and has thus been linked to the strength of the Indo-Australian summer monsoon (Griffiths et al., 2009). Furthermore, it was suggested, that ENSO and the IOD might be controlling factors on an interannual scale.

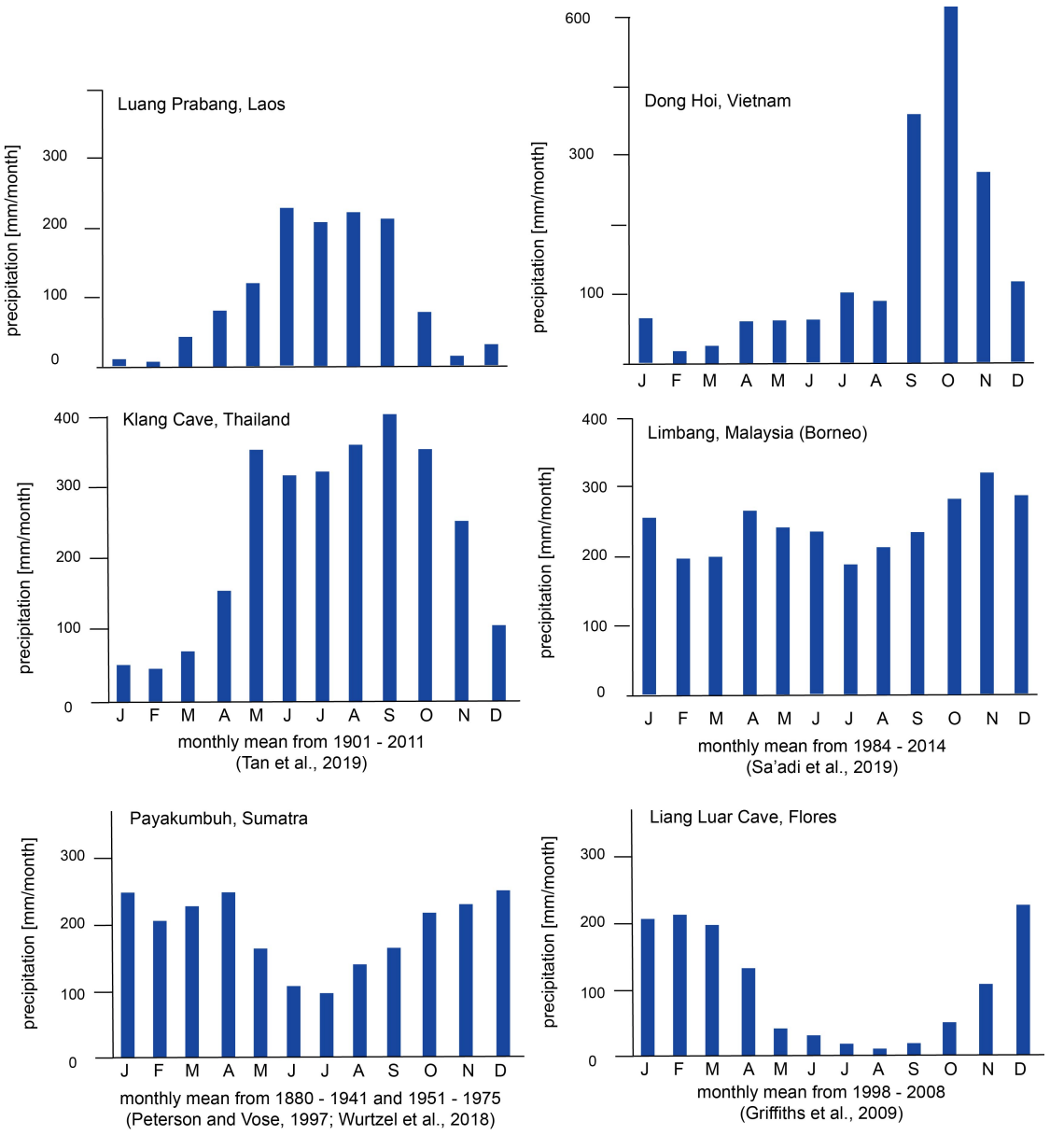

Figure 3.7: Multi-average monthly rainfall distribution at **a** GNIP data from Luang Prabang Station, close to Tham Mai Cave, **b** GNIP data from Dong Hoi station, close to Thien Duong Cave, **c** at Klang Cave (Tan et al., 2019a), **d** at Limbamg close to Bukit Assam Cave (Saadi et al., 2019), **e** at Payakumbuh close to Tangga Cave (Peterson and Vose, 1997; Wurtzel et al., 2017) and **f** at Liang Luar Cave (Griffiths et al., 2009).

Chapter 4

General Methodology

This chapter summarises the methodology used for results presented in Chapter 5, Chapter 6 and Chapter 7. Each chapter has additional methods which are further explained in the individual chapters.

The dating of stalagmite TD3 was conducted by David McGee, the laser ablation ICP-MS was done by Amanda French and the IRMS measurements, in part, by Stefano Bernasconi and Madalina Jaggi (see Chapter 1 for details).

4.1 Analytical methods

4.1.1 Speleothem sampling

Stalagmite TD3 was cut in half along the growth axis with a saw blade of 1.5 mm thickness and both halves were polished. The halves were used for drilling powder subsamples, with the high-resolution records and U-Th dating samples on one half and low-resolution stable isotopes on the other half (Figure 4.1). Powder samples were taken in 50 μm steps for the high-resolution record in a continuing trench (Figure 4.1). For the low-resolution record samples were drilled in 1 mm steps, creating discrete punctures. Samples were drilled concordant to layering using a Sherline2010 computer-controlled micromill with stainless steel tungsten carbide drill bits, with a 0.5 mm diameter. Every 10 samples notes were scratched into the stalagmites with a scalpel to allow for spatial referencing of the sample depth later on.

20 Samples for U-Th dating, with an average of 2 mg per sample were taken from TD3. 10 of these samples were drilled by hand drill and the samples were taken prior to any subsampling to establish an initial age model. 10 were drilled in the remaining trench after subsampling for stable isotopes, using the Sherline micro mill. This approach assures that U-Th ages are located as close as possible to the subsamples for stable isotope analysis. Between each sample the drill bit was cleaned with compressed air and weak hydrochloric acid to avoid cross contamination.

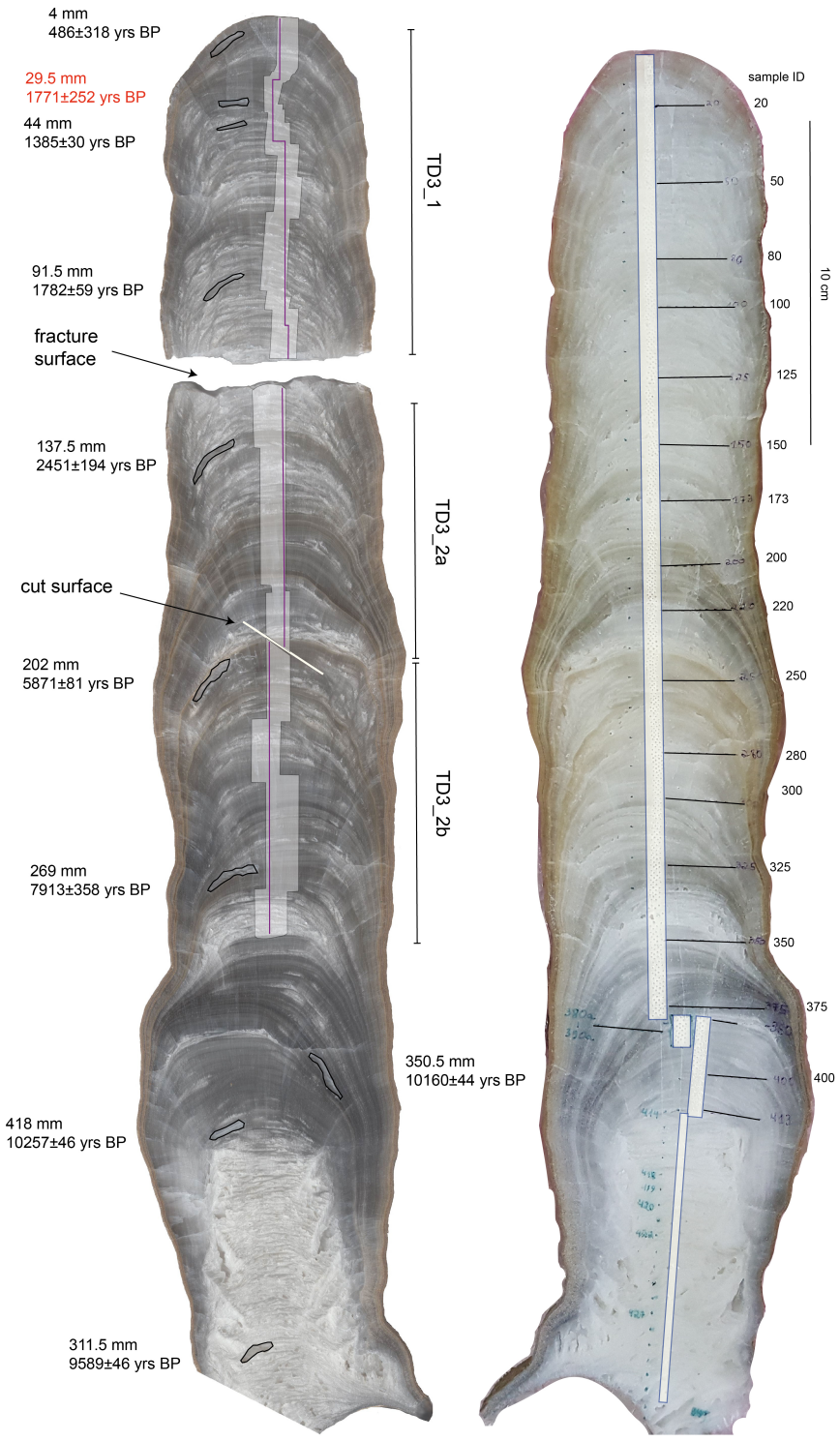

Figure 4.1: Scan of stalagmite TD3 with the location of drilled samples for the initial U-Th dating, distance from top and age including 2σ error. White lines shows the micromilled tracks and the purple line indicates the laser track. TD3 was cut (TD3_2a and TD3_2b) to fit on the sample holder for trace elemental analysis.

4.1.2 Stable isotopes in stalagmites

In total 371 low-resolution and 853 high-resolution samples were drilled and analysed. Carbonate stable isotope analyses were performed using a Delta V Advantage isotope ratio mass spectrometer (IRMS) (ThermoFisherScientific) interfaced with a GasBench II and a CTC GC PAL autosampler at ETH in Zurich (high-resolution) and Northumbria University (low-resolution). Dual in-let and continuous-flow systems are widely used for stable isotope analysis due to their high precision, rapid working speed and requirement of small sample amounts (50-100 μg) (Spötl and Vennemann, 2003; Breitenbach and Bernasconi, 2011). Results were normalized against the international NBS 18 and NBS 19 standards and in-house standard Wiley. Results are reported in respect to Vienna Pee Dee Belemnite (VPDB) [‰] using the conventional delta notation: $\delta^{18}O/\delta^{13}C = (R_{sample} - R_{standard})/R_{standard}$ with $R = ([^{18}O])/([^{16}O])$ or $R = ([^{13}C])/([^{12}C])$; (Brand and Coplen, 2012).

4.1.3 Mineral determination

Fourier-transform infrared spectroscopy (FTIR) was used to determine speleothem mineralogy at Northumbria University, Newcastle. The FTIR emits infrared radiation onto a sample to determine the structural properties of minerals. Certain wavelengths of the radiation are absorbed by the sample, whereas the remains are reflected into the instrument. This reflected signal is detected as a spectrum representing a molecular structure of the sample. 3 mg of stalagmite powder was analysed on a PerkinElmer Spectrum RX I FTIR over a spectrum of 640-4200 cm^{-1} with 32 replications. The detection limit was about 5 wt% and the measurement had a precision of approximately $\pm$10% and the resolution is 0.8 cm^{-1}. Before each run the background spectrum was measured and automatically subtracted from the sample spectrum. Three samples of stalagmite TD3 were analysed (Figure 4.2) and show a typical calcite FTIR spectrum (Chakrabarty and Mahapatra, 1999), with pronounced peaks at 712 cm^{-1} and 872 cm^{-1}.

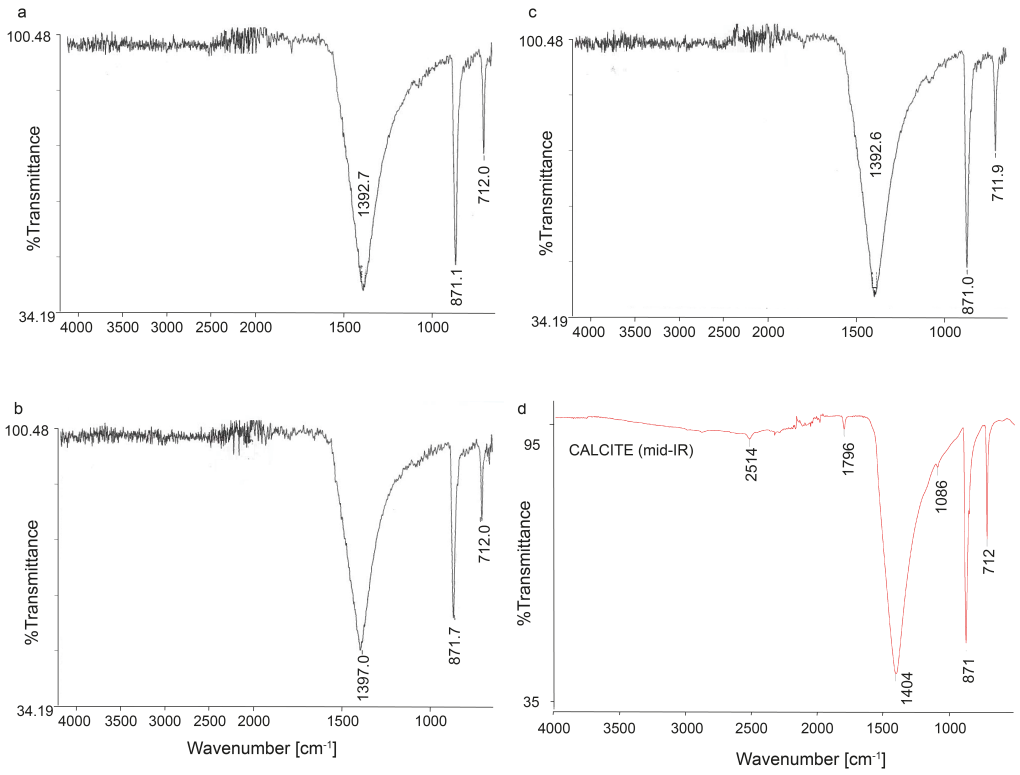

Figure 4.2: FTIR spectra of TD3 samples **a**, **b** and **c** in comparison to a typical calcite spectrum **d** from the database of ATR FTIR spectra of various materials at http://lisa.chem.ut.ee/IR_spectra/paint/fillers/calcite/ (Vahur et al., 2016).

4.1.4 Trace elements

Trace element measurements were made using a RESOlution-SE Compact 193nm excimer laser ablation (LA) system in tandem with an Agilent 8900 Inductively Coupled Plasma Mass Spectrometer (ICP-MS) at the Waikato University, New Zealand. Analyses are conducted by pulsing the laser at 15 Hz with a 50 μm spot size and energy density of 5 J/cm^2 at a scan speed of 26.118 μm/s. The laser measured inside the milled track to ensure that stable isotope and trace elemental data have the same depth-age relation. Ultra-high purity helium is used as the carrier gas to deliver the ablated sample from the LA system to the ICP-MS. The ICP-MS is optimised to maximum sensitivity daily (Table 4.1). Background counts (gas background, measured with the laser off) are collected for 40 seconds between samples. NIST glass standards (610, 612) are analysed after each sample track to account for any instrument drift. Data processing is performed using Iolite (v3.32; (Paton et al., 2011)). Background counts are subtracted from the raw data and all data are standardised to NIST 612 glass. NIST 610 glass is utilized as a secondary standard. GeoReM

database (Jochum et al., 2005) is utilized for NIST glass values.

Table 4.1: LA-ICP-MS parameters for trace elemental analysis.

ICP-MS Conditions	
Forward (reflected) power [watt]	1550
Gas flows [L/min]	
Plasma	15 (Ar)
Auxiliary	0.90
Carrier	1.05
Sampling Depth [mm]	4.0
Detector mode	Pulse counting
Sweep mode	Peak hopping
Dwell time [s]	0.01 - 0.1
Points per peak	1

4.1.5 Uranium-Thorium dating

The dating was conducted on a Nu Plasma II-ES MC-ICP-MS at Massachusetts Institute of Technology, USA. Reported errors for ^{238}U and ^{232}Th concentrations are estimated to be $\pm$1% due to uncertainties in spike concentration and analytical uncertainties are smaller. Ages were corrected for detrital ^{230}Th assuming an initial ^{230}Th/^{232}Th of (4.4$\pm$2.2) $\times$ 10^{-6}, which is the initial ^{230}Th/^{232}Th ratio in most crustal materials (Wedepohl, 1995), and the age was reported as before present, where the present is defined as 1950 C.E (Table 4.2). Decay constants for ^{230}Th and ^{234}U were taken from Cheng et al. (2013), with a decay constant for ^{238}U of 1.55125 $\times$ 10^{-10} yr^{-1} (Jaffey et al., 1971).

4.2 Statistical analysis

4.2.1 Depth-age modelling

The depth-age model for TD3 is based on 20 U-Th dates, of which five samples were excluded from the age modelling (Figure 4.3). Samples with an age correction of more than 200 years have been excluded.

Table 4.2: Summary of U-Th dating results. Dates with a $^{230}Th/^{232}Th$ ratio below 60 ppm have been excluded from the age model

Sample ID	Distance from top [mm]	^{238}U [ng/g]	$\pm(2\sigma)$	^{232}Th [pg/g]	$\pm(2\sigma)$	$\delta^{234}U$ [‰]	$\pm(2\sigma)$	$(^{230}Th/^{238}U)$ activity	$\pm(2\sigma)$
TD3_1_U7	0.9	158.0	3.2	733.9	14.7	51.5	3.7	0.011653725	0.000143
VM-1	3.5	265	5	2132	43	51.51	0.83	0.01138	0.00013
TD3_1_U8	8.7	204.3	4.1	234.4	4.7	50.6	1.9	0.010655254	0.000123
3-V1-Top	30.3	206	4	1317	26	52.59	1.57	0.02234	0.00018
TD3-4.4cm	43.5	201	4	86	3	53	4	0.01427	0.00023
TD3_1_U9	71.5	218.8	4.4	151.3	3.1	53.9	1.9	0.016135806	0.000138
VM-2	93	372	7	543	11	54.88	0.68	0.01882	0.00015
TD3_1_U10	112.5	269.1	5.4	133.4	2.7	54.8	1.6	0.018808099	0.00014
TD3_2a_U5	131.1	272.2	5.4	111.3	2.3	56.2	1.7	0.019863826	0.000159
VM-3	139.3	277	6	1378	28	63.35	0.69	0.02795	0.00019
TD3_2a_U1	165.2	201.9	4.0	908.9	18.2	50.1	1.8	0.032625833	0.000212
TD3_2a_U2	181.2	249.3	5.0	775.7	15.6	58.9	1.5	0.043315095	0.00025
VM-4	204.2	189	4	366	7	63.4	0.69	0.05778	0.00027
TD3_2b_U3	219.4	220.8	4.4	309.4	6.2	60.9	1.6	0.063661025	0.000386
TD3_2b_U3B	233.7	204.2	4.1	264.1	5.3	60.3	1.6	0.065639409	0.000339
TD3_2b_U4	250.9	339.8	6.8	16.0	0.5	55.2	1.4	0.067799862	0.000266
VM-5	269	221	4	2004	40	55.78	0.77	0.08092	0.00034
TD3_2b_U6	279.6	229.5	4.6	62.2	1.3	63.6	1.8	0.08170932	0.00034
VM-6	311.5	228	5	41	1	72.55	0.93	0.0911	0.0004
2-V1-Bottom-1	350.5	323	6	62	2	77.34	1.36	0.09667	0.00037
1-V1-Bottom	418	422	8	235	5	79.76	1.13	0.09802	0.00044

$^{230}Th/^{232}Th$ [ppm atomic]	±(2σ)	Age (uncorr) [yr]	±(2σ)	Age (corr) [yr]	±(2σ)	$\delta^{234}U$ init [‰]	±(2σ)	Age (corr) [yr BP]	±(2σ)
39.8	0.5	1215	16	1082	69	52	4	1011	69
22.4	0.3	1186	14	954	117	52	1	888	117
147.4	1.7	1111	13	1078	21	51	2	1007	21
55.5	0.5	2339	19	2155	94	53	2	2089	94
531	17	1487	25	1475	25	53	4	1406	25
370.4	3.3	1682	15	1662	18	54	2	1591	18
204.8	1.6	1963	15	1921	26	55	1	1855	26
602.3	5.0	1962	15	1948	17	55	2	1876	17
771.2	6.6	2070	17	2058	18	57	2	1987	18
89.3	0.6	2904	20	2763	73	64	1	2696	73
115.1	0.7	3441	23	3311	69	51	2	3240	69
221.1	1.3	4552	28	4464	52	60	2	4393	52
473	2.3	6089	29	6034	40	64	1	5967	40
721.3	4.5	6744	43	6705	48	62	2	6634	48
805.7	4.2	6964	39	6928	43	62	2	6856	43
22893.2	462.5	7238	31	7236	31	56	1	7165	31
141.5	0.6	8690	39	8430	136	57	1	8364	136
4784.9	29.5	8710	41	8702	41	65	2	8631	41
8092.7	123.3	9670	45	9665	45	75	1	9598	45
8002.9	134.8	10241	43	10235	43	80	1	10169	43
2792.1	15.7	10366	50	10350	50	82	1	10284	50

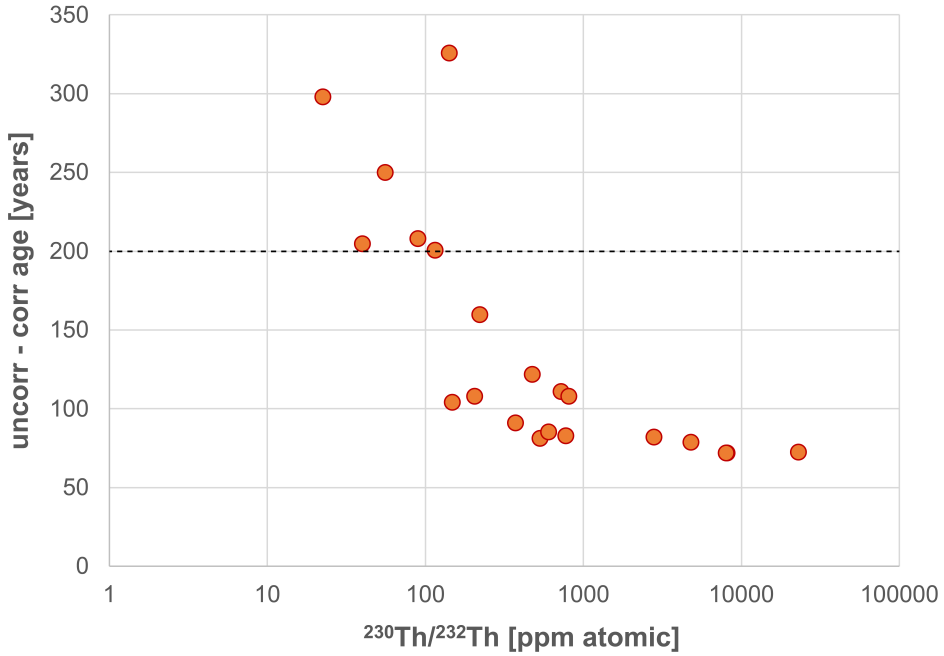

Figure 4.3: Relation between the $^{230}Th/^{232}Th$ ratio and the age correction. Ages plotting above the line have been excluded from the age model, due to the large age correction. $^{230}Th/^{232}Th$ ratio is plotted on a logarithmic scale.

The depth-age model is constructed using 2000 Monte-Carlo simulations and cubic interpolation in COPRA (Figure 4.4a). COPRA anchors proxy values to time values, considering the age uncertainty and calculates the proxy confidence limits for each time step (Breitenbach et al., 2012). Based on the U-Th dates, the growth rate was calculated (Figure 4.4b).

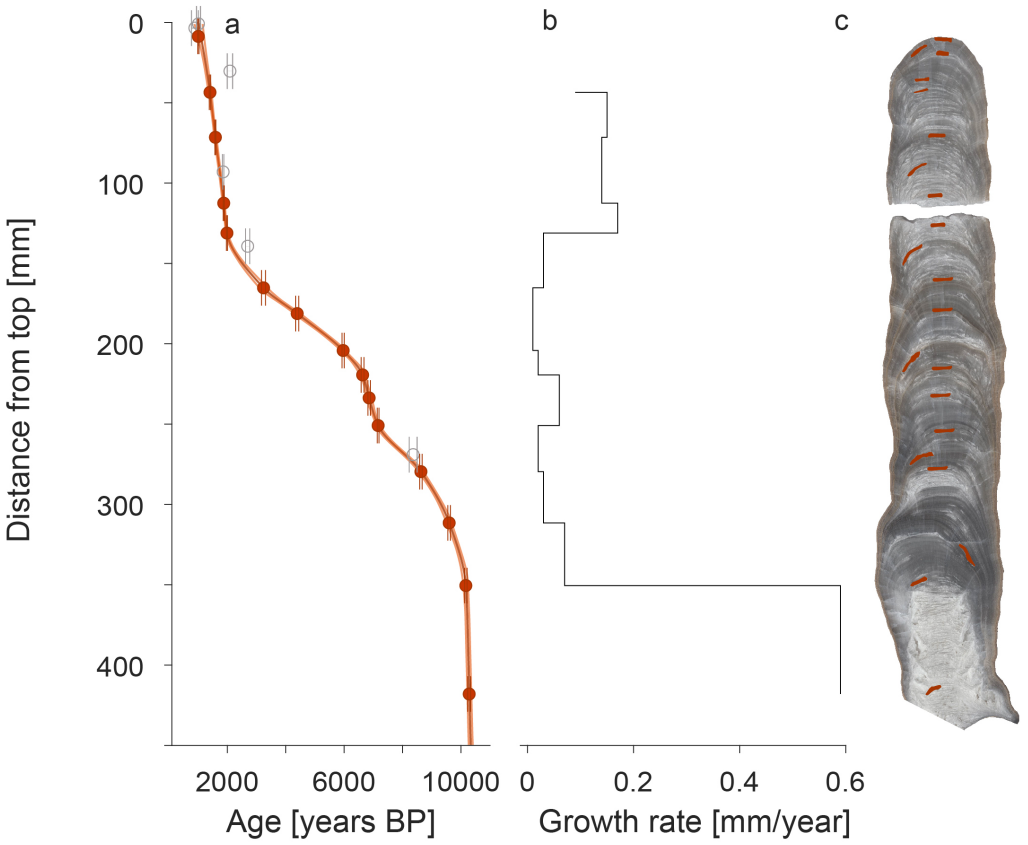

Figure 4.4: **a** Depth-age model of TD3 reconstructed with COPRA. The line plot shows the mean age, including the 95% confidence intervals. Dots mark U-Th dates including the age uncertainty as error bars. Grey dates have been excluded from the age model. **b** shows changes in growth rate calculated from the U-Th dates. **c** scan of TD3 with the drill location of U-Th dates on the stalagmite marked in red.

4.2.2 Gaussian smoothing

Irregular sampling of the TD3 proxy record requires special treatment for the extraction of multi-centennial trends. Thus, proxy time series were smoothed using a Gaussian-kernel weighted filter which is well-suited to extract trends from irregularly sampled time series (Rehfeld et al., 2011). Kernel width is varied adaptively such that sampling intervals with little deviation from the average sampling interval contribute to the weighted sum with higher weights. We use the implementation provided by (Rehfeld et al., 2011) in the MATLAB package NESToolbox.

4.2.3 Principal Component Analysis (PCA)

A Principal Component Analysis is used to reduce the dimensionality of continuous multivariate data, and summarises variables in components to break down shared information between the

variables. PCA was conducted on the smoothed trace element time series to establish their relationship to each other. The analysis was conducted using the R package FactoMineR (Lê et al., 2008) for calculating the PCA and plotting the results on a variable factor map.

Chapter 5

Proxy Interpretation

5.1 Chapter summary

Correct proxy interpretation is one of the main challenges in speleothem-based research. $\delta^{18}O$ in rainfall from central Vietnam reflects moisture source dynamics rather than rainfall amount (Chapter 2), thus, additional proxies are needed to understand changes in the hydrological regime. This chapter aims to investigate the local processes controlling carbon isotopic and trace elemental variability in stalagmite TD3. Firstly, a short summary of the theoretical background on carbon isotope and trace elemental variability in soils and the karst is provided. This is followed by an investigation of the relationship between certain elements and $\delta^{13}C$ in TD3. By using high-resolution trace elements provided by LA-ICP-MS and by analysing the results with a PCA the relationship between proxies in TD3 is determined. The results show that $\delta^{13}C$ and Mg/Ca variability is closely linked to local hydrology and can be interpreted as reflecting wet/dry conditions in central Vietnam.

5.2 $\delta^{13}C$ as a proxy for local climate variability

The use of $\delta^{13}C$ as a tracer for local climate has recently increased in popularity e.g. (Breitenbach et al., 2019; Fohlmeister et al., 2017, 2020; Ridley et al., 2015), especially in combination with trace element records. While processes driving $\delta^{13}C$ and trace element variability have been investigated for decades, the use of speleothem $\delta^{18}O$ as a rainfall proxy dominated research based

in Asia e.g. (Cheng et al., 2016; Dykoski et al., 2005; Kathayat et al., 2017; Mohtadi et al., 2016; Wang et al., 2005; Wang, 2001). This has recently been subject to change and the use of $\delta^{13}C$ and trace elements has become more important in reconstructing local climate conditions e.g. (Cheng et al., 2016a; Cosford et al., 2009; Griffiths et al., 2020; Lechleitner et al., 2017; Zhang et al., 2018).

There are two main sources for carbon isotopes in speleothems: the soil and the bedrock. Soil CO_2 derives from atmospheric CO_2, plant respiration and decomposition of organic matter, whereas input of dissolved inorganic carbon (DIC) from the bedrock is controlled by the rock composition (Dreybrodt and Scholz, 2011; Noronha et al., 2015). Increased microbial oxidation and plant respiration supplying CO_2 inversely controls the $\delta^{13}C$ signature in the soil and cave waters, leading to lower $\delta^{13}C$ values when plant activity is increased (Fairchild et al., 2006). Low soil moisture reduces microbial activity and plant respiration leading to increased $\delta^{13}C$ values (Moyano et al., 2013) and the plant type e.g. trees vs grass (C3:C4) or no vegetation also affect the resulting carbon isotopic signature (Zhang et al., 2006).

$\delta^{13}C$ values in the cave water reflect the $\delta^{13}C$ and DIC signature of the soil, which can be modified in the karst by various processes (Frisia et al., 2011). For example, an increase in the ionic strength of the cave water due to CO_2 degassing results in higher $\delta^{13}C$ values in the speleothem (Frisia et al., 2011). During dry events the karst partly fills with air, allowing for carbonate precipitation prior to downstream speleothem formation. This process is described as prior carbonate precipitation (PCP) and can manifest in both calcite and aragonite growth (Wassenburg et al., 2016). PCP preferentially removes light carbon isotopes from the solution via degassing of CO_2 (Fairchild and McMillan, 2007) and thus enriches the remaining $\delta^{13}C$ values in the cave waters and resulting speleothems.

Cave air ventilation as a driver for CO_2 degassing is a further component influencing PCP and thus $\delta^{13}C$. At high latitudes, the strong seasonal temperature difference between summer and winter often drives the seasonal cycle in cave ventilation and controls the CO_2 concentration (Baldini, 2010). For example, surface air cooling outside the cave during winter, can drive the relatively warmer cave air to circulate towards the entrance. In the (sub-)tropics, where seasonal temperature gradients are smaller compared to high latitudes, the difference between day and night can be more important (James et al., 2015).

5.3 Trace elements as local environmental proxies

In order to distinguish between soil derived and karst/cave internal controls on carbon isotopes it is useful to investigate additional proxies (Oster et al., 2010, Griffiths et al., 2012; (Fohlmeister et al., 2017; Oster et al., 2010). This is because PCP does not only affect isotopic fractionation between the solid and liquid phase, but also the ionic content of the remaining cave waters (Day and Henderson, 2013; Johnson et al., 2006; Sinclair et al., 2012). The enrichment or depletion of certain elements in cave water in respect to Ca is based on the disproportional incorporation of trace elements. This process is controlled by the distribution coefficient, which gives a comparison of the solubilities of elements (Sinclair et al., 2012). Ions with a distribution coefficient below 1, are typically found to be enriched in waters following PCP, these elements usually include Mg, Sr, and Ba (Huang and Fairchild, 2001; Sinclair et al., 2012). However, PCP is not always the main control, as Mg can can be reflecting by sea spray (Baldini et al., 2015). Sr and Ba are sometimes linked to growth rate (Huang and Fairchild, 2001; Tremaine and Froelich, 2013)and can be outcompeted by increased Mg/Ca ratios in the solution (Wassenburg et al., 2020). Further, the type of carbonate formed during PCP is important to consider, since Sr and U are positively correlated to prior calcite precipitation, but negative correlated to prior aragonite precipitation (Wassenburg et al., 2016). U and also P can be sensitive to infiltration rather than PCP, further complicating the interpretation (Hartland et al., 2012; Huang and Fairchild, 2001; Johnson et al., 2006). The residence time of percolating waters in the karst can also control the elemental content of cave waters (Fairchild et al., 2000). During dry periods the extended residence time allows for leaching of certain elements from the bedrock (Sinclair et al., 2012). Especially in Mg-rich bedrocks, such as dolomites, the additional uptake of Mg disproportionally increases the Mg concentration in cave waters in respect to Sr. This can lead to an amplification of Mg variability during dry and wet periods.

In order to determine the process that mainly controls certain elements with a cave system, it is thus important to investigate the relation between elements and stable isotopes. In the following section it is examined which proxies are controlled by the local hydroclimate in central Vietnam and how they can be interpreted in terms of palaeoclimate variability.

5.4 Local climate proxies in Thien Duong Cave

Due to the various processes that can control carbon isotopic and trace elemental variability, it is important to closely investigate the relation between elements to gather information on their main drivers. The most prominent feature of the TD3 proxy record is the strong correlation between δ^{13}C and Mg/Ca ratios (Figure 5.1). PCP and leaching of additional Mg from the bed rock can both increase the Mg content in an associated speleothem (Sinclair et al., 2012). The correlation observed in the plot is high, especially during the dry phases (Figure 5.1), however, the calculated correlation (r=0.6389, p-value<0.05) is lower than expected, which is likely due to the large difference in sampling frequency between stable isotopes and trace elements (δ^{13}C has 312 samples, Mg has 23000 samples). The Mg/Ca time series was smoothed before calculating the correlation.

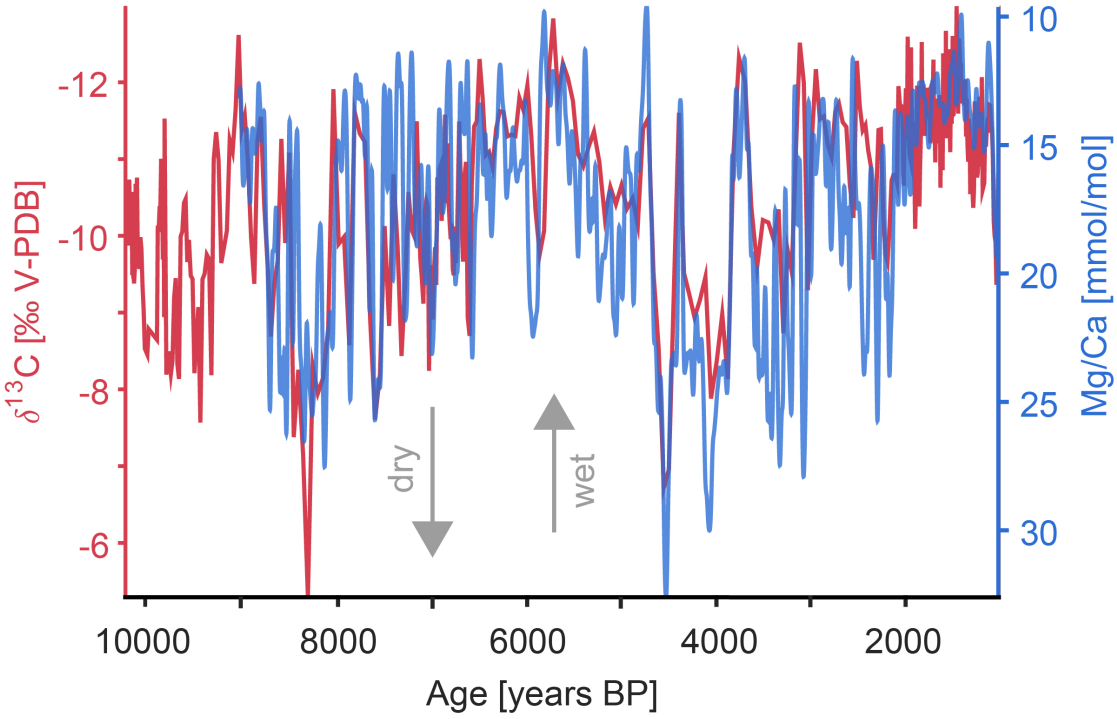

Figure 5.1: Carbon isotopes and smoothed time series of Mg/Ca ratios of TD3 over the Holocene. In general lower values are found in the early and late Holocene and highest values in the mid-Holocene, indicating wet and dry climate in Vietnam, respectively.

As an explanation for the strong co-variance of δ^{13}C and Mg/Ca ratios, PCP is invoked as a possible driver. Further evidence for this is provided by elements, that are typically found as weathering products of soils (Nesbitt and Young, 1982) or indicative of flooding events (Finné et al., 2014;

Frisia et al., 2012). The high abundance of Si, Al, Ti and Fe, in the late Holocene coincides with low δ^{13}C values and Mg/Ca ratios. This inverse connection supports the hypothesis that δ^{13}C and Mg are proxies recording wet versus dry conditions. For example, Si, Al, Ti, and Fe are strongly reduced during extremely dry periods, around 5000 to 3600 BP, when δ^{13}C and Mg show the highest values of the record (Figure 5.1 and 5.2). Al and Ti are likely the most reliable proxies for weathering in this dataset, as Fe and Si can be influenced by interference with other elements during LA-ICP-MS (Jochum et al., 2012). Yet, the strong replication of the signal in all four elements hints towards a common driver.

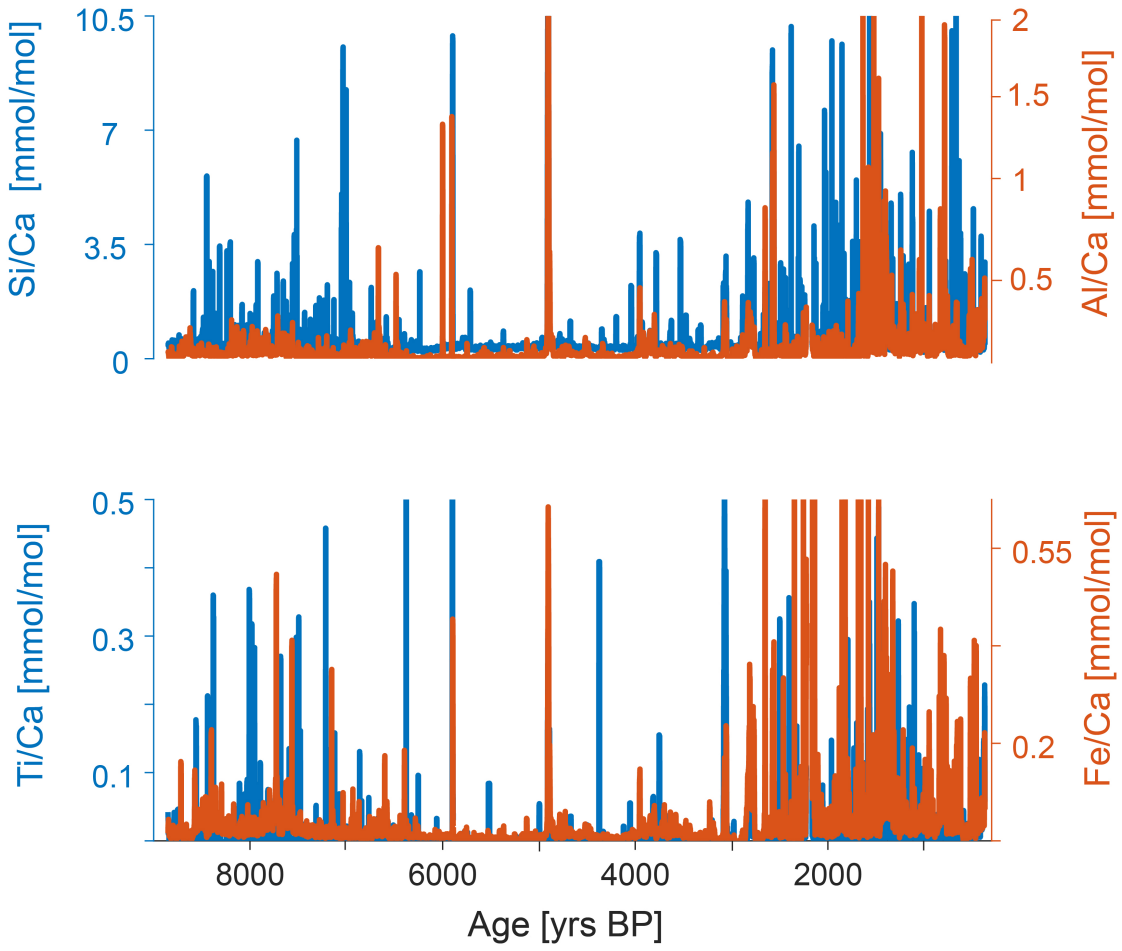

Figure 5.2: Time series of Si/Ca, Al/Ca, Fe/Ca and Ti/Ca ratios indicating increased weathering/flooding during the early and late Holocene. These elements show an increase in abundance after 3000 years BP and the lowest concentrations are found between 6000 to 3000 years BP.

Some elements, such as U, can be linked to both PCP and infiltration (Huang and Fairchild, 2001; Johnson et al., 2006). A strong correlation between U/Ca and P/Ca ratios is an indicator for infiltration being a first order control on U (Johnson et al., 2006; Treble et al., 2003). U/Ca and

P/Ca are indicators of infiltration, when they travel bound to colloids Hartland et al. (2012) and are washed into the cave. Thus, tight coupling between U and P in TD3 strongly hints towards infiltration as a driver of these elements (Figure 5.3). Additionally, U/Ca and P/Ca are inversely correlated to δ^{13}C and Mg/Ca (r=-0.4, p-value < 0.05), which further corroborates the conclusion that δ^{13}C and Mg/Ca are reflecting local hydrology.

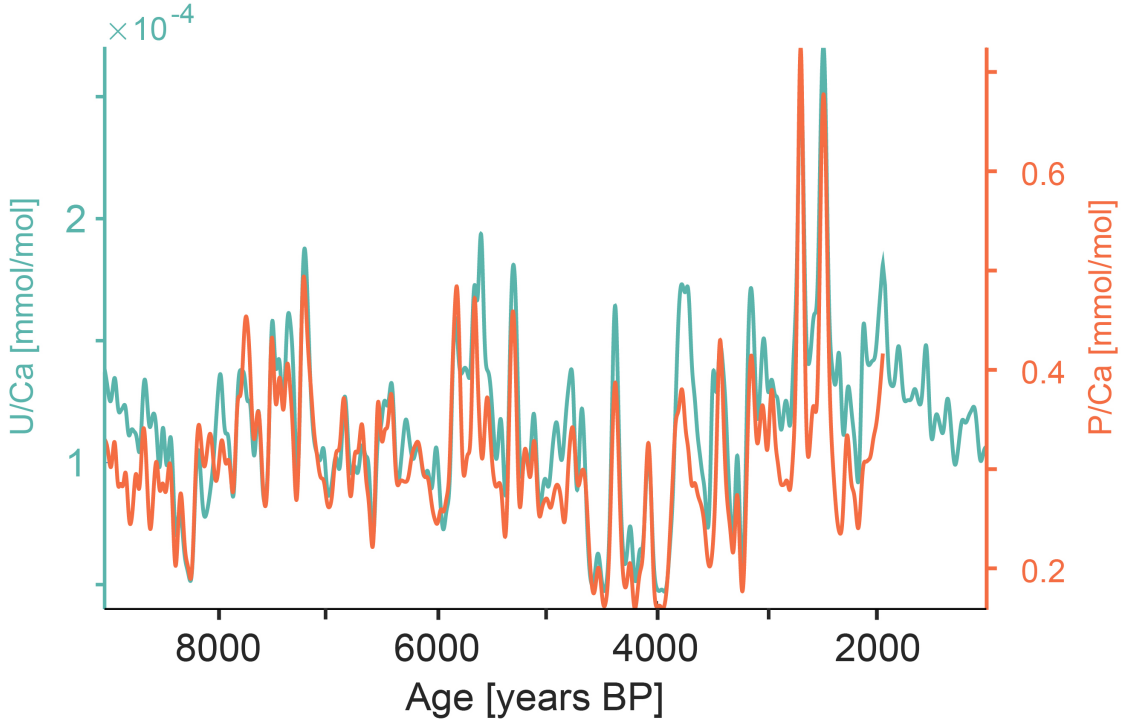

Figure 5.3: Smoothed time series of U/Ca and P/Ca over the Holocene. Both elements show a similar pattern and appear to positively correlate, over the record. P/Ca is only available for the time period of 9000 to 2000 years BP.

The inverse coupling of U/Ca and P/Ca versus δ^{13}C and Mg/Ca is constant on different time scales, from millennial to centennial and decadal time scales (Figure 5.4). This is an important observation suggesting that the controls on Mg/Ca and δ^{13}C remained constant during the Holocene. Both proxies are reliable indicators for local hydrology over an extended period of time. Taking these observation together, it is likely that Mg/Ca and δ^{13}C are driven by PCP and can be used as indicators for locally dry versus wet conditions over the Holocene.

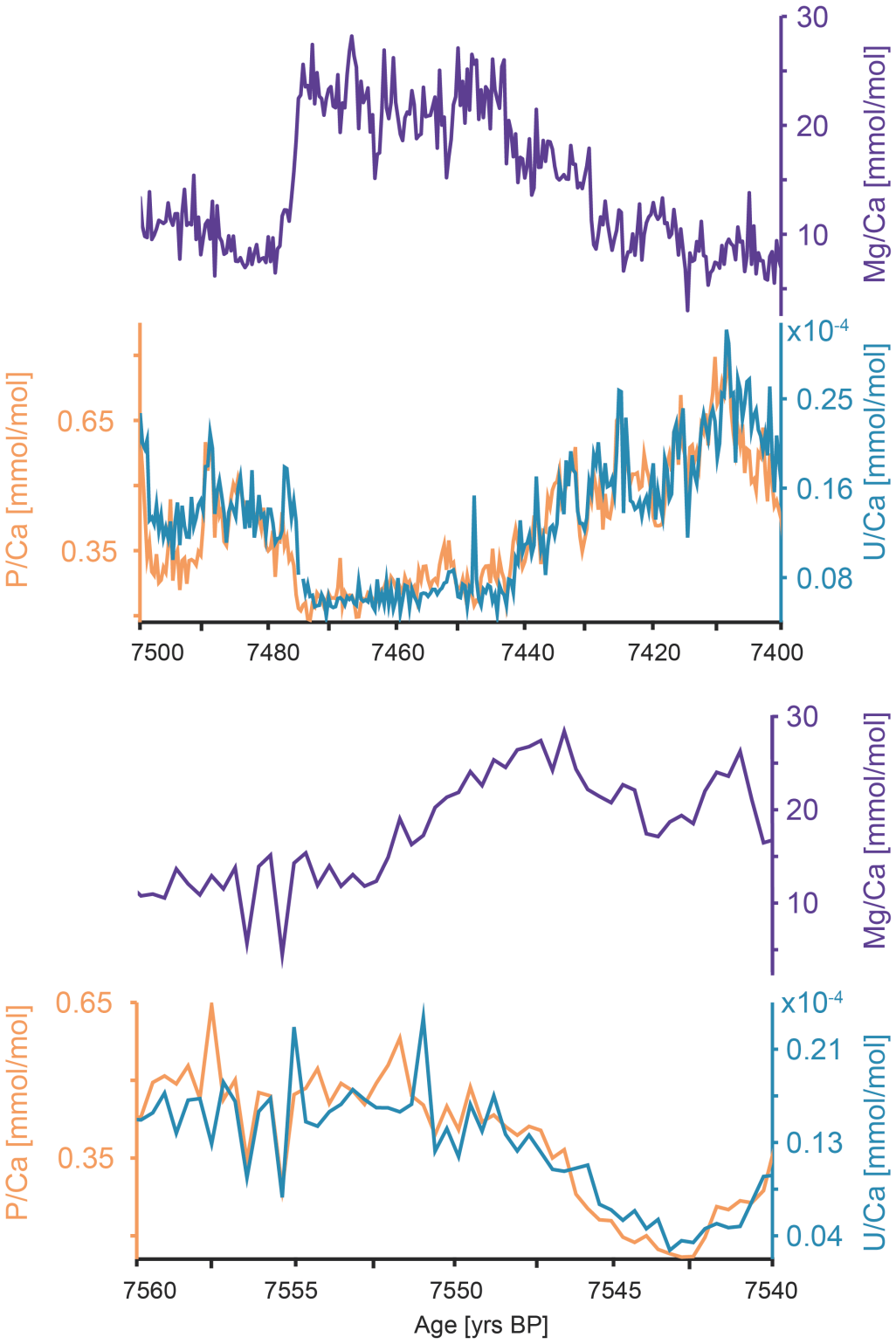

Figure 5.4: Comparison of the relation between Mg and U and P over centennial (top) and decadal (bottom) time scales

The relation between Sr/Ca and Mg/Ca ratios in TD3 is less obviously explainable and needs further

elucidation, as usually the positive correlation between Mg/Ca and Sr/Ca is used as a supporting argument for PCP. Sinclair et al. (2012) predicted that the slope between ln(Sr/Ca) vs ln(Mg/Ca) should be 0.88, in order for both elements to indicative of PCP. In TD3, Sr/Ca and Mg/Ca have no correlation (r=-0.07) based on the raw data and a negative correlation for smoothed data (r=-0.4, p-value<0.05). However, this relation varies depending on the prevailing climate conditions. The elements are negatively correlated during extended dry periods, whereas during wetter periods the proxy time series vary between a negative and positive correlation (Figure 5.5). One explanation for the inverse relation during dry periods could be leaching of additional Mg from the bedrock. During dry periods, the extended residence time of cave waters in the karst can increase the Mg/Ca concentration relativ to Sr/Ca. The bedrock of Thien Duong Cave, consists of partly dolomitized limestone (Debevec et al., 2012), which allows for additional contribution of Mg during extended dry periods. Higher Mg/Ca ratios in cave waters can discriminate Sr against Mg during downstream speleothem formation (Wassenburg et al., 2020), reducing the incorporation of Sr into the crystal lattice. Thus, the increased Mg/Ca ratio in cave water, can lead to decreased Sr values in the downstream speleothem during dry periods.

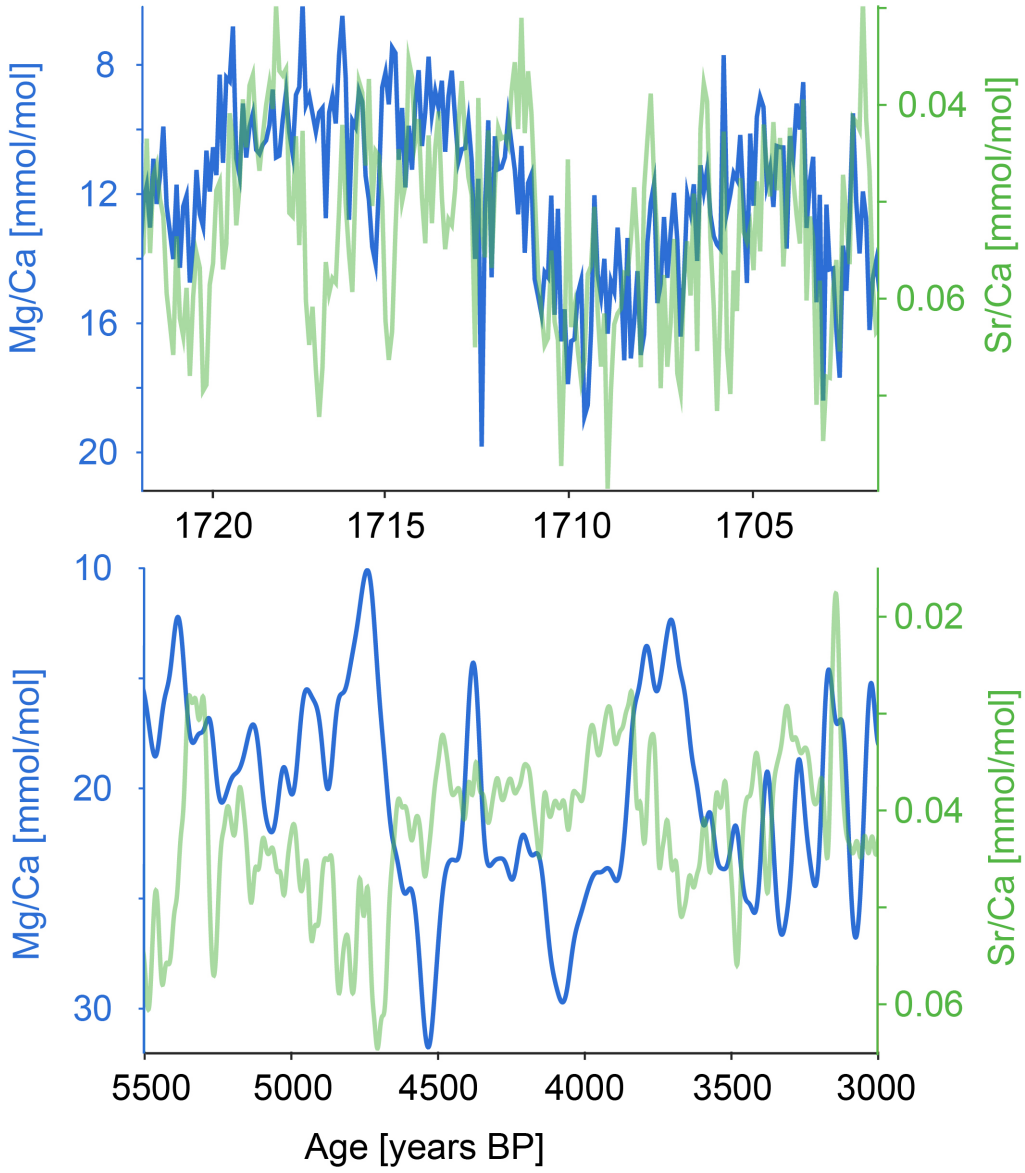

Figure 5.5: Plots showing the correlation of Sr/Ca and Mg/Ca, as the original and smoothed times series, for **a** wet and **b** dry periods. There is a coherency between both times series during wet periods, whereas during dry periods the elements decouple.

To further examine the drivers of Sr and Ba in comparison to Mg, a PCA analysis (Figure 5.6) was conducted using the R package FactoMineR (Lê et al., 2008). PC1 and PC2 indicate that elements typical for weathering (Si, Al, Th, Ti and Fe) cluster narrowly together (Figure 5.6 upper right corner). Proxies for infiltration are U, P and Y and cluster within the lower right section. While P and U can be proxies for various processes (Frisia et al., 2012), Y has been shown to be typically associated with infiltration from the soil (Hartland et al., 2012). Despite not following the model of Sinclair et al. (2012), Mg, Sr and Ba cluster within the same section. This shows that all three

elements are controlled by processes within the bedrock. Ba and Sr show the direct opposite trend to U, P and Y, which suggests that Ba and Sr are likely dominated by water supply, rather than PCP. The PCA suggests that infiltration is inversely driving Ba and Sr, which means that during time of high infiltration, there is little incorporation of Ba and Sr, with the opposite being true for dry periods. While this is also true for Mg, there is the additional influence of PCP on the Mg/Ca ratios in TD3.

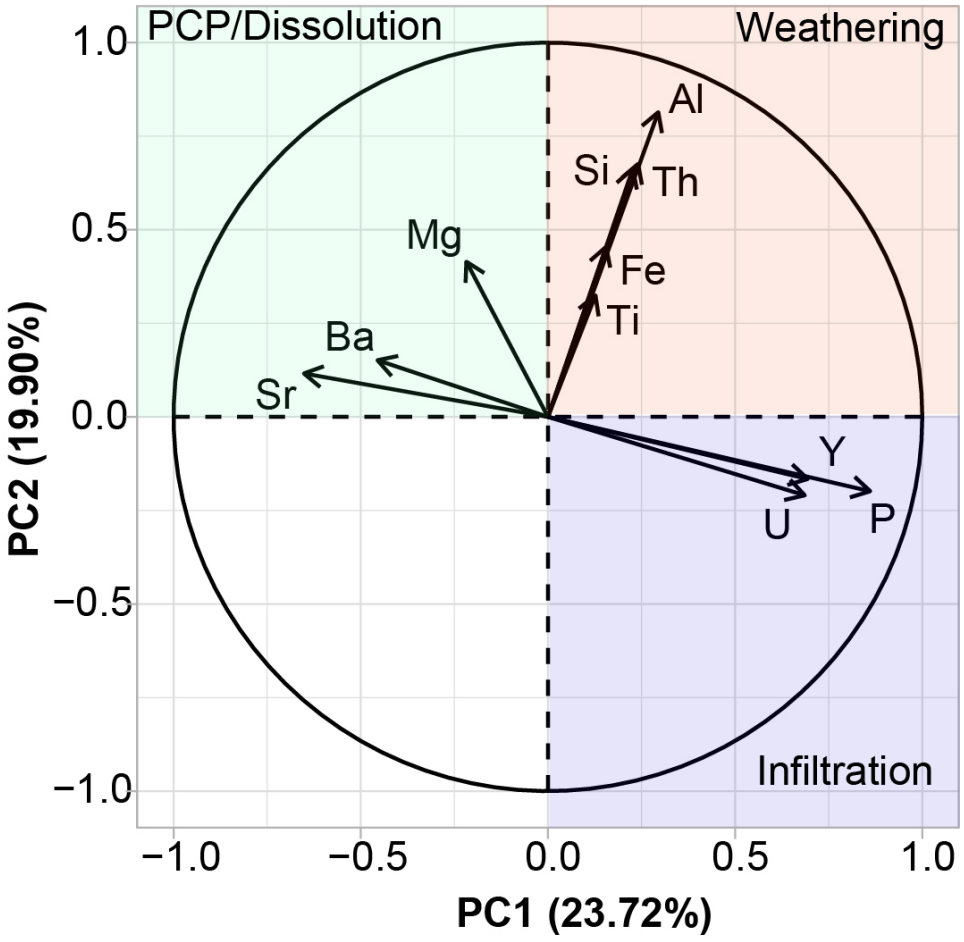

Figure 5.6: Variable factor map showing the PCA loadings of smoothed trace element time series from stalagmite TD3. Element concentration within TD3 can be divided into three clusters: PCP/dissolution, weathering and infiltration. The PCA analysis confirms the observations that Mg/Ca can be used as a proxy for local hydrology in conjunction with proxies of weathering and infiltration.

5.5 Conclusion

The use of $\delta^{13}C$ in combination with trace element concentrations in speleothems is a powerful tool for hydroclimatic reconstructions. However, a diverse set of processes can control variability

and an interpretation of climatic parameters should be considered carefully. This chapter presents evidence that Mg/Ca ratios and δ^{13}C are reflecting locally dry versus wet conditions in central Vietnam. Supported by other elements sensitive to infiltration and weathering, there is strong evidence that PCP is the main control of variability in δ^{13}C and Mg in TD3. These processes are summarised in Figure 5.7. Dry periods are reflected as increased δ^{13}C and Mg/Ca values, in contrast low values indicate wet conditions. These findings are fundamental for the correct interpretation of the TD3 proxy record.

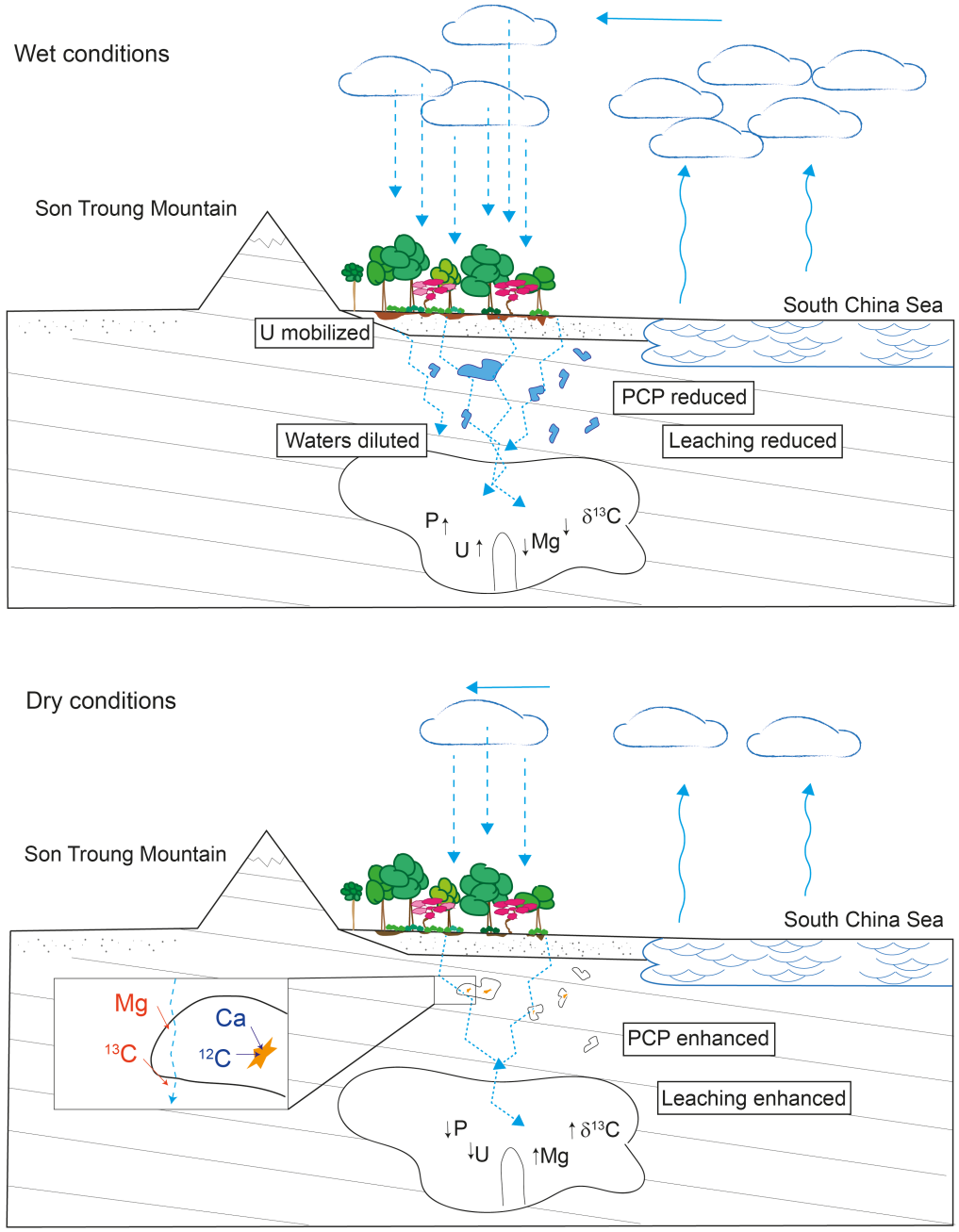

Figure 5.7: Schematic showing the processes in the soil, karst and cave during wet and dry events at Thien Duong Cave. During wet events the karst is filled with water, which is transported fast into the cave. The reduced residence time of the water, decreases the amount of Mg leached from the bedrock and PCP is reduced due to the lack of air in the karst. During dry events the karst fills partly with air enabling PCP to occur, which enriches the Mg and ^{13}C in the remaining solution and thus the speleothem. Due to the prolong residence time, more Mg can be dissolved in the waters, increasing the Mg content even further. U and P are enriched in the speleothem during wet conditions, since they are mobilized in the soil and washed into the cave.

Chapter 6

Climate of the Holocene

6.1 Chapter summary

The relationship between the Asian winter and summer monsoon over the Holocene is highly debated. Proxy records and climate modelling studies give inconclusive results, leaving especially the winter monsoon evolution largely unknown. This chapter uses the proxy record retrieved from stalagmite TD3 to investigate hydroclimatic changes and the evolution history of the Northeast Winter Monsoon in Southeast Asia over the Holocene. The Mg/Ca and δ^{13}C values indicate the Northeast Winter Monsoon rainfall was relatively strong during the early and late Holocene, but was substantially weaker during the mid-Holocene from 5000 to 3000 years BP. The prevailing dry conditions during the mid-Holocene have also been identified in Southwest Summer Monsoon records across Southeast Asia, suggesting that rainfall was affected in both seasons. The results show that rainfall related to the Northeast Winter and Southwest Summer Monsoon in Southeast Asia was positively correlated during the early and mid-Holocene and shifted towards an negative correlation during the late Holocene. By performing a frequency analysis, this chapter shows that interannual variability of rainfall in central Vietnam was strongly suppressed during the early and mid-Holocene and became most active after 3000 years BP. This work suggests that the positive correlation between Northeast Winter and Southwest Summer Monsoon is likely driven by shifts in the Walker Circulation during the early and mid-Holocene. During the late Holocene, the teleconnection between the Pacific and rainfall in central Vietnam became dominant, similar to today's climate in this region, whereas the Southwest Monsoon is more affected by changes in

the Indian Ocean. The results reconcile the ongoing debate on the nature and drivers of winter monsoon variability across Asia during the Holocene.

Tobias Braun developed and conducted the MC-PCA for this chapter.

6.2 Introduction

The Asian winter monsoon is mainly associated with cold and dry north-westerlies across East Asia and north-easterlies in Southeast Asia (Sengupta and Nigam, 2019). Yet, in some coastal regions, such as Vietnam, the Philippines, Southeast India, Sri Lanka, and Japan, the winter monsoon leads to intensive rainfall and flooding, threatening the livelihood of millions. There is some consensus on the co-evolution of the monsoons in the two seasons over glacial-interglacial time scales (An, 2000; Clemens et al., 2008; Maher, 2016). However, whether these two monsoon systems were similarly linked during the Holocene remains an open question (An et al., 2017; Hao et al., 2017; Liu et al., 2009b; Sone et al., 2013; Steinke et al., 2011; Wang, Wu, Chang, Liu, Li and Zhou, 2010; Wang et al., 2021; Wen et al., 2016; Yancheva et al., 2007; Zhao et al., 2021). This is particularly true for coastal Vietnam which hitherto contains no information on how the winter monsoon has varied in the past. The following sections summarise the current knowledge of winter and summer monsoon co-variability during the Holocene in Asia and highlight outstanding issues regarding winter monsoon reconstructions.

Recent modelling studies suggest that the winter and summer monsoons in Asia are positively correlated on orbital time scales (>3000 years) (Wen et al., 2016; Yan et al., 2020). This positive correlation is argued to be forced by Earth's precession of the equinoxes: Increased summer insolation leads to enhanced warming of the land surface during summers, and as a result increased summer monsoon circulation; stronger cooling of the land during winters results in stronger winter monsoons. However, terrestrial proxy data disagree, linking-insolation induced displacements of the ITCZ with an inverse relationship between summer and winter monsoons (An et al., 2017; Shi et al., 2012; Sone et al., 2013; Yancheva et al., 2007). This latter hypothesis suggests a northward shift of the ITCZ, such as was the case under higher summer insolation, which is accompanied by a stronger summer monsoon and a weak winter monsoon, whereas the opposite is true for a southward shift (Yancheva et al., 2007).

Furthermore, modelling studies (Yan et al., 2020) highlighted that the negative correlation on time-scales less than 2000 years has also been linked to internal variability in the coupled ocean-atmosphere system, mainly related to ice sheet and Atlantic Meridional Overturning Circulation (AMOC) forcing. In contrast, proxy records and other modelling studies have shown that, especially in the lower latitudes, insolation-induced variability of the ITCZ position and ENSO variability can lead to more complex pattern (An et al., 2017; Shi et al., 2012; Yancheva et al., 2007). Marine records from the Okinawa Trough show an anti-correlation between the summer and winter monsoons on centennial time scales (Sagawa et al., 2014; Xiao et al., 2006; Zheng et al., 2014). Invoked drivers are solar activity (Sagawa et al., 2014; Xiao et al., 2006) and the displacement of the ITCZ (Zheng et al., 2014). Insolation-induced displacements of the ITCZ as drivers of winter monsoon variability have been supported by other studies (Sone et al., 2013; Yancheva et al., 2007; Zheng et al., 2014). This mechanism extends beyond millennial time-scales, contrasting with model observations (Wen et al., 2016) and other proxy records from this region (Steinke et al., 2011; Tian et al., 2010; Wang et al., 2012). Thus, the nature of Asian summer and winter monsoon variability, and the mechanisms to explain their co-evolution, is still unknown for the Holocene. One of the causes lies in the use of proxies from different regions within Asia.

For example, studies based on proxy records from northern and southern China, the South China Sea and Yellow Sea found that the Asian Winter Monsoon consists of two modes: a northern and a southern mode (Zhang et al., 2015; Zhao et al., 2019). The northern mode is usually named the East Asian Winter Monsoon, and the southern mode the Northeast Monsoon, although clear definitions for the geographic extent are lacking (Chapter 1). The Arctic Oscillation is controlling the northern mode via the Siberian High, which is regulating surface pressure over central Siberia (He et al., 2017). The Siberian High over the Asian Continent and the Aleutian Low to its east are forcing northwesterly winds east of the Siberian High (Wu and Wang, 2002). The southern mode is strongly affected by SST variability in the Pacific, which influences the circulation pattern over the South China Sea and the Philippine Sea (Jin et al., 2016; Sengupta and Nigam, 2019).

On decadal time-scales, recent palaeoclimate studies highlighted the influence of ENSO and changes in the mean ocean state of the Pacific on winter monsoon variability (Hao et al., 2017; Zhao et al., 2019; Zheng et al., 2014). It is suggested that a weaker winter monsoon coincides with El Niño events and a stronger winter monsoon occurs during La Niña events (Wang et al.,

2000). This is in agreement with modern climatological observations, suggesting a strong control of ENSO on the winter monsoon in southern East Asia (Chen et al., 2014; He et al., 2008; Wang, Wu, Chang, Liu, Li and Zhou, 2010), whereas, the controls of ENSO on the winter monsoon in the higher latitudes are limited (Zhang et al., 2015). Yet, modelling studies also showed that the influence of ENSO on winter monsoon variability can be enhanced or diminished by changes in the mean ocean state, affecting the anticyclonic circulation in the western Pacific (An et al., 2017; Kim et al., 2014). Thus, the interaction between interannual variability in the Pacific Ocean and the winter monsoon on longer time scales, remains uncertain.

A further issue in understanding the winter monsoon arises from the disagreement of winter monsoon proxy records within the same region. Reconstructions based on marine sediment cores in the South China Sea (Huang et al., 2011; Steinke et al., 2011; Tian et al., 2010), found a positive correlation between summer and winter monsoons over the Holocene. However, more recent studies suggest an inverse relation between summer and winter monsoons in the South China Sea (Zhang et al., 2019a). Further, findings showed that the relation between winter and summer monsoons can vary during warm or cold phases of the Holocene (Ge et al., 2017b). Similar disputes have been reported from terrestrial winter monsoon records from southern China (Jia et al., 2015; Wang et al., 2012; Yancheva et al., 2007), showing opposing trends over the Holocene. These mismatches, combined with the lack of terrestrial winter monsoon records from Southeast Asia, leave the evolution of the winter monsoon in this region largely unknown.

Not only is the disagreement between winter monsoon records from the same region a challenge, but also concerns regarding the use of speleothem δ^{18}O as a summer monsoon proxy are adding complexity. Reconstructions of the Asian summer monsoon are mainly derived from speleothem δ^{18}O records, reflecting changes in regional precipitation and circulation pattern. Recent research has shown that δ^{18}O in rainfall can be affected by numerous processes, not necessarily related to rainfall variability, such as moisture source and convection dynamics (Aggarwal et al., 2016; Konecky et al., 2019). Cave internal processes additionally alter the δ^{18}O signal of an associated speleothem, limiting the use of δ^{18}O as a proxy for monsoon intensity, if not supported by additional proxies (Baker et al., 2019; Fohlmeister et al., 2020). Most δ^{18}O speleothem records share similarities between sites across Asia, and also show a connection to summer monsoon records across the globe (Deininger et al., 2020; Wang et al., 2017a). However, there is growing

evidence that the driver of δ^{18}O in precipitation depends on the region: δ^{18}O in speleothems from the East Asian Monsoon region is more related to changes in atmospheric circulation, such as moisture source and pathways, whereas δ^{18}O in speleothems from the Indian Monsoon region better reflects regional precipitation, yet to some extent circulation dynamics as well (Parker et al., 2021). In comparison, to the speleothems δ^{18}O, winter monsoon records are mostly based on loess, lake or marine records, and are therefore reconstructing the wind strength or water temperatures, rather than precipitation or moisture source dynamics.

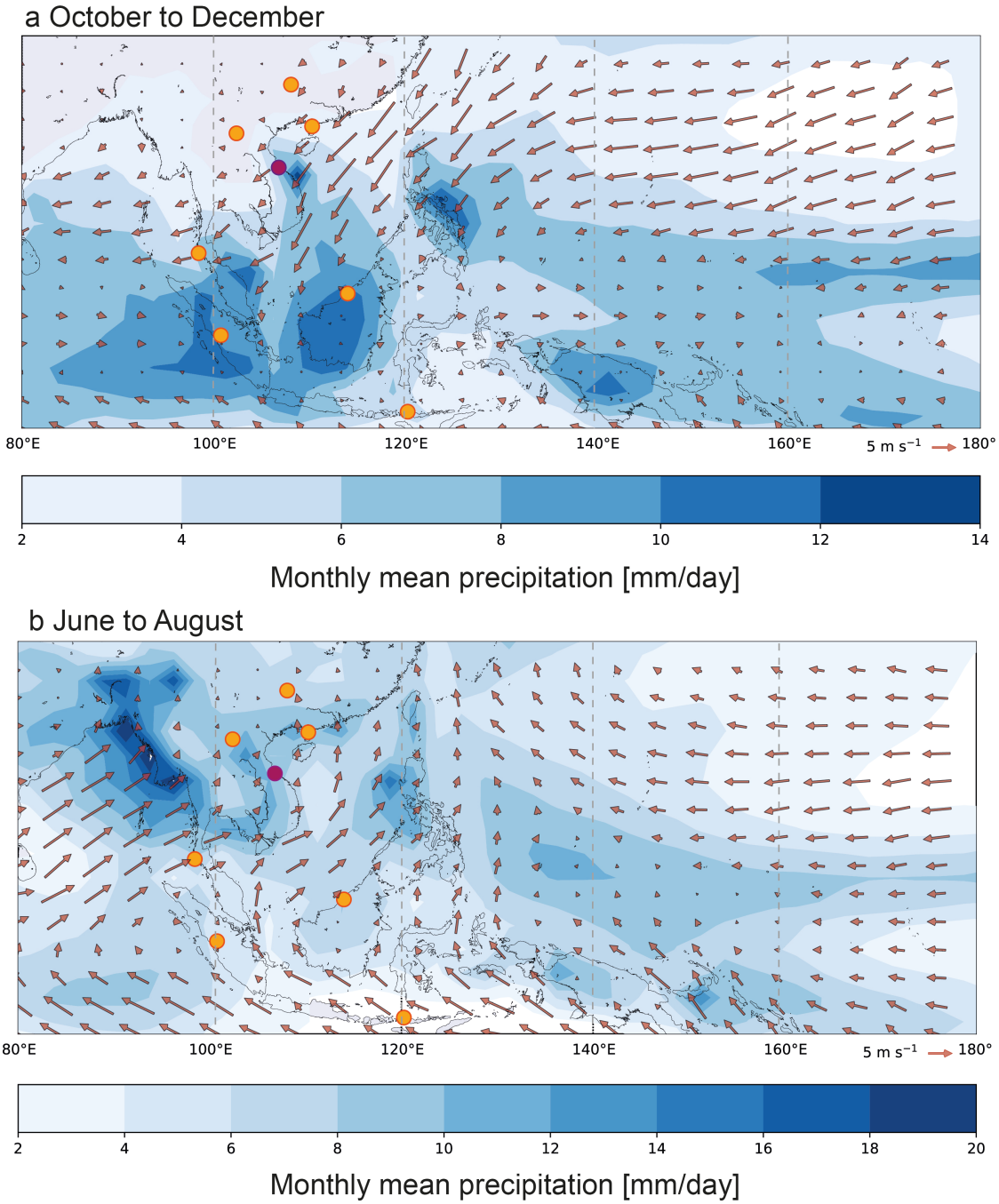

Figure 6.1: Precipitation and wind fields during **a** the winter monsoon season and **b** the summer monsoon season in Southeast Asia. During the winter strong north-easterly winds carry moisture into central Vietnam. During summer, strong south-westerlies prevail over mainland Southeast Asia. Shading shows long term mean average monthly precipitation rate from the GPCP Version 2.3 Combined Precipitation Dataset (NOAA, 2020*c*). The arrows indicate surface wind strength at 10 m using the u and v components of the ERA5 data set (Copernicus Climate Change Service (C3S), 2020). Yellow dots show the location of proxy records used in this work and Thien Duong Cave is marked in purple.

Usually, speleothem records of monsoonal areas are of limited use for reconstructions of winter

monsoonal rainfall, as the total annual rainfall is often strongly biased towards the summer monsoon season. Only few locations within Asia allow a reconstruction of winter monsoon induced precipitation (Figure 6.1). Central Vietnam is one of these locations, where more than 75% of the annual rainfall is related to the north-easterly winds of the winter monsoon (Chapter 2). Additionally, SSTs anomalies in the Pacific are a major control of interannual rainfall variability in central Vietnam, making the region ideal to investigate the evolution of rainfall related to the winter monsoon circulation. Further, the close geographic proximity between caves in central Vietnam to other cave sites across mainland Southeast Asia, which capture the Holocene summer monsoon, allows for a unique comparison of the two monsoon systems. Finally, recent reconstructions of summer monsoonal variability in Southeast Asia addressed the uncertainties arising by the use of δ^{18}O, from using additional proxies like carbon isotopes and trace elements.

Towards this end, this chapter presents the first Northeast Winter Monsoon rainfall record from stalagmite TD3, which covers the Holocene. The reconstruction, based on a suite of geochemical tracers preserved in the calcite at the time of precipitation, shows significant changes in both the Southwest Summer and Northeast Winter Monsoon, particularly during the mid-Holocene between ca. 6000 and 4000 years BP.

6.3 Methods

6.3.1 Spectral Analysis

Spectral Analysis was performed on TD3 to identify changes in the interannual variability. The analysis was performed using the MATLAB tool box red2con, which is based upon REDFIT, a Fortran 90 program (Schulz and Mudelsee, 2002). REDFIT allows processing of unevenly spaced time series, without the need for interpolation, which avoids the occurrence of artificial frequencies. The spectral analysis was used to analyse frequencies from the Mg/Ca time series of stalagmite TD3. The Mg/Ca time series has a very high resolution varying between monthly to two samples per year and is thus suitable for identifying ENSO-scale frequencies. The time series was divided into three sections: the early Holocene from 9000 to 6000 years BP, the mid Holocene from 6000 to 3500 years BP and the late Holocene from 3500 to 1000 years BP, to investigate potential changes in the frequency over longer time scales. In order to avoid a sampling bias, each section was

divided into subsections containing the same number of sample points. The section for the late Holocene was divided in 5 subsections, the mid Holocene had 2 subsections and 3 subsections were chosen for the early Holocene, to ensure an equal distribution of samples in each section. These results, thus, show the average of each of these subsection, e.g. the mid-Holocene contains 2 subsections and the power spectra is thus the average of these 2 subsections. Significance is estimated by calculating first-order autoregressive (AR1) time series. The oversampling factor for Lomb-Scargle Fourier transform was set to 2, the maximum frequency was set to 0.55. The analysis was performed on three age model realisations, which are the median and the lower and upper limits of COPRA ages realisations. Doing so covers three different age realisations provided by the model, helping to ensure that the calculated power spectra are not artefacts introduced by the age uncertainties.

6.3.2 Monte-Carlo Principle Component Analysis (MC-PCA)

In order to calculate the spatio-temporal coherency between 'n' records (where n is the number of proxy records) across Southeast Asia, an age uncertainty-aware Principal Component Analysis (PCA) is applied. The approach largely follows Deininger et al. (2017), using Monte-Carlo sampling of age model realizations to adjust for the age uncertainties in all records. Firstly, all speleothem age models have been recalculated in COPRA using the initially published U-Th ages. With COPRA, 2000 distinct time axes compatible with age uncertainty are sampled employing a Monte-Carlo sampling scheme and subsequently transferred into uncertainty of the proxy values (Breitenbach et al., 2012). This results in a single 'error-free' time axis and 2000 distinct proxy realisations which are compatible with the U-Th dating uncertainties. The PCA method requires constant sampling intervals in order to compute and decompose the covariance matrix of normalized proxy time series. Based on the lowest resolution record used in the PCA (Tangga Cave record (Wurtzel et al., 2017)) all records are resampled with a constant sampling interval of 75 years adapting to the lowest resolution. An overlap of 80% between consecutive windows was used to ensure an equal sampling resolution. As proposed by Deininger et al. (2017), Gaussian Kernel-based smoothing is applied in this step to align the temporal variability between the differently resolved proxy records. Smoothing windows are centered of the resulting regularly sampled dates. Smoothed proxy realizations are z-normalized, yielding zero mean and unit standard deviation. Finally, MC-PCA is applied to each of the 2000 sets of smoothed and z-normalized proxy realizations. Since every

proxy realization can be regarded as a shifted and stretched/compressed version of the underlying 'real' proxy time series, each set of proxy realizations yields an individual characterization of spatiotemporal coherency represented by $m \leqslant n$ modes, where m is the number of modes. Each mode consists of a principal component (PC) and n EOFs (empirical orthogonal functions, also called 'loadings'). EOFs are normalized such that they are equivalent to the linear correlation between the respective PC and a proxy realization.

When the MC-PCA is performed, a 'flipping-effect' and a 'smoothing- effect' are known to occur (Deininger et al., 2017). The former effect results firstly from the intrinsic sign ambiguity in the singular value decomposition used to numerically solve the eigendecomposition of the data covariance matrix (Bro et al., 2008). Small deviations in one of the n proxy records can suffice to result in a 'random' sign flip of the resulting PCs and EOFs, irrespective of the MC-based procedure. This will in some cases result in a bimodal distribution of the EOFs for a given PC. Secondly, the age uncertainty can cause sign flips as it introduces a mixture of phased and anti-phased proxy realizations into the PCA. Sign flips of the resulting PCs and loadings, thus, need to be accounted for when averaging over distinct MC iterations of the PCA. This averaging also results in a smoothing of the resulting PCs, whereas the degree of smoothing depends on the dating errors. In order to obtain meaningful estimates of the median and confidence limits for the PCs and EOFs, the flipping effect requires additional processing of the ensemble of results.

Therefore, k-means clustering is applied for each ensemble of the m PCs to distinguish flipped and non-flipped solutions (Lloyd, 1982). In this context, another effect was observed when age uncertainty of any of the included proxy records is large: apart from the flipped and non-flipped solution for the 1st PC, a third distinct solution can be identified which exhibits strong similarity to the 2nd PC. This results from an overlap between the variance explained by each of the modes and may occur between any given pair of *i*-th and *i*+1-th PC if dating uncertainties are large. While in most cases (e.g. 1800 out of 2000) the 1st mode is represented by strongly correlated (flipped and non-flipped) PCs, in fewer cases variance may be maximized by what is largely identified as the 2nd mode. Such a scenario is identified successfully by the proposed k-means clustering of PCs with $k = 3$ and should be considered in future application of the MC-PCA method. In this work, dating uncertainties were found to be sufficiently low such that this effect does not result in a significant number of 'swapped' modes. Consequently, EOFs and PCs of the flipped modes

identified by k-means clustering are sign-flipped and a single median PC/EOF is computed from the respective ensemble of solutions for each mode. Age uncertainty is propagated by computation of the 2σ-error bars of the respective PC and explained variance. The statsmodel package was used to compute PCA solutions for each set of proxy realizations and the sklearn package was used for k-means clustering.

The MC-PCA is applied to δ^{13}C and δ^{18}O records respectively from Tham Mai Cave (Laos) (Griffiths et al., 2020), Thien Duong Cave (Vietnam) this study, Tangga Cave (Sumatra) (Wurtzel et al., 2017), Bukit Assam Cave (Borneo) (Chen et al., 2016a). Additionally, a lake record from Lake Huguang Maar in China (Yancheva et al., 2007) was included. However, COPRA is specifically built for speleothem records, therefore the original age model without age uncertainties in all 2000 realisation was used. For the δ^{18}O MC-PCA, Dongge Cave record was included instead of the Lake Huguang Maar lake record, but no δ^{13}C record was accessible (Dykoski et al., 2005). For both applications, three modes were computed motivated by their interpretability.

The individual records reflect different seasonal parts of the monsoon system in Southeast Asia. Dongge Cave record is representative of changes in the East Asian Summer Monsoon circulation, and the Laos record reflects the Southeast Summer Monsoon circulation. The record from Sumatra partly reflects the Southwest Summer Monsoon, but is also influenced by the Australian Monsoon system. In Borneo, rainfall falls year-round with no distinct seasonality. The record based on TD3 reflects hydrological changes related to the Northeast Winter Monsoon and the Huguang Maar lake record reflects the East Asian Winter Monsoon. More details about the seasonality of rainfall in each location can be found in Chapter 3.

6.4 Results

6.4.1 Multiproxy records of Southeast Asian monsoon precipitation

Stalagmite TD3 is dated based on 20 U-Th ages and covers most of the Holocene. In total 371 low resolution samples were analysed for stable isotopes and about 23.000 data points for trace elements. On average, this results in a sub-decadal resolution for stable isotopes and a sub-annual resolution for trace elements. Both proxy records span the time between 8000 to 1000 years BP. Time series for each proxy are constructed with the COPRA model (see Chapter 3).

δ^{18}O in precipitation in central Vietnam is controlled by the seasonal shift between moisture sources, which are the Indian Ocean during summer and the Pacific during the rest of the year. Cave monitoring, installed in a cave about 50 km from Thien Duong Cave, showed that the seasonal cycle in δ^{18}O is preserved in drip waters, however, the signal is bias towards the rainy season in autumn/winter. Here it is proposed that the δ^{18}O in TD3 likely contains some information from the δ^{18}O in precipitation, where increased moisture from the Indian Ocean leads to lower δ^{18}O values. However, most of this information could be overprinted by the local hydrology, and the bias of low value to the rainy season. From 8000 to 6000 years δ^{18}O shows a gradual decline from increased to decreased values, which is followed by a sharp increase in δ^{18}O values at ca. 5000 years BP (Figure 6.2a). Afterwards values decrease again towards 1200 years BP.

A similar trend is observed in proxies reflecting local hydrology: The local precipitation related to the Northeast Winter Monsoon circulation over the Holocene, is reconstructed by using high-resolution trace elements (Mg, P, U, Al, Ti) and stable isotope data (δ^{13}C) retrieved from stalagmite TD3. δ^{13}C and Mg/Ca variability is driven by prior carbonate precipitation and thus, a tracer for locally wet and dry conditions. Further evidence for this interpretation is derived from other trace elements including U and P, which show an opposite trend compared to δ^{13}C and Mg, and are indicators for infiltration (Chapter 5).

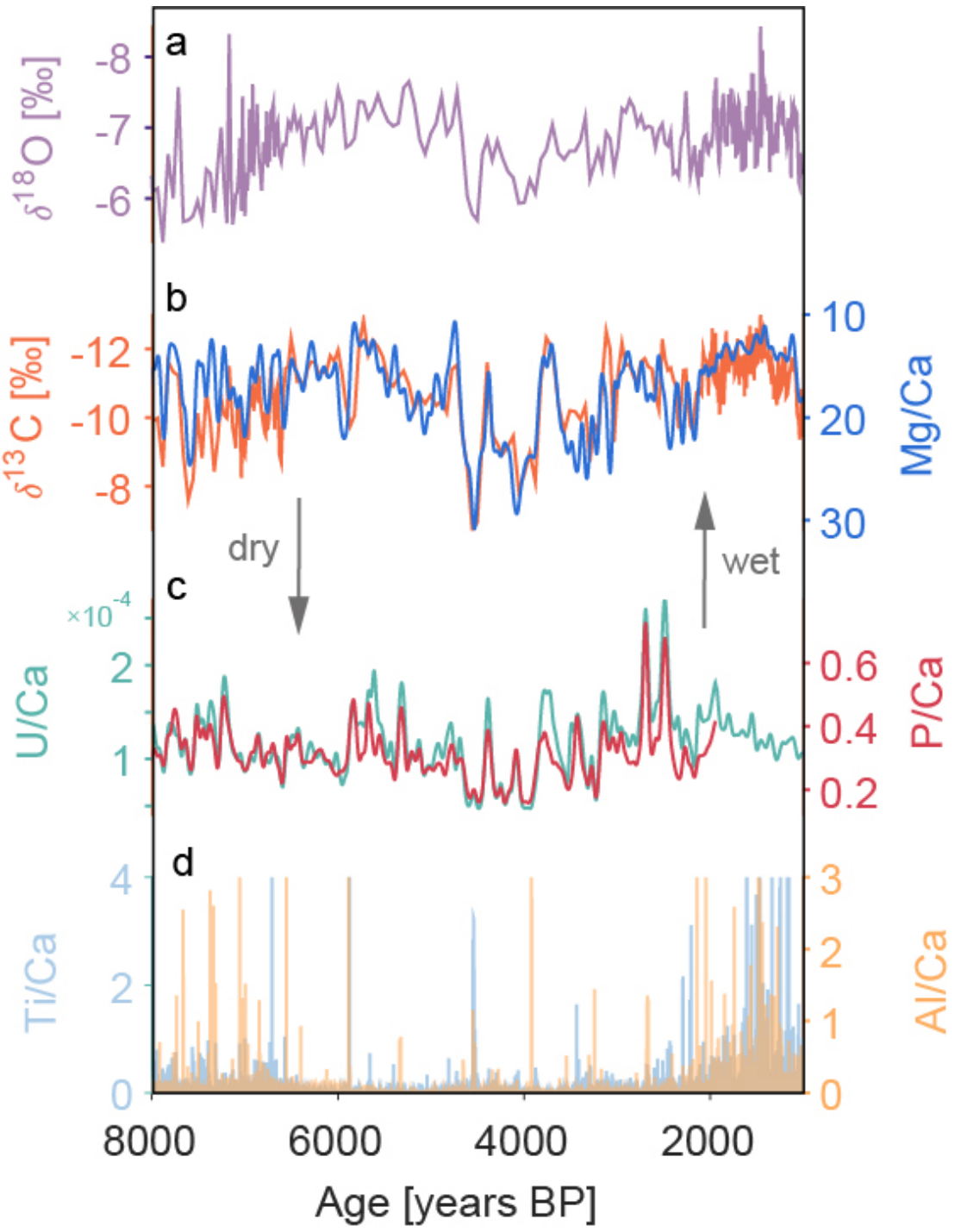

Figure 6.2: Multi-proxy record of stalagmite TD3: **a** δ^{18}O is reflecting changes in moisture source dynamics, **b** δ^{13}C superimposed with a smoothed timeseries of Mg/Ca, indicating wet and dry conditions, **c** smoothed U/Ca and P/Ca as indicators for infiltration. **d** Ti/Ca and Al/Ca, used as proxy for increased weathering/infiltration.

The most prominent feature of the TD3 record is the pronounced drought during the mid-Holocene, which starts at around 5000 years BP and lasts until ~3000 years BP. The drought started and

ended abruptly, and was interrupted by two brief wet episodes at ~4500 and ~3500 years BP. Other speleothem records from Southeast Asia indicate similarly dry conditions during the mid-Holocene (Figure 6.3). Specifically, Mg/Ca ratios, carbon isotopes, and δ^{18}O in a suite of speleothem records from northern Laos, which is the closest to central Vietnam, also shows a pronounced local drought (Figure 6.3b), beginning around 5000 years BP and lasting until around 3000 years BP (Griffiths et al., 2020). At the same time a δ^{18}O record from southern Thailand exhibits a 2000-years-long hiatus, potentially indicating a lack of water supply to sustain speleothem growth, in the south of mainland Southeast Asia (Figure 6.3c). Meanwhile in Borneo, the δ^{18}O record suggests increase regional precipitation from 5000 years BP to 3000 years BP (Figure 6.3d), though interestingly, the δ^{13}C record shows a positive peak at 4000 years BP, likely indicating locally dry conditions, although the use of δ^{13}C as a local climate proxy is not certain in this cave (Partin et al., 2013). Two speleothem records from the Maritime Continent show a shift towards dry conditions at 5000 years BP in Sumatra (Figure 6.3e) (Wurtzel et al., 2017) and Flores (Figure 6.3f) (Griffiths et al., 2009). The δ^{13}C record of Tangga Cave (Sumatra) has been interpreted to represent changes in vegetation, due to shifts in local climate on glacial-interglacial time scales (Wurtzel et al., 2017). Therefore, the Tangga Cave record shows dry conditions after 5000 years BP, suggesting that the drought prevailed across most of Southeast Asia (Figure 6.3e). The initial U content in a speleothem from Flores, peaks simultaneously with the record from Tham Mai Cave (Laos) and also indicates dry conditions during the mid-Holocene (Figure 6.3f). The drought conditions have also been reported from lake sediments in northern Thailand (Chabangborn and Wohlfarth, 2014), Cambodia (Hamilton et al., 2019; Maxwell, 2001; Penny, 2006) and southern China (Hillman et al., 2017).

Thus far, the drought during the mid-Holocene was only observed in summer monsoon records. Now the rainfall proxies in central Vietnam highlight that rainfall related to the Northeast Winter Monsoon was also strongly reduced. These findings indicate that, at least during the mid-Holocene, rainfall related to the summer and winter monsoon had a common controlling mechanism. By establishing the coherency between speleothem records across Southeast Asia the evolution of both monsoonal systems can be investigated further.

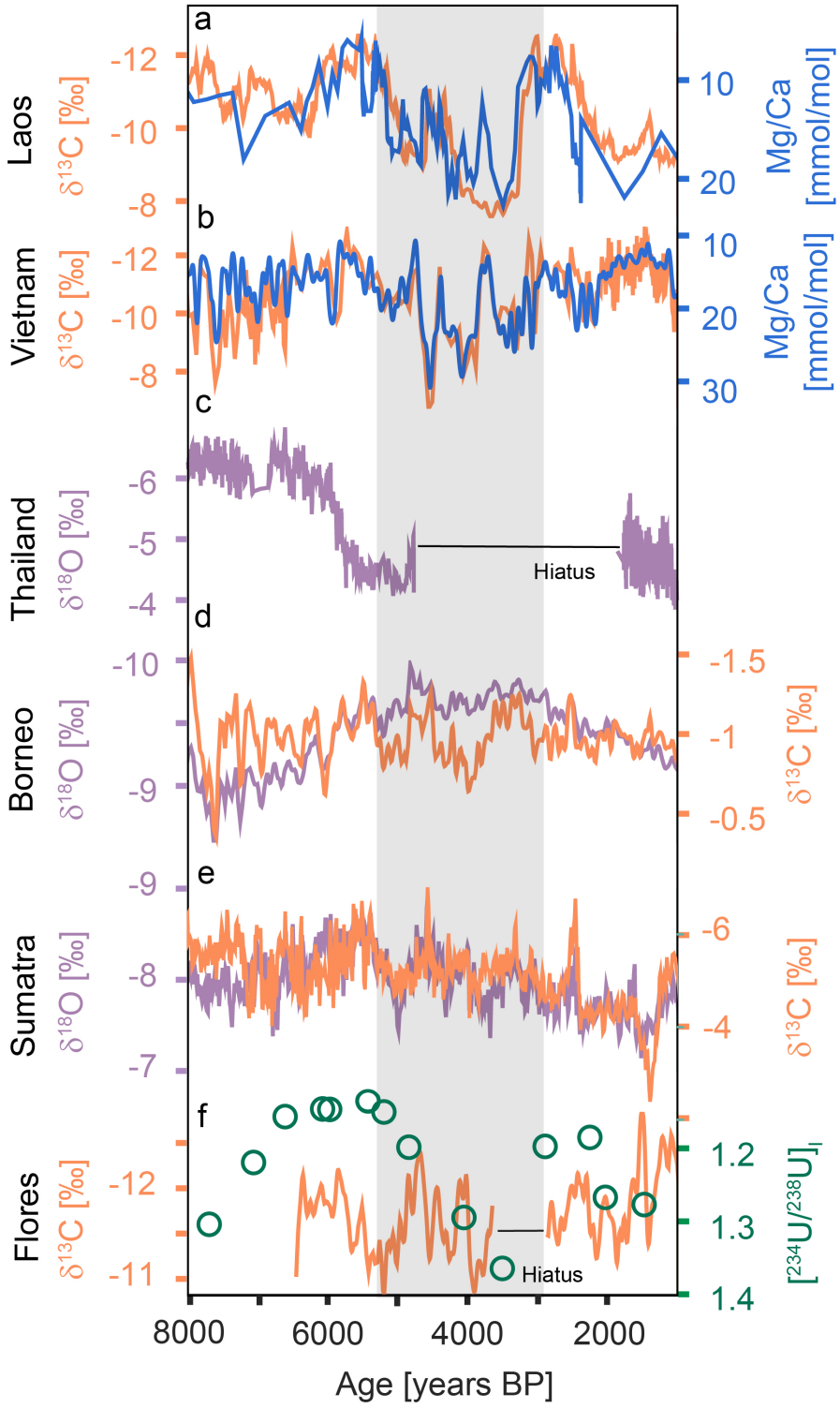

Figure 6.3: **a** δ^{13}C and Mg/Ca record of TD3, **b** δ^{13}C and Mg/Ca record from Tham Mai Cave, Laos **c** δ^{18}O record from Klang Cave, southern Thailand **d** δ^{18}O and δ^{13}C from Bukit Assam Cave, Borneo, **e** δ^{18}O and δ^{13}C record from Tangga Cave, Sumatra. **f** δ^{13}C and initial U record from Liang Luar Cave, Flores. Grey shading indicates the extreme dry conditions in Southeast Asia during the Holocene.

To gain a spatiotemporal view of the regional monsoon circulation changes across Southeast Asia during the Holocene published speleothem records (δ^{18}O and δ^{13}C) (Figure 6.1) are synthesized using a Monte-Carlo Principal Component Analysis (MC-PCA) approach. In this work, both δ^{13}C and δ^{18}O are used for an intercomparison to understand the advantages and limitations of each proxy. For example, the drought evident in local records from Southeast Asia, is not observed in δ^{18}O speleothem records from China (Wang et al., 2005; Yang et al., 2019; Zhang et al., 2019a). This is an issue, since speleothem δ^{18}O records are often used as classical summer monsoon records.

The leading PC1 of the δ^{18}O data explains 54% of the variance (Figure 6.4a) and illustrates the dominant orbital-scale trend of the monsoon across Southeast Asia, interpreted to reflect changes in insolation, which impact the monsoon systems (Figure 6.4c). PC1 exhibits a strong correlation with Tham Mai (0.58) and Dongge Cave (0.57), and a modest correlation of 0.27 with Sumatra. By contrast, PC1 displays a strong negative correlation with Borneo (-0.5) and a weak negative correlation with Vietnam (-0.16) (Figure 6.4b). These loadings reflect the controls of summer insolation on the summer monsoon circulation in southern China and Laos, and the inverse relation to boreal autumn insolation for regional rainfall in Borneo. The results for Sumatra are surprising due to the high coherency between the Tangga Cave record and other speleothem records from India and East Asia over glacial-inter-glacial time-scales (Wurtzel et al., 2018), which seem less pronounced during the Holocene. The weak correlation between PC1 of the δ^{18}O record from Vietnam is likely due to the bias of dripwater δ^{18}O to the autumn-winter rainy season (Chapter 3).

The orbital trend in δ^{18}O of the five records is aligned with either summer or autumn insolation (Figure 6.4b). However, the information contained in the higher-frequency millennial trends (i.e. PC2) shows that all records share, to some extent, a common forcing. Indeed, PC2 shows a strong positive correlation with Sumatra (0.68), Vietnam (0.62), and Borneo (0.36), while a rather and weak correlation with Laos (0.07) and China (Dongge) (0.08) (Figure 6.4b). Similar to the hydroclimate changes in Laos and Vietnam (Figure 6.3a and b), PC2 shows a trend towards higher values (i.e. weaker monsoon circulation) from ~5500 to ~4000 years BP. Thus, the millennial-scale mode of Southeast Asian monsoon variability is consistent with regional droughts, most notably in both Laos and Vietnam. However, while PC2 clearly contains some link with the local

hydrological signal, the much stronger control of insolation on the δ^{18}O records (PC1) is potentially the limiting factor in deconvolving summer and winter monsoon variability across these sites. Thus, it is proposed that more local rainfall proxies, such as δ^{13}C and trace elements in speleothems, potentially contain more information on summer and winter monsoon rainfall variability.

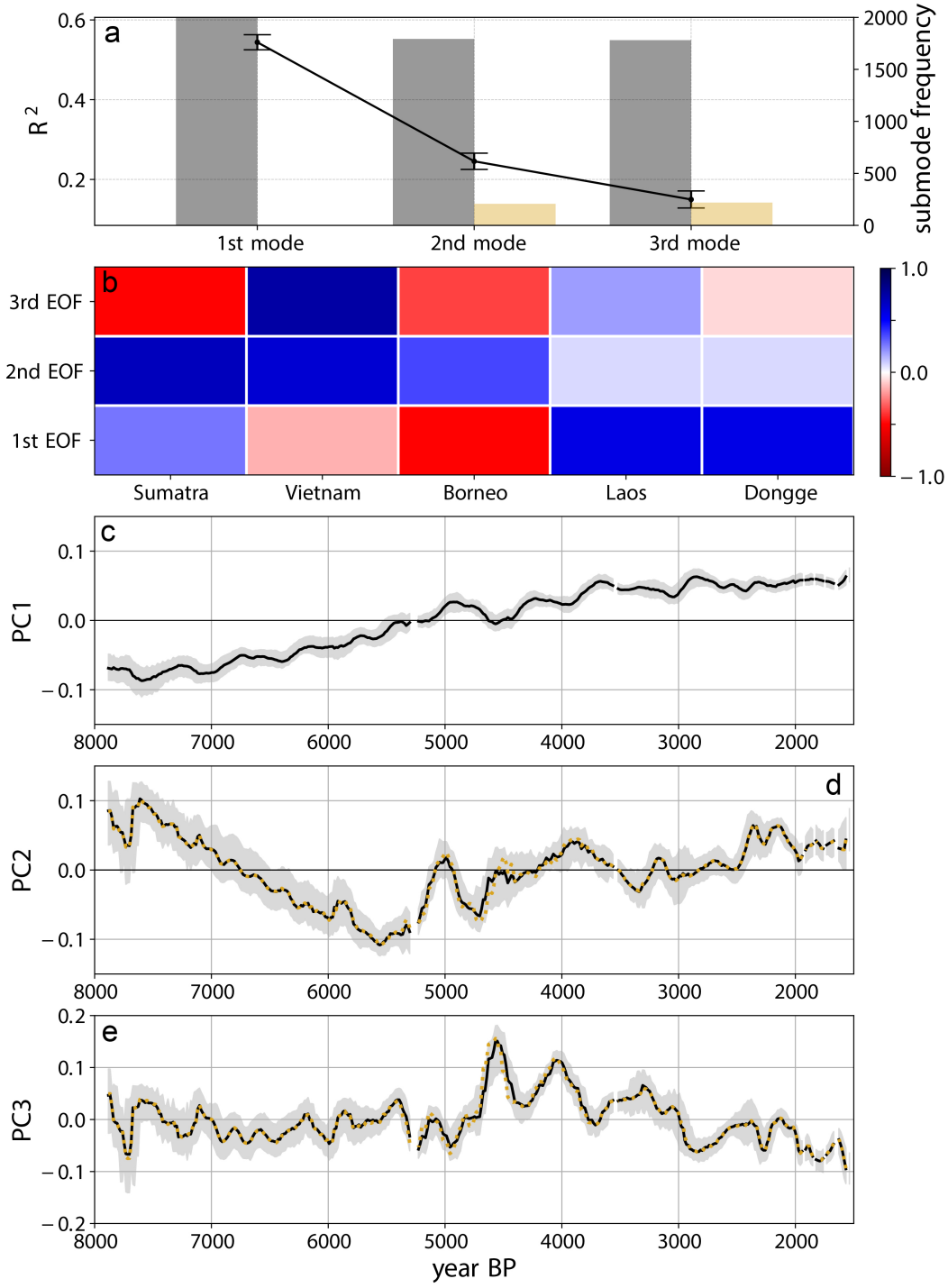

Figure 6.4: MC-PCA on the δ^{18}O records of Sumatra, Vietnam, Borneo, Laos and Southern China (Dongge Cave). **a** mean R^2 indicates the variance explained by each mode (dashed lines), with 2σ-error bars for different R^2-estimates, resulting from the different age realizations. Due to the clustering there is a dominant mode (grey bar), which uses most of the age model realisations and a mirrored mode describing the residuals (yellow bar). **b** Averaged EOF for each mode and each ensemble of proxy time series. The EOF gives a value of correlation between proxy time series and the individual PC. **c**, **d** and **e** three leading PCs extracted from the five δ^{18}O records. The solid line shows the dominant PC, dashed yellow line the sign-flipped PC (after flipping) and the shading represents the 2σ-error region propagated from the dating uncertainties for **c** PC1, **d** PC2 and **e** PC3.

Results of the PCA on the δ^{13}C profiles shows that all records load heavily on to PC1 (Figure 6.5b). The strongest positive correlation between PC1 and the proxy records is found for Laos (0.62), followed by Sumatra (0.46), and Borneo (0.41). The winter monsoon records - e.g. the stalagmite from Vietnam (TD3) and Lake Huguang Maar record from southern China (Yancheva et al., 2007) - show a weaker, but also positive correlation with PC1 (Vietnam: 0.27 and southern China: 0.37). These findings show that the first PC from stalagmite δ^{13}C records across Southeast Asia share a common forcing(s) throughout the Holocene, despite the different modern rainfall regimes unique to each site (Chapter 3). Worth noting, however, is that the records more dominated by the winter monsoon have a higher correlation with PC2, with a correlation of 0.57 for Vietnam and 0.43 for southern China (Huguang Maar). Additionally, Sumatra shows a strong negative correlation with PC2 of -0.59. This can be explained by the local hydroclimate, which has a minimum in rainfall during the boreal summer and a strong influence of the Indo-Australian summer monsoon (Chapter 3). The Borneo record loads most heavily on PC3 (-0.81). This could be explained either by the local climate, with year-round rainfall or, as suggested by Partin et al. (2013), indicate that local hydrology is not the primary control of δ^{13}C variability in Bukit Assam Cave.

Nevertheless combined, the first three PCs explain 77% of the variance, covering most of the variability of all five records. Crucially, the dry conditions observed in the proxy records between 5000 to 4000 years BP are evident in both PC1 and PC2, suggesting a strong coherency between the sites during this time. These results highlight that the drought affected most of Southeast Asia, with reduced rainfall, not just confined to the summer monsoon season, but also to the autumn/winter season. Further, the results indicate that the spatio-temporal pattern observed from hydrological records across Southeast Asia share similarity over the Holocene. Due to the differences in seasonality of peak rainfall at each site, the speleothem record from Laos is likely to reflect the Southwest Summer Monsoon, whereas the record from central Vietnam reflects the Northeast Monsoon best (Figure 6.1).

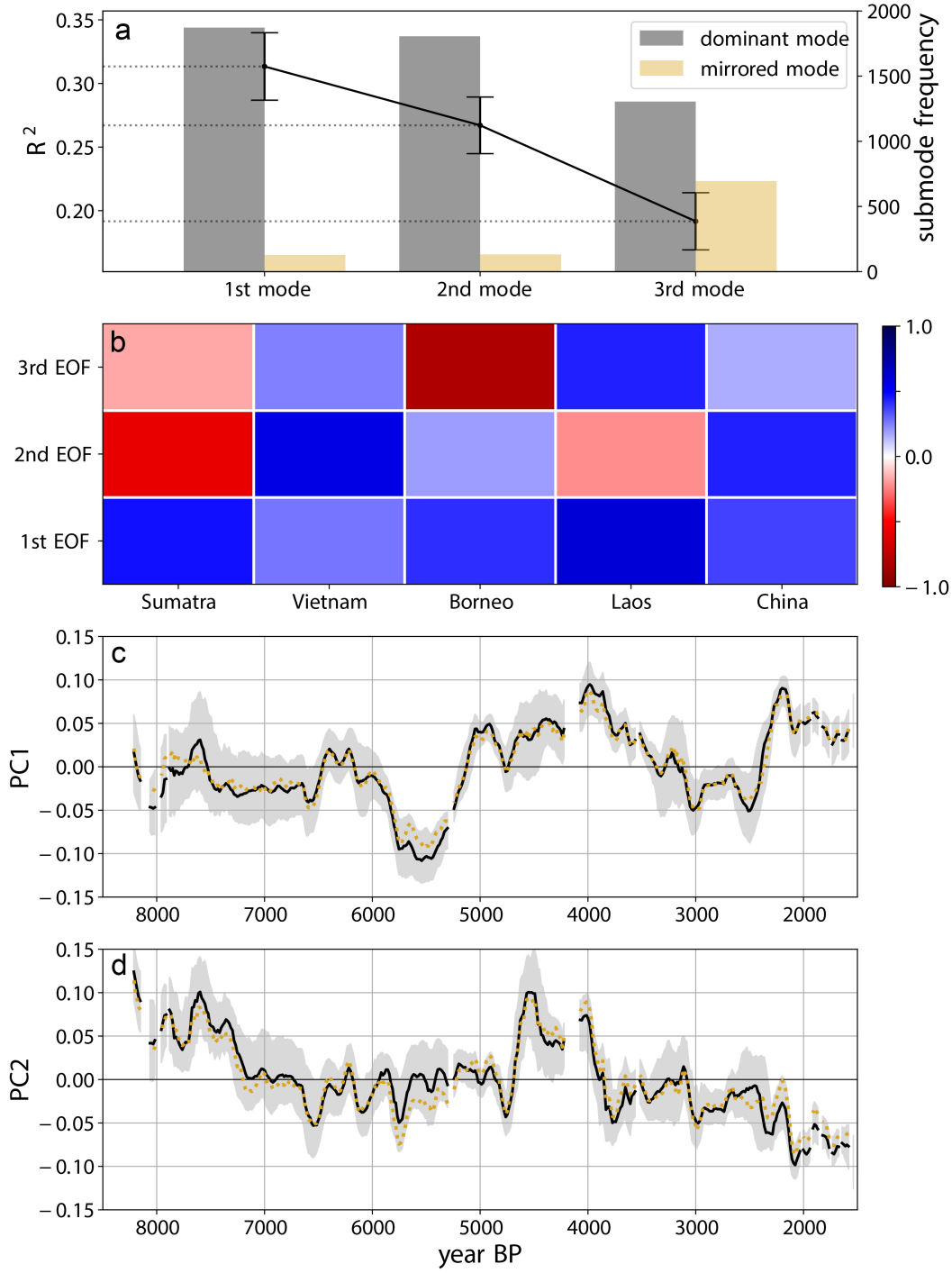

Figure 6.5: MC-PCA on the δ^{13}C records of Sumatra, Vietnam, Borneo, Laos and the lake record from Southern China (Huguang Maar). **a** mean R^2 indicates the variance explained by each mode (dashed lines), with 2σ-error bars for different R^2-estimates, resulting from the different age realizations. Due to the clustering there is a dominant mode (grey bar), which uses most of the age model realisations and a mirrored mode describing the remains (yellow bar). **b** Averaged EOF for each mode and each ensemble of proxy time series. The EOF gives a value of correlation between proxy time series and the individual PC. **c/d** Two leading PCs extracted from the five δ^{13}C records. The solid line shows the dominant PC, dashed yellow line the sign-flipped PC (after flipping) and the shading represents the 2σ-error region propagated from the dating uncertainties for **c** PC1 and **d** PC2 respectively.

6.4.2 The relation of summer and winter monsoon

A recent study addressed the concerns regarding using only speleothem $\delta^{18}O$ records as summer monsoon proxies and used several lake and marine cores instead to produce stacked East Asian Summer and East Asian Winter Monsoon records (Kaboth-Bahr et al., 2021). By doing so, they found that the summer and winter monsoon in Asia were highly correlated between 10,000 to 4500 years BP and this relationship became much weaker afterwards. A summer/winter comparative analysis with a similar level of detail is currently not achievable for Southeast Asia due to the paucity of published records from the region. However, the close proximity of well-dated speleothem records from Tham Mai Cave (Laos) and Thien Duong Cave (central Vietnam), combined with their distinct summer and winter monsoon climatologies respectively (Figure 6.1), makes them ideal places for deconvolving the evolution and interrelationships between the two monsoon systems (Chapter 3).

The multiproxy hydroclimate records from Vietnam and Laos show pronounced declines in both summer and winter monsoonal rainfall respectively, from 5000 to 3500 years BP and enhanced monsoon rainfall between 8000 to 6000 years BP. However, similar to the lake/marine reconstructions from East Asia, the relationship between the two monsoon systems appears to break down during the late Holocene (Figure 6.6b and d); while central Vietnam becomes progressively wetter during the late Holocene, Laos becomes progressively drier (Figure 6.6a and c). In contrast to findings based on Chinese speleothem $\delta^{18}O$ records alone, the stacked summer monsoon records based on lake and marine sediments, along with hydrological proxies from Laos speleothems shows that East Asian summer monsoon rainfall is not simply driven by summer insolation, rather millennial-scale drivers may have been more dominant. The general agreement amongst the different proxies and archives of both summer and winter monsoon variability across East Asia therefore suggests a generally coherent pattern of Holocene monsoon co-evolution.

These results from Vietnam are significant in that they show that the prolonged period of the drought, that swept across Southeast Asia during the mid-Holocene, was not only driven by significant declines in summer rainfall, but also large deficits in winter monsoon precipitation. It is therefore likely that both summer and winter rainfall changes had a common forcing, at least for the early- and mid-Holocene.

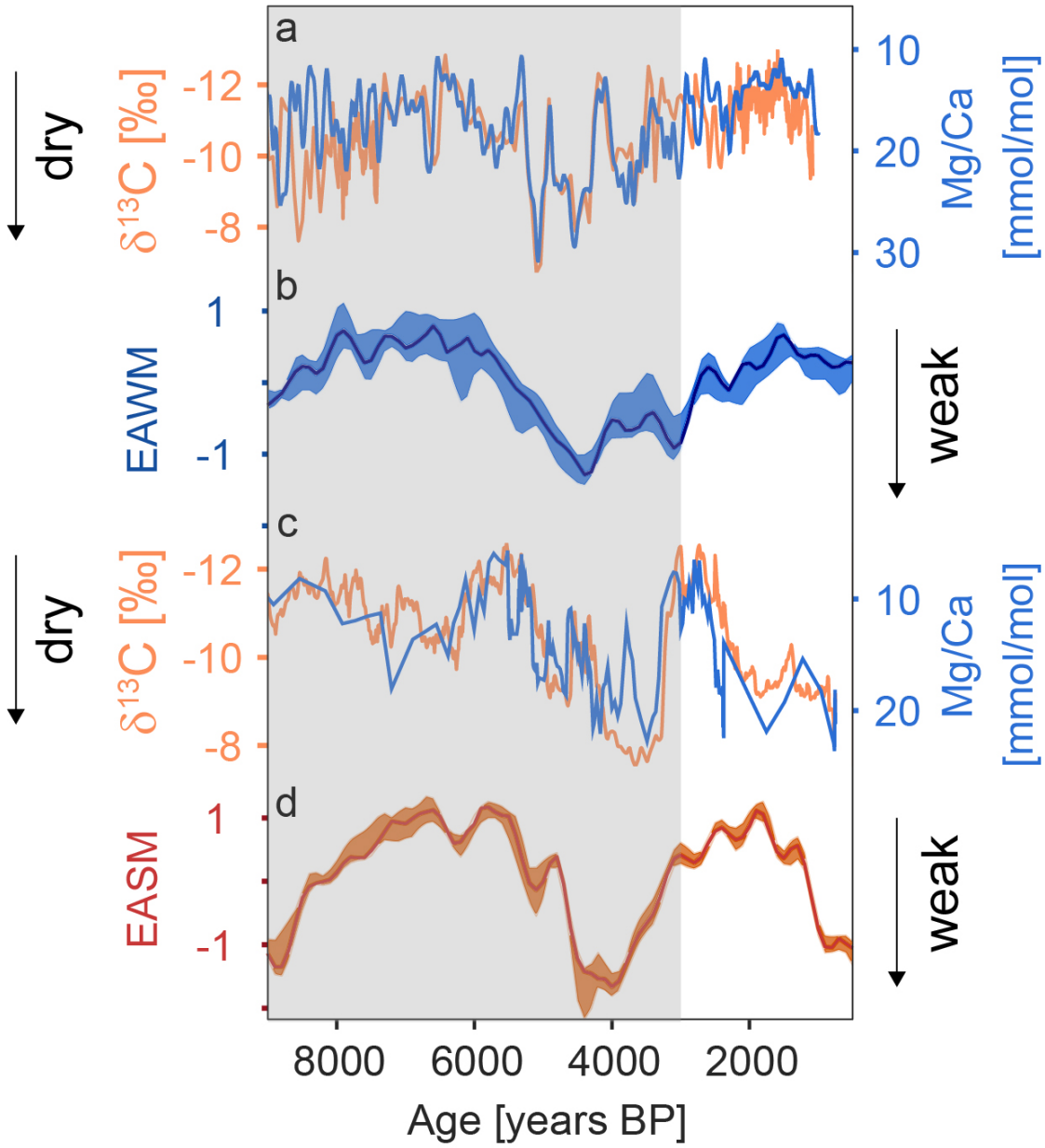

Figure 6.6: **a** δ^{13}C and Mg/Ca record of TD3 in comparison to **b** stacked Asian winter monsoon index, reconstructed by Kaboth-Bahr et al. (2021) from five sediment cores in Asia. **c** δ^{13}C and Mg/Ca record from Laos (Tham Mai Cave) in comparison to **d** stacked Asian summer monsoon index, reconstructed by Kaboth-Bahr et al. (2021) from five sediment cores in Asia. The shading indicates the time period where summer and winter monsoon follow the same trend, which is until ca. 3000 years BP. Afterwards the stacked records decouple and the speleothem records indicate an opposing trend, with central Vietnam getting wetter and northern Laos drier.

6.5 Discussion

6.5.1 Causes of mid- to late Holocene winter monsoon failure

Traditionally, research has suggested that the decline in Asian summer monsoon over the Holocene was a result of a southwards shift in the ITCZ (Chabangborn and Wohlfarth, 2014; Maxwell, 2001; Sachs et al., 2018; Schneider et al., 2014) due to declining summer insolation (Schneider et al., 2014). Since around 8,000 years ago, the declining interhemispheric temperature gradient has been linked to decreasing summer monsoon rains in India and East Asia over this time (Sachs et al., 2018). A weak temperature gradient between the hemispheres would drive the ITCZ mean position towards the equator. This explanation is not corroborated by proxy studies across Southeast Asia, which indicate a spatio-temporally diverse pattern (Figure 6.3). Records from the north and south of mainland Southeast Asia and from the Maritime Continent all indicate relatively dry conditions around 5000 to 3000 years BP (Chawchai et al., 2021; Griffiths et al., 2009, 2020; Wurtzel et al., 2018) (Figure 6.3). While a southward shift of the ITCZ during the mid-Holocene could explain the dry conditions across mainland Southeast Asia, it would likely have resulted in wet conditions over the Maritime Continent. However, this is not the case for Sumatra and Flores, both indicating dry conditions during this time. Thus, a simple north-south shift in the ITCZ mean position over the Holocene, does not adequately explain palaeo-monsoon variability across Southeast Asia.

More recently, Griffiths et al. (2020) used speleothem multi-proxy data along with mid-Holocene climate model-simulations (Pausata et al., 2017) to attribute the drought in Laos with an increase in dust load and reduction in vegetation at the end of the Green Sahara between 5000-4000 years BP. More precisely, the decline in summer insolation after 6000 years BP reduced summer monsoon rainfall across the African monsoon region (McGee and deMenocal, 2017), leading to significant drying of northern Africa which, combined with amplifying vegetation and dust climate feedbacks, formed the Sahara Desert around 3000 years BP (Kröpelin et al., 2008). The lack of vegetation led to an increase in dust loading of the atmosphere, which, in conjunction with decreasing summer insolation caused a drop in SSTs in the Indo-Pacific Warm Pool, especially in the eastern Indian Ocean. This period of cooling between ~5600 and ~4200 years BP, observed in both the eastern and western boundaries of the tropical Indian Ocean (Abram et al., 2009; Kuhnert et al., 2014), was accompanied by an eastward shift in the Pacific Walker Circulation. Analogous to a modern-day

El Niño event where increased convection and uplift of air masses over the western Pacific is replaced by drier descending air; this shift resulted in lower summer monsoon precipitation in Laos (Griffiths et al., 2020).

In the context of this prior work, the record from central Vietnam, therefore, suggests that not only was Southwest Summer monsoonal rainfall affected, but also rainfall related to the Northeast Monsoon. The summer monsoon in Laos is mainly derived from south-westerlies bearing moisture from the Indian Ocean (Yang et al., 2016). Thus, a decline in SSTs in the Indian Ocean can force changes in the summer monsoonal circulation in mainland Southeast Asia. Collectively, observations from the western Pacific do not exhibit such a drastic decline in SSTs between 5600 and 4200 years ago, but rather a continuous decline in SSTs over the Holocene (Figure 6.7c). Though on the other hand, further northward over the East China Sea, SSTs plummeted to their lowest values of the Holocene between 5000-4000 years BP during the peak of the drought in Vietnam (Kajita et al., 2018).

To further investigate changes in the mean ocean state as a potential driver of the monsoons in Southeast Asia the following section focuses on interannual variability of rainfall in central Vietnam.

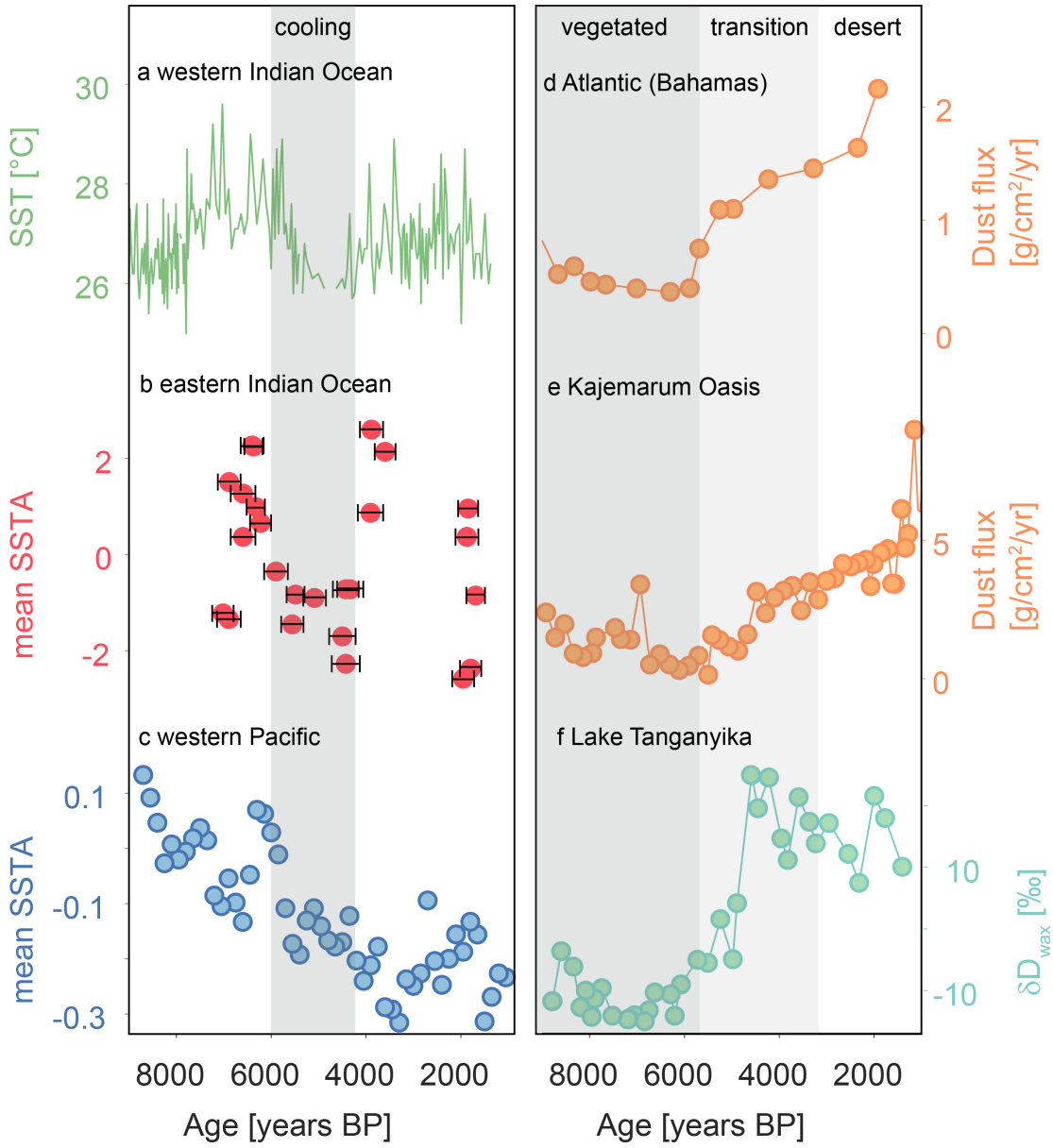

Figure 6.7: **a** Annual mean sea surface temperature based on Mg/Ca from a marine core of the coast of Tanzania (Kuhnert et al., 2014), **b** sea surface temperature anomalies (SSTA) reconstructed from corals in the eastern Indian Ocean (Abram et al., 2009) and **c** stacked SST anomalies from several records across the western Pacific (Dang et al., 2020). The shading indicates strong cooling across the Indian Ocean, whereas the western Pacific shows a gradual cooling over the Holocene. The right panel indicates the evolution of the desertification of the Sahara, by **d** a marine sediment core from the northern Atlantic recording airborne dust emission from Africa, **e** dust flux recorded in an oasis in the Sahel and **f** leaf wax δ^2H from lake Tanganyika in central Africa. The shading indicates the state of the Sahara, from a vegetated to a desertifed region.

6.5.2 Interannual variability and the Northeast Monsoon

Palaeoclimate data suggest ENSO variance was reduced during the mid-Holocene around 5,000 years ago relative to pre-industrial (Carré et al., 2014; McGregor et al., 2013) (Figure 6.9), when dry conditions prevailed across Southeast Asia. Traditionally, it has been hypothesized that changes in orbital forcing was the primary driver for this reduction in ENSO variance (Clement et al., 2000). However, more recent work has shown no simple link between decadal-scale ENSO variability and orbital forcing during the Holocene (Emile-Geay et al., 2016). An alternative hypothesis invokes land surface changes across Africa as the main culprit. Indeed, Pausata et al. (2017) recently demonstrated, using idealized climate model sensitivity experiments, that internal climate feedbacks associated with Saharan vegetation and atmospheric dust loads had a significant influence on both ENSO variance and mean state. In particular, they showed that vegetation-dust feedbacks during the Green Sahara (decreased dust load) increased the strength of the west African monsoon, which, via changes in Atlantic and Pacific ocean-atmosphere dynamics, caused the Pacific Walker Circulation to shift westward analogous to modern-day La Niña conditions. Such a shift would have lead to increased rainfall across Southeast Asia, which is evident in the reconstructions from Laos and Vietnam (Figure 6.3a and b). Following this period of enhanced monsoon rainfall, Griffiths et al. (2020) proposed an opposing mechanism, leading to a eastward shift in the Pacific Walker Circulation and dry conditions in Southeast Asia. The following sections investigate changes in interannual variability of rainfall in central Vietnam, and compare these results to ENSO records from the Pacific. Change in ENSO variance can be symptomatic for underlying changes in the mean ocean state of the Pacific (Roberts et al., 2014) and therefore might confirm the hypothesis of a shifting Walker Circulation.

Modern observational data show that there is a close link between the Northeast Winter monsoonal rainfall and ENSO variability in central Vietnam at present (Chen et al., 2012a; Vu et al., 2015). However, it remains unclear whether a similar relation was evident during the Holocene. The trace element record of TD3 has a sufficient temporal resolution (at least >2 samples per year) to explore ENSO and decadal variability over the Holocene. Due to the uncertainties related to age modelling, the analysis was applied to three different age model realisations. The power spectra of the Mg/Ca time series shows significant peaks at ENSO and lower decadal frequencies during the late Holocene (Figure 6.8). The ENSO band is evident during the late Holocene in

all three power spectra, showing that despite the age uncertainties, an ENSO frequency can be detected. Contrasting to this is the absence of significant decadal or lower frequencies during the mid-Holocene for all three age realisations. The early Holocene does not show a clear ENSO frequency, but two of the age realisations suggest some (sub)decadal frequencies.

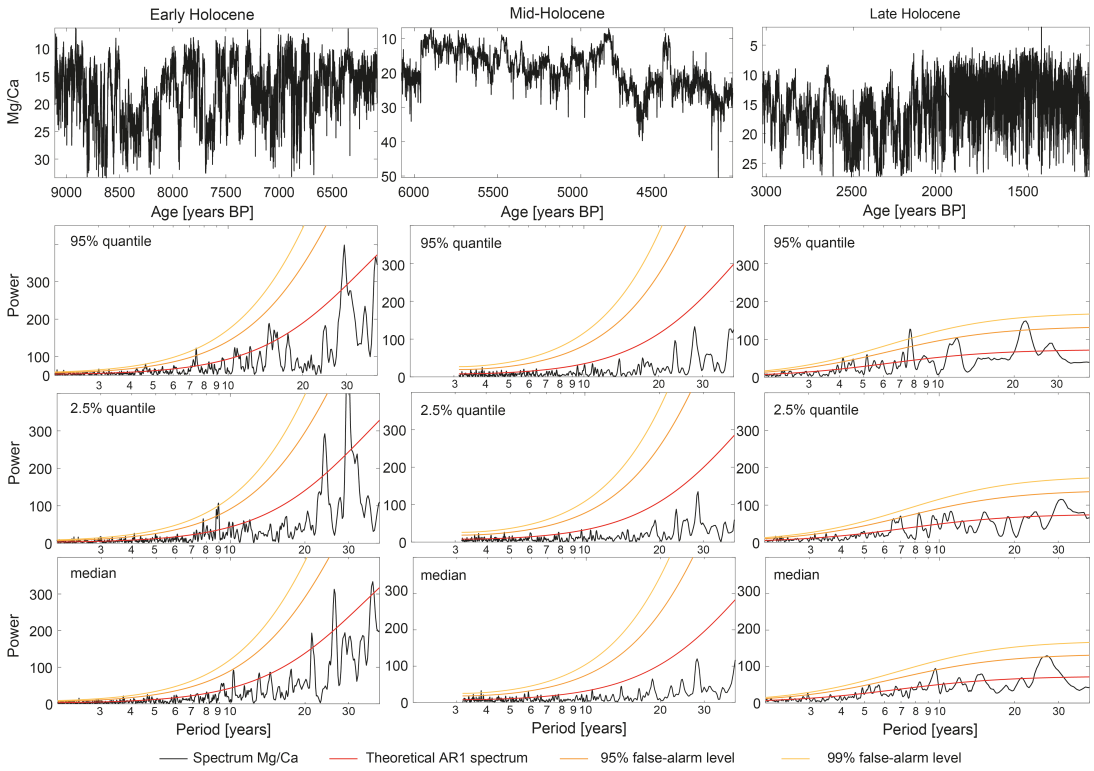

Figure 6.8: Mg/Ca time series and power spectra for each section, using the higher age uncertainty limit (95% quantile), the lower age uncertainty limit (2.5% quantile) and the median calculated by COPRA. The lines on the power spectra give value of significance, with the 99% quantile being the most significant. Peaks below the 95% quantile are not significant. Important significant peaks are labelled. It is evident that the mid-Holocene is strongly significant lacking interdecadal and decadal variability, compared to the early and late Holocene.

To further investigate (sub)decadal variability over the Holocene, the variance is calculated from the TD3 Mg/Ca time series. Here the ENSO- and decadal-scale variance of the Mg/Ca time series is extracted by, firstly, removing the millennial-scale trend, which is determined by a sliding Gaussian kernel average. The time series is left with annual to multi-centennial-scale variability, from which secondly, the ENSO and decadal variance is calculated again using Gaussian kernel windows (Rehfeld and Kurths, 2014). Lastly, the resulting variances in each section of the time series are averaged, according to the subsections described in the section '6.3.1 Spectral Analysis', to avoid a sampling bias.

Compared to the power spectra, using the variance of the ENSO and other frequency bands, has the advantage that more information is contained (Russon et al., 2015). The variance of an ENSO band encompasses not only changes in frequency, but also in amplitude or general trend of the data. For ENSO events, this would mean a shift in the variance can represent variability in the frequency of ENSO or a change in the strength of ENSO.

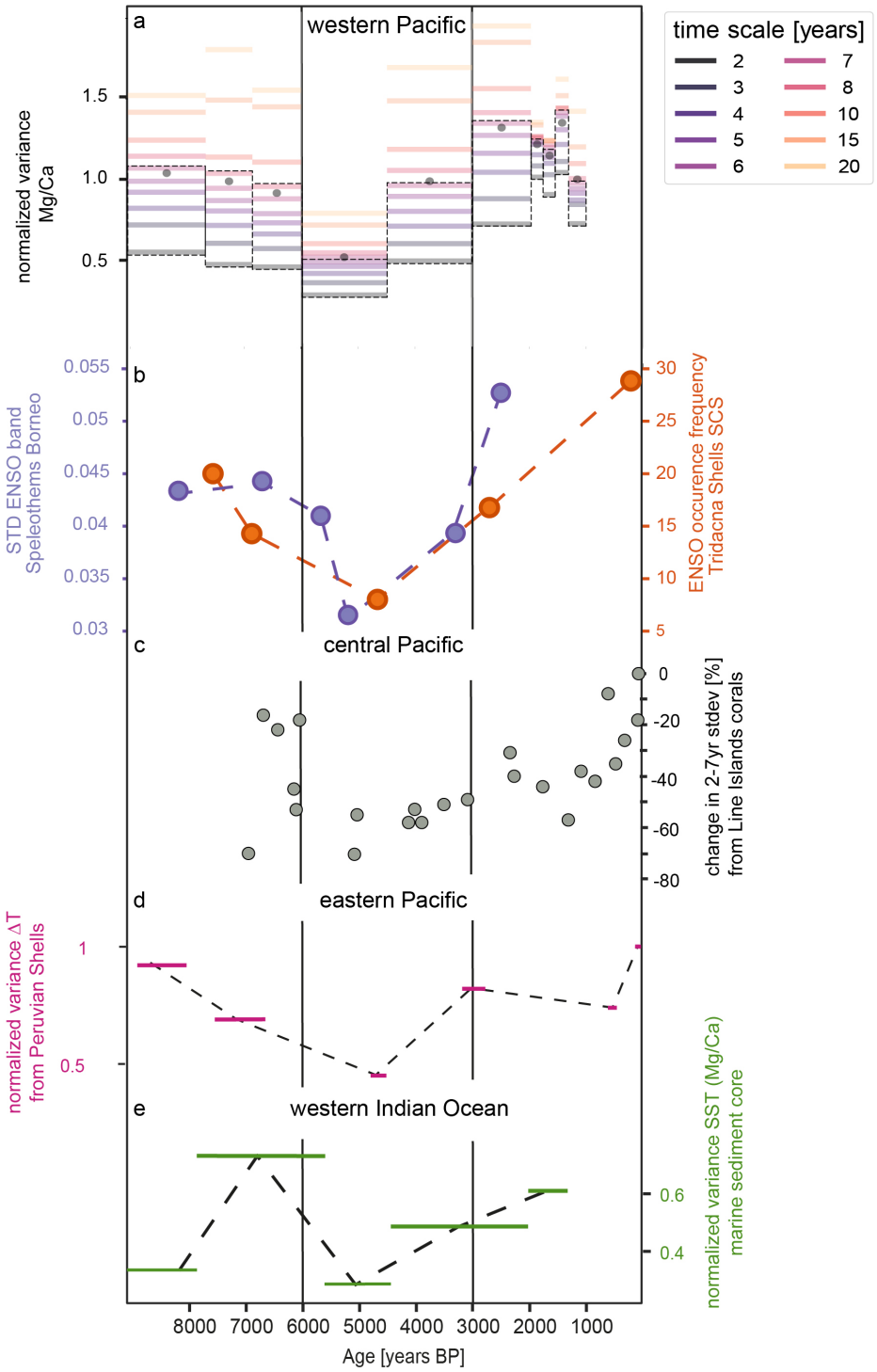

Figure 6.9: **a** Normalized variance (2 to 20 years) calculated from the Mg/Ca record of TD3, where each bar is referring to a section of the spectra analysis (Figure 6.8). The dots show the mean variance for 2 to 20 years and the dash boxes indicate the ENSO band variance (2 to 7 years). The Mg/Ca record is compared to **b** ENSO reconstructions from a Borneo stalagmite (purple) (Chen et al., 2016a) and the frequency of ENSO event occurrence retrieved from a Tridacna shell in the South China Sea (Shao et al., 2020), **c** ENSO variance reconstructed from central Pacific corals (Cobb et al., 2007) **d** normalized ENSO variance based on Peruvian shells (Carré et al., 2014) and **e** decadal SST variability retrieved from Mg/Ca ratios from a marine core in the eastern Indian Ocean (Kuhnert et al., 2014).

The Mg/Ca variance shows a similar pattern to the power spectra, indicating that Northeast Winter Monsoon rainfall variability declined from the early to mid-Holocene, in concert with the decreasing trend in ENSO variance (Figure 6.9a). The wettest interval across southeast Asia, between ~6-5000 years ago (Figure 6.3b), coincides with the lowest variability in Northeast Winter Monsoon rainfall and lowest ENSO variance (Figure 6.9). Shortly thereafter, the autumn/winter rainfall variance in Vietnam exhibits a trend reversal beginning around 4500 years ago that is also associated with the reconstructed increasing trend in ENSO variance during the end of the Green Sahara. Therefore, the changes in ENSO variance during the Holocene are likely reflecting the lower-frequency changes in Southeast Asian hydroclimate.

The hypotheses of Pausata et al. (2017) and Griffiths et al. (2020) - i.e. zonal shifts in the Pacific Walker Circulation were modulated by amplifying vegetation and dust feedbacks impacting the west African monsoon - are sufficient in explaining the regional-scale hydroclimate across central Vietnam, Laos and Flores during the early to late Holocene period. However, this mechanism cannot explain the decoupling of summer and winter monsoon variability after 3000 years BP. The TD3 Mg/Ca record shows increased Northeast Winter Monsoon variability in central Vietnam after 3000 years BP was superimposed on a generally wetter hydroclimate. By contrast, the Southwest Summer Monsoon record from Laos indicates generally drier conditions (Figure 6.3a and b) during the late Holocene, coinciding with increased ENSO activity observed across the Pacific (Figure 6.9). Northeast Winter Monsoon rainfall variability in central Vietnam increased after 3000 years BP, when the Sahara was desertified as today.

The late Holocene western Pacific is characterised by cool SSTs (Figure 6.7c) (Dang et al., 2020; Zhang et al., 2019a). Colder SSTs in the western Pacific can lead to stronger trade winds creating a cyclonic circulation over the Philippines, enhancing the Northeast Winter Monsoon circulation over Southeast Asia (Zhao et al., 2019). This could potentially explain increased rainfall in central Vietnam. Laos on the other hand, receives moisture from the Indian Ocean during the summer monsoon season, rather than from the Pacific (Yang et al., 2016). For the late Holocene it has been proposed that the Indian Walker Circulation slowed down over the last 3000 years (Mohtadi et al., 2017), which would result in reduced Southwest Monsoon rainfall, as reconstructed in Laos (Figure 6.3a). This slowdown of the Indian Walker Circulation has been linked to stronger upwelling and a shallower thermocline in the eastern Indian Ocean, resulting in stronger surface

cooling, weakling convection in this region (Mohtadi et al., 2017). The different forcing from the Indian and Pacific Ocean on seasonal rainfalls in Southeast Asia could potentially explain the inverse relationship between Southwest and Northeast Monsoon rainfall in Southeast Asia during the late Holocene. The onset of modern day ENSO activity, which imprinted on interannual rainfall variability in central Vietnam also hints towards a stronger influence of Pacific SSTs on climate in central Vietnam in the late Holocene.

6.6 Conclusions

This chapter investigated the Holocene hydroclimate in Southeast Asia, with a particular focus on the Northeast Winter Monsoon in central Vietnam. Based on a MC-PCA which was applied to 5 records across Southeast Asia and China, it is shown that the first PC of speleothem δ^{18}O is dominated by an orbital trend, following insolation. While some information about monsoonal rainfall is contained in the second PC of speleothem δ^{18}O, it is found that more local proxies, such as δ^{13}C are better suited as proxies for rainfall variability. The proxy records of Southeast Summer and Northeast Winter Monsoon, both indicate relatively wet conditions between 7000 and 6000 years BP, which is followed by pronounced dry conditions between 5000 and 3000 years BP. After 3000 years BP the Southeast Summer appears to weaken and drier conditions prevail, whereas the Northeast Winter Monsoon strengthens and central Vietnam receives increased rainfall. Therefore, the Southeast Summer and Northeast Winter Monsoon likely share a common forcing for most of the Holocene, but decouple after 3000 years BP. During the mid-Holocene changes in the west African monsoon, impacted the vegetation cover of the Sahara, which in turn lead to changes in SST in the Atlantic and Indian Ocean. Here it is proposed that one possible result was a westward shift in the Pacific Walker Circulation, increasing rainfall in Southeast Asia between 7000 and 6000 years BP. Between 5000 and 3000 years BP an eastward shift in the Pacific Walker Circulation led to an opposing result, with strongly decreased monsoon rainfall. This is also evident in the interannual variability of rainfall in central Vietnam and ENSO records from the Pacific, which indicate a strongly reduced ENSO variance during the mid-Holocene. A change in ENSO variance can be indicative of a change in the mean ocean state of the Pacific and thus of the Walker Circulation. The spatial footprint of ENSO across Southeast Asia became much larger during the late Holocene as the climate mode became more extreme. After 3000 years BP the Southwest and Northeast

Monsoon show opposing trend for local rainfall, which could potentially be attributed to increase Pacific ocean forcing on Northeast Monsoon variability, whereas the Southwest Monsoon is mainly impacted by changes in the Indian Ocean. This chapter highlights that the forcing of summer and winter monsoon in Southeast Asia varied over the Holocene, explaining the mismatch between proxy records of both monsoons over the Holocene.

Chapter 7

Climate of the Common Era

7.1 Chapter summary

Climate changes over the last 2000 years are often used to set the current warm phase into perspective. However, high-resolution climate records from Southeast Asia are sparse, particularly for the period between 2000 and 1000 years BP. Consequently, centennial and decadal changes and their climate drivers are not fully explained by current research. This chapter aims to identify climate drivers in the recent past in central Vietnam and Southeast Asia. By using 18 proxy records from the Asian and Australian monsoon regions, this chapter found changes in the ITCZ during a northern hemisphere cool phase. The proxy reconstructions show that only records located in the northern part of mainland Southeast Asia and the southern part of the Maritime Continent indicated wetter conditions during the cool phase from 1600 to 1300 years BP. In contrast, the edges and core region of the ITCZ were drier during this time. This cold phase was mainly a result of cooler winter temperatures in Southeast Asia and the seasonal bias in cooling potentially drove a faster southwards migration of the ITCZ during boreal winter, shortening the rainy season over the northern Maritime Continent, but enhancing it over mainland Southeast Asia and Australia. Alternatively, the hydrological pattern could be explained by a squeeze of the ITCZ belt over its seasonal extreme positions, enhancing rainfall over these regions. These findings highlight that the timing and position of the ITCZ seasonal migration could be a key factor controlling local seasonal climate variability. Current state-of-the-art climate models are still limited in simulating seasonal changes in the ITCZ rather than the mean. Thus, identifying controls on seasonal climate

variability in Southeast Asia improves the confidence in climate predictions of near-future climate in this region.

7.2 Introduction

The anthropogenically induced warming of recent years is projected to cause a rise in extreme climate events such as heatwaves, droughts, and flooding (Masson-Delmotte et al., 2013). The reliability of climate models is validated by comparing simulations of past climate to palaeoclimate reconstructions (Atwood et al., 2020). Therefore, future rainfall patterns in Asia remain unresolved due to the lack of high-resolution climate data extending beyond the last century in this region (Mohtadi et al., 2016; Taylor et al., 2012). One of the challenges in predicting the impacts of anthropogenic climate change is separating the natural climate variability, which is not forced by greenhouse gases, from the currently observed changes (Atwood et al., 2020). Therefore, palaeoclimate records from the Common Era covering the last two millennia (2000 to -70 years BP), during which there was no anthropogenic greenhouse gas forcing, are often used for understanding past climate variability. On a global scale, these records have shaped the understanding of climate mechanisms in recent times, helping to set the current warm phase into context of previous warm periods (Neukom et al., 2019a). Pronounced cold and warm phases were observed over the Common Era, some with almost global effects like the Little Ice Age (LIA) in 1350-1850 CE or the Medieval Warm Period (MWP) (also called the Medieval Climate Anomaly) during 900-1300 CE (Ahmed et al., 2013) (Figure 7.1). A growing body of highly resolved proxy records spanning the globe are available for the Common Era (Neukom et al., 2019b), linking climate variability mainly to external forcing, such as solar insolation and volcanic activity (Mann et al., 1998; Schurer et al., 2013; Sigl et al., 2015; Stoffel et al., 2015). However, most of these records cover the later half of the Common Era (from 1000 years BP on), thus, more proxy data is needed to confirm these findings. Especially, the first half of the Common Era (2000 to 1000 years BP) is lacking proxy coverage (Neukom et al., 2019a), despite the few records available showing that major societal changes in Europa and Asia can be linked to climatic shifts during this time (Büntgen et al., 2016).

For the Asian Summer Monsoon region, it is suggested that major controls on monsoonal rainfall during the Common Era are solar forcing (Tan et al., 2011; Wang et al., 2019; Yan et al., 2015a;

Zhang et al., 2008), ENSO (Chen et al., 2015; Cobb et al., 2003; Conroy et al., 2010) and volcanic activity (Anchukaitis et al., 2010; Liu et al., 2016). For the Asian Winter Monsoon some studies proposed that centennial-scale variability over the Common Era is controlled by solar activity (Sagawa et al., 2014), whereas other proxy records found a link between periods of intensified winter monsoon circulation and North Atlantic cooling events (Hao et al., 2017; Li et al., 2018), or ENSO events (Wang et al., 2008). Regions closer to the equator, such as Southeast Asia, have very limited proxy coverage for (Northeast) Winter Monsoon variability over the Common Era, leaving an important part of the Asian monsoon underrepresented. Chapter 6 of this work and other studies e.g. (Griffiths et al., 2020) showed that the mid-Holocene warm phase was characterised by an eastwards shift of the Walker Circulation causing drier conditions over Southeast Asia, affecting both summer and autumn/winter monsoon precipitation. The question therefore arises does the climate of the Common Era in Southeast Asia respond to warm and cool phases in the same way as in the more distant mid-Holocene? Results from Chapter 2 showed that the timing of ITCZ migration is the main factor controlling the general circulation and the relative contribution to rainfall from the summer versus winter monsoon circulation. However, it is not clear whether the ITCZ was a primary climate driver over the last 2000 years and how it was impacted by cool or warm phases.

Studies reconstructing hydroclimate variability in the Asian and Australian monsoon region have found that meridional and zonal shifts of convection cells in the Indo-Pacific region are a major factor modulating regional precipitation patterns over the Common Era (Denniston et al., 2016; Griffiths et al., 2016; Oppo et al., 2009; Tan et al., 2019a; Tierney et al., 2010). However, it is uncertain whether a meridional shift in the Walker Circulation or a zonal shift in the ITCZ is the dominant driver over the Common Era in the Asian-Australian monsoon region. Studies from the Indo-Pacific Warm Pool and the Maritime Continent (Konecky et al., 2013; Oppo et al., 2009; Tierney et al., 2010) suggest that on centennial timescales ITCZ displacements drive monsoon intensity in East Asia and the Indo-Pacific region. More evidence for mainly ITCZ controlled precipitation changes is found from the Asian-Australian monsoon region (Denniston et al., 2016; Yan et al., 2015a) indicating that the contraction or expansion of the ITCZ belt is the main control for spatial variability of rainfall. These studies suggest a contraction in the latitudinal range of the ITCZ during cold phases of the Common Era. It was further proposed that not only are meridional

shifts of the ITCZ modulating climate over the Common Era in this region, but also zonal shifts in the ascending branch of the Walker Circulation and the Pacific Ocean mean state are important factors (Griffiths et al., 2016; Yan et al., 2011). During cool phases the Walker Circulation can enhance and shift westwards, leading to wetter conditions in the Indo-Pacific region (Yan et al., 2011). Following studies combined both explanations and argued that a strengthened Walker Circulation likely occurred in conjunction with a latitudinal contraction of the ITCZ (Griffiths et al., 2016; Tan et al., 2019a). In summary, palaeoclimate records from Southeast Asia and Australia, suggest a contraction of the ITCZ's latitudinal extent and possible a westward shift of the ascending branch of the Walker Circulation during the cool phases.

However, a recent study based on speleothem records from the tropical regions of America suggests an expansion of the ITCZ region, rather than a contraction during the most recent cool phase (Asmerom et al., 2020). This is supported by modelling studies which show that a contraction of the ITCZ region is projected under future warming, suggesting that the ITCZ would expand during a cooling (Byrne et al., 2018). The average uplift within the ITCZ is projected to narrow and weaken (Byrne et al., 2018) under future warming, which in turn would result in increased rainfall across the Indo-Pacific region, but reduced rainfall over mainland Southeast Asia. However, this prediction is in contrast with proxy observations during warm phases of the Common Era, such as the Medieval Warm Period (MWP) in this region (Denniston et al., 2016; Griffiths et al., 2016; Tan et al., 2019a).

In summary, predicting future rainfall patterns in Southeast Asia, is limited by a lack of palaeoclimate records, which could validate climate simulations. Furthermore, our understanding of natural climate variability during the Common Era in tropical Asia, is limited due to a lack of consensus among proxy records and missing proxy data, especially, during the first half of the Common Era. This chapter aims to fill these gaps, with sub-annually resolved proxy data covering the time between 2000 and 1000 years BP in central Vietnam.

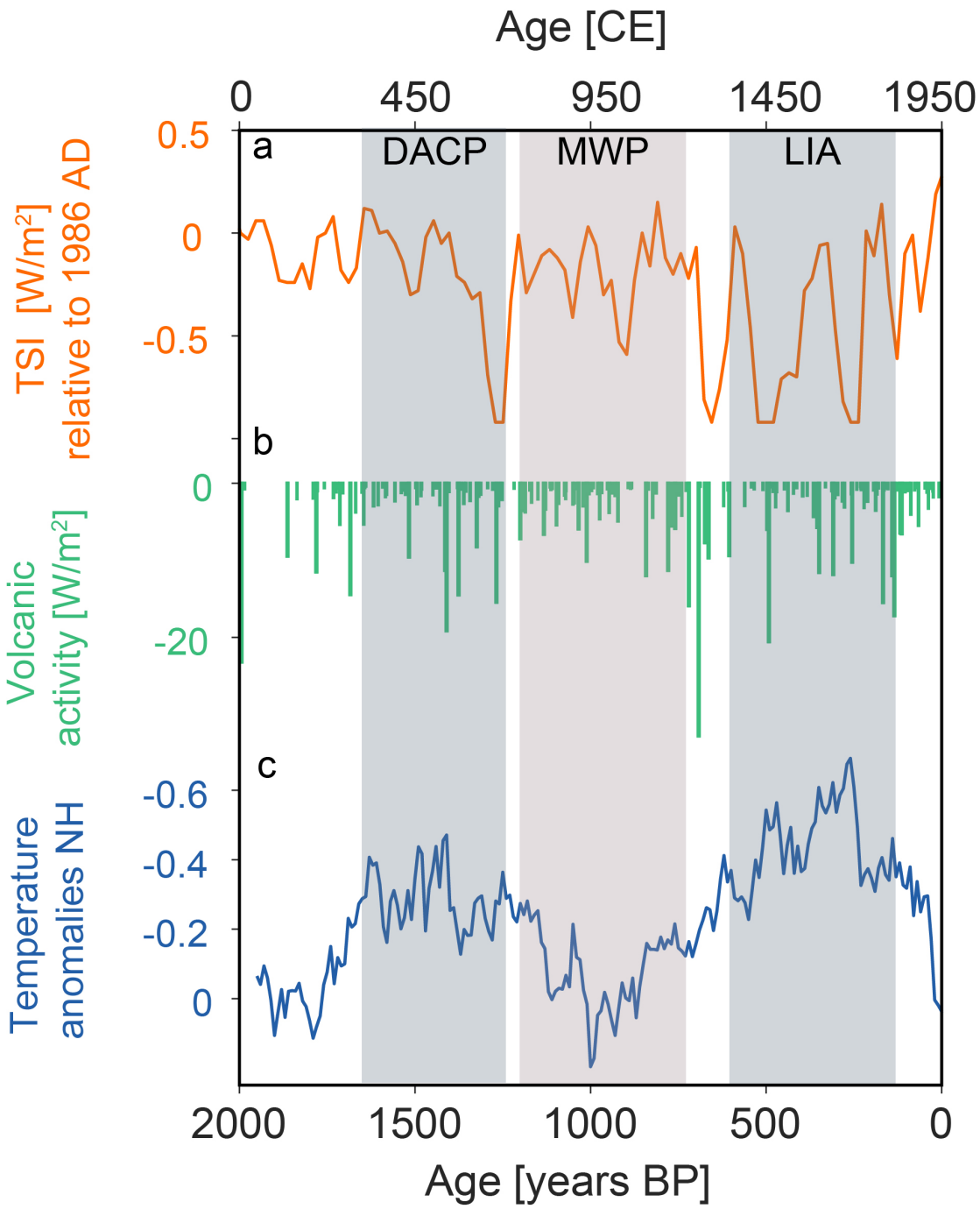

Figure 7.1: **a** Total Solar Irridance (TSI) relative to the year 1986 (Steinhilber et al., 2012), **b** global volcanic activity (Sigl et al., 2015) and northern hemisphere temperature anomalies (Ljungqvist, 2010). The grey boxes mark times of cool periods during the Common Era: Dark Ages Cold Period (DACP) and the Little Ice Age (LIA), and warm phases: Medieval Warm Period (MWP).

7.3 Data

TD3-1, the topmost 12 cm of stalagmite TD3, has an average age resolution of 2.6 years for stable isotopes and an average of 10 samples per year for trace elements and covers the time period between 1900 to 1000 years BP. Trace elements were down-sampled using a Gaussian smoothing with a kernel width of 5 (ca. 10 years), to reduce the noise and make decadal trends visible in the Mg/Ca time series. The interpretation of the proxies remains equal to Chapter 6, with carbon isotopes and Mg/Ca ratios reflecting local hydrology and oxygen isotopes reflecting moisture source dynamics, however, overprinted by local hydrology in the cave.

7.3.1 Age uncertainties

Research has strongly focused on warm phases during the Common Era, aiming to identify natural variability compared to the current warm phase. For TD3-1, the age uncertainties over the Common Era strongly limit directly correlating this record to others (Griffiths et al., 2016; Tan et al., 2019a). The age uncertainties are largest in the top age of TD3-1 (Figure 7.2e) with an error of up to 150 years. This means that the drought after 1100 years BP could correspond to increased temperatures during the MWP (Figure 7.2a, b and c) or to a drop in winter temperatures prior to the MWP (Figure 7.2d). Despite the uncertainties in the topmost section of TD3-1, the section prior to 1200 years BP has a lower age uncertainty. In this chapter, the focus will be on the Dark Ages Cold Period (DACP) due to the better age control.

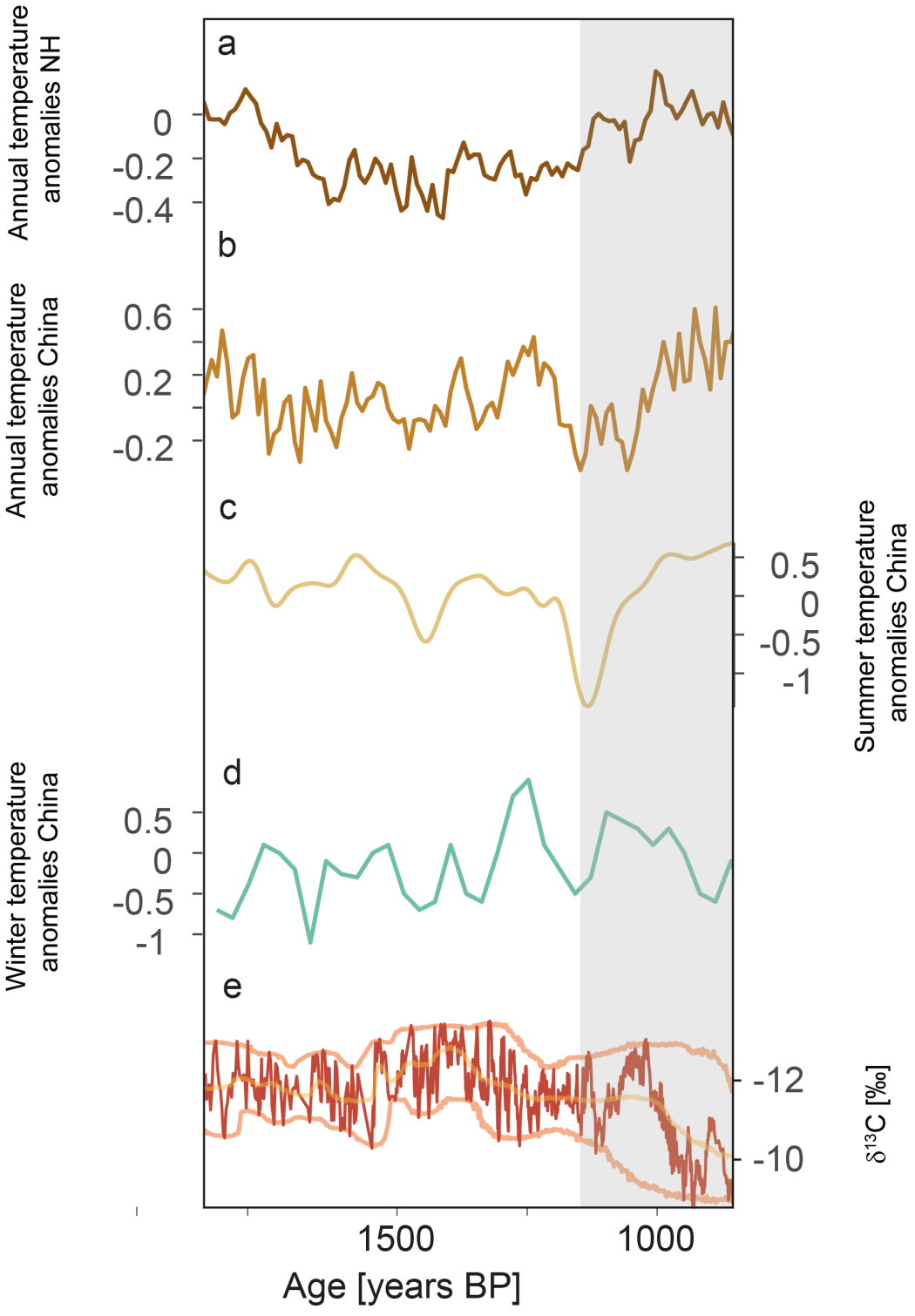

Figure 7.2: **a** Temperature anomalies from the northern hemisphere (Ljungqvist, 2010) **b** Temperature anomalies from China (Ge et al., 2013) **c** Summer temperature anomalies from China (Tan et al., 2003), **d** Winter temperature anomalies from China (Ge et al., 2003). **e** TD3 δ^{13}C record including upper and lower confidence intervals from COPRA.

7.3.2 Trends in rainfall from central Vietnam

The oxygen isotopes show a peak in low values at around 1420 years BP and a shift towards increased values after 1100 years BP. A similar trend can be observed in the carbon isotopes and the Mg/Ca ratios. The high-resolution stable isotope record in combination with the high-resolution trace elements allows for a unique investigation of decadal to seasonal variability of rainfall in central Vietnam. Generally, the δ^{13}C record suggests relatively wet conditions between 1700 to 1350 years BP, followed by a pronounced drought beginning at 1100 years BP (Figure 7.3). This general trend is also visible in the Mg/Ca record of TD3-1 (Figure 7.3c). The results show that central Vietnam was relatively wet prior to 1100 years BP, with a peak in rainfall from ca. 1600 to 1300 years BP, which is followed by a drought beginning at around 1100 years BP.

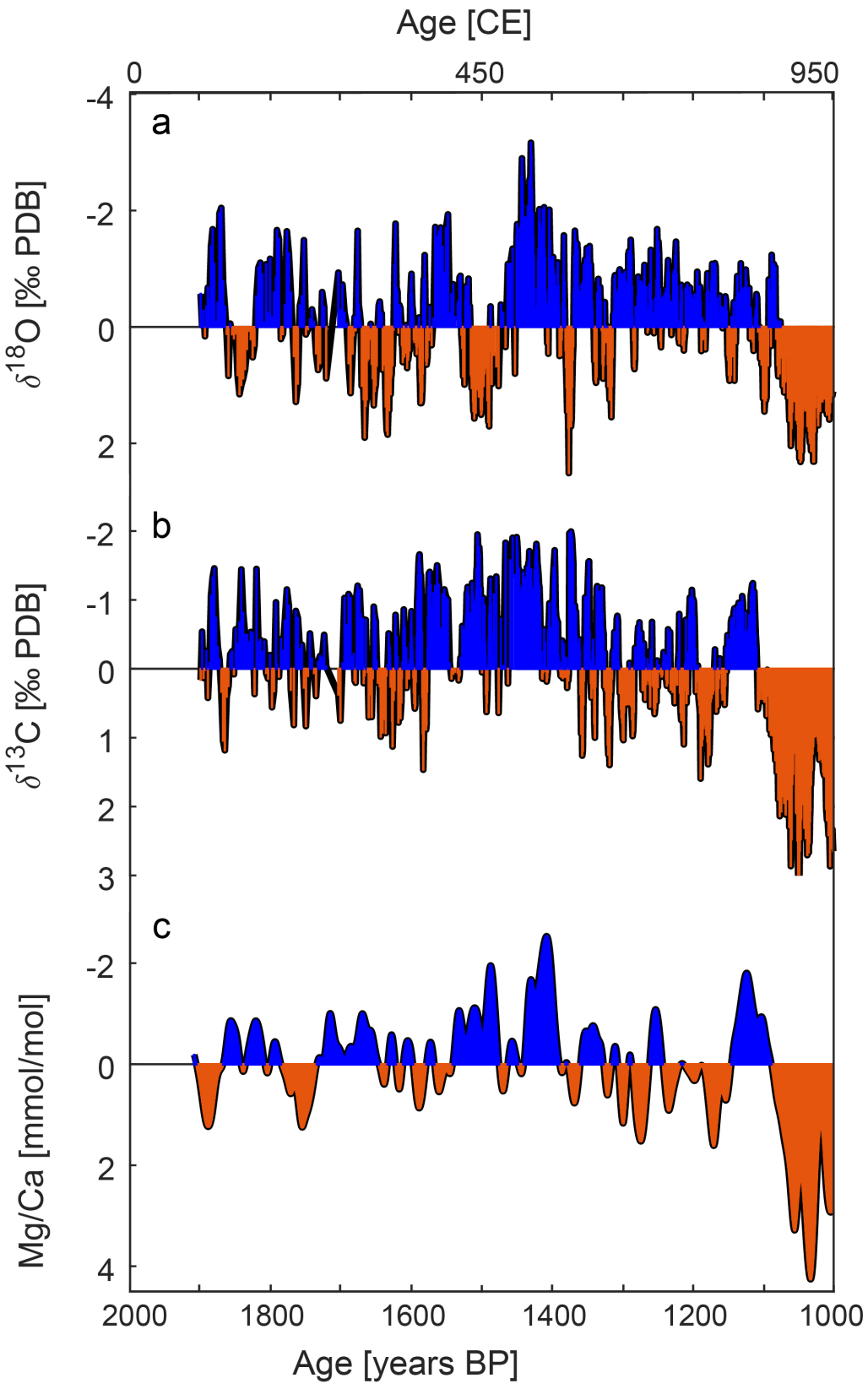

Figure 7.3: Z-normalised times series for TD3-1 of **a** δ^{18}O **b** δ^{13}C and **c** Mg/Ca. For Mg/Ca and δ^{13}C orange indicates dry and blue indicates wet conditions. Mg/Ca is smoothed to a resolution of 250 years to show the long-term pattern. The original time proxy record has a monthly resolution. The z-score of δ^{13}C reveals wetter conditions between 1650 to 1300 years BP.

7.3.3 Influence of tropical cyclones

Tropical cyclones contribute around 70 % of rainfall to the rainy season in central Vietnam during the winter monsoon season (Chen et al., 2012b). Therefore, the question arises whether rainfall derived from tropical cyclones in central Vietnam can be reconstructed from TD3-1. Counts of tropical cyclones recorded in historical documents show that tropical cyclones were observed throughout the Common Era across the coast of China, with a peak in tropical cyclones making landfall around 1450 and 1150 to 1250 years BP (Chen et al., 2019). Tropical cyclone activity reconstructed from broken shells and corals in the South China Sea, based on marine cores from Xisha Island (Yue et al., 2019) (Figure 7.4 b), indicate a decline in tropical cyclones after 1550 years BP. The cyclone activity is related to SSTs in the Indo-Pacific Warm Pool (Figure 7.4b). High SSTs coincide with increased tropical cyclone activity and the opposite is true for low SSTs (Oppo et al., 2009).

Periods of wet and dry climate in central Vietnam show no relation to tropical cyclone activity in the South China Sea (Figure 7.4). The tropical cyclone record from Xisha Island is located just offshore central Vietnam and would likely record any tropical cyclones making landfall in central Vietnam. Tropical cyclones are daily events, which might not be transferred into the cave immediately (Chapter 3). Further, the contribution of tropical cyclones to the annual mean could have been reduced during this time (Figure 7.4a).

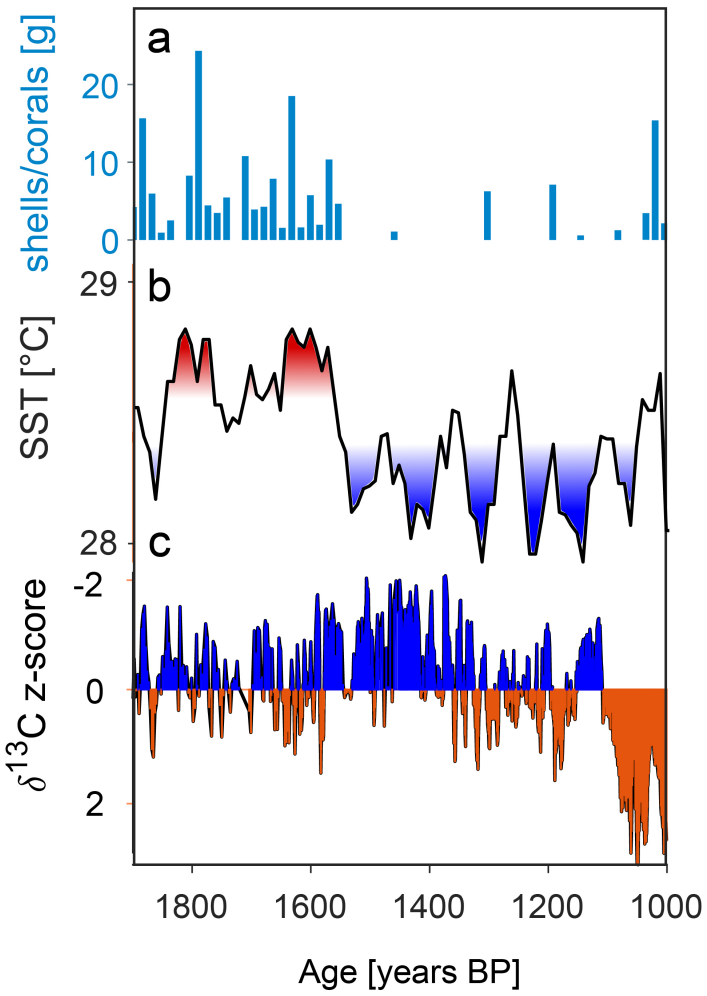

Figure 7.4: **a** Tropical cyclone activity reconstructed from broken shells and corals on Xisha Island in the South China Sea (Yue et al., 2019). **b** SSTs reconstructed from δ^{18}O of foraminifera in the Indo-Pacific Warm pool (Oppo et al., 2009), **c** δ^{13}C record from central Vietnam. There is a clear disagreement between historical and reconstructed tropical cyclone records in the western Pacific.

7.4 Cold climate forcing and rainfall in Southeast Asia

As described at the beginning of this chapter, in the Indo-Pacific region it is not clear whether warm or cool phases of the recent past imply changes in the ITCZ extent or the position of the Walker Circulation. Especially, during the first half of the Common Era, a substantial lack of palaeoclimate records leaves unknown how future warming will affect precipitation in this region. In order to understand the behaviour of the ITCZ and Walker Circulation during the Common Era, speleothem records from the Asian-Australian monsoon region are invoked for comparison (Figure 7.5). Focus is on the DACP, due to the time coverage and age uncertainties of TD3-1.

We begin by examining the changes during the early part of the Common Era from 2000 to 1000 years BP. Between 2000 and 1200 years BP, the δ^{13}C records from Laos and Vietnam show a generally declining trend of local rainfall. The Tangga Cave record from Sumatra shows pronounced dry conditions between 1650 and 1300 years BP (Figure 7.5c). The record from Liang Luar Cave, Flores, indicates wet conditions compared to the last millennium (Griffiths et al., 2016). A record from the north of Australia indicates relatively dry conditions prior to 1300 years BP (Denniston et al., 2013). In summary, these speleothem records suggest wet conditions in mainland Southeast Asia and Flores and dry conditions over most parts of the Maritime Continent and northern Australia during the DACP.

The dry condition in Sumatra and northern Australia during the DACP suggest that a shift in the Walker Circulation to the west is unlikely as a response to cooler temperatures (Figure 7.5c and e). To further corroborate the results and to investigate the changes of the ITCZ during the DACP, additional palaeoclimate records are used (Figure 7.6 and Table 7.1).

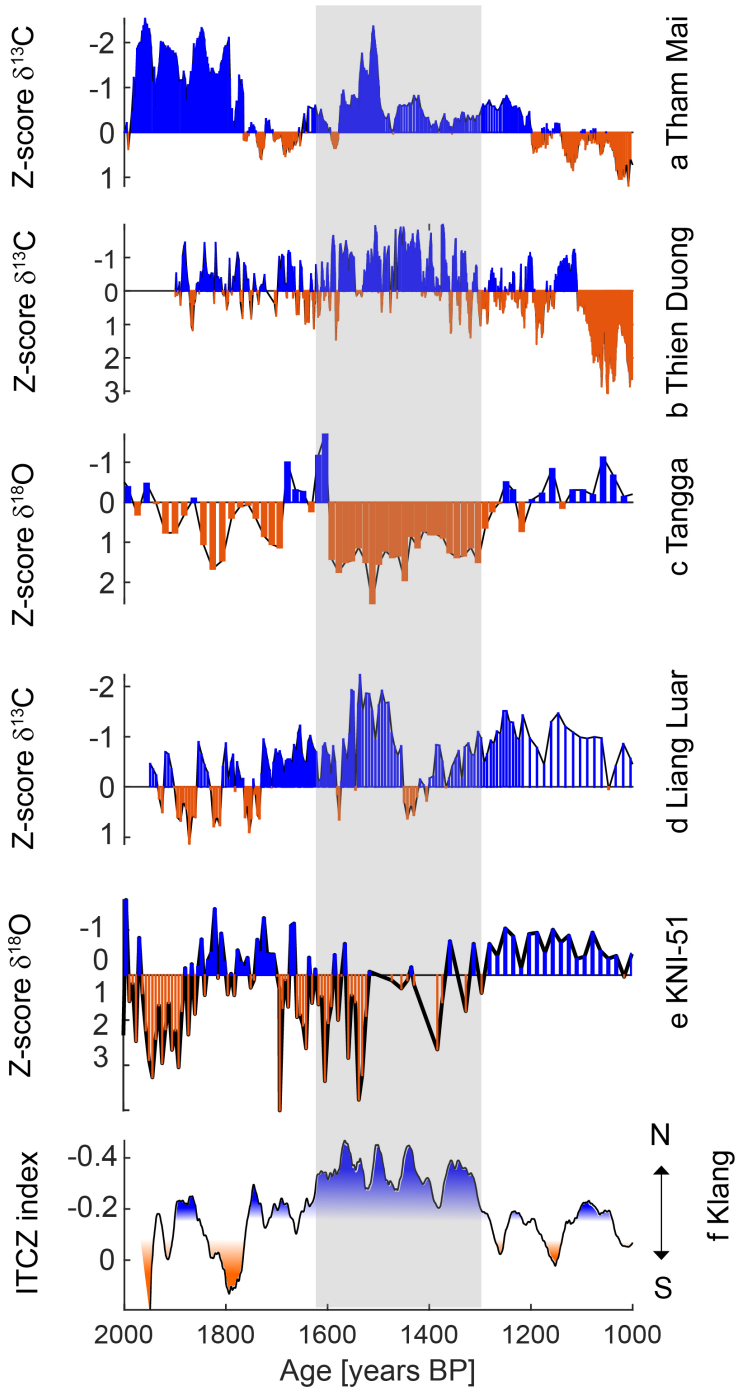

Figure 7.5: Speleothem proxy records from the Asian and Australian monsoon region, covering a cross sections from 20°N to 15°S. **a** Tham Mai Cave (Laos), **b** Thien Duong Cave (central Vietnam), **c** Tangga Cave (Sumatra), **d** Liang Luar Cave (Flores), KNI-51 (Australia), references are listed in Table 7.1. The grey bar indicates the time of cooling the northern hemisphere during the DACP (Figure 7.1). Proxy records are shown as z-normalised time series, to identify relatively wet and dry periods between 2000 to 1000 years BP. Except for Sumatra (Tangga Cave) and northern Australia, the records indicate wet conditions during this time.

At present most regions located between 25°N and 15°S receive rainfall related to the ITCZ

convection either during boreal summer or winter (Figure 7.6) (Denniston et al., 2016; Waliser and Gautier, 1993). Therefore, palaeoclimate reconstructions from these regions are ideal to investigate changes in the ITCZ position and width. In total 18 records covering the time period between 1600 to 1300 years BP (DACP) are available within this region (Table 7.1).

Firstly, the additional proxy records confirm, that a westwards shift in the Walker Circulations is unlikely (Figure 7.7). Dry conditions during the DACP are observed in Sumatra, Southern Thailand, and the Andaman Islands. Speleothem records from Borneo indicate a drying trend over the Common Era, however, no particular shift during the DACP can be observed. Thus, changes in the ITCZ position are more plausible in explaining the observed precipitation pattern during the DACP.

Tan et al. (2019a) developed a speleothem-based ITCZ index for the Common Era and suggested that the ITCZ moved north during the DACP (Figure 7.5f). Today, Laos and Vietnam receive rainfall when the ITCZ is located north of 15°N and southern China lies at the northern most edge of the ITCZ during boreal summer when the ITCZ is around 25°N. Dry conditions are observed in southern China during the DACP, indicating that the ITCZ does not extend farther north than at present. Laos and Vietnam indicate wetter conditions indicating that the ITCZ either extended its stay over this region or that precipitation within the ITCZ was enhanced. A northwards shift of the ITCZ is therefore not a sufficient explanation to explain these records.

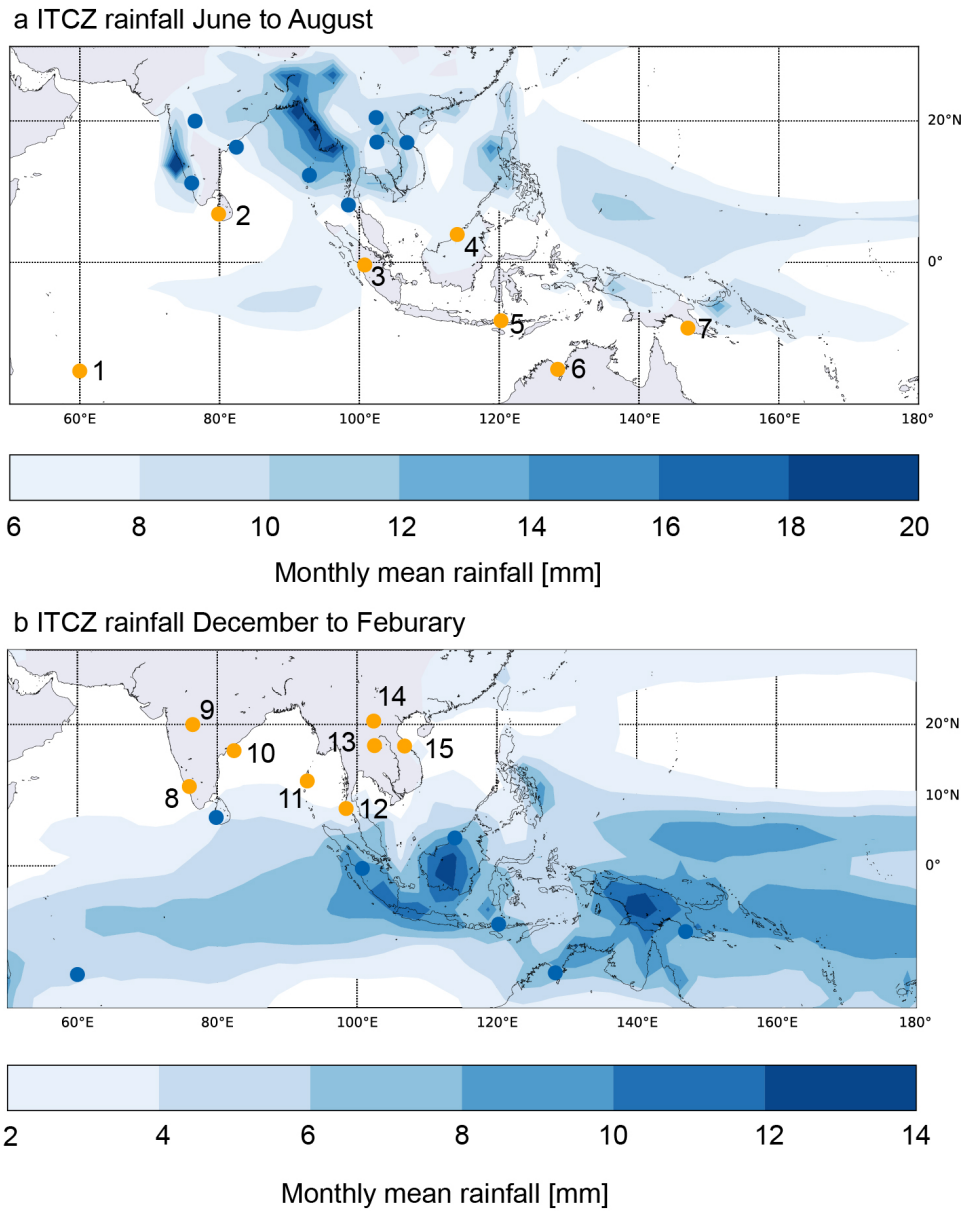

Figure 7.6: Monthly mean rainfall from the CPC dataset (NOAA, 2020*a*) during **a** June to August and **b** December to February. Most regions in India and mainland Southeast Asia receive rainfall during boreal summer, when the ITCZ lies above 15°N. The Maritime Continent and northern Australia, receive rainfall during boreal winter, when the ITCZ lies South of 8°S.

Table 7.1: List of records shown in Figure 7.6 and Figure 7.7.

ID on map	Location	Archive	Reference
1	Mauritius	Sediment core	De Boer et al. (2014)
2	Sri Lanka	Sediment core	Ranasinghe et al. (2013)
3	Sumatra	Speleothem	Wurtzel et al. (2018)
4	Borneo	Speleothem	Chen et al. (2016a)
5	Flores	Speleothem	Griffiths et al. (2016)
6	Australia	Speleothem	Denniston et al. (2015, 2013)
7	Papua New Guinea	Sediment core	Osborne et al. (1993)
8	India	Sediment core	Veena et al. (2014)
9	India	Sediment core	Prasad et al. (2014)
10	Bay of Bengal	Sediment core	Ponton et al. (2012)
11	Andaman Islands	Speleothem	Laskar et al. (2013)
12	Thailand	Speleothem	Tan et al. (2019a)
13	Thailand	Sediment core	Chawchai et al. (2015)
14	Laos	Speleothem	Wang et al. (2019)
15	Vietnam	Speleothem	This study
16	Java	Sediment record	Tierney et al. (2010)
17	Australia	Sediment record	McGowan et al. (2012)
18	China	Sediment record	Zhong et al. (2014)

Proxy records available from the Asian and Australian monsoon region covering the DACP show that sites located around 20°N and 6°S were wetter during the DACP while regions in the centre (0° to 12°N) and at the outer rim (25°N and 15°S) were drier (Figure 7.7). These observations are in contrast to previous findings, which suggested a contraction of the ITCZ rain belt during cold periods, which led to increased rainfall over the Maritime Continent (core region of the ITCZ) and drying over northern Australian and southern China (Denniston et al., 2016; Yan et al., 2015a).

7.4.1 ITCZ dynamics during the DACP

The following sections explore two potential mechanisms, which can explain the reconstructed hydrology in Southeast Asia during the DACP.

Firstly, the reconstructed rainfall pattern could be explained with a narrowing of the ITCZ rain belt in its northern and southernmost position. A narrowing in the seasonal extreme positions would leave the regions in the centre between both extrema and the edges north and south of the seasonal extreme positions drier (Figure 7.7). Model simulations showed that a narrowing of the ITCZ can strengthen the ascent in its core region and enhance rainfall (Lau and Kim, 2015). The

wetter conditions over central Vietnam, Laos, and Flores suggest that this squeeze of the ITCZ in its seasonal extreme positions could be a possible explanation. However, current literature is mainly focusing on the mean state of the ITCZ rather than its extremes, therefore validation of this theory based on modern observational or simulated data is difficult. In terms of past climate reconstructions, studies suggested a contraction of the latitudinal range of the ITCZ, based on observations from northern Australia, southern China and proxy records from Flores and Java (Denniston et al., 2016; Griffiths et al., 2016; Tierney et al., 2010; Yan et al., 2015a). However, these studies lacked proxy records from the region between 0° and 15°N, which now highlight that this region underwent drying during the DACP (Figure 7.7). Therefore, the palaeoclimate reconstructions need to be set into a new perspective.

A second explanation could be based on the different timing of rainfalls across Southeast Asia. Central Vietnam shows wet conditions during the DACP similar to proxy records in close proximity in northern Laos (Wang et al., 2019) and Thailand (Chawchai et al., 2015). This precipitation pattern suggests that both the Southwest Summer and the Northeast Winter Monsoon were affected equally during this time. While there is no correlation between the Laos and Vietnam records over the whole Common Era, as suggested in Chapter 6, both show relatively wetter conditions during the DACP than during the rest of the Common Era (Figure 7.5a and b). One explanation for this pattern could be a shift in the timing of the ITCZ. At present, the seasonal movement of the ITCZ determines the length of the rainy season across Southeast Asia (Misra and Dinapoli, 2014; Wang and Chang, 2008). Therefore, changes in its seasonal migration directly impact the length of the rainy season. For example, a longer seasonal migration during autumn/winter (ITCZ withdrawal) would results in an extended rainy season in Vietnam, whereas a fast withdrawal would shorten the rainy season.

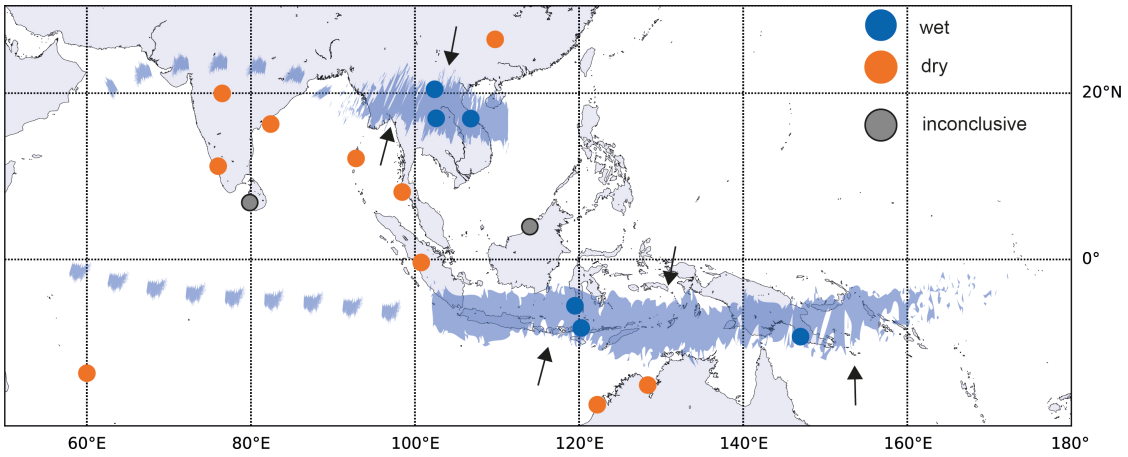

Figure 7.7: Climatic conditions reconstructed by proxy records (Table 7.1) for the time between 1600 to 1300 years BP. The blue shading indicates the potential positions of the ITCZ in summer and autumn/winter during the DACP. The black arrows indicate the direction of narrowing of the ITCZ rain belt. The Borneo speleothem indicates a general drying trend over the Common Era, but no particular shifts during the DACP. Records from Sri Lanka show a shift from wet to dry at 1400 years BP (Ranasinghe et al., 2013), or dry conditions (Premathilake and Risberg, 2003), thus no clear signal could be concluded. Speleothem records from southern China, suggest that the East Asian Summer monsoon was reduced during this time, supporting dry conditions in this region (Zhang et al., 2008).

Shifts in the ITCZ are the atmospheric response to additional energy uptake in one hemisphere (Byrne and Schneider, 2016). Energy deficits in the northern hemisphere, like during the LIA, drive the ITCZ to shift south (Sachs et al., 2018). Not only is the mean position affected, but also the latitudinal extent is larger, thus a widening can be observed (Asmerom et al., 2020; Byrne et al., 2018). However, a different pattern is observed in proxy records during the DACP in the Asian-Australian monsoon region. Thus, the cooling during DACP was likely different from the LIA. On a global scale, the DACP showed strong diversity in the timing of peak cooling, whereas the LIA showed a more coherent temporal pattern (Neukom et al., 2019a). This suggests that surface cooling during DACP and LIA was different. On a regional scale, a study based on Tridacna shells in the South China Sea (Yan et al., 2015) found that annual SSTs cooled during both cold phases, but the cooling during the DACP is mainly a result of winter SST cooling, whereas the LIA cooling affected both seasons equally. Therefore, the cooling during the DACP was likely much stronger during boreal winter than during summer (Yan et al., 2015). One explanation for the observed precipitation pattern could be that the timing of the ITCZ movement changed. Today the ITCZ moves northwards quickly, within days, but retreats south very slowly over three months in autumn to winter. This seasonal asymmetry is explained by the different land-ocean thermal memories,

favouring the southwards movement during boreal autumn but hindering the northwards movement of the ITCZ during boreal spring (Chang et al., 2005; Wang and Chang, 2008). Hindering the ITCZ movement is associated with a prolonged stay at the southerly location during spring followed by an abrupt jump northwards. A strong cooling during boreal winter could have initiated a shorter retreat phase of the ITCZ compared to today. Cool SSTs anomalies in the South China Sea could lead to a more abrupt southwards migration of the ITCZ. At present the ITCZ is kept near the equator during spring due to a lagged ocean response, resulting in cool SSTs until mid-May (Chang et al., 2005; Wang and Chang, 2008). The gradual retreat during autumn is favoured by warmer SSTs, when the oceans responds slower to atmospheric cooling. Therefore, it is proposed that the strong cooling of winter SSTs during the DACP hindered the ITCZ in its southwards movement and resulting in an abrupt retreat, rather than a gradual retreat. A faster retreat could shorten the rainy season in sites located between the most pole-ward positions of the ITCZ and lengthening the rainy season over sites at the northern and southernmost positions. This would explain the observed precipitation pattern over the Asian-Australian monsoon region, with increased rainfall over mainland Southeast Asia and Flores, but drying in the regions located in-between.

Modern rainfall in Southeast Asia is strongly affected by the timing of ITCZ migration (Misra and Dinapoli, 2014; Wang and Chang, 2008) (Chapter 2). Therefore, it is likely that a change in the timing of the ITCZ migration in the past altered the length of the rainy season across Southeast Asia.

7.5 Outlook and conclusions

This chapter investigated the climatic conditions in Southeast Asia during the Common Era with a focus on the DACP, a cool phase in the northern hemisphere between 1600 and 1300 BP. Dry conditions prevailed in southern Thailand, Sumatra, the Andaman Islands, Borneo, southern China, and northern Australia. Thus, regions around 10° to 25°N and 5° to 8°S received increased rainfall, whereas other regions of Southeast Asia and northern Australia underwent drying.

Here, two hypotheses are outlined in order to explain the constructed hydrological patterns in Southeast Asia. One explanation could be that the ITCZ narrowed and enhanced in its core region while being located at the seasonal extremes north and south of the Equator. This explains the

wetter conditions over mainland Southeast Asia and Flores, whereas the regions in the inner region and at the edges of the ITCZ become drier. Another explanation is the timing of the ITCZ migration, with an extended stay over the pole-ward positions but a reduced stay and thus reduced rainfall over the core region (Maritime Continent). These findings suggest that the seasonal extreme positions and the timing of the ITCZ migration are key drivers of hydroclimate variability in Southeast Asia during the Common Era.

Some limitations of this work are based on the age uncertainties in TD3-1, which do not allow for a profound investigation of the effects of warm phases on rainfall in central Vietnam. Proxy observations from Indonesia and southern Thailand linked the current warm phase to a decrease in summer monsoonal rainfall. The proxy observations from TD3-1 indicate a decline of rainfall during the medieval warm period, but further U-Th dates are necessary to gain confidence in the age uncertainties of the proxy data. Additionally, a stalagmite that is still actively growing today and covers the late Holocene would be ideal to estimate the effects of the current warm phase on rainfall in central Vietnam and place it in relation to previous known warm phases.

Further, to gain more confidence in the results presented in this chapter more palaeoclimate records are needed, especially, from the Philippines, Borneo, southern mainland Southeast Asia and northern Australia. Finally, climate modelling is needed to gain confidence in the suggested drivers of the observed hydrological changes.

Chapter 8

General Conclusions

8.1 Summary

In this chapter, aims and objectives from Chapter 1 will be revisited and advances made in the understanding of climate in Southeast Asia will be outlined. The main aim of this work, was to reconstruct the Holocene evolution of the winter monsoon and to identify long- and short-term climate drivers of seasonal rainfall in Southeast Asia. To achieve this a high-resolution record of winter monsoon rainfall covering the Holocene was established based on speleothem proxies from central Vietnam. Modern environmental monitoring was conducted in central Vietnam to ensure a correct proxy interpretation. δ^{18}O is one the most commonly used proxies in speleothem research, often invoked as a record of rainfall. However, rainwater stable isotopes in central Vietnam are controlled by the seasonal shift of the rainfall source from the Indian Ocean in boreal summer to the western Pacific in autumn to spring. The amount of vapour contributed from each oceanic source is driven by the timing of the onset and offset of the seasonal ITCZ migration. These findings are the fundamental basis for any palaeoclimate research based on δ^{18}O and δ^{2}H as rainfall proxies in the region. This also includes not only research using speleothems but also using other archives, such as lake cores and tree ring cellulose. The results also show that isotopic fractionation of rainfall in this region is not dominated by the amount of rainfall, but rather by changes in the large-scale circulation. Following these findings, the δ^{18}O signal transfer between the land surface and the cave environment was investigated.

Drip water δ^{18}O in Soong Cave is controlled by the seasonal cycle in δ^{18}O of surface precipitation

and the season of recharge. Lowest values are found during autumn, when precipitation is highest. This is in contrast to δ^{18}O in surface precipitation, which shows lowest values during summer. These findings highlight that δ^{18}O is likely reflecting both, the δ^{18}O signature of surface precipitation and local water supply. These results are setting the scene for future speleothem samples from Soong Cave, but also show that δ^{18}O is a complex proxy and additional proxies are needed for a correct interpretation. The interpretation of proxies from stalagmite TD3 are based on these findings.

Stalagmite TD3 from Thien Duong Cave was analysed for stable isotopes and trace elements. Using a principle component analysis it was found that Mg/Ca and carbon isotopes are sensitive to prior carbonate precipitation and thus tracers for wet versus dry conditions at Thien Doung Cave. Al, Fe, Si, Ti and Th are indicator for weathering processes or flooding events, and U, Y and P trace infiltration rates. δ^{18}O shows similar trends to Mg/Ca and δ^{13}C, however, with some deviations, related to the δ^{18}O composition of rainfall. Mg/Ca and δ^{13}C are powerful proxies for local rainfall and are interpreted as proxies for rainfall related to the Northeast Winter Monsoon.

Using this proxy interpretation, winter monsoon rainfall over the Holocene in central Vietnam was reconstructed. The long-term reconstruction of the winter monsoon rainfall variability in central Vietnam resolves some of the uncertainty related the co-evolution of winter and summer monsoon over the Holocene. The results show that changes in the winter monsoon are in-phase with changes in the summer monsoon during the early and mid-Holocene. After 3000 years BP, winter and summer monsoon show opposing trends, with the summer monsoon declining in rainfall, whereas winter monsoon rainfall enhances. One possible explanation for the observed in-phase relation of the monsoons are zonal shifts in the Pacific Walker Circulation, affecting both, summer and winter monsoonal rainfall. These shifts could be forced by changes in SST in the Indian and Atlantic Ocean, induced by increased or decreased dust loading from the Sahara. For example, a pronounced drought affecting Southeast Asia between 5000 to 3500 years BP, was likely caused by an eastwards shift of the Pacific Walker Circulation resulting from increased dust emission at the end of the Green Sahara. The inverse relationship of the monsoon after 3000 years BP, can be explained by a slowdown of the Indian Walker Circulation, weakening the summer monsoon in Southeast Asia, whereas SST changes in the western Pacific enhance winter monsoon rainfall.

Further, the findings of this work show that speleothem δ^{18}O as a proxy for summer monsoonal

strength is not ideal for comparisons with winter monsoon proxies, since speleothem δ^{18}O is a proxy for regional circulation in East Asia, whereas many winter monsoon proxies record more localised climate variability. These findings are important for future palaeoclimate reconstructions in this region and settle the long lasting debate about the Holocene winter monsoon evolution.

In addition to the long-term development of the winter monsoon in Southeast Asia, climate drivers on centennial to decadal time scales were identified for the Common Era. Based on 18 proxy records covering the Asian and Australian monsoon region, the precipitation pattern related to cool phases of the recent past were identified. During the DACP, a cool phase between 1600 to 1300 years BP, proxy records suggest a drying at the outer edges of the ITCZ and in the core region. This pattern can be explained by a disproportional cooling of SSTs in the South China Sea during the winter season. The anomalously cool winter SSTs delayed the withdrawal of the ITCZ and the rainy season was shorten in the core region of the ITCZ between 2°S and 10°N. These findings have implications for studies of future climate in Southeast Asia, highlighting that the timing of the onset and offset of the ITCZ needs to be considered in future simulations.

In summary, the two key points of this work are:

- For most of the Holocene the relationship between summer and winter monsoon in Southeast Asia is positive. This can be attributed to shifts in the Pacific Walker Circulation affecting rainfall in both seasons. In the late Holocene changes in the Indian Walker Circulation and SST in the western Pacific affect the monsoons in opposite way, leading to increased rainfall in autumn/winter and decrease rainfall in summer.
- Over the recent past (the Common Era) the position and timing of the seasonal migration of the ITCZ is the major control of locally dry and wet conditions. Cool phases lead to increased rainfall in central Vietnam.

8.2 Implications

Recent observations suggest that summer rainfall from July to September has increased in central Vietnam over the recent decades (Li et al., 2019). This is in accordance with climate simulations predicting an increase in rainfall by up to 20% for southern and central Vietnam (Thuc et al., 2016). The evolution of winter monsoonal rainfall over the Holocene highlighted that changes dust load

from the Sahara can impact climate over Southeast Asia. Some modelling studies predict that the monsoon over Africa will strengthen in future and likely lead to a decreased dust loading into the atmosphere from the Sahara region. This could lead to increased winter and summer monsoonal rainfall across Southeast Asia in long-term future.

On the other hand, modelling studies (Byrne et al., 2018) indicate that the ITCZ will likely narrow in its latitudinal extent in future. This would centre intense rainfall over the Maritime Continent and leave the other regions, such as mainland Southeast Asia drier. Based on the proxy observations of rainfall during cool events of the Common Era, which suggests drier conditions in the centre region of the ITCZ, this could be a possible scenario in near future. Droughts would become more severe even and more enhanced by increased temperatures.

Projections suggest that the total number of tropical cyclones may decrease in future, but the occurrence is projected to be more concentrated towards the end of the tropical cyclone season (Thuc et al., 2016). For central Vietnam, where most tropical cyclones make landfall during September and October, this could mean an increase in more intense tropical cyclones during late autumn. The additional rainfall deficits in the dry season, would cause less rainfall during spring and early summer in central Vietnam.

In summary, the dry season will likely extend, while the rainy season will shorten, but be more intense in central Vietnam in near-term future. These findings are important signposts for adaptation strategies in preparing for future climate change.

8.3 Outlook

Future work in central Vietnam should focus on extending the paleoclimate record of winter monsoonal rainfall into the past, beyond the Holocene and the last millennium. This work contributed to the understanding of long-term climate drivers, but it remains unknown how the climate of central Vietnam changed over more extreme climate shifts like during the last glacial period. Further, finding a speleothem record covering the last millennium until today would be ideal to set the current warm phase into perspective of past warm phases. Subsequently, one focus should be on extending cave monitoring, ideally over five years, in caves where speleothems were sampled. This approach ensures a better understanding of the proxies interpretation.

Focusing on seasonally resolved proxy records from central Vietnam could help to understand the seasonal cycle and identify changes in the length of the rainy season. At the moment most climate models simulate changes in the annual mean of the ITCZ. Research presented in this work, however, has highlighted that the seasonal migration is key to unravel past and future precipitation patterns. Addressing these uncertainties could potentially improve models and avoid known biases such as the double ITCZ problem (Lin, 2007).

Once these issues are resolved and future predictions of rainfall in Vietnam and Southeast Asia have more confidence, research should focus on climate change adaption strategies. Due to the intense agriculture based on crops in Southeast Asia, main focus should be on the development of more resilient crops which can endure more pronounced droughts and flooding.

References

Abram, N. J., Gagan, M. K., Liu, Z., Hantoro, W. S., McCulloch, M. T. and Suwargadi, B. W. (2007), 'Seasonal characteristics of the Indian Ocean Dipole during the Holocene epoch', *Nature* **445**(7125), 299–302.

Abram, N. J., McGregor, H. V., Gagan, M. K., Hantoro, W. S. and Suwargadi, B. W. (2009), 'Oscillations in the southern extent of the Indo-Pacific Warm Pool during the mid-Holocene', *Quaternary Science Reviews* **28**(25-26), 2794–2803.

Affek, H. P., Bar-Matthews, M., Ayalon, A., Matthews, A. and Eiler, J. M. (2008), 'Glacial/interglacial temperature variations in Soreq cave speleothems as recorded by clumped isotopethermometry', *Geochimica et Cosmochimica Acta* **72**(22), 5351–5360.

Aggarwal, P. K., Fröhlich, K., Kulkarni, K. M. and Gourcy, L. L. (2004), 'Stable isotope evidence for moisture sources in the asian summer monsoon under present and past climate regimes', *Geophysical Research Letters* **31**(8).

Aggarwal, P. K., Romatschke, U., Araguas-Araguas, L., Belachew, D., Longstaffe, F. J., Berg, P., Schumacher, C. and Funk, A. (2016), 'Proportions of convective and stratiform precipitation revealed in water isotope ratios', *Nature Geoscience* **9**(8), 624–629.

Ahmed, M., Anchukaitis, K. J., Asrat, A., Borgaonkar, H. P., Braida, M., Buckley, B. M., Büntgen, U., Chase, B. M., Christie, D. A., Cook, E. R. et al. (2013), 'Continental-scale temperature variability during the past two millennia', *Nature Geoscience* **6**(5), 339.

Allan, M., Fagel, N., Van Rampelbergh, M., Baldini, J., Riotte, J., Cheng, H., Edwards, R. L., Gillikin, D., Quinif, Y. and Verheyden, S. (2015), 'Lead concentrations and isotope ratios in

speleothems as proxies for atmospheric metal pollution since the industrial revolution', *Chemical Geology* **401**, 140–150.

Amante, C. and Eakins, B. W. (2009), 'ETOPO1 arc-minute global relief model: procedures, data sources and analysis'.

An, S.-I., Kim, H.-J., Park, W. and Schneider, B. (2017), 'Impact of ENSO on East Asian winter monsoon during interglacial periods: effect of orbital forcing', *Climate Dynamics* **49**(9), 3209–3219.

An, Z. (2000), 'The history and variability of the east asian paleomonsoon climate', *Quaternary Science Reviews* **19**(1-5), 171–187.

An, Z., Porter, S. C., Kutzbach, J. E., Xihao, W., Suming, W., Xiaodong, L., Xiaoqiang, L. and Weijian, Z. (2000), 'Asynchronous holocene optimum of the east asian monsoon', *Quaternary Science Reviews* **19**(8), 743–762.

Anchukaitis, K., Buckley, B., Cook, E., Cook, B., D'Arrigo, R. and Ammann, C. (2010), 'Influence of volcanic eruptions on the climate of the asian monsoon region', *Geophysical Research Letters* **37**(22).

Anders, A. M. and Nesbitt, S. W. (2015), 'Altitudinal precipitation gradients in the tropics from tropical rainfall measuring mission (trmm) precipitation radar', *Journal of Hydrometeorology* **16**(1), 441–448.

Araguás-Araguás, L., Froehlich, K. and Rozanski, K. (1998), 'Stable isotope composition of precipitation over southeast Asia', *Journal of Geophysical Research* **103**, 28721.

As-syakur, A. R., Adnyana, I. W. S., Mahendra, M. S., Arthana, I. W., Merit, I. N., Kasa, I. W., Ekayanti, N. W., Nuarsa, I. W. and Sunarta, I. N. (2014), 'Observation of spatial patterns on the rainfall response to ENSO and IOD over Indonesia using TRMM Multisatellite Precipitation Analysis (TMPA)', *International Journal of Climatology* **34**(15), 3825–3839.

Asmerom, Y., Baldini, J. U., Prufer, K. M., Polyak, V. J., Ridley, H. E., Aquino, V. V., Baldini, L. M., Breitenbach, S. F., Macpherson, C. G. and Kennett, D. J. (2020), 'Intertropical convergence zone variability in the neotropics during the common era', *Science Advances* **6**(7), eaax3644.

Atwood, A. R., Battisti, D., Wu, E., Frierson, D. and Sachs, J. P. (2020), 'Data-model comparisons of tropical hydroclimate changes over the common era', *Paleoceanography and Paleoclimatology* p. e2020PA003934.

Augustin, L., Barbante, C., Barnes, P. R., Barnola, J. M., Bigler, M., Castellano, E., Cattani, O., Chappellaz, J., Dahl-Jensen, D., Delmonte, B. et al. (2004), 'Eight glacial cycles from an antarctic ice core', *Nature* **429**, 623–628.

Baker, A., Hartmann, A., Duan, W., Hankin, S., Comas-Bru, L., Cuthbert, M. O., Treble, P. C., Banner, J., Genty, D., Baldini, L. M. et al. (2019), 'Global analysis reveals climatic controls on the oxygen isotope composition of cave drip water', *Nature communications* **10**(1), 1–7.

Baker, A. J., Sodemann, H., Baldini, J. U. L., Breitenbach, S. F. M., Johnson, K. R., van Hunen, J. and Zhang, P. (2015), 'Seasonality of westerly moisture transport in the East Asian summer monsoon and its implications for interpreting precipitation δ^{18}O', *Journal of Geophysical Research: Atmospheres* **120**(12), 5850–5862.

Baldini, J., McDermott, F. and Fairchild, I. (2006), 'Spatial variability in cave drip water hydrochemistry: Implications for stalagmite paleoclimate records', *Chemical Geology* **235**(3-4), 390–404.

Baldini, J. U. (2010), 'Cave atmosphere controls on stalagmite growth rate and palaeoclimate records', *Geological Society, London, Special Publications* **336**(1), 283–294.

Baldini, L. M., McDermott, F., Baldini, J. U., Arias, P., Cueto, M., Fairchild, I. J., Hoffmann, D. L., Mattey, D. P., Müller, W., Nita, D. C. et al. (2015), 'Regional temperature, atmospheric circulation, and sea-ice variability within the younger dryas event constrained using a speleothem from northern iberia', *Earth and Planetary Science Letters* **419**, 101–110.

Berkelhammer, M., Sinha, A., Stott, L., Cheng, H., Pausata, F. S. and Yoshimura, K. (2012), 'An abrupt shift in the indian monsoon 4000 years ago', *Geophys. Monogr. Ser* **198**, 75–87.

Bertler, N., Mayewski, P. and Carter, L. (2011), 'Cold conditions in antarctica during the little ice age implications for abrupt climate change mechanisms', *Earth and Planetary Science Letters* **308**(1), 41 – 51.

Bjerknes, J. (1969), 'Atmospheric teleconnections from the equatorial pacific', *Monthly weather review* **97**(3), 163–172.

Blyth, A. J., Baker, A., Collins, M. J., Penkman, K. E., Gilmour, M. A., Moss, J. S., Genty, D. and Drysdale, R. N. (2008), 'Molecular organic matter in speleothems and its potential as an environmental proxy', *Quaternary Science Reviews* **27**(9-10), 905–921.

Blyth, A. J., Farrimond, P. and Jones, M. (2006), 'An optimised method for the extraction and analysis of lipid biomarkers from stalagmites', *Organic Geochemistry* **37**(8), 882–890.

Blyth, A. J., Hartland, A. and Baker, A. (2016), 'Organic proxies in speleothems–new developments, advantages and limitations', *Quaternary Science Reviews* **149**, 1–17.

Bony, S., Risi, C. and Vimeux, F. (2008), 'Influence of convective processes on the isotopic composition (δ18O and δD) of precipitation and water vapor in the tropics: 1. Radiative-convective equilibrium and Tropical Ocean-Global Atmosphere-Coupled Ocean-Atmosphere Response Experiment (TOGA-COARE)', *Journal of Geophysical Research Atmospheres* **113**(19), 1–21.

Bowen, G. J. (2008), 'Spatial analysis of the intra-annual variation of precipitation isotope ratios and its climatological corollaries', *Journal of Geophysical Research: Atmospheres* **113**(D5).

Brand, W. A. and Coplen, T. B. (2012), 'Stable isotope deltas: tiny, yet robust signatures in nature', *Isotopes in environmental and health studies* **48**(3), 393–409.

Breitenbach, S. F., Lechleitner, F. A., Meyer, H., Diengdoh, G., Mattey, D. and Marwan, N. (2015), 'Cave ventilation and rainfall signals in dripwater in a monsoonal setting–a monitoring study from ne india', *Chemical Geology* **402**, 111–124.

Breitenbach, S. F. M., Adkins, J. F., Meyer, H., Marwan, N., Kumar, K. K. and Haug, G. H. (2010), 'Strong influence of water vapor source dynamics on stable isotopes in precipitation observed in Southern Meghalaya, NE India', *Earth and Planetary Science Letters* **292**(1-2), 212–220.

Breitenbach, S. F. M., Rehfeld, K., Goswami, B., Baldini, J. U., Ridley, H. E., Kennett, D. J., Prufer, K. M., Aquino, V. V., Asmerom, Y., Polyak, V. J. et al. (2012), 'Constructing proxy records from age models (copra)', *Climate of the Past* **8**(5), 1765–1779.

Breitenbach, S. F., Plessen, B., Waltgenbach, S., Tjallingii, R., Leonhardt, J., Jochum, K. P., Meyer, H., Goswami, B., Marwan, N. and Scholz, D. (2019), 'Holocene interaction of maritime and continental climate in central europe: New speleothem evidence from central germany', *Global and Planetary Change* **176**, 144–161.

Bro, R., Acar, E. and Kolda, T. G. (2008), 'Resolving the sign ambiguity in the singular value decomposition', *Journal of Chemometrics: A Journal of the Chemometrics Society* **22**(2), 135–140.

Buckley, B. M., Anchukaitis, K. J., Penny, D., Fletcher, R., Cook, E. R., Sano, M., Wichienkeeo, A., Minh, T. T., Hong, T. M. et al. (2010), 'Climate as a contributing factor in the demise of angkor, cambodia', *Proceedings of the National Academy of Sciences* **107**(15), 6748–6752.

Buckley, B. M., Stahle, D. K., Luu, H. T., Wang, S.-Y. S., Nguyen, T. Q. T., Thomas, P., Le, C. N., Ton, T. M., Bui, T. H. and Nguyen, V. T. (2017), 'Central Vietnam climate over the past five centuries from cypress tree rings', *Climate Dynamics* **48**(11-12), 3707–3723.

Budyko, M. I., Miller, D. H. and Miller, D. H. (1974), *Climate and life*, Vol. 508, Academic press New York.

Büntgen, U., Myglan, V. S., Ljungqvist, F. C., McCormick, M., Di Cosmo, N., Sigl, M., Jungclaus, J., Wagner, S., Krusic, P. J., Esper, J. et al. (2016), 'Cooling and societal change during the late antique little ice age from 536 to around 660 ad', *Nature Geoscience* **9**(3), 231–236.

Byrne, M. P., Pendergrass, A. G., Rapp, A. D. and Wodzicki, K. R. (2018), 'Response of the intertropical convergence zone to climate change: Location, width, and strength', *Current climate change reports* **4**(4), 355–370.

Byrne, M. P. and Schneider, T. (2016), 'Energetic constraints on the width of the intertropical convergence zone', *Journal of Climate* **29**(13), 4709–4721.

Cai, Y., Zhang, H., Cheng, H., An, Z., Edwards, R. L., Wang, X., Tan, L., Liang, F., Wang, J. and Kelly, M. (2012), 'The holocene indian monsoon variability over the southern tibetan plateau and its teleconnections', *Earth and Planetary Science Letters* **335**, 135–144.

Cai, Z. and Tian, L. (2016), 'Atmospheric controls on seasonal and interannual variations in the precipitation isotope in the East Asian Monsoon region', *Journal of Climate* **29**(4), 1339–1352.

Cai, Z., Tian, L. and Bowen, G. J. (2017), 'Enso variability reflected in precipitation oxygen isotopes across the asian summer monsoon region', *Earth and Planetary Science Letters* **475**, 25 – 33.

Cai, Z., Tian, L. and Bowen, G. J. (2018), 'Spatial-seasonal patterns reveal large-scale atmospheric controls on Asian Monsoon precipitation water isotope ratios', *Earth and Planetary Science Letters* **503**, 158–169.

Carré, M., Sachs, J. P., Purca, S., Schauer, A. J., Braconnot, P., Falcón, R. A., Julien, M. and Lavallée, D. (2014), 'Holocene history of ENSO variance and asymmetry in the eastern tropical Pacific', *Science* **345**(6200), 1045–1048.

Center, J. T. W. (2014-2018), 'annual typhoon report, US Navy: JTWC Annual Tropical Cyclone Reports'.

CGIAR-CS (2020), 'CGIAR-CSI Global-Aridity and Global-PET Databas', *Accessible at:* http://www.cgiar-csi.org.

Chabangborn, A. and Wohlfarth, B. (2014), 'Climate over mainland southeast asia 10.5–5 ka', *Journal of Quaternary Science* **29**(5), 445–454.

Chan, J. C. L. and Li, C. (2004), *The East Asian Winter Monsoon*, Heidelberg: Springer, chapter 5, pp. 54–106.

Chang, C.-P., Lu, M.-M. and Wang, S. (2011), The east asian winter monsoon, *in* 'The global monsoon system: research and forecast', World Scientific, pp. 99–109.

Chang, C.-P., Wang, Z., McBride, J. and Liu, C.-H. (2005), 'Annual cycle of Southeast Asia–Maritime Continent rainfall and the asymmetric monsoon transition', *Journal of climate* **18**(2), 287–301.

Chawchai, S., Chabangborn, A., Fritz, S., Väliranta, M., Mörth, C.-M., Blaauw, M., Reimer, P. J., Krusic, P. J., Löwemark, L. and Wohlfarth, B. (2015), 'Hydroclimatic shifts in northeast thailand during the last two millennia–the record of lake pa kho', *Quaternary Science Reviews* **111**, 62–71.

Chawchai, S., Chabangborn, A., Kylander, M., Löwemark, L., Mörth, C.-M., Blaauw, M., Klubseang, W., Reimer, P., Fritz, S. and Wohlfarth, B. (2013), 'Lake Kumphawapi an archive of Holocene palaeoenvironmental and palaeoclimatic changes in northeast Thailand', *Quaternary Science Reviews* **68**, 59 – 75.

Chawchai, S., Tan, L., Löwemark, L., Wang, H.-C., Yu, T.-L., Chung, Y.-C., Mii, H.-S., Liu, G., Blaauw, M., Gong, S.-Y. et al. (2021), 'Hydroclimate variability of central indo-pacific region during the holocene', *Quaternary Science Reviews* **253**, 106779.

Chen, H.-F., Liu, Y.-C., Chiang, C.-W., Liu, X., Chou, Y.-M. and Pan, H.-J. (2019), 'China's historical record when searching for tropical cyclones corresponding to Intertropical Convergence Zone (ITCZ) shifts over the past 2 kyr', *Climate of the Past* **15**(1), 279–289.

Chen, J., Chen, F., Feng, S., Huang, W., Liu, J. and Zhou, A. (2015), 'Hydroclimatic changes in china and surroundings during the medieval climate anomaly and little ice age: spatial patterns and possible mechanisms', *Quaternary Science Reviews* **107**, 98–111.

Chen, S., Hoffmann, S. S., Lund, D. C., Cobb, K. M., Emile-Geay, J. and Adkins, J. F. (2016a), 'A high-resolution speleothem record of western equatorial Pacific rainfall: Implications for Holocene ENSO evolution', *Earth and Planetary Science Letters* **442**, 61–71.

Chen, T.-C., Tsay, J. D., Yen, M. C. and Matsumoto, J. (2012b), 'Interannual variation of the late fall rainfall in central Vietnam', *Journal of Climate* **25**(1), 392–413.

Chen, T.-C., Yen, M.-C., Tsay, J.-D., Tan Thanh, N. T. and Alpert, J. (2012a), 'Synoptic Development of the Hanoi Heavy Rainfall Event of 3031 October 2008: Multiple-Scale Processes', *Monthly Weather Review* **140**(4), 1219–1240.

Chen, Z., Wu, R. and Chen, W. (2014), 'Distinguishing interannual variations of the northern and southern modes of the east asian winter monsoon', *Journal of Climate* **27**(2), 835–851.

Cheng, H., Edwards, R. L., Shen, C.-C., Polyak, V. J., Asmerom, Y., Woodhead, J., Hellstrom, J., Wang, Y., Kong, X., Spötl, C. et al. (2013), 'Improvements in 230th dating, 230th and 234u half-life values, and u–th isotopic measurements by multi-collector inductively coupled plasma mass spectrometry', *Earth and Planetary Science Letters* **371**, 82–91.

Cheng, H., Edwards, R. L., Sinha, A., Spötl, C., Yi, L., Chen, S., Kelly, M., Kathayat, G., Wang, X., Li, X. et al. (2016), 'The Asian monsoon over the past 640,000 years and ice age terminations', *Nature* **534**(7609), 640–646.

Cheng, H., Sinha, A., Wang, X., Cruz, F. W. and Edwards, R. L. (2012), 'The Global Paleomonsoon as seen through speleothem records from Asia and the Americas', *Climate dynamics* **39**(5), 1045–1062.

Cheng, H., Spotl, C., Breitenbach, S., Sinha, A., Wassenburg, J., Jochum, K. P., Scholz, D., Li, X., Yi, L., Peng, Y., Lv, Y., Zhang, P., Votintseva, A., Loginov, V., Ning, Y., Kathayat, G. and Edwards, L. (2016a), 'Climate variations of central asia on orbital to millennial timescales', *Scientific Reports* **6**(1), 1–11.

Cheong, W., Timbal, B., Golding, N., Sirabaha, S., Kwan, K., Cinco, T., Archevarahuprok, B., Vo, V., Gunawan, D. and Han, S. (2018), 'Observed and modelled temperature and precipitation extremes over Southeast Asia from 1972 to 2010', *International Journal of Climatology* **38**(7), 3013–3027.

Chiang, J. C., Fung, I. Y., Wu, C.-H., Cai, Y., Edman, J. P., Liu, Y., Day, J. A., Bhattacharya, T., Mondal, Y. and Labrousse, C. A. (2015), 'Role of seasonal transitions and westerly jets in east asian paleoclimate', *Quaternary Science Reviews* **108**, 111–129.

Clark, I. and Fritz, P. (1997), 'The environmental isotopes', *Environmental isotopes in hydrogeology* pp. 2–34.

Clemens, S. C., Prell, W. L., Sun, Y., Liu, Z. and Chen, G. (2008), 'Southern Hemisphere forcing of Pliocene δ^{18}O and the evolution of Indo-Asian monsoons', *Paleoceanography* **23**(4).

Clemens, S., Holbourn, A., Kubota, Y., Lee, K., Liu, Z., Chen, G., Nelson, A. and Fox-Kemper, B. (2018), 'Precession-band variance missing from east asian monsoon runoff', *Nature Communications* **9**(1), 1–12.

Clement, A. C., Seager, R. and Cane, M. A. (2000), 'Suppression of El Niño during the mid-Holocene by changes in the Earth's orbit', *Paleoceanography* **15**(6), 731–737.

Cobb, K. M., Adkins, J. F., Partin, J. W. and Clark, B. (2007), 'Regional-scale climate influences

on temporal variations of rainwater and cave dripwater oxygen isotopes in northern Borneo', *Earth and Planetary Science Letters* **263**(3-4), 207–220.

Cobb, K. M., Charles, C. D., Cheng, H. and Edwards, R. L. (2003), 'El Niño/Southern Oscillation and tropical Pacific climate during the last millennium', *Nature* **424**(6946), 271–276.

Cobb, K. M., Westphal, N., Sayani, H. R., Watson, J. T., Di Lorenzo, E., Cheng, H., Edwards, R. and Charles, C. D. (2013), 'Highly variable El Niño–Southern Oscillation throughout the Holocene', *Science* **339**(6115), 67–70.

Comas-Bru, L., Atsawawaranunt, K., Harrison, S. et al. (2020), 'Sisal (speleothem isotopes synthesis and analysis working group) database version 2.0'.

Conroy, J. L., Overpeck, J. T. and Cole, J. E. (2010), 'El Niño/Southern Oscillation and changes in the zonal gradient of tropical Pacific sea surface temperature over the last 1.2 ka', *PAGES news* **18**(1), 32–34.

Copernicus Climate Change Service (C3S) (2020), 'ERA5: Fifth generation of ECMWF atmospheric reanalyses of the global climate. Copernicus Climate Change Service Climate Data Store (CDS)', *Accessible at:* https://cds.climate.copernicus.eu/cdsapp#!/home.

Cosford, J., Qing, H., Mattey, D., Eglington, B. and Zhang, M. (2009), 'Climatic and local effects on stalagmite δ^{13}c values at lianhua cave, china', *Palaeogeography, Palaeoclimatology, Palaeoecology* **280**(1-2), 235–244.

Craig, H. (1961), 'Isotopic variations in meteoric waters', *Science* **133**(3465), 1702–1703.

Craig, H., Gordon, L. and Horibe, Y. (1963), 'Isotopic exchange effects in the evaporation of water: 1. Low-temperature experimental results', *Journal of Geophysical Research* **68**(17), 5079–5087.

Cross, M. (2015), Pysplit: A package for the generation, analysis, and visualizations of hysplit air parcel trajectories, *in* 'Proc. 14th Ann. Scientific Computing with Python Conf.(SciPy 15)'.

Dang, H., Jian, Z., Wang, Y., Mohtadi, M., Rosenthal, Y., Ye, L., Bassinot, F. and Kuhnt, W. (2020), 'Pacific warm pool subsurface heat sequestration modulated Walker circulation and ENSO activity during the Holocene', *Science Advances* **6**(42), eabc0402.

Dansgaard, W. (1964), 'Stable isotopes in precipitation', *Tellus* **16**(4), 436–468.

Day, C. C. and Henderson, G. M. (2013), 'Controls on trace-element partitioning in cave-analogue calcite', *Geochimica et Cosmochimica Acta* **120**, 612–627.

De Boer, E. J., Tjallingii, R., Vélez, M. I., Rijsdijk, K. F., Vlug, A., Reichart, G.-J., Prendergast, A. L., de Louw, P. G., Florens, F. V., Baider, C. et al. (2014), 'Climate variability in the SW Indian Ocean from an 8000-yr long multi-proxy record in the Mauritian lowlands shows a middle to late Holocene shift from negative IOD-state to ENSO-state', *Quaternary Science Reviews* **86**, 175–189.

De Deckker, P. (2016), 'The indo-pacific warm pool: critical to world oceanography and world climate', *Geoscience Letters* **3**(1), 1–12.

Debevec, B., Knez, M., Kranjc, A., Pahor, M., Prelovšek, M. and Slabe, T. (2012), 'Preliminary study for the adaptation of the Heaven's Cave for tourist purposes (Phong Nha-Ke Bang national park, Vietnam)', *Acta carsologica* **41**(1).

Deininger, M., McDermott, F., Cruz, F. W., Bernal, J. P., Mudelsee, M., Vonhof, H., Millo, C., Spötl, C., Treble, P. C., Pickering, R. et al. (2020), 'Inter-hemispheric synchroneity of holocene precipitation anomalies controlled by earths latitudinal insolation gradients', *Nature communications* **11**(1), 1–9.

Deininger, M., McDermott, F., Mudelsee, M., Werner, M., Frank, N. and Mangini, A. (2017), 'Coherency of late Holocene European speleothem δ^{18}O records linked to North Atlantic Ocean circulation', *Climate Dynamics* **49**(1), 595–618.

Demény, A., Kern, Z., Czuppon, G., Németh, A., Leél-Őssy, S., Siklósy, Z., Lin, K., Hu, H.-M., Shen, C.-C., Vennemann, T. W. et al. (2017), 'Stable isotope compositions of speleothems from the last interglacial–spatial patterns of climate fluctuations in europe', *Quaternary Science Reviews* **161**, 68–80.

Denniston, R. F., Houts, A. N., Asmerom, Y., Wanamaker Jr, A. D., Haws, J. A., Polyak, V. J., Thatcher, D. L., Altan-Ochir, S., Borowske, A. C., Breitenbach, S. F. et al. (2018), 'A stalagmite test of north atlantic sst and iberian hydroclimate linkages over the last two glacial cycles', *Climate of the Past* **14**(12), 1893–1913.

Denniston, R. F., Ummenhofer, C. C., Wanamaker, A. D., Lachniet, M. S., Villarini, G., Asmerom, Y., Polyak, V. J., Passaro, K. J., Cugley, J., Woods, D. et al. (2016), 'Expansion and contraction of the indo-pacific tropical rain belt over the last three millennia', *Scientific reports* **6**(1), 1–9.

Denniston, R. F., Villarini, G., Gonzales, A. N., Wyrwoll, K.-H., Polyak, V. J., Ummenhofer, C. C., Lachniet, M. S., Wanamaker, A. D., Humphreys, W. F., Woods, D. et al. (2015), 'Extreme rainfall activity in the Australian tropics reflects changes in the El Niño/Southern Oscillation over the last two millennia', *Proceedings of the National Academy of Sciences* **112**(15), 4576–4581.

Denniston, R. F., Wyrwoll, K.-H., Polyak, V. J., Brown, J. R., Asmerom, Y., Wanamaker Jr, A. D., LaPointe, Z., Ellerbroek, R., Barthelmes, M., Cleary, D. et al. (2013), 'A stalagmite record of holocene indonesian–australian summer monsoon variability from the australian tropics', *Quaternary Science Reviews* **78**, 155–168.

Domínguez-Villar, D., Krklec, K., Pelicon, P., Fairchild, I. J., Cheng, H. and Edwards, L. R. (2017), 'Geochemistry of speleothems affected by aragonite to calcite recrystallization–potential inheritance from the precursor mineral', *Geochimica et Cosmochimica Acta* **200**, 310–329.

Dong, W., Lin, Y., Wright, J. S., Ming, Y., Xie, Y., Wang, B., Luo, Y., Uang, W., Huang, J., Wang, L., Tian, L., Peng, Y. and Xu, F. (2016), 'Summer rainfall over the southwestern Tibetan Plateau controlled by deep convection over the Indian subcontinent', *Nature Communications* **7**, 1–9.

Donohoe, A., Marshall, J., Ferreira, D. and Mcgee, D. (2013), 'The relationship between ITCZ location and cross-equatorial atmospheric heat transport: From the seasonal cycle to the Last Glacial Maximum', *Journal of Climate* **26**(11), 3597–3618.

Dreybrodt, W. and Scholz, D. (2011), 'Climatic dependence of stable carbon and oxygen isotope signals recorded in speleothems: From soil water to speleothem calcite', *Geochimica et Cosmochimica Acta* **75**(3), 734–752.

Duc, H. N., Bang, H. Q. and Quang, N. X. (2018), 'Influence of the Pacific and Indian Ocean climate drivers on the rainfall in Vietnam', *International Journal of Climatology* **2018**(April), 5717–5732.

Dykoski, C. A., Edwards, R. L., Cheng, H., Yuan, D., Cai, Y., Zhang, M., Lin, Y., Qing, J., An, Z. and Revenaugh, J. (2005), 'A high-resolution, absolute-dated Holocene and deglacial Asian

monsoon record from Dongge Cave, China', *Earth and Planetary Science Letters* **233**(1-2), 71–86.

Ellis, S. A., Cobb, K. M., Moerman, J. W., Partin, J. W., Bennett, A. L., Malang, J., Gerstner, H. and Tuen, A. A. (2020), 'Extended cave drip water time series captures the 2015–2016 El Niño in Northern Borneo', *Geophysical Research Letters* **47**(5), no–no.

Emile-Geay, J., Cobb, K. M., Carré, M., Braconnot, P., Leloup, J., Zhou, Y., Harrison, S. P., Corrège, T., McGregor, H. V., Collins, M. et al. (2016), 'Links between tropical pacific seasonal, interannual and orbital variability during the holocene', *Nature Geoscience* **9**(2), 168–173.

Engel, J., Woodhead, J., Hellstrom, J., White, S., White, N. and Green, H. (2020), 'Using speleothems to constrain late cenozoic uplift rates in karst terranes', *Geology* **48**(8), 755–760.

Fairchild, I. J. and Baker, A. (2012), *Speleothem science: from process to past environments*, Vol. 3, John Wiley & Sons.

Fairchild, I. J., Borsato, A., Tooth, A. F., Frisia, S., Hawkesworth, C. J., Huang, Y., McDermott, F. and Spiro, B. (2000), 'Controls on trace element (Sr–Mg) compositions of carbonate cave waters: implications for speleothem climatic records', *Chemical Geology* **166**(3-4), 255–269.

Fairchild, I. J. and McMillan, E. A. (2007), 'Speleothems as indicators of wet and dry periods', *International Journal of Speleology* **36**(2), 2.

Fairchild, I. J., Smith, C. L., Baker, A., Fuller, L., Spötl, C., Mattey, D., McDermott, F. et al. (2006), 'Modification and preservation of environmental signals in speleothems', *Earth-Science Reviews* **75**(1-4), 105–153.

Fairchild, I. J. and Treble, P. C. (2009), 'Trace elements in speleothems as recorders of environmental change', *Quaternary Science Reviews* **28**(5-6), 449–468.

Festi, D., Hoffmann, D. L. and Luetscher, M. (2016), 'Pollen from accurately dated speleothems supports alpine glacier low-stands during the early holocene', *Quaternary Research* **86**(1), 45–53.

Finné, M., Kylander, M., Boyd, M., Sundqvist, H. S. and Löwemark, L. (2014), 'Can xrf scanning

of speleothems be used as a non-destructive method to identify paleoflood events in caves?', *International Journal of Speleology* **44**(1), 2.

Fohlmeister, J., Plessen, B., Dudashvili, A. S., Tjallingii, R., Wolff, C., Gafurov, A. and Cheng, H. (2017), 'Winter precipitation changes during the medieval climate anomaly and the little ice age in arid central asia', *Quaternary Science Reviews* **178**, 24–36.

Fohlmeister, J., Voarintsoa, N. R. G., Lechleitner, F. A., Boyd, M., Brandtstätter, S., Jacobson, M. J. and L. Oster, J. (2020), 'Main controls on the stable carbon isotope composition of speleothems', *Geochimica et Cosmochimica Acta* **279**, 67–87.

Frisia, S. (2014), 'Microstratigraphic logging of calcite fabrics in speleothems as tool for palaeoclimate studies', *International Journal of Speleology* **44**(1), 1.

Frisia, S., Borsato, A., Drysdale, R., Paul, B., Greig, A. and Cotte, M. (2012), 'A re-evaluation of the palaeoclimatic significance of phosphorus variability in speleothems revealed by high-resolution synchrotron micro xrf mapping', *Climate of the Past* **8**(6), 2039–2051.

Frisia, S., Borsato, A., Fairchild, I. J. and McDermott, F. (2000), 'Calcite fabrics, growth mechanisms, and environments of formation in speleothems from the italian alps and southwestern ireland', *Journal of Sedimentary Research* **70**(5), 1183–1196.

Frisia, S., Fairchild, I. J., Fohlmeister, J., Miorandi, R., Spötl, C. and Borsato, A. (2011), 'Carbon mass-balance modelling and carbon isotope exchange processes in dynamic caves', *Geochimica et Cosmochimica Acta* **75**(2), 380–400.

Galewsky, J., Steen-Larsen, H. C., Field, R. D., Worden, J., Risi, C. and Schneider, M. (2016), 'Stable isotopes in atmospheric water vapor and applications to the hydrologic cycle', *Reviews of Geophysics* **54**(4), 809–865.

Gat, J. R. and Airey, P. L. (2006), 'Stable water isotopes in the atmosphere/biosphere/lithosphere interface: Scaling-up from the local to continental scale, under humid and dry conditions', *Global and Planetary Change* **51**(1), 25 – 33.

Gat, J. R., Bowser, C. J. and Kendall, C. (1994), 'The contribution of evaporation from the great lakes to the continental atmosphere: estimate based on stable isotope data', *Geophysical Research Letters* **21**(7), 557–560.

Gázquez, F., Columbu, A., De Waele, J., Breitenbach, S. F., Huang, C.-R., Shen, C.-C., Lu, Y., Calaforra, J.-M., Mleneck-Vautravers, M. J. and Hodell, D. A. (2018), 'Quantification of paleo-aquifer changes using clumped isotopes in subaqueous carbonate speleothems', *Chemical Geology* **493**, 246–257.

Ge, F., Zhi, X., Babar, Z. A., Tang, W. and Chen, P. (2017a), 'Interannual variability of summer monsoon precipitation over the Indochina Peninsula in association with ENSO', *Theoretical and applied climatology* **128**(3-4), 523–531.

Ge, Q., Hao, Z., Zheng, J. and Shao, X. (2013), 'Temperature changes over the past 2000 yr in china and comparison with the northern hemisphere', *Climate of the Past* **9**(3), 1153–1160.

Ge, Q., Xue, Z., Yao, Z., Zang, Z. and Chu, F. (2017b), 'Anti-phase relationship between the east asian winter monsoon and summer monsoon during the holocene?', *Journal of Ocean University of China* **16**(2), 175–183.

Ge, Q., Zheng, J., Fang, X., Man, Z., Zhang, X., Zhang, P. and Wang, W.-C. (2003), 'Winter half-year temperature reconstruction for the middle and lower reaches of the Yellow River and Yangtze River, China, during the past 2000 years', *The Holocene* **13**(6), 933–940.

Geen, R., Bordoni, S., Battisti, D. S. and Hui, K. (2020), 'Monsoons, ITCZs, and the Concept of the Global Monsoon', *Reviews of Geophysics* **58**(4), e2020RG000700.

Gobin, A., Nguyen, H. T., Pham, V. Q. and Pham, H. T. (2016), 'Heavy rainfall patterns in Vietnam and their relation with ENSO cycles', *International Journal of Climatology* **36**(4), 1686–1699.

Gonfiantini, R., Roche, M.-A., Olivry, J.-C., Fontes, J.-C. and Zuppi, G. M. (2001), 'The altitude effect on the isotopic composition of tropical rains', *Chemical Geology* **181**(1-4), 147–167.

Good, S. P., Noone, D. and Bowen, G. (2015), 'Hydrologic connectivity constrains partitioning of global terrestrial water fluxes', *Science* **349**(6244), 175–177.

Griffiths, M. L., Drysdale, R. N., Gagan, M. K., Zhao, J., Ayliffe, L. K. and Hellstrom, J. C. (2009), 'Increasing Australian Indonesian monsoon rainfall linked to early Holocene sea-level rise', *Nature Geoscience* **2**(9), 636–639.

Griffiths, M. L., Johnson, K. R., Pausata, F. S., White, J. C., Henderson, G. M., Wood, C. T., Yang, H., Ersek, V., Conrad, C. and Sekhon, N. (2020), 'End of Green Sahara amplified mid-to late Holocene megadroughts in mainland Southeast Asia', *Nature communications* **11**(1), 1–12.

Griffiths, M. L., Kimbrough, A. K., Gagan, M. K., Drysdale, R. N., Cole, J. E., Johnson, K. R., Zhao, J.-X., Cook, B. I., Hellstrom, J. C. and Hantoro, W. S. (2016), 'Western pacific hydroclimate linked to global climate variability over the past two millennia', *Nature Communications* **7**(1), 1–9.

Gu, G., Adler, R. F. and Huffman, G. J. (2016), 'Long-term changes/trends in surface temperature and precipitation during the satellite era (1979–2012)', *Climate Dynamics* **46**(3-4), 1091–1105.

Guo, Y.-P. and Tan, Z.-M. (2018), 'Relationship between El Niño–Southern Oscillation and the symmetry of the Hadley circulation: Role of the sea surface temperature annual cycle', *Journal of Climate* **31**(13), 5319–5332.

Hamilton, R., Penny, D. and Hua, Q. (2019), 'A 4700-year record of hydroclimate variability over the asian monsoon intersection zone inferred from multi-proxy analysis of lake sediments', *Global and Planetary Change* **174**, 92–104.

Hao, T., Liu, X., Ogg, J., Liang, Z., Xiang, R., Zhang, X., Zhang, D., Zhang, C., Liu, Q. and Li, X. (2017), 'Intensified episodes of east asian winter monsoon during the middle through late holocene driven by north atlantic cooling events: High-resolution lignin records from the south yellow sea, china', *Earth and Planetary Science Letters* **479**, 144–155.

Hartland, A., Fairchild, I. J., Lead, J. R., Borsato, A., Baker, A., Frisia, S. and Baalousha, M. (2012), 'From soil to cave: Transport of trace metals by natural organic matter in karst dripwaters', *Chemical Geology* **304**, 68–82.

He, S., Gao, Y., Li, F., Wang, H. and He, Y. (2017), 'Impact of arctic oscillation on the east asian climate: A review', *Earth-Science Reviews* **164**, 48–62.

He, X.-c., Ding, Y.-h. and He, J.-h. (2008), 'Response characteristics of the East Asian winter monsoon to ENSO events', *CHINESE JOURNAL OF ATMOSPHERIC SCIENCES-CHINESE EDITION-* **32**(2), 335.

Held, I. M. and Soden, B. J. (2006), 'Robust responses of the hydrological cycle to global warming', *Journal of climate* **19**(21), 5686–5699.

Hendricks, M., DePaolo, D. and Cohen, R. (2000), 'Space and time variation of δ^{18}O andδD in precipitation: Can paleotemperature be estimated from ice cores?', *Global Biogeochemical Cycles* **14**(3), 851–861.

Herzschuh, U., Cao, X., Laepple, T., Dallmeyer, A., Telford, R. J., Ni, J., Chen, F., Kong, Z., Liu, G., Liu, K.-B. et al. (2019), 'Position and orientation of the westerly jet determined holocene rainfall patterns in china', *Nature Communications* **10**(1), 1–8.

Hijioka, Y., Lin, E., Pereira, J., Corlett, R., X. Cui and, G. I., Lasco, R., Lindgren, E. and Surjan, A. (2014), 'Asia. In: Climate Change 2014: Impacts, Adaptation, and Vulnerability. Part B: Regional Aspects. Contribution of Working Group II to the Fifth Assessment Report of the Intergovernmental Panel on Climate Change', *IPCC Report* pp. 1327–1370.

Hillman, A. L., Abbott, M. B., Finkenbinder, M. S. and Yu, J. (2017), 'An 8,600 year lacustrine record of summer monsoon variability from yunnan, china', *Quaternary Science Reviews* **174**, 120–132.

Hu, P., Chen, W., Huang, R. and Nath, D. (2019), 'Climatological characteristics of the synoptic changes accompanying south china sea summer monsoon withdrawal', *International Journal of Climatology* **39**(2), 596–612.

Hua, Q., McDonald, J., Redwood, D., Drysdale, R., Lee, S., Fallon, S. and Hellstrom, J. (2012), 'Robust chronological reconstruction for young speleothems using radiocarbon', *Quaternary Geochronology* **14**, 67–80.

Huang, E., Tian, J. and Steinke, S. (2011), 'Millennial-scale dynamics of the winter cold tongue in the southern south china sea over the past 26 ka and the east asian winter monsoon', *Quaternary Research* **75**(1), 196–204.

Huang, Y. and Fairchild, I. J. (2001), 'Partitioning of Sr2+ and Mg2+ into calcite under karst-analogue experimental conditions', *Geochimica et Cosmochimica Acta* **65**(1), 47–62.

IAEA/WMO (2020), 'The GNIP Database', *Accessible at:* http://www.iaea.org/water.

Izumo, T., Vialard, J., Lengaigne, M., de Boyer Montegut, C., Behera, S. K., Luo, J.-J., Cravatte, S., Masson, S. and Yamagata, T. (2010), 'Influence of the state of the Indian Ocean Dipole on the following years El Niño', *Nature Geoscience* **3**(3), 168–172.

Jaffey, A., Flynn, K., Glendenin, L., Bentley, W. t. and Essling, A. (1971), 'Precision measurement of half-lives and specific activities of u 235 and u 238', *Physical review C* **4**(5), 1889.

James, E. W., Banner, J. L. and Hardt, B. (2015), 'A global model for cave ventilation and seasonal bias in speleothem paleoclimate records', *Geochemistry, Geophysics, Geosystems* **16**(4), 1044–1051.

Jia, G., Bai, Y., Yang, X., Xie, L., Wei, G., Ouyang, T., Chu, G., Liu, Z. et al. (2015), 'Biogeochemical evidence of holocene east asian summer and winter monsoon variability from a tropical maar lake in southern china', *Quaternary Science Reviews* **111**, 51–61.

Jiao, Y., Liu, C., Liu, Z., Ding, Y. and Xu, Q. (2020), 'Impacts of moisture sources on the temporal and spatial heterogeneity of monsoon precipitation isotopic altitude effects', *Journal of Hydrology* p. 124576.

Jin, C.-X., Zhou, T.-J., Guo, Z., Wu, B. and Chen, X.-L. (2016), 'Improved simulation of the East Asian winter monsoon interannual variation by IAP/LASG AGCMs', *Atmospheric and Oceanic Science Letters* **9**(3), 204–210.

Jochum, K. P., Nohl, U., Herwig, K., Lammel, E., Stoll, B. and Hofmann, A. W. (2005), 'Georem: a new geochemical database for reference materials and isotopic standards', *Geostandards and Geoanalytical Research* **29**(3), 333–338.

Jochum, K. P., Scholz, D., Stoll, B., Weis, U., Wilson, S. A., Yang, Q., Schwalb, A., Börner, N., Jacob, D. E. and Andreae, M. O. (2012), 'Accurate trace element analysis of speleothems and biogenic calcium carbonates by LA-ICP-MS', *Chemical Geology* **318**, 31–44.

Johnsen, S. J., Dahl-Jensen, D., Gundestrup, N., Steffensen, J. P., Clausen, H. B., Miller, H., Masson-Delmotte, V., Sveinbjörnsdottir, A. E. and White, J. (2001), 'Oxygen isotope and palaeotemperature records from six Greenland ice-core stations: Camp Century, Dye-3, GRIP, GISP2, Renland and NorthGRIP', *Journal of Quaternary Science: Published for the Quaternary Research Association* **16**(4), 299–307.

Johnson, K. R., Hu, C., Belshaw, N. S. and Henderson, G. M. (2006), 'Seasonal trace-element and stable-isotope variations in a chinese speleothem: The potential for high-resolution paleomonsoon reconstruction', *Earth and Planetary Science Letters* **244**(1-2), 394–407.

Jouzel, J., Masson-Delmotte, V., Cattani, O., Dreyfus, G., Falourd, S., Hoffmann, G., Minster, B., Nouet, J., Barnola, J.-M., Chappellaz, J. et al. (2007), 'Orbital and millennial antarctic climate variability over the past 800,000 years', *science* **317**(5839), 793–796.

Julian, P. R. and Chervin, R. M. (1978), 'A study of the southern oscillation and walker circulation phenomenon', *Monthly Weather Review* **106**(10), 1433–1451.

Kaboth-Bahr, S., Bahr, A., Zeeden, C., Yamoah, K. A., Lone, M. A., Chuang, C.-K., Löwemark, L. and Wei, K.-Y. (2021), 'A tale of shifting relations: East asian summer and winter monsoon variability during the holocene', *Scientific reports* **11**(1), 1–10.

Kajita, H., Kawahata, H., Wang, K., Zheng, H., Yang, S., Ohkouchi, N., Utsunomiya, M., Zhou, B. and Zheng, B. (2018), 'Extraordinary cold episodes during the mid-holocene in the yangtze delta: Interruption of the earliest rice cultivating civilization', *Quaternary Science Reviews* **201**, 418–428.

Kathayat, G., Cheng, H., Sinha, A., Spötl, C., Edwards, R. L., Zhang, H., Li, X., Yi, L., Ning, Y., Cai, Y. et al. (2016), 'Indian monsoon variability on millennial-orbital timescales', *Scientific reports* **6**(1), 1–7.

Kathayat, G., Cheng, H., Sinha, A., Yi, L., Li, X., Zhang, H., Li, H., Ning, Y. and Edwards, R. L. (2017), 'The indian monsoon variability and civilization changes in the indian subcontinent', *Science Advances* **3**(12), e1701296.

Kaufman, A., Bar-Matthews, M., Ayalon, A. and Carmi, I. (2003), 'The vadose flow above soreq cave, israel: a tritium study of the cave waters', *Journal of Hydrology* **273**(1-4), 155–163.

Kaushal, N., Breitenbach, S. F. M., Lechleitner, F. A., Sinha, A., Tewari, V. C., Ahmad, S. M., Berkelhammer, M., Band, S., Yadava, M., Ramesh, R. and Henderson, G. M. (2018), 'The Indian Summer Monsoon from a Speleothem δ^{18}O Perspective - a Review', **3**(September), 1–26.

Kilbourne, K. H., Quinn, T. M. and Taylor, F. W. (2004), 'A fossil coral perspective on western tropical pacific climate 350 ka', *Paleoceanography* **19**(1).

Kim, J.-W., Yeh, S.-W. and Chang, E.-C. (2014), 'Combined effect of El Niño-Southern Oscillation and Pacific decadal oscillation on the East Asian winter monsoon', *Climate dynamics* **42**(3-4), 957–971.

Konecky, B. L., Noone, D. C. and Cobb, K. M. (2019), 'The In fl uence of Competing Hydroclimate Processes on Stable Isotope Ratios in Tropical Rainfall Geophysical Research Letters', *Geophysical Research Letters* pp. 1622–1633.

Konecky, B. L., Russell, J. M., Rodysill, J. R., Vuille, M., Bijaksana, S. and Huang, Y. (2013), 'Intensification of southwestern indonesian rainfall over the past millennium', *Geophysical Research Letters* **40**(2), 386–391.

Kousky, V. E., Kagano, M. T. and Cavalcanti, I. F. (1984), 'A review of the southern oscillation: oceanic-atmospheric circulation changes and related rainfall anomalies', *Tellus A* **36**(5), 490–504.

Kröpelin, S., Verschuren, D., Lézine, A.-M., Eggermont, H., Cocquyt, C., Francus, P., Cazet, J.-P., Fagot, M., Rumes, B., Russell, J. M. et al. (2008), 'Climate-driven ecosystem succession in the sahara: the past 6000 years', *Science* **320**(5877), 765–768.

Kuhnert, H., Kuhlmann, H., Mohtadi, M., Meggers, H., Baumann, K.-H. and Pätzold, J. (2014), 'Holocene tropical western indian ocean sea surface temperatures in covariation with climatic changes in the indonesian region', *Paleoceanography* **29**(5), 423–437.

Kukla, T., Winnick, M. J., Maher, K., Ibarra, D. E. and Chamberlain, C. P. (2019), 'The Sensitivity of Terrestrial δ^{18}O Gradients to Hydroclimate Evolution', *Journal of Geophysical Research: Atmospheres* **124**(2), 563–582.

Kurita, N., Ichiyanagi, K., Matsumoto, J., Yamanaka, M. D. and Ohata, T. (2009), 'The relationship between the isotopic content of precipitation and the precipitation amount in tropical regions', *Journal of Geochemical Exploration* **102**(3), 113–122.

Kutzbach, J., Liu, X., Liu, Z. and Chen, G. (2008), 'Simulation of the evolutionary response of global summer monsoons to orbital forcing over the past 280,000 years', *Climate Dynamics* **30**(6), 567–579.

Lachniet, M. S. (2009), 'Climatic and environmental controls on speleothem oxygen-isotope values', *Quaternary Science Reviews* **28**(5-6), 412–432.

Laskar, A. H., Yadava, M., Ramesh, R., Polyak, V. and Asmerom, Y. (2013), 'A 4 kyr stalagmite oxygen isotopic record of the past indian summer monsoon in the andaman islands', *Geochemistry, Geophysics, Geosystems* **14**(9), 3555–3566.

Lau, K.-M. and Yang, S. (2015), Tropical meteorology & climate - walker circulation, *in* G. R. North, J. Pyle and F. Zhang, eds, 'Encyclopedia of Atmospheric Sciences (Second Edition)', second edition edn, Academic Press, Oxford, pp. 177–181.

Lau, K. and Yang, S. (1997), 'Climatology and interannual variability of the Southeast Asian summer monsoon', *Advances in Atmospheric Sciences* **14**(2), 141–162.

Lau, W. K. and Kim, K.-M. (2015), 'Robust Hadley circulation changes and increasing global dryness due to CO_2 warming from CMIP5 model projections', *Proceedings of the National Academy of Sciences* **112**(12), 3630–3635.

Le Duy, N., Heidbüchel, I., Meyer, H., Merz, B. and Apel, H. (2018), 'What controls the stable isotope composition of precipitation in the Mekong Delta? A model-based statistical approach', *Hydrology and Earth System Sciences* **22**(2), 1239–1262.

Lê, S., Josse, J., Husson, F. et al. (2008), 'Factominer: an r package for multivariate analysis', *Journal of statistical software* **25**(1), 1–18.

Lechleitner, F. A., Breitenbach, S. F., Cheng, H., Plessen, B., Rehfeld, K., Goswami, B., Marwan, N., Eroglu, D., Adkins, J., Haug, G. and et al. (2017), 'Climatic and in-cave influences on $\delta^{18}O$ and $\delta^{13}C$ in a stalagmite from northeastern India through the last deglaciation', *Quaternary Research* **88**(3), 458471.

Lechleitner, F. A., Fohlmeister, J., McIntyre, C., Baldini, L. M., Jamieson, R. A., Hercman, H., Gąsiorowski, M., Pawlak, J., Stefaniak, K., Socha, P. et al. (2016), 'A novel approach for construction of radiocarbon-based chronologies for speleothems', *Quaternary Geochronology* **35**, 54–66.

LeComte, D. (2021), 'International weather highlights 2020: Record atlantic tropical season, historic flooding in asia and africa', *Weatherwise* **74**(3), 26–35.

Li, D., Li, T., Jiang, H., Björck, S., Seidenkrantz, M.-S., Zhao, M., Sha, L. and Knudsen, K. L. (2018), 'East asian winter monsoon variations and their links to arctic sea ice during the last millennium, inferred from sea surface temperatures in the okinawa trough', *Paleoceanography and Paleoclimatology* **33**(1), 61–75.

Li, R., Wang, S.-Y., Gillies, R. R., Buckley, B., Yoon, J.-H. and Cho, C. (2019), 'Regional trends in early-monsoon rainfall over Vietnam and CCSM4 attribution', *Climate Dynamics* **52**(1), 363–372.

Li, Y., Wang, N., Zhou, X., Zhang, C. and Wang, Y. (2014), 'Synchronous or asynchronous holocene indian and east asian summer monsoon evolution: A synthesis on holocene asian summer monsoon simulations, records and modern monsoon indices', *Global and planetary Change* **116**, 30–40.

Limbert, H., Limbert, D., Ponta, G. M., Xuan, N. N., Stoiciu, F. and Mocioiu, A.-M. (2020), 'Preliminary hydrogeological observations in phong nha–ke bang national park and tu lan karst area, quang binh province, vietnam', *Carbonates and Evaporites* **35**(3), 1–26.

Lin, J.-L. (2007), 'The double-ITCZ problem in IPCC AR4 coupled GCMs: Ocean–atmosphere feedback analysis', *Journal of Climate* **20**(18), 4497–4525.

Liu, F., Chai, J., Wang, B., Liu, J., Zhang, X. and Wang, Z. (2016), 'Global monsoon precipitation responses to large volcanic eruptions', *Scientific reports* **6**(1), 1–11.

Liu, J., Chen, S., Chen, J., Zhang, Z. and Chen, F. (2017), 'Chinese cave δ18o records do not represent northern east asian summer monsoon rainfall', *Proceedings of the National Academy of Sciences* **114**(15), E2987–E2988.

Liu, J., Song, X., Yuan, G., Sun, X. and Yang, L. (2014), 'Stable isotopic compositions of precipitation in China', *Tellus, Series B: Chemical and Physical Meteorology* **66**(1).

Liu, X., Dong, H., Yang, X., Herzschuh, U., Zhang, E., Stuut, J.-B. W. and Wang, Y. (2009b), 'Late holocene forcing of the asian winter and summer monsoon as evidenced by proxy records from the northern qinghai–tibetan plateau', *Earth and Planetary Science Letters* **280**(1-4), 276–284.

Liu, Z., Wen, X., Brady, E., Otto-Bliesner, B., Yu, G., Lu, H., Cheng, H., Wang, Y., Zheng, W.,

Ding, Y. et al. (2014), 'Chinese cave records and the east asia summer monsoon', *Quaternary Science Reviews* **83**, 115–128.

Ljungqvist, F. C. (2010), 'A new reconstruction of temperature variability in the extra-tropical northern hemisphere during the last two millennia', *Geografiska Annaler: Series A, Physical Geography* **92**(3), 339–351.

Lloyd, S. (1982), 'Least squares quantization in pcm', *IEEE transactions on information theory* **28**(2), 129–137.

Lough, J. M. (2010), 'Climate records from corals', *Wiley interdisciplinary reviews: climate change* **1**(3), 318–331.

Maher, B. A. (2008), 'Holocene variability of the east asian summer monsoon from chinese cave records: a re-assessment', *The Holocene* **18**(6), 861–866.

Maher, B. A. (2016), 'Palaeoclimatic records of the loess/palaeosol sequences of the chinese loess plateau', *Quaternary Science Reviews* **154**, 23–84.

Mahmud, K., Mariethoz, G., Baker, A. and Treble, P. C. (2018), 'Hydrological characterization of cave drip waters in a porous limestone: Golgotha cave, western australia', *Hydrology and Earth System Sciences* **22**(2), 977–988.

Mann, M. E., Bradley, R. S. and Hughes, M. K. (1998), 'Global-scale temperature patterns and climate forcing over the past six centuries', *Nature* **392**(6678), 779–787.

Masson-Delmotte, V., Schulz, M., Abe-Ouchi, A., Beer, J., Ganopolski, A., Rouco, J. G., Jansen, E., Lambeck, K., Luterbacher, J., Naish, T. et al. (2013), 'Information from paleoclimate archives in: Climate change 2013: The physical science basis contribution of working group i to the fifth assessment report of the intergovernmental panel on climate change ed tf stocker et al', *Cambridge, United Kingdom and New York, NY, USA* **435**.

Matley, K. A., Sniderman, J. K., Drinnan, A. N. and Hellstrom, J. C. (2020), 'Late-holocene environmental change on the nullarbor plain, southwest australia, based on speleothem pollen records', *The Holocene* **30**(5), 672–681.

Matsumoto, J. (1992), 'The seasonal changes in asian and australian monsoon regions', *Journal of the Meteorological Society of Japan. Ser. II* **70**(1B), 257–273.

Maxwell, A. L. (2001), 'Holocene monsoon changes inferred from lake sediment pollen and carbonate records, northeastern cambodia', *Quaternary Research* **56**(3), 390–400.

McDermott, F. (2004), 'Palaeo-climate reconstruction from stable isotope variations in speleothems: a review', *Quaternary Science Reviews* **23**(7-8), 901–918.

McGarry, S. F. and Caseldine, C. (2004), 'Speleothem palynology: an undervalued tool in quaternary studies', *Quaternary Science Reviews* **23**(23-24), 2389–2404.

McGee, D. and deMenocal, P. B. (2017), 'Climatic changes and cultural responses during the african humid period recorded in multi-proxy data', *Oxford Research Encyclopedia of Climate Science* **November 20**.

McGowan, H., Marx, S., Moss, P. and Hammond, A. (2012), 'Evidence of ENSO mega-drought triggered collapse of prehistory Aboriginal society in northwest Australia', *Geophysical Research Letters* **39**(22).

McGregor, H., Fischer, M. J., Gagan, M., Fink, D., Phipps, S. J., Wong, H. and Woodroffe, C. (2013), 'A weak el niño/southern oscillation with delayed seasonal growth around 4,300 years ago', *Nature Geoscience* **6**(11), 949–953.

Merlivat, L. and Jouzel, J. (1979), 'Global climatic interpretation of the deuterium-oxygen 18 relationship for precipitation', *Journal of Geophysical Research: Oceans* **84**(C8), 5029–5033.

Misra, V. and Dinapoli, S. (2014), 'The variability of the Southeast Asian summer monsoon', *International Journal of Climatology* **34**(3), 893–901.

Moerman, J. W., Cobb, K. M., Adkins, J. F., Sodemann, H., Clark, B. and Tuen, A. A. (2013), 'Diurnal to interannual rainfall δ18O variations in northern Borneo driven by regional hydrology', *Earth and Planetary Science Letters* **369-370**, 108–119.

Mohtadi, M., Prange, M., Schefuß, E. and Jennerjahn, T. C. (2017), 'Late holocene slowdown of the indian ocean walker circulation', *Nature Communications* **8**(1), 1–8.

Mohtadi, M., Prange, M. and Steinke, S. (2016), 'Palaeoclimatic insights into forcing and response of monsoon rainfall', *Nature* **533**(7602), 191–199.

Moyano, F. E., Manzoni, S. and Chenu, C. (2013), 'Responses of soil heterotrophic respiration to moisture availability: An exploration of processes and models', *Soil Biology and Biochemistry* **59**, 72–85.

Munksgaard, N. C., Kurita, N., Sánchez-Murillo, R., Ahmed, N., Araguas, L., Balachew, D. L., Bird, M. I., Chakraborty, S., Kien Chinh, N., Cobb, K. M., Ellis, S. A., Esquivel-Hernández, G., Ganyaglo, S. Y., Gao, J., Gastmans, D., Kaseke, K. F., Kebede, S., Morales, M. R., Mueller, M., Poh, S. C., dos Santos, V., Shaoneng, H., Wang, L., Yacobaccio, H. and Zwart, C. (2019), 'Data Descriptor: Daily observations of stable isotope ratios of rainfall in the tropics', *Scientific Reports* **9**(1), 1–7.

Nava-Fernandez, C., Hartland, A., Gázquez, F., Kwiecien, O., Marwan, N., Fox, B., Hellstrom, J., Pearson, A., Ward, B., French, A. et al. (2020), 'Pacific climate reflected in waipuna cave drip water hydrochemistry', *Hydrology and Earth System Sciences* **24**(6), 3361–3380.

NCEP (2020), 'NCEP Global Data Assimilation System data', *provided by NOAA/OAR/ESRL PSL Boulder, Colorado, USA, from their Web site at* https://psl.noaa.gov/.

Nesbitt, H. and Young, G. (1982), 'Early proterozoic climates and plate motions inferred from major element chemistry of lutites', *Nature* **299**(5885), 715–717.

Neukom, R., Barboza, L. A., Erb, M. P., Shi, F., Emile-Geay, J., Evans, M. N., Franke, J., Kaufman, D. S., Lücke, L., Rehfeld, K. et al. (2019b), 'Consistent multi-decadal variability in global temperature reconstructions and simulations over the common era', *Nature Geoscience* **12**(8), 643.

Neukom, R., Steiger, N., Gómez-Navarro, J. J., Wang, J. and Werner, J. P. (2019a), 'No evidence for globally coherent warm and cold periods over the preindustrial common era', *Nature* **571**(7766), 550–554.

Nguyen-Thi, H. A., Matsumoto, J., Ngo-Duc, T. and Endo, N. (2012), 'A Climatological Study of Tropical Cyclone Rainfall in Vietnam', *Sola* **8**(0), 41–44.

NOAA (2020*a*), 'CPC Global Unified Precipitation data', *provided by NOAA/OAR/ESRL PSL Boulder, Colorado, USA, from their Web site at* https://psl.noaa.gov/.

NOAA (2020*b*), 'Dipole Mode Index (DMI)', *provided by NOAA/OAR/ESRL PSL Boulder, Colorado, USA, from their Web site at* https://psl.noaa.gov/gcos_wgsp/Timeseries/DMI/.

NOAA (2020*c*), 'GPCC Precipitation data', *provided by NOAA/OAR/ESRL PSL Boulder, Colorado, USA, from their Web site at* https://psl.noaa.gov/.

NOAA (2020*d*), 'Interpolated OLR data', *provided by NOAA/OAR/ESRL PSL Boulder, Colorado, USA, from their Web site at* https://psl.noaa.gov/.

Noipow, N. (2015), Seasonal Variation of the Stable Isotope Fingerprints in daily precipitations and Mekong River, the implication on Hydrological Study of Thailand and Lao PDR., *in* 'The 3rd Lao-Thai Technical Conference, July 7-8, 2015', pp. 201–208.

Noronha, A. L., Johnson, K. R., Southon, J. R., Hu, C., Ruan, J. and McCabe-Glynn, S. (2015), 'Radiocarbon evidence for decomposition of aged organic matter in the vadose zone as the main source of speleothem carbon', *Quaternary Science Reviews* **127**, 37–47.

Oppo, D. W., Rosenthal, Y. and Linsley, B. K. (2009), '2,000-year-long temperature and hydrology reconstructions from the indo-pacific warm pool', *Nature* **460**(7259), 1113–1116.

Osborne, P., Humphreys, G. and Polunin, N. (1993), 'Sediment deposition and late Holocene environmental change in a tropical lowland basin: Waigani Lake, Papua New Guinea', *Journal of Biogeography* pp. 599–613.

Oster, J. L., Ibarra, D. E., Harris, C. R. and Maher, K. (2012), 'Influence of eolian deposition and rainfall amounts on the u-isotopic composition of soil water and soil minerals', *Geochimica et Cosmochimica Acta* **88**, 146–166.

Oster, J. L., Montanez, I. P., Guilderson, T. P., Sharp, W. D. and Banner, J. L. (2010), 'Modeling speleothem δ^{13}C variability in a central Sierra Nevada cave using ^{14}C and ^{87}Sr/^{86}Sr', *Geochimica et Cosmochimica Acta* **74**(18), 5228–5242.

Owen, R., Day, C., Hu, C.-Y., Liu, Y.-H., Pointing, M., Blättler, C. and Henderson, G. (2016),

'Calcium isotopes in caves as a proxy for aridity: Modern calibration and application to the 8.2 kyr event', *Earth and Planetary Science Letters* **443**, 129–138.

Parker, S. E., Harrison, S. P., Comas-Bru, L., Kaushal, N., LeGrande, A. N. and Werner, M. (2021), 'A data–model approach to interpreting speleothem oxygen isotope records from monsoon regions', *Climate of the Past* **17**(3), 1119–1138.

Partin, J. W., Cobb, K. M., Adkins, J. F., Tuen, A. A. and Clark, B. (2013), 'Trace metal and carbon isotopic variations in cave dripwater and stalagmite geochemistry from northern Borneo', *Geochemistry, Geophysics, Geosystems* **14**(9), 3567–3585.

Paton, C., Hellstrom, J., Paul, B., Woodhead, J. and Hergt, J. (2011), 'Iolite: Freeware for the visualisation and processing of mass spectrometric data', *Journal of Analytical Atomic Spectrometry* **26**(12), 2508–2518.

Pausata, F. S., Battisti, D. S., Nisancioglu, K. H. and Bitz, C. M. (2011), 'Chinese stalagmite δ18o controlled by changes in the indian monsoon during a simulated heinrich event', *Nature Geoscience* **4**(7), 474.

Pausata, F. S., Zhang, Q., Muschitiello, F., Lu, Z., Chafik, L., Niedermeyer, E. M., Stager, J. C., Cobb, K. M. and Liu, Z. (2017), 'Greening of the Sahara suppressed ENSO activity during the mid-Holocene', *Nature Communications* **8**(1), 1–12.

Peng, T.-R., Wang, C.-H., Huang, C.-C., Fei, L.-Y., Chen, C.-T. A. and Hwong, J.-L. (2010), 'Stable isotopic characteristic of taiwan's precipitation: A case study of western pacific monsoon region', *Earth and Planetary Science Letters* **289**(3), 357 – 366.

Penny, D. (2006), 'The Holocene history and development of the Tonle Sap, Cambodia', *Quaternary Science Reviews* **25**(3-4), 310–322.

Peterson, T. C. and Vose, R. S. (1997), 'An overview of the global historical climatology network temperature database', *Bulletin of the American Meteorological Society* **78**(12), 2837–2850.

Petit, J.-R., Jouzel, J., Raynaud, D., Barkov, N. I., Barnola, J.-M., Basile, I., Bender, M., Chappellaz, J., Davis, M., Delaygue, G. et al. (1999), 'Climate and atmospheric history of the past 420,000 years from the vostok ice core, antarctica', *Nature* **399**(6735), 429–436.

Phuong, L. T. H., Biesbroek, G. R., Sen, L. T. H. and Wals, A. E. (2018), 'Understanding smallholder farmers' capacity to respond to climate change in a coastal community in central vietnam', *Climate and Development* **10**(8), 701–716.

Pickering, R., Herries, A. I., Woodhead, J. D., Hellstrom, J. C., Green, H. E., Paul, B., Ritzman, T., Strait, D. S., Schoville, B. J. and Hancox, P. J. (2019), 'U–Pb-dated flowstones restrict South African early hominin record to dry climate phases', *Nature* **565**(7738), 226–229.

Poage, M. A. and Chamberlain, C. P. (2001), 'Empirical relationships between elevation and the stable isotope composition of precipitation and surface waters: considerations for studies of paleoelevation change', *American Journal of Science* **301**(1), 1–15.

Ponton, C., Giosan, L., Eglinton, T. I., Fuller, D. Q., Johnson, J. E., Kumar, P. and Collett, T. S. (2012), 'Holocene aridification of India', *Geophysical Research Letters* **39**(3).

Prasad, S., Anoop, A., Riedel, N., Sarkar, S., Menzel, P., Basavaiah, N., Krishnan, R., Fuller, D., Plessen, B., Gaye, B. et al. (2014), 'Prolonged monsoon droughts and links to indo-pacific warm pool: A holocene record from lonar lake, central india', *Earth and Planetary Science Letters* **391**, 171–182.

Premathilake, R. and Risberg, J. (2003), 'Late Quaternary climate history of the Horton plains, central Sri Lanka', *Quaternary Science Reviews* **22**(14), 1525–1541.

Ranasinghe, P., Ortiz, J. D., Smith, A., Griffith, E., Siriwardana, C., De Silva, S. and Wijesundara, D. (2013), 'Mid-to late-holocene indian winter monsoon variability from a terrestrial record in eastern and southeastern coastal environments of sri lanka', *The Holocene* **23**(7), 945–960.

Rehfeld, K. and Kurths, J. (2014), 'Similarity estimators for irregular and age-uncertain time series', *Climate of the Past* **10**(1), 107–122.

Rehfeld, K., Marwan, N., Heitzig, J. and Kurths, J. (2011), 'Comparison of correlation analysis techniques for irregularly sampled time series', *Nonlinear Processes in Geophysics* **18**(3), 389–404.

Reynard, L., Day, C. and Henderson, G. (2011), 'Large fractionation of calcium isotopes during cave-analogue calcium carbonate growth', *Geochimica et cosmochimica acta* **75**(13), 3726–3740.

Ridley, H. E., Asmerom, Y., Baldini, J. U., Breitenbach, S. F., Aquino, V. V., Prufer, K. M., Culleton, B. J., Polyak, V., Lechleitner, F. A., Kennett, D. J. et al. (2015), 'Aerosol forcing of the position of the intertropical convergence zone since ad 1550', *Nature Geoscience* **8**(3), 195–200.

Roberts, W. H., Battisti, D. S. and Tudhope, A. W. (2014), 'ENSO in the mid-Holocene according to CSM and HadCM3', *Journal of climate* **27**(3), 1223–1242.

Robinson, P. J. and Henderson-Sellers, A. (2014), *Contemporary Climatology*, Routledge.

Ropelewski, C. F. and Jones, P. D. (1987), 'An extension of the tahitidarwin southern oscillation index', *Monthly Weather Review* **115**(9), 2161–2165.

Rozanski, K., Araguás-Araguás, L. and Gonfiantini, R. (1993), 'Isotopic Patterns in Modern Global Precipitation', *Geophysical Monograph* pp. 1–36.

Ruan, J., Zhang, H., Cai, Z., Yang, X. and Yin, J. (2019), 'Regional controls on daily to interannual variations of precipitation isotope ratios in southeast china: Implications for paleomonsoon reconstruction', *Earth and Planetary Science Letters* **527**, 115794.

Russon, T., Tudhope, A., Collins, M. and Hegerl, G. (2015), 'Inferring changes in ENSO amplitude from the variance of proxy records', *Geophysical Research Letters* **42**(4), 1197–1204.

Sachs, J., Blois, J. L., McGee, T., Wolhowe, M., Haberle, S., Clark, G. and Atahan, P. (2018), 'Southward shift of the Pacific ITCZ during the Holocene', *Paleoceanography and Paleoclimatology* **33**(12), 1383–1395.

Sachs, L. (1984), Statistical decision techniques, *in* 'Applied Statistics', Springer, pp. 23–194.

Sagawa, T., Kuwae, M., Tsuruoka, K., Nakamura, Y., Ikehara, M. and Murayama, M. (2014), 'Solar forcing of centennial-scale east asian winter monsoon variability in the mid-to late holocene', *Earth and Planetary Science Letters* **395**, 124–135.

Sánchez-Murillo, R., Durán-Quesada, A. M., Esquivel-Hernández, G., Rojas-Cantillano, D., Birkel, C., Welsh, K., Sánchez-Llull, M., Alonso-Hernández, C. M., Tetzlaff, D., Soulsby, C. et al. (2019), 'Deciphering key processes controlling rainfall isotopic variability during extreme tropical cyclones', *Nature communications* **10**(1), 1–10.

Sano, M., Xu, C. and Nakatsuka, T. (2012), 'A 300-year Vietnam hydroclimate and ENSO variability record reconstructed from tree ring δ^{18}O', *Journal of Geophysical Research: Atmospheres* **117**(D12).

Saadi, Z., Shahid, S., Ismail, T., Chung, E.-S. and Wang, X.-J. (2019), 'Trends analysis of rainfall and rainfall extremes in Sarawak, Malaysia using modified Mann–Kendall test', *Meteorology and Atmospheric Physics* **131**(3), 263–277.

Schneider, T., Bischoff, T. and Haug, G. H. (2014), 'Migrations and dynamics of the intertropical convergence zone', *Nature* **513**(7516), 45–53.

Schulz, M. and Mudelsee, M. (2002), 'Redfit: estimating red-noise spectra directly from unevenly spaced paleoclimatic time series', *Computers & Geosciences* **28**(3), 421–426.

Schurer, A. P., Hegerl, G. C., Mann, M. E., Tett, S. F. and Phipps, S. J. (2013), 'Separating forced from chaotic climate variability over the past millennium', *Journal of Climate* **26**(18), 6954–6973.

Sengupta, A. and Nigam, S. (2019), 'The northeast winter monsoon over the indian subcontinent and southeast asia: evolution, interannual variability, and model simulations', *Journal of Climate* **32**(1), 231–249.

Shao, D., Mei, Y., Yang, Z., Wang, Y., Yang, W., Gao, Y., Yang, L. and Sun, L. (2020), 'Holocene ENSO variability in the South China Sea recorded by high-resolution oxygen isotope records from the shells of Tridacna spp.', *Scientific reports* **10**(1), 1–10.

Shi, Z., Liu, X. and Cheng, X. (2012), 'Anti-phased response of northern and southern East Asian summer precipitation to ENSO modulation of orbital forcing', *Quaternary Science Reviews* **40**, 30–38.

Sigl, M., Winstrup, M., McConnell, J. R., Welten, K. C., Plunkett, G., Ludlow, F., Büntgen, U., Caffee, M., Chellman, N., Dahl-Jensen, D. et al. (2015), 'Timing and climate forcing of volcanic eruptions for the past 2,500 years', *Nature* **523**(7562), 543–549.

Sinclair, D. J., Banner, J. L., Taylor, F. W., Partin, J., Jenson, J., Mylroie, J., Goddard, E., Quinn, T., Jocson, J. and Miklavič, B. (2012), 'Magnesium and strontium systematics in tropical speleothems from the western pacific', *Chemical Geology* **294**, 1–17.

Smith, R. B. (1979), The influence of mountains on the atmosphere, *in* 'Advances in geophysics', Vol. 21, Elsevier, pp. 87–230.

Sodemann, H., Schwierz, C. and Wernli, H. (2008), 'Interannual variability of Greenland winter precipitation sources: Lagrangian moisture diagnostic and North Atlantic Oscillation influence', *Journal of Geophysical Research: Atmospheres* **113**(D3).

Sone, T., Kano, A., Okumura, T., Kashiwagi, K., Hori, M., Jiang, X. and Shen, C.-C. (2013), 'Holocene stalagmite oxygen isotopic record from the japan sea side of the japanese islands, as a new proxy of the east asian winter monsoon', *Quaternary Science Reviews* **75**, 150–160.

Stein, A. F., Draxler, R. R., Rolph, G. D., Stunder, B. J., Cohen, M. D. and Ngan, F. (2015), 'NOAA's HYSPLIT atmospheric transport and dispersion modeling system', *Bulletin of the American Meteorological Society* **96**(12), 2059–2077.

Steinhilber, F., Abreu, J. A., Beer, J., Brunner, I., Christl, M., Fischer, H., Heikkilä, U., Kubik, P. W., Mann, M., McCracken, K. G. et al. (2012), '9,400 years of cosmic radiation and solar activity from ice cores and tree rings', *Proceedings of the National Academy of Sciences* **109**(16), 5967–5971.

Steinke, S., Glatz, C., Mohtadi, M., Groeneveld, J., Li, Q. and Jian, Z. (2011), 'Past dynamics of the east asian monsoon: No inverse behaviour between the summer and winter monsoon during the holocene', *Global and Planetary Change* **78**(3-4), 170–177.

Stoffel, M., Khodri, M., Corona, C., Guillet, S., Poulain, V., Bekki, S., Guiot, J., Luckman, B. H., Oppenheimer, C., Lebas, N. et al. (2015), 'Estimates of volcanic-induced cooling in the northern hemisphere over the past 1,500 years', *Nature Geoscience* **8**(10), 784–788.

Sturm, C., Hoffmann, G. and Langmann, B. (2007), 'Simulation of the stable water isotopes in precipitation over south america: Comparing regional to global circulation models', *Journal of Climate* **20**(15), 3730–3750.

Sun, G., Li, Y. and Li, S. (2019), 'The differences in cloud vertical structures between active and break spells of the east asian summer monsoon based on cloudsat data', *Atmospheric Research* **224**, 157–167.

Tan, L., Cai, Y., An, Z., Yi, L., Zhang, H. and Qin, S. (2011), 'Climate patterns in north central china during the last 1800 yr and their possible driving force', *Climate of the Past* **7**(3), 685–692.

Tan, L., Shen, C.-C., Löwemark, L., Chawchai, S., Edwards, R. L., Cai, Y., Breitenbach, S. F. M., Cheng, H., Chou, Y.-C., Duerrast, H., Partin, J. W., Cai, W., Chabangborn, A., Gao, Y., Kwiecien, O., Wu, C.-C., Shi, Z., Hsu, H.-H. and Wohlfarth, B. (2019a), 'Rainfall variations in central Indo-Pacific over the past 2,700 y', *Proceedings of the National Academy of Sciences* **116**(35), 17201–17206.

Tan, M., Liu, T., Hou, J., Qin, X., Zhang, H. and Li, T. (2003), 'Cyclic rapid warming on centennial-scale revealed by a 2650-year stalagmite record of warm season temperature', *Geophysical Research Letters* **30**(12).

Tan, P.-H., Tu, J.-Y., Wu, L., Chen, H.-S. and Chen, J.-M. (2019), 'Asymmetric relationships between El Niño–Southern Oscillation and entrance tropical cyclones in the South China Sea during fall', *International Journal of Climatology* **39**(4), 1872–1888.

Tang, Y., Pang, H., Zhang, W., Li, Y., Wu, S. and Hou, S. (2015), 'Effects of changes in moisture source and the upstream rainout on stable isotopes in precipitation, a case study in Nanjing, eastern China', *Hydrology and Earth System Sciences* **19**(10), 4293–4306.

Taylor, K. E., Stouffer, R. J. and Meehl, G. A. (2012), 'An overview of CMIP5 and the experiment design', *Bulletin of the American meteorological Society* **93**(4), 485–498.

Thuc, T., Van Thang, N., Huong, H. T. L., Van Khiem, M., Hien, N. X. and Phong, D. H. (2016), 'Climate change and sea level rise scenarios for vietnam', *Ministry of Natural resources and Environment. Hanoi, Vietnam* .

Tian, J., Huang, E. and Pak, D. K. (2010), 'East asian winter monsoon variability over the last glacial cycle: insights from a latitudinal sea-surface temperature gradient across the south china sea', *Palaeogeography, Palaeoclimatology, Palaeoecology* **292**(1-2), 319–324.

Tierney, J. E., Oppo, D. W., Rosenthal, Y., Russell, J. M. and Linsley, B. K. (2010), 'Coordinated hydrological regimes in the indo-pacific region during the past two millennia', *Paleoceanography* **25**(1).

Tierney, J. E., Pausata, F. S. and Demenocal, P. (2016), 'Deglacial indian monsoon failure and north atlantic stadials linked by indian ocean surface cooling', *Nature Geoscience* **9**(1), 46–50.

Törnqvist, T. E. and Hijma, M. P. (2012), 'Links between early holocene ice-sheet decay, sea-level rise and abrupt climate change', *Nature Geoscience* **5**(9), 601–606.

Treble, P., Shelley, J. and Chappell, J. (2003), 'Comparison of high resolution sub-annual records of trace elements in a modern (1911–1992) speleothem with instrumental climate data from southwest australia', *Earth and Planetary Science Letters* **216**(1-2), 141–153.

Tremaine, D. M. and Froelich, P. N. (2013), 'Speleothem trace element signatures: A hydrologic geochemical study of modern cave dripwaters and farmed calcite', *Geochimica et Cosmochimica Acta* **121**, 522–545.

Tremaine, D. M., Froelich, P. N. and Wang, Y. (2011), 'Speleothem calcite farmed in situ: Modern calibration of δ^{18}O and δ^{13}C paleoclimate proxies in a continuously-monitored natural cave system', *Geochimica et Cosmochimica Acta* **75**(17), 4929–4950.

Trinh, D. A., Trinh, Q. H., Fernández-Cortés, A., Mattey, D. and Guinea, J. G. (2018), 'First assessment on the air co 2 dynamic in the show caves of tropical karst, vietnam', *International Journal of Speleology* **47**(1), 8.

Tung, Y.-S., Wang, S.-Y. S., Chu, J.-L., Wu, C.-H., Chen, Y.-M., Cheng, C.-T. and Lin, L.-Y. (2020), 'Projected increase of the East Asian summer monsoon (Meiyu) in Taiwan by climate models with variable performance', *Meteorological Applications* **27**(1), e1886.

United Nations Report, R. (2020), 'Viet Nam: Floods, Landslides and Storms, Office of the UN Resident Coordinator', **1**.

Vaks, A., Woodhead, J., Bar-Matthews, M., Ayalon, A., Cliff, R., Zilberman, T., Matthews, A. and Frumkin, A. (2013), 'Pliocene–Pleistocene climate of the northern margin of Saharan–Arabian Desert recorded in speleothems from the Negev Desert, Israel', *Earth and Planetary Science Letters* **368**, 88–100.

Vanghi, V., Iriarte, E. and Aranburu, A. (2015), 'High resolution x-ray computed tomography for petrological characterization of speleothems.', *Journal of Cave & Karst Studies* **77**(1).

Veena, M., Achyuthan, H., Eastoe, C. and Farooqui, A. (2014), 'A multi-proxy reconstruction of monsoon variability in the late Holocene, South India', *Quaternary International* **325**, 63–73.

Vu, T. V., Nguyen, H. T., Nguyen, T. V., Nguyen, H. V., Pham, H. T. T. and Nguyen, L. T. (2015), 'Effects of ENSO on autumn rainfall in central Vietnam', *Advances in Meteorology* **2015**(3).

Waliser, D. E. and Gautier, C. (1993), 'A satellite-derived climatology of the ITCZ', *Journal of climate* **6**(11), 2162–2174.

Walker, G. T. (1933), 'Seasonal weather and its prediction', *Nature* **132**, 805–808.

Wang, B., Huang, F., Wu, Z., Yang, J. and Fu, X. (2009), 'Dynamics of Atmospheres and Oceans Multi-scale climate variability of the South China Sea monsoon : A review', *Dynamics of Atmospheres and Oceans* **47**, 15–37.

Wang, B. and Lin, H. (2002), 'Rainy season of the Asian–Pacific summer monsoon', *Journal of Climate* **15**(4), 386–398.

Wang, B., LinHo, Zhang, Y. and Lu, M.-M. (2004), 'Definition of South China Sea Monsoon Onset and Commencement of the East Asia Summer Monsoon', *American Meteorological Society* pp. 699–710.

Wang, B., Wu, R. and Fu, X. (2000), 'Pacific–East Asian teleconnection: how does ENSO affect East Asian climate?', *Journal of Climate* **13**(9), 1517–1536.

Wang, B., Wu, Z., Chang, C.-P., Liu, J., Li, J. and Zhou, T. (2010), 'Another look at interannual-to-interdecadal variations of the east asian winter monsoon: The northern and southern temperature modes', *Journal of Climate* **23**(6), 1495–1512.

Wang, J. K., Johnson, K. R., Borsato, A., Amaya, D. J., Griffiths, M. L., Henderson, G. M., Frisia, S. and Mason, A. (2019), 'Hydroclimatic variability in southeast asia over the past two millennia', *Earth and Planetary Science Letters* **525**, 115737.

Wang, L., Chen, W. and Huang, R. (2008), 'Interdecadal modulation of PDO on the impact of ENSO on the East Asian winter monsoon', *Geophysical Research Letters* **35**(20).

Wang, L., Li, G., Wang, L., Zhang, W., Zhang, Y., Liu, Y., Wang, X. and Wang, H. (2021), 'In-phase and out-of-phase behavior of the east asian summer and winter monsoons recorded in the south yellow sea sediment over the past 9.5 ka', *Quaternary Research* **99**, 96–113.

Wang, L., Li, J., Lu, H., Gu, Z., Rioual, P., Hao, Q., Mackay, A. W., Jiang, W., Cai, B., Xu, B. et al. (2012), 'The east asian winter monsoon over the last 15,000 years: its links to high-latitudes and tropical climate systems and complex correlation to the summer monsoon', *Quaternary Science Reviews* **32**, 131–142.

Wang, P., Wang, B., Cheng, H., Fasullo, J., Guo, Z., Kiefer, T. and Liu, Z. (2014), 'The global monsoon across time scales: Is there coherent variability of regional monsoons?', *Climate of the Past Discussions* **10**(3).

Wang, P. X., Wang, B., Cheng, H., Fasullo, J., Guo, Z., Kiefer, T. and Liu, Z. (2017a), 'The global monsoon across time scales: Mechanisms and outstanding issues', *Earth-Science Reviews* **174**, 84–121.

Wang, Y., Cheng, H., Edwards, R. L., He, Y., Kong, X., An, Z., Wu, J., Kelly, M. J., Dykoski, C. A. and Li, X. (2005), 'The Holocene Asian monsoon: links to solar changes and North Atlantic climate', *Science* **308**(5723), 854–857.

Wang, Y. J. (2001), 'A High-Resolution Absolute-Dated Late Pleistocene Monsoon Record from Hulu Cave, China', *Science* **294**(5550), 2345–2348.

Wang, Y., Liu, X. and Herzschuh, U. (2010), 'Asynchronous evolution of the Indian and East Asian Summer Monsoon indicated by Holocene moisture patterns in monsoonal central Asia', *Earth-Science Reviews* **103**(3-4), 135–153.

Wang, Z. and Chang, C. (2008), 'Mechanism of the asymmetric monsoon transition as simulated in an agcm', *Journal of climate* **21**(8), 1829–1836.

Wang, Z. and Chang, C.-P. (2012), 'A Numerical Study of the Interaction between the Large-Scale Monsoon Circulation and Orographic Precipitation over South and Southeast Asia', *Journal of Climate* **25**(7), 2440–2455.

Ward, B. M., Wong, C. I., Novello, V. F., McGee, D., Santos, R. V., Silva, L. C., Cruz, F. W., Wang, X., Edwards, R. L. and Cheng, H. (2019), 'Reconstruction of Holocene coupling between

the South American Monsoon System and local moisture variability from speleothem $\delta^{18}O$ and $^{87}Sr/^{86}Sr$ records', *Quaternary Science Reviews* **210**, 51–63.

Wassenburg, J. A., Riechelmann, S., Schröder-Ritzrau, A., Riechelmann, D. F., Richter, D. K., Immenhauser, A., Terente, M., Constantin, S., Hachenberg, A., Hansen, M. et al. (2020), 'Calcite mg and sr partition coefficients in cave environments: Implications for interpreting prior calcite precipitation in speleothems', *Geochimica et Cosmochimica Acta* **269**, 581–596.

Wassenburg, J. A., Scholz, D., Jochum, K. P., Cheng, H., Oster, J., Immenhauser, A., Richter, D. K., Haeger, T., Jamieson, R., Baldini, J. et al. (2016), 'Determination of aragonite trace element distribution coefficients from speleothem calcite–aragonite transitions', *Geochimica et Cosmochimica Acta* **190**, 347–367.

Wedepohl, K. H. (1995), 'The composition of the continental crust', *Geochimica et cosmochimica Acta* **59**(7), 1217–1232.

Wei, W., Wu, Y., Yang, S. and Zhou, W. (2019), 'Role of the south asian high in the onset process of the asian summer monsoon during spring-to-summer transition', *Atmosphere* **10**(5).

Wei, Z., Lee, X., Liu, Z., Seeboonruang, U., Koike, M. and Yoshimura, K. (2018), 'Influences of large-scale convection and moisture source on monthly precipitation isotope ratios observed in thailand, southeast asia', *Earth and Planetary Science Letters* **488**, 181 – 192.

Weller, E., Min, S.-K., Cai, W., Zwiers, F. W., Kim, Y.-H. and Lee, D. (2016), 'Human-caused indo-pacific warm pool expansion', *Science Advances* **2**(7), e1501719.

Wen, X., Liu, Z., Wang, S., Cheng, J. and Zhu, J. (2016), 'Correlation and anti-correlation of the east asian summer and winter monsoons during the last 21,000 years', *Nature communications* **7**(1), 1–7.

Wheeler, M. C. and Hendon, H. H. (2004), 'An all-season real-time multivariate mjo index: Development of an index for monitoring and prediction', *Monthly weather review* **132**(8), 1917–1932.

Williams, A. P. and Funk, C. (2011), 'A westward extension of the warm pool leads to a westward extension of the walker circulation, drying eastern africa', *Climate Dynamics* **37**(11-12), 2417–2435.

Williams, P. W. (2008), 'The role of the epikarst in karst and cave hydrogeology: a review', *International Journal of Speleology* **37**(1), 1.

Winnick, M. J., Chamberlain, C. P., Caves, J. K. and Welker, J. M. (2014), 'Quantifying the isotopic 'continental effect'', *Earth and Planetary Science Letters* **406**, 123–133.

Wodzicki, K. R. and Rapp, A. D. (2016), 'Long-term characterization of the pacific itcz using trmm, gpcp, and era-interim', *Journal of Geophysical Research: Atmospheres* **121**(7), 3153–3170.

Wolf, A., Roberts, W. H., Ersek, V., Johnson, K. R. and Griffiths, M. L. (2020), 'Rainwater isotopes in central vietnam controlled by two oceanic moisture sources and rainout effects', *Scientific Reports* **10**(1), 1–14.

Woodhead, J., Hellstrom, J., Maas, R., Drysdale, R., Zanchetta, G., Devine, P. and Taylor, E. (2006), 'U–pb geochronology of speleothems by mc-icpms', *Quaternary Geochronology* **1**(3), 208–221.

Wortham, B. E., Wong, C. I., Silva, L. C., McGee, D., Montañez, I. P., Rasbury, E. T., Cooper, K. M., Sharp, W. D., Glessner, J. J. and Santos, R. V. (2017), 'Assessing response of local moisture conditions in central brazil to variability in regional monsoon intensity using speleothem 87sr/86sr values', *Earth and Planetary Science Letters* **463**, 310–322.

Wu, B. and Wang, J. (2002), 'Winter arctic oscillation, siberian high and east asian winter monsoon', *Geophysical research letters* **29**(19), 3–1.

Wu, C.-H. and Hsu, H.-H. (2016), 'Role of the indochina peninsula narrow mountains in modulating the east asianwestern north pacific summer monsoon', *Journal of Climate* **29**(12), 4445–4459.

Wu, C.-H., Huang, W.-R. and Wang, S.-Y. S. (2018), 'Role of indochina peninsula topography in precipitation seasonality over east asia', *Atmosphere* **9**(7), 255.

Wurtzel, J. B., Abram, N. J., Lewis, S. C., Bajo, P., Hellstrom, J. C., Troitzsch, U. and Heslop, D. (2018), 'Tropical indo-pacific hydroclimate response to north atlantic forcing during the last deglaciation as recorded by a speleothem from sumatra, indonesia', *Earth and Planetary Science Letters* **492**, 264–278.

Wurtzel, J. B. et al. (2017), 'Reading the rain in rocks: A late deglacial speleothem record from sumatra, indonesia'.

Xiao, S., Li, A., Liu, J. P., Chen, M., Xie, Q., Jiang, F., Li, T., Xiang, R. and Chen, Z. (2006), 'Coherence between solar activity and the east asian winter monsoon variability in the past 8000 years from yangtze river-derived mud in the east china sea', *Palaeogeography, Palaeoclimatology, Palaeoecology* **237**(2-4), 293–304.

Xu, C., Buckley, B. M., Promchote, P., Wang, S.-Y. S., Pumijumnong, N., An, W., Sano, M., Nakatsuka, T. and Guo, Z. (2019), 'Increased Variability of Thailand's Chao Phraya River Peak Season Flow and Its Association With ENSO Variability: Evidence From Tree Ring δ^{18}O', *Geophysical Research Letters* **46**(9), 4863–4872.

Xu, C., Pumijumnong, N., Nakatsuka, T., Sano, M. and Guo, Z. (2018), 'Inter-annual and multi-decadal variability of monsoon season rainfall in central Thailand during the period 1804–1999, as inferred from tree ring oxygen isotopes', *International Journal of Climatology* **38**(15), 5766–5776.

Xu, C., Pumijumnong, N., Nakatsuka, T., Sano, M. and Li, Z. (2015), 'A tree-ring cellulose δ^{18}O-based July–October precipitation reconstruction since AD 1828, northwest Thailand', *Journal of Hydrology* **529**, 433–441.

Xu, C., Sano, M. and Nakatsuka, T. (2011), 'Tree ring cellulose δ^{18}O of Fokienia hodginsii in northern Laos: A promising proxy to reconstruct ENSO?', *Journal of Geophysical Research: Atmospheres* **116**(D24).

Yamoah, K. A., Chabangborn, A., Chawchai, S., Schenk, F., Wohlfarth, B. and Smittenberg, R. H. (2016), 'A 2000-year leaf wax-based hydrogen isotope record from Southeast Asia suggests low frequency ENSO-like teleconnections on a centennial timescale', *Quaternary Science Reviews* **148**, 44 – 53.

Yan, H., Soon, W. and Wang, Y. (2015), 'A composite sea surface temperature record of the northern south china sea for the past 2500 years: A unique look into seasonality and seasonal climate changes during warm and cold periods', *Earth-Science Reviews* **141**, 122–135.

Yan, H., Wei, W., Soon, W., An, Z., Zhou, W., Liu, Z., Wang, Y. and Carter, R. M. (2015a), 'Dynamics of the intertropical convergence zone over the western pacific during the little ice age', *Nature Geoscience* **8**(4), 315–320.

Yan, H., Yang, H., Yuan, Y. and Li, C. (2011), 'Relationship between east asian winter monsoon and summer monsoon', *Advances in Atmospheric Sciences* **28**(6), 1345–1356.

Yan, M., Liu, Z., Ning, L. and Liu, J. (2020), 'Holocene easm-eawm relationship across different timescales in ccsm3', *Geophysical Research Letters* **47**(17), e2020GL088451.

Yan, X.-H., Ho, C.-R., Zheng, Q. and Klemas, V. (1992), 'Temperature and size variabilities of the western pacific warm pool', *Science* **258**(5088), 1643–1645.

Yancheva, G., Nowaczyk, N. R., Mingram, J., Dulski, P., Schettler, G., Negendank, J. F., Liu, J., Sigman, D. M., Peterson, L. C. and Haug, G. H. (2007), 'Influence of the intertropical convergence zone on the east asian monsoon', *Nature* **445**(7123), 74–77.

Yang, H., Johnson, K. R., Griffiths, M. L. and Yoshimura, K. (2016), 'Interannual controls on oxygen isotope variability in asian monsoon precipitation and implications for paleoclimate reconstructions', *Journal of Geophysical Research: Atmospheres* **121**(14), 8410–8428.

Yang, X., Yang, H., Wang, B., Huang, L.-J., Shen, C.-C., Edwards, R. L. and Cheng, H. (2019), 'Early-holocene monsoon instability and climatic optimum recorded by chinese stalagmites', *The Holocene* **29**(6), 1059–1067.

Yasmi, Y. (2021), 'Transitioning toward equitable, profitable, and environmentally sound rice agri-food systems', *Regional strategy for Southeast Asia 2020-2025* pp. 1–8.

Yen, M.-C., Chen, T.-C., Hu, H.-L., Tzeng, R.-Y., Dinh, D. T., Nguyen, T. T. T. and Wong, C. J. (2011), 'Interannual Variation of the Fall Rainfall in Central Vietnam', *Journal of the Meteorological Society of Japan* **89A**(1), 259–270.

Yihui, D. and Chan, J. C. (2005), 'The east asian summer monsoon: an overview', *Meteorology and Atmospheric Physics* **89**(1), 117–142.

Yokoi, S. and Matsumoto, J. (2008), 'Collaborative Effects of Cold Surge and Tropical DepressionType Disturbance on Heavy Rainfall in Central Vietnam', *Monthly Weather Review* **136**(9), 3275–3287.

Yokoi, S., Satomura, T. and Matsumoto, J. (2007), 'Climatological characteristics of the intrasea-

sonal variation of precipitation over the Indochina Peninsula', *Journal of Climate* **20**(21), 5301–5315.

Yue, Y., Yu, K., Tao, S., Zhang, H., Liu, G., Wang, N., Jiang, W., Fan, T., Lin, W. and Wang, Y. (2019), '3500-year western pacific storm record warns of additional storm activity in a warming warm pool', *Palaeogeography, Palaeoclimatology, Palaeoecology* **521**, 57–71.

Zhang, H., Ait Brahim, Y., Li, H., Zhao, J., Kathayat, G., Tian, Y., Baker, J., Wang, J., Zhang, F., Ning, Y. et al. (2019b), 'The asian summer monsoon: Teleconnections and forcing mechanismsa review from chinese speleothem δ^{18}o records', *Quaternary* **2**(3), 26.

Zhang, H., Griffiths, M. L., Chiang, J. C., Kong, W., Wu, S., Atwood, A., Huang, J., Cheng, H., Ning, Y. and Xie, S. (2018), 'East asian hydroclimate modulated by the position of the westerlies during termination i', *Science* **362**(6414), 580–583.

Zhang, J., Griffis, T. J. and Baker, J. M. (2006), 'Using continuous stable isotope measurements to partition net ecosystem co2 exchange', *Plant, Cell & Environment* **29**(4), 483–496.

Zhang, P., Cheng, H., Edwards, R. L., Chen, F., Wang, Y., Yang, X., Liu, J., Tan, M., Wang, X., Liu, J. et al. (2008), 'A test of climate, sun, and culture relationships from an 1810-year chinese cave record', *Science* **322**(5903), 940–942.

Zhang, X., Jin, L. and Li, N. (2015), 'Asynchronous variation in the east asian winter monsoon during the holocene', *Journal of Geophysical Research: Atmospheres* **120**(11), 5357–5370.

Zhang, Y., Zhu, K., Huang, C., Kong, D., He, Y., Wang, H., Liu, W., Xie, Z., Wei, G. and Liu, Z. (2019a), 'Asian winter monsoon imprint on holocene sst changes at the northern coast of the south china sea', *Geophysical Research Letters* **46**(22), 13363–13370.

Zhang, Z., Chan, J. C. and Ding, Y. (2004), 'Characteristics, evolution and mechanisms of the summer monsoon onset over Southeast Asia', *International Journal of Climatology: A Journal of the Royal Meteorological Society* **24**(12), 1461–1482.

Zhao, D., Wan, S., Song, Z., Gong, X., Zhai, L., Shi, X. and Li, A. (2019), 'Asynchronous variation in the Quaternary East Asian winter monsoon associated with the tropical Pacific ENSO-like system', *Geophysical Research Letters* **46**(12), 6955–6963.

Zhao, J., Tan, L., Yang, Y., Pérez-Mejías, C., Brahim, Y. A., Lan, J., Wang, J., Li, H., Wang, T., Zhang, H. et al. (2021), 'New insights towards an integrated understanding of ne asian monsoon during mid to late holocene', *Quaternary Science Reviews* **254**, 106793.

Zheng, X., Li, A., Wan, S., Jiang, F., Kao, S. J. and Johnson, C. (2014), 'ITCZ and ENSO pacing on East Asian winter monsoon variation during the Holocene: Sedimentological evidence from the Okinawa Trough', *Journal of Geophysical Research: Oceans* **119**(7), 4410–4429.

Zhong, W., Xue, J., Ouyang, J., Cao, J. and Peng, Z. (2014), 'Evidence of late holocene climate variability in the western nanling mountains, south china', *Journal of paleolimnology* **52**(1-2), 1–10.

Zhou, J., Lundstrom, C. C., Fouke, B., Panno, S., Hackley, K. and Curry, B. (2005), 'Geochemistry of speleothem records from southern illinois: Development of (234u)/(238u) as a proxy for paleoprecipitation', *Chemical Geology* **221**(1-2), 1–20.

Zhu, M., Stott, L., Buckley, B., Yoshimura, K. and Ra, K. (2012), 'Indo-Pacific Warm Pool convection and ENSO since 1867 derived from Cambodian pine tree cellulose oxygen isotopes', *Journal of Geophysical Research: Atmospheres* **117**(D11).

Zomer, R. J., Trabucco, A., Bossio, D. A. and Verchot, L. V. (2008), 'Climate change mitigation: A spatial analysis of global land suitability for clean development mechanism afforestation and reforestation', *Agriculture, Ecosystems & Environment* **126**(1-2), 67–80.